The physical, genetic, and social priorities of dynamic plant mitochondria

By

Joanna Chustecki

A thesis submitted to
the University of Birmingham
for the degree of
DOCTOR OF PHILOSOPHY

Stochastic Biology Group
School of Biosciences
College of Life and Environmental Sciences
University of Birmingham
December 2021

ABSTRACT

Mitochondria are key energy providers of eukaryotic cells. They are dynamic organelles and, within plants, exist in a fragmented, individual state. Mitochondrial function and positioning is vital for energy provision, metabolite exchange, proteostasis and genetic stability. Previous work has characterised plant mitochondrial motion, as well as connectivity of mitochondria in other kingdoms, but how these dynamics benefit the cell and organism remain poorly understood. Within this thesis, the physical, genetic, and "social" priorities of these organelle dynamics are explored, and we investigate why the plant cell controls its bioenergetic organelles in this way. Physical priorities encompass how mitochondria move, positioning within the cell and interactions with other organelles. In plants, there has not yet been a broad analysis of the entire cellular mitochondrial population and the connectivity across it. Here, connectivity between these individual organelles is quantified using a "social" paradigm- used to describe mitochondria as individual entities capable of communicating, and networks of encounters between these individuals are demonstrated. Genetic priorities stem from each mitochondrion harbouring its own genomic material, that within plant mitochondria is recombinatorally active- it can be rearranged, swapped and fragmented, and can be transferred between individual mitochondria, opening the question of how genetic priorities may be shaped by the physical dynamics of these organelles.

Using imaging, modelling and molecular biology approaches, we quantify physical characteristics and close encounters of mitochondria in single *Arabidopsis thaliana* cells to build social networks, revealing a trade-off between social connectivity and even cellular spread. We also investigate the physical-genetic link between sharing and spacing of these organelles within the cell using two fluorescent mutant lines, mtGFP-*friendly* and mtGFP-

msh1, showing that amongst other effects, disrupted recombination surveillance of the mitochondrial genome shifts this trade-off towards increased connectivity. The unique genetic dynamics of plant mitochondria impact upon the health of the chondriome and the successive generations, and we look for evidence of mitochondrial genome recombination ability correlating with long life span across the eukaryotic tree of life. Together, the evidence put forwards demonstrates the importance of the motility and connectivity of the mitochondrial population, and its impact upon genetic stability both within plants and broader eukaryotes.

For my family

ACKNOWLEDGMENTS

My sincere thanks to my supervisor Prof. Iain Johnston, who has encouraged, inspired and supported me throughout this project, and consistently helped me develop as a well-rounded scientist. Thankyou to Prof. Dan Gibbs for taking me on and the care and support you have shown not just me, but so many other PhDs here at Birmingham. Thankyou to Prof. George Bassel for inspiring my research interests, steadfast advice, and welcoming me as an undergraduate summer student back in 2016. Thankyou to the BBSRC and University of Birmingham for funding via the MIBTP doctoral training scheme (grant number BB/M01116X/1).

Thankyou to my amazing colleagues past and present who have taught me so much about science, resilience, kindness, and buffets. Thanks to members of the Bassel lab, Matt Jackson, Hao Xu, Jack Mitchell and Salva Duran-Nebreda. Thanks to Clare Ziegler for your tolerance and maths advice. Thankyou to Alice Darbyshire, Miguel Pachón Peñalba, Ross Etherington, Alex Phokas, Anne-Marie Labandera, Mark Bailey, Sjon Hartmann, Tumie Akintewe, Xulyu Cao, Rory Osborne, for the moral support, laughs and lessons in molecular biology. Thanks to Kostas Giannakis and the Stochastic Biology group for your support, and making doing science throughout a global pandemic less lonely.

Thankyou to my family, my mother and late father. You both knew I could do it. To my grandparents for being the strongest, bravest role models. And finally, thankyou to my partner Lewis, for your patience. Thankyou for helping me write my first ever for loop, letting me bombard you with my talks and programming questions, and your enduring belief in me. Thankyou for your support throughout this, I couldn't have done it without ya'.

CONTRIBUTIONS AND PUBLICATIONS

Chustecki, J. M., Gibbs, D. J., Bassel, G. W., Johnston, I. G. (2021) 'Network analysis of *Arabidopsis* mitochondrial dynamics reveals a resolved tradeoff between physical distribution and social connectivity', *Cell Systems*. Elsevier, 12(0), pp. 1–13. ***Cover article***

Contribution: Performed experimental work, collected and analysed image data. Shared responsibility with I.G.J for analysis code, model analysis, and manuscript drafting. Designed experiments alongside I.G.J and G.W.B.

Chustecki, J. M., Etherington, R. D., Gibbs, D. J., Johnston, I. G.(2021) 'Altered collective mitochondrial dynamics in an *Arabidopsis* msh1 mutant compromising organelle DNA maintenance', *BioRxiv*. Cold Spring Harbor Laboratory.

Contribution: Created plant lines, performed microscopy and image analysis, performed statistical analysis. Shared responsibility with R.D.E for performing sequencing and validation. Shared responsibility with I.G.J for manuscript drafting.

Giannakis, K., **Chustecki, J. M.** and Johnston, I. G. (2021) 'Encounter networks from collective mitochondrial dynamics support the emergence of effective mtDNA genomes in plant cells', *BioRxiv*. Cold Spring Harbor Laboratory.

Contribution: Performed experimental work, microscopy, video analysis, and experimental network extraction. Edited manuscript alongside K.G and I.G.J.

Edwards D. M., Røyrvik E. C., **Chustecki J. M.**, Giannakis K., Glastad R. C., Radzvilavicius A. L., Johnston I. G. (2021) 'Avoiding organelle mutational meltdown across eukaryotes with or without a germline bottleneck', *PLoS Biology*. Public Library of Science, 19(4), p. e3001153. ***Cover article***

Contribution: Literature review and helped develop theory on MSH1 across eukaryotes and contributed bioinformatics support.

Giannakis, K., Arrowsmith, S. J., Richards, L., Gasparini, S., **Chustecki, J. M.**, Røyrvik, E. C., Johnston, I. G. (2021). Universal features shaping organelle gene retention. *BioRxiv*. Cold Spring Harbor Laboratory.

Contribution: Helped develop theory for oDNA maintenance and contributed bioinformatics support.

Ibne Kamal, A. K., Batty, L., Bartlett, R., Suleiman, S., **Chustecki J. M.** (2020) Germination potential of *Sesbania cannabina* in 2 Chromium (Cr) spiked growth media, *EGU (European Geosciences Union) General Assembly 2020*

Contribution: Assisted with staining and confocal microscopy of *Sesbania* root and hypocotyl.

OUTREACH

- Postgraduate **Certificate** (Advanced Research Methods and Skills), PGCARMS Research Communication and Public Engagement, University of Birmingham, 2020
  Designed and released mitochondriamove.com, a **website** aimed at engaging a broad audience in plant science and computational approaches.
- Co-wrote a **blog post** for Botany One with Prof. Iain Johnston on our Cell Systems publication (www.botany.one/2021/06/the-social-networks-of-plant-mitochondria/)
- Wrote a **blog post** for the John Innes Centre in association with the Journal of Quantitative Plant Biology on my research interests, our publications and future directions (www.jic.ac.uk/blog/the-social-networks-of-plant-mitochondria)
- **Talk** for Birmingham Science Branch of University of the Third Age seniors' group, with some great discussions – "The social networks of mitochondria in plant cell"
- Shape Your Future series **webinar** for 15–17 year old students – "The social network of dynamic organelles within plant cells – towards understanding mitochondrial motion"

CONFERENCES, AWARDS, SEMINARS

- Plant Science Seminar Series, 2021, University of Birmingham – *Seminar*
- Society Of Experimental Biology Annual conference, 2021, Virtual – *Invited short talk*
- American Society of Plant Biologists Plant Biology conference, 2021, Plant plastid origins and evolution symposium, Virtual – *Rapid talk and poster*
- International Plant Systems Biology EMBO conference, 2021, Virtual – *Invited short talk*

  Awarded the Plant Journal Talk Prize for this talk
- MIBTP Annual Symposium, 2021, Virtual – *Invited plenary talk*

  Awarded the Plenary Talk Prize for the symposium

- MitOX, 2020, Virtual, University of Oxford – *Lightning presentation*
- Biosciences Graduate Research Symposium, 2020, University of Birmingham – *Short talk*

  Awarded the New England Biolabs Talk Prize for this talk
- Lunchtime Applied Mathematics seminar, 2020, University of Birmingham – *Seminar*
- Plant Science Seminar Series, 2019, University of Birmingham – *Seminar*
- Research Poster Conference, 2019, University of Birmingham – *Poster presentation*
- GARNet Workshop on Advances in Plant Imaging, 2019, University of Warwick – *Lightning talk and poster presentation*
- MitOX, 2019, University of Oxford – *Poster presentation*
- MIBTP Annual Symposium, 2019, University of Warwick – *Poster presentation*
- European Open Science Forum, 2018, University of Toulouse – *Organising workshops*

TEACHING

- Demonstrating and marking across modules in BSc Biological Sciences, 2018 - 2021
  - Ecological Concepts and Plant Sciences
  - Human Nutrition & Metabolism
  - Plant Science: from cells to environment
  - Human structure and Function
- Pedagogical training from Centre for Learning and Academic Development, University of Birmingham, 2018
  - Introduction to learning and teaching in higher education for postgraduates
  - Introduction to Assessment and Feedback
- Undergraduate open days demonstrator for Biological Sciences/Biochemistry/Natural Sciences, 2019

Contents

List of Figures

List of Tables

Chapter One

Introduction

1.1 The plant mitochondrion

Mitochondria are key energy providers within eukaryotic cells. They are involved in multiple functions including stress responses, metabolic pathways and cell death (Yoshinaga et al., 2005; Jacoby et al., 2012; Shutt and McBride, 2013; Wang, Berkowitz, et al., 2018; Dopp et al., 2021). They produce ATP through the process of oxidative phosphorylation (OXPHOS) by passing electrons through the electron transport chain, providing a main source of energy for the cell. Mitochondria move within the cytoplasm and, within plants, are actively transported along actin filaments. They colocalise with each other and other organelles throughout cellular space, sharing metabolites and proteins in order to maintain both a healthy cell and processes that rely on them, such as photosynthesis, photorespiration and OXPHOS.

Mitochondrial morphology is highly variable. As individuals, these membrane-bound organelles are diverse in shape, able to fluctuate between bean-like, elongate or very punctate structures rapidly, demonstrated through elegant imaging experiments across kingdoms (Bereiter-Hahn and Vöth, 1994; Yaffe, 1999; Logan and Leaver, 2000; Day et al., 2004;

De Vos, Allan, et al., 2005; Zhao et al., 2013; Simula and Campello, 2018). Yeast and most mammalian mitochondria typically exist as elongated, reticulated structures that can form physical branched networks (Shaw and Nunnari, 2002; Sukhorukov, Dikov, et al., 2012; Rafelski, 2013). Mitochondria exist as populations within most eukaryotic cells, with the number of mitochondria in yeast cells typically between 1-10 (Nunnari et al., 1997), and in humans the number varies, from ~80-1000s (Cole, 2016), with high-energy demand cells typically having more. These populations are also dynamic, able to split apart and fuse together by joining membranes. In yeast, there is typically one fusion or fission event once per cell per minute, and fusion happens typically side-on, between the end of a tubule and the side of another, forming a branch structure (Rafelski, 2013; Nunnari et al., 1997). Fission occurs either at the branch structure, or in the middle of a tubule. The network distribution is usually well-spread across the cell, but can be asymmetric, over-fused, over-fragmented, swollen or completely non tubular (a big spherical shape)- all dependant of the cell-cycle stage, altered conditions or mutations (Rafelski, 2013). Mitochondria with reduced membrane potential, a sign of reduced energetic capacity, will not fuse as readily with the network, and so be segregated from the population and targeted for mitophagy (Twig, Elorza, et al., 2008). In contrast, plant mitochondria exist as individual, discrete, punctate structures of ~1µm in length (Logan and Leaver, 2000; Jaipargas, Barton, et al., 2015; Logan and Paszkiewicz, 2018), although exceptions do exist- such as in the reticulated cage-like structure of the Shoot Apical Meristem (SAM) in *Arabidopsis* (Seguí-Simarro, Coronado, et al., 2008; Seguí-Simarro and Staehelin, 2009), and during germination (Paszkiewicz et al., 2017). They too exist as populations, and in mesophyll cells, there are ~200-400 mitochondria (Logan, 2006a).

Within plants, fragmented mitochondria move about rapidly, interacting with each other through transient fission and fusion events (Logan, 2006b; Logan, 2010a; Arimura, Yamamoto, et al., 2004; Logan and Paszkiewicz, 2018). This behaviour is similar to the 'kiss-and-run' dynamics of bacteria (Liu, Weaver, et al., 2009) (note the Liu, Weaver, et al. (2009)

experiments were done in mammalian cells). Plant mitochondria transiently encounter each other in this way, allowing diffusion and exchange of mitochondrial contents, whether partial or full fusion occurs (Arimura, Yamamoto, et al., 2004). The proteins involved in plant mitochondrial fusion are still being elucidated (Logan, 2010a; Johnston, 2019a; Rose, 2021), but key works demonstrate the roles of the cytosolic protein FRIENDLY (*FMT*) in mitochondrial fusion (Logan, Scott, et al., 2003; El Zawily et al., 2014). Mitochondrial fission in plants is controlled by two homologs of human and yeast Fis1, named BIGYIN 1 and 2 –a Scottish colloquialism for 'the big one'– as one or two large mitochondria are formed when the gene is disrupted, implicating it in mitochondrial fission (Scott, Tobin, et al., 2006; Logan, 2010a). Two other proteins, DRP3A and DRP3B are also implicated in controlling mitochondrial division in *Arabidopsis* (Arimura, Tsutsumi, et al., 2002; Logan, Scott, et al., 2004).

Positioning of mitochondria within the cell is cell-type specific, for example, mitochondria will colocalise to chloroplasts within leaf cells, particularly in response to light fluctuations– a key environmental response (Islam, Niwa, et al., 2009). This colocalisation is also seen in plant protoplasts (Oikawa et al., 2021), and mitochondria move in streaming motions in root hairs cells (Zheng, Beck, et al., 2009). Mitochondrial positioning in the cell needs to be contextualised with the fact that the cell is a busy place. Plant mitochondria navigate space between the cell wall, a central vacuole, and the many other organelles. Even moving through the cytoplasm itself is difficult. For example, if a monomeric (single molecule) protein was moving about in water, its diffusion constant might be 100 $\mu m^2/s$, but inside the cell it might be 10$\mu m^2/s$ (Milo and Phillips, 2015). Time taken to traverse the cell scales with distance, with an estimate for a protein to traverse 1µm being 0.01 seconds (*Escherichia coli* cell), but increasing to 10 seconds for a 20µm distance (HeLa human cell) (Milo and Phillips, 2015), showing the difficulty of moving biomolecules efficiently through the cell. Over long distances, mitochondria use cytoskeletal strands (of actin in plants, using

the motor protein myosin) to traverse cellular space, and streaming can occur from high velocity motion of organelles through the cell, carrying individual mitochondria along (Doniwa et al., 2007; Van Gestel et al., 2002; Avisar et al., 2009). However, non-random movement uses energy, and so these organelles pay an energetic toll for each step along actin strands, contributing to the cost of maintaining a dynamic population with efficient movement across the cell.

This population of dynamic individuals interlinked through transient connectivity and intermitochondrial signals can be described as a 'discontinuous whole' (Logan, 2006b). This describes the higher plant chondriome as being physically fragmented, but functionally connected. Chondriome is the collective term for all mitochondria in the cell, used interchangeably herein with 'mitochondrial population'. Transient fission and fusion events are linked with mitochondrial quality control (Arimura, 2018). These events allow the vital mixing of mitochondrial components across the chondriome, such as genomic material or proteins (Bereiter-Hahn and Vöth, 1994; Arimura, Yamamoto, et al., 2004; Busch et al., 2014; Logan, 2006a; El Zawily et al., 2014; Møller, 2016). These events also ensure the monitoring of quality across all individuals (Shutt and McBride, 2013) and removal of unhealthy mitochondria via mitophagy (El Zawily et al., 2014; Nakamura et al., 2021). This ensures continuing proteostasis (the maintenance of the correct amount and type of proteins required for normal function) (Clavel and Dagdas, 2021), helping to maintain the health of the plant.

It is curious however, why plants keep their powerhouses as individuals, and fusion rates are not as high as within fungi or metazoans. As mentioned, poorly performing 'unhealthy' mitochondria are targeted for degradation through the process of mitophagy (in which FRIENDLY is also implicated to be a key regulator (Ma et al., 2021)). Keeping the mitochondrial population in a fragmented state may help the cell clear out underperforming individuals more effectively (Johnston, 2019a). Also, this fragmented population may provide a *physical barrier* to recombination and exchange of the genomic information mito-

chondria carry, acting as a control on unregulated proliferation of certain genetic elements (Johnston, 2019a; Rose, 2021). It could also be postulated that a fragmented mitochondrial population provides the sessile plant with an opportunity to quickly respond to environmental changes, such as alterations in light levels, and the need to relocate to energy demanding areas or organelles. Considering the common ancestry of mitochondria across major eukaryotic lineages, it is a key question as to why plant mitochondria exist at the fragmented end of a mitochondrial population state, and fungal and metazoans exist in a more fused and networked state. Key examples across the plant life cycle such as massive mitochondrial reticulation, studies into the sequence and structural states of mitochondrial DNA, dynamic responses to environmental fluctuations and quantification and modelling of network states will help us further investigate this dynamic mitochondrial population and begin to answer these key questions.

Ultrastructure and energy requirements are interlinked, as these highly dynamic organelles invest large a amount of energy in active travel across the cell on cytoskeletal strands. Why do they invest so much energy? Why stay as individuals? Why move at all? The cellular principles behind their ultrastructure and motility patterns still remain poorly understood (Takagi et al., 2011; Hoitzing et al., 2015).

1.1.1 Mitochondrial genomes

Mitochondria retain their own genomes, a relic of their evolutionary past. The plant mitochondrial genome has undergone both massive expansion and loss of genes (Adams and Palmer, 2003; Sloan, Alverson, et al., 2012; Skippingtona et al., 2015; Petersen et al., 2017; Kozik et al., 2019), rendering much of the genome as non-coding introns and repeat sequences. Only genes encoding proteins central to energy production and functionality remain in the organellar genome, with other ancestral genes either lost or transferred to the nucleus (Gray

et al., 1999). Remaining in *Arabidopsis* mitochondria are 57 genes (33 protein coding) across 366kb of mtDNA (Unseld et al., 1997; Ladoukakis and Zouros, 2017; Sloan, Wu, et al., 2018). The mtDNA encoded proteins are the most energetically central to subunits making up the electron transport chain (Johnston and Williams, 2016), and so any mutation in these genes can have catastrophic effects on the organism, particularly in animal mitochondria, where the majority of mtDNA is protein coding exons.

mtDNA (mitochondrial DNA) molecules are highly polyploid and each cell contains many different versions of the same genome. In contrast to other kingdoms, each individual mitochondrion within plants does not necessarily carry the full mtDNA genome (Preuten et al., 2010). Some mitochondria carry the full mtDNA complement, some only a subgenomic molecule carrying a few genes, and some carry no mtDNA at all (Arimura, Yamamoto, et al., 2004; Gualberto, Mileshina, et al., 2014; Kozik et al., 2019). In contrast to mammalian organellar DNA, plant mtDNA is recombinatorally active (Maréchal and Brisson, 2010; Woloszynska, 2010; Klucnika and Ma, 2020), meaning that mtDNA molecules can be exchanged both within the nucleoid structures they are arranged as, and between these structures, leading to a very dynamic organisation of the mitochondrial genome (Arrieta-Montiel and Mackenzie, 2011). The plant mitochondrial genome has very low mutation rates (Palmer and Herbon, 1988), evolving slowly in nucleotide sequence (i.e. base by base), but has a rapid structural evolutionary rate. In contrast, animal mtDNA mutation rates are high, and the nucleotide sequence evolves rapidly, but its structure changes very slowly (Brown et al., 1979).

Plant mtDNA also has an unusual structural organization- instead of being organised into one central ring structure, mtDNA can be found in circular, linear and branched molecules (Gualberto, Mileshina, et al., 2014; Morley and Nielsen, 2017; Kozik et al., 2019). This unusual structure and distribution is linked to recombination and exchange of mtDNA in plants, with these processes key to maintaining the arrangement of mtDNA (Gray et

al., 1999; Bellaoui et al., 1998; Arrieta-Montiel, Shedge, et al., 2009; Davila et al., 2011; Gualberto and Newton, 2017; Johnston, 2019b). As stated by Lonsdale et al. (1988) it is "an impossibility" for the complex structure of mtDNA to arise from a single punctate mitochondrion, that may not even contain any mtDNA, and recombination cannot be facilitated within one single mitochondrion; therefore it is the act of intermixing, fusion and the dynamic syncytium between mitochondria that facilitates this recombination (Rose, 2021).

Recombination is one of the main driving forces behind the multi-partite structure seen in plant mtDNA (Kmiec et al., 2006). The plant mitochondrial genome contains repeats regions, some long (several kb in length), and some short (100s of base pairs). Long repeat sequences have been shown to be sites of frequent homologous recombination (Arrieta-Montiel and Mackenzie, 2011). Recombination is less frequent in wild-type plants at short repeats sequences, but it can happen, dynamically forming small sections of mtDNA called sublimons, that are detected at a substoichiometric level (very low levels of subgenomic molecules). When DNA repair and maintenance machinery is mutated, these short sequences become sites of frequent recombination (Shedge et al., 2007), and genome instability. Generally, mtDNA genome instability leads to a detrimental phenotype, and can have a deleterious effect, as mtDNA encodes the most important bioenergetic proteins (Wallace and Chalkia, 2013; Ahmad and Nielsen, 2020), as mentioned previously. Genome instability and the build-up of mitochondrial mutations can lead to many mitochondrial diseases in humans, and is implicated in cancers, ageing and neurodegenerative diseases (Lee, Yin, et al., 2005; Stenton and Prokisch, 2020; Lawless et al., 2020). Recombination in the plant mitochondrial genome and the associated repair proteins allow the maintenance of the genome on a nucleotide level i.e at a genic level (Johnston, 2019a). However, this recombination can lead to structural rearrangements on a genomic level leading to the multipartite structures described above. Selection will act to remove inaccurate fixes at a sequence level, and so a balance between recombination allowing genetic control and maintenance of a healthy genome and control by

the cell to mitigate proliferation of damaging sequences arises.

1.1.2 Organellar interactions

Historically, compartments within cells have been considered as isolated entities, each with a specific role– whether energy production, protein synthesis, storage or degradation (Schrader et al., 2015). We now know that there are more involved, functional interactions *between* membrane-bound organelles within the eukaryotic cell (Simmen and Tagaya, 2017). For example, the interaction of mitochondria and the endoplasmic reticulum (ER) has been observed in morphological studies since the early 1970s (Morré et al., 1971; Franke and Kartenbeck, 1971). Mitochondrial associated membrane proteins were found stuck to the outer membrane of extracted mitochondria, and thought to be an artefact of the extraction process (Dolgin, 2019). However, they were shown to be part of the ER, bound to the mitochondrion during lipid transfer and calcium regulation from the ER to the mitochondrion, having a role in monitoring apoptosis, and controlling the morphology and dynamics of mitochondria (Vance, 2014).

Diverse evidence of interorganellar interactions has since been demonstrated. These interactions are temporally and spatially dynamic (Takagi et al., 2011). Nearly all organelles can interact directly using their own portfolios of membrane proteins (Schrader et al., 2015; Perico and Sparkes, 2018). For example, in yeast; peroxisomes, lipid droplets, mitochondria, the plasma membrane, vacuole and the ER have been shown to interact with one another via membrane contact sites (Shai, Yifrach, et al., 2018). In plants, mitochondria are known to colocalise to chloroplasts (Jouhet et al., 2004; Islam, Niwa, et al., 2009; Islam and Takagi, 2010), the ER (Jaipargas, Barton, et al., 2015; Mueller and Reski, 2015; White et al., 2020) and peroxisomes (Scott, Sparkes, et al., 2007; Jaipargas, Mathur, et al., 2016). Direct communication and transfer of metabolites has been demonstrated between organelles in

plants, such as lipid transfer from chloroplasts to mitochondria (Jouhet et al., 2004), and bidirectional ability of chloroplasts and the ER to access non-polar metabolites (Mehrshahi et al., 2013). Many organelles also use membrane protrusions for interorganellar signalling (Mullineaux et al., 2020). These are named stromules in plastids, matrixules in mitochondria and peroxules in peroxisomes (Mathur et al., 2012; Mathur, 2021). They enable rapid responses, for plastid sugar metabolism/light response, mitochondrial fusion/fission, and peroxisome H_2O_2 scavenging (Schattat et al., 2011; Mathur et al., 2012; Mathur, 2021).

Indirect interorganellar communication can occur between mitochondria, chloroplasts and the nucleus using anterograde (from the nucleus) and retrograde signalling (to the nucleus) in the plant (Pesaresi et al., 2007). Direct plastid– nuclear complexes also facilitate this signalling (Mullineaux et al., 2020). It is important for the nucleus and mitochondria/ plastids to be in communication– these compartments contain their own genomes, and encode subunits for proteins that will be complexed together with subunits encoded by the nucleus. Each organelle needs to maintain its own collection of proteins- one reason for organelles to maintain their own genomes (Johnston, 2019a). Intra-organellar signalling is vital to maintain proteostasis in both chloroplasts and mitochondria and dual-targeting proteins (often transcription factors) enable control of this 'genome communication' (Woodson and Chory, 2008; Krupinska et al., 2020).

1.1.3 Inheritance and recombination in mitochondrial populations

The mitochondrial genome is dynamic, and has an unusual structure that is changeable with recombination as a driving force. But how does the plant manage a dynamic population of nucleoids? The renamed *MSH1* is a homolog of bacterial MutS, a mismatch repair protein (Abdelnoor, Yule, et al., 2003), with a structure that allows it to make double stranded incisions in DNA (Chevalier and Stoddard, 2001). The prevailing view is that plant *MSH1*

is involved in recombination surveillance of mtDNA. Wu et al. (2020) present two different models for MSH1 function in plants. One, that as a MutS homolog, MSH1 functions as a mismatch repair protein, and directs cleavage to the newly synthesised strand of DNA. Or two, that it induces DSB (double-strand breaks) at mismatches, and the site is then subject to homology-directed repair, using another unaffected genome copy (Fukui et al., 2018). This would happen before the mismatch becomes embedded as a true double strand base substitution. From this, various outcomes can occur: long homology-based repair, leading to gene conversion (the overwriting of one gene by another due to DSB formation and either chromosome paired or ectopic homologous sequences being used as the template); Short homology-based repair, leading to break-induced replication and genome expansion/rearrangements; Or non-homologous repair where inaccurate repair takes place and leads to genome expansion and chimeric gene production (Christensen, 2014). This DSB-led model would result in high repair accuracy, and would not rely on the choosing of which single strand the error is on at mismatched sites (Wu et al., 2020). It would, however, lead to an expanded mitochondrial genome, which we do observe in plants, as each instance of damage would be repaired using homologous templates to fill DSB sites.

There is also discussion of the expression and availability of *MSH1* being lower in plant vegetative tissues (Virdi et al., 2016) (or at least higher in meristematic tissues than other types (Edwards et al., 2021)), and fewer template strands available in vegetative tissues (Wynn et al., 2020). The shoot apical meristem (SAM) is the origin of aerial tissues including leaves and flowers, and so alterations to the cytoplasmic and nuclear genomes here influence the germ line. Cells in the SAM are sites of active DNA synthesis, with this activity changing according to developmental stages (Fujie et al., 1994). The SAM is also the site of massive reticulation between mitochondria– a state not seen within the vegetative tissues of plants, where mitochondria exist as individuals (that themselves can transiently fuse) (Bendich and Gauriloff, 1984). This massive reticulation, paired with high expression of *MSH1* allows

high levels of mtDNA recombination, providing DNA repair but also homogenization of the mitochondrial genome across daughter cells before going on to form gametes (Seguí-Simarro, Coronado, et al., 2008; Seguí-Simarro and Staehelin, 2009; Edwards et al., 2021). Massive mitochondrial mixing events also occur at zygote, germination and regeneration stages in the plant, potentially providing an increase in energy production in the face of large developmental change (Rose, 2021). This homogenization and bringing together of mtDNA copies give opportunity for the DSB repair to occur, as there would be ample opportunity for utilization of template strands for repair (Wu et al., 2020; Christensen, 2014). This situation is a direct link between physical mitochondrial dynamics and the genome stability of individual mtDNA molecules.

In metazoans, build-up of mitochondrial mutations is subject to a 'threshold effect', discussed by Rossignol et al. (2003), when the disease is presented phenotypically, biochemically or translationally only upon reaching a certain threshold of mutational variants within the mtDNA. Any build-up of mutational damage is termed Muller's ratchet (Muller, 1964), and is avoided in mtDNA by organisms with a germ line through the genetic mitochondrial bottleneck (Garone et al., 2018; Johnston, 2019a). This is where generation of heteroplasmy variance is induced, with purifying selection disposing of germ cells with high level of mtDNA damage, reducing the amount of damaged mtDNA passed to the next generation. For plants and other organisms without a fixed germline, gene conversion and mtDNA recombination are implemented instead (Edwards et al., 2021). These mechanisms are responsible for generating beneficial variance that would allow segregation of mtDNA types and homoplasmy within cells, to be subjected to purifying selection, and going on to form the next generation.

1.1.4 Linking physical and genetic dynamics

As with many processes, plants deal with damage to their mitochondrial genome differently to other organisms. Recombination at the many repeat sequences generates a level of variation in the plant mitochondrial genome that can be useful for the plant under fluctuating environmental conditions, from which it cannot move away, as well as allowing rapid mtDNA evolution, using the non-coding regions as a "reservoir of genetic diversity" (Chevigny et al., 2020). However, the mitochondrial genome is also subject to damage, in the form of ROS produced through bioenergetic processes within the mitochondrial matrix, UV damage and genotoxic stress; these all lead to a constant need to repair mtDNA (Mahapatra et al., 2021). This is done through direct repair, mismatch repair, nucleotide excision repair, base excision repair or recombination. This repair is often facilitated by the exchange of mtDNA between mitochondria (Møller, 2016; Chevigny et al., 2020). These repair mechanisms all contribute to keeping mutation rates low in plant mtDNA.

mtDNA exchange occurs between molecules of DNA and also between individual mitochondria. Upon the close, proximal encounter of two or more mitochondria, membrane fusion can occur; followed by the exchange of membranes, contents mixing and mtDNA transfer (El Zawily et al., 2014; Arimura, Yamamoto, et al., 2004; Sheahan et al., 2005; Rose, 2021). This information exchange leads to the mitochondrial population acting as a 'discontinuous whole' (Logan, 2006a; Logan, 2006b), physically discrete individual organelles capable of intermixing and sharing contents. It also links physical dynamics and fission/ fusion of mitochondria to the genetic dynamics across the population, with recombination, complementation and sharing both shaped and limited by the physical dynamics of these organelles (Belliard et al., 1979; Lonsdale et al., 1988; Ono et al., 2001; Arimura, Yamamoto, et al., 2004; Mouli et al., 2009; Arrieta-Montiel and Mackenzie, 2011; Gualberto and Newton, 2017; Johnston, 2019b; Aryaman et al., 2019; Rose, 2021).

As well as genetic exchange, physical proximity facilitates both metabolic exchange and the process of mitochondrial quality control which relies on cycles of fission and fusion (Jones, 1986; Karbowski and Youle, 2003; Arimura, Yamamoto, et al., 2004; Logan, 2006b; Takanashi et al., 2006; Twig, Elorza, et al., 2008; Liu, Weaver, et al., 2009; Figge et al., 2012; Shutt and McBride, 2013; Agrawal et al., 2018). This mitochondrial mixing and matrix sharing is vital for maintaining a healthy mitochondrial population (Mouli et al., 2009). It allows the exchange of biomolecules, genetic material and protein machinery (Arimura, Yamamoto, et al., 2004; Logan, 2006b; Takanashi et al., 2006; Arimura, 2018), ensuring these organelles have everything they need to continue their vital functions. The performance of the cellular population is also improved, as mitochondrial mixing helps to compensate for damaged material (Karbowski and Youle, 2003; Twig, Elorza, et al., 2008; Figge et al., 2012; Shutt and McBride, 2013), such as the electron transport chain proteins that are susceptible to oxidative damage (Guo et al., 2013). It is not just direct fusion between mitochondria that the cell can benefit from, as there are functional metabolic effects of close adjacency between these organelles and others (Jones, 1986), such as modulating glucose concentration (Agrawal et al., 2018), metabolite flow in the processes of photorespiration (Bauwe et al., 2010; Shai, Schuldiner, et al., 2016), and C4 photosynthesis (Sage, Sage, and Kocacinar, 2012). Close proximity between mitochondria can also influence membrane potential (Santo-Domingo et al., 2013), calcium waves (Ichas et al., 1997) and cristae alignment (Picard, McManus, et al., 2015) (all from mouse or human cells), demonstrating the functional implications of intermitochondrial connectivity, even without fusion. Close encounters do not necessarily imply fusion between individuals, or exchange of genetic content, but it *is* a prerequisite for this to occur.

However, it is also beneficial for mitochondria to remain evenly spread across the cell, for a variety of reasons. These include an even spread of mitochondria allowing a quick response to metabolic and energetic demands across cellular space, a primed and swift response

to environmental fluctuations, colocalisation and communication with other organelles and avoidance of uneven local mutagen build-up (Bereiter-Hahn, 1990; Wada and Suetsugu, 2004; Chen and Chan, 2006; Seguí-Simarro and Staehelin, 2009; Logan, 2010a; Bauwe et al., 2010; Sage, Sage, and Kocacinar, 2012; Liesa and Shirihai, 2013; Spillane et al., 2013; Zorov et al., 2014; Shai, Schuldiner, et al., 2016; Yu, Lee, et al., 2016; Schuler et al., 2017; Yu and Pekkurnaz, 2018). This reasoning is substantiated by evidence of aberrant distributions of mitochondria within the cell leading to cellular stress, and from that detrimental transcriptomic, and whole-plant phenotypes (Feng et al., 2004; El Zawily et al., 2014). Even spread of mitochondria within the cell has been demonstrated in yeast, and demonstrates a system primed to have equal exposure to all areas of the cell (Yaffe, 1999; Sukhorukov, Dikov, et al., 2012; Rafelski, 2013; Viana et al., 2020). Mitochondria demonstrate swift responses to local energy demand by relocating to areas with high energy needs, such as within neurons of mammalian cells (Rintoul et al., 2003; Yi et al., 2004; Hollenbeck and Saxton, 2005; Chen and Chan, 2006; Yu, Lee, et al., 2016), and surrounding locations of high energy use such as in the dividing plant meristem (Seguí-Simarro and Staehelin, 2009). Mitochondria have also been shown to associate with energy-hungry organelles, providing ATP and vital reducing equivalents to various sub-cellular compartments (Bereiter-Hahn, 1990; Bereiter-Hahn and Vöth, 1994; Logan, 2006a; Paszkiewicz et al., 2017). A well-spaced mitochondrial population does not align with the exchange of genomic material, metabolites and functional inter-mitochondrial encounters, without the dynamic motion of these organelles.

The link between physical and genetic dynamics of mitochondria also extends to the intramitochondrial environment. In mammalian mitochondria, the nucleoid structure (a collection of proteins packaging mtDNA) holds one copy of the genome, specifying it as one unit of inheritance (Kukat, Wurm, et al., 2011; Kukat, Davies, et al., 2015). These complexes give rise to structural control of mtDNA inheritance. There are protein structures involved in anchoring the nucleoid to the inner mitochondrial membrane, limiting their spread

throughout the cell, and also in part dictating the even spread of these nucleoids throughout the reticulated mitochondrial network, key to even division into daughter cells during mitosis (Xin and Butow, 2005; Nicholls and Gustafsson, 2018).

Each mtDNA molecule has also been described as having a 'sphere of influence' within the mitochondrion, with the diffusion of mitochondrially encoded protein products being limited to the space immediately around these nucleoids (Dieteren et al., 2011; Busch et al., 2014; Jakubke et al., 2021). Jakubke et al. (2021) found that in yeast, removal of mutant mtDNA is not entirely dependant on selective fission and removal of defective or reduced capacity regions. Quality control can happen within mitochondrial reticulated networks, and the mitochondrion has a working spatial 'knowledge' of mutant mtDNA location due to physiological defects in the mitochondrial subdomain in which they reside. Upon mutation of cristae formations, these 'spheres of influence' become less well-defined and the cell has a harder time getting rid of mutant mtDNA. If defects exist, the mitochondrion can selectively degrade mutant mtDNA. Therefore, even inside the mitochondrial structure itself, there is control of genetic priorities through the formation of sub-mitochondrial regions in which each nucleoid can influence the surrounding area.

1.2 Quantifying the cell

The establishment of the central dogma of molecular biology in which information is passed from DNA to proteins through genes and transcripts has historically encouraged a reductionist approach to discovery (Watson and Crick, 1953; Crick, 1970). Over the past two decades, the field of cell and molecular biology has undergone a paradigm shift away from this reductionist approach (Westerhoff and Palsson, 2004). Advances in high-throughput methodologies have allowed the complexity of many biological process to be examined, and

a broader view of the system taken into account, such as the role of a single protein in many different pathways, the dynamics of feedback loops, as well as interactions and influence of the environment (Alm and Arkin, 2003; Van Regenmortel, 2004).

Biology is inherently complex, with all life composed of elements that are selective, functionally diverse and interact in non-linear ways to produce a response. Communication occurs across every level of life, from protein-protein interactions, organellar interactions, signalling between cells, across organs, right up to the intricate relationships between different organisms (Picard and Sandi, 2021)– all of which are dynamic in both time and space. There is spatio-temporal regulation within cells, and separation; for example, of metabolite pools between the compartments (organelles) that make up the cell (Bruggeman et al., 2002), or between sub-populations of organelles (Willingham et al., 2021), often based on energy demand within the cell ((Porat-Shliom, Harding, et al., 2019), in mice). This intricate regulation across levels of organisation must be taken into account if we are to gain a true picture of the live cell (Bruggeman et al., 2002). Therefore the term 'systems-biology' should taken as Kitano (2002) defines, an integration of experimental and computational research, and not be limited to only gene-regulatory networks or quantification of genomic data as is often the definition (Breitling, 2010).

Cell biology needs to be, and is becoming, quantitative (Howard, 2014). Why? The process of quantifying and theorising cellular features not only helps our intuition of complex biological situations, but also highlights knowledge gaps, and the influences of unconsidered factors (Milo and Phillips, 2015; Flamholz et al., 2014). By modelling complex processes, we can gain a deeper understanding of the components that go into the produced response, and we need quantification of these processes to get there. The quantification of biological processes is not a new idea– the 'father of genetics' Gregor Mendel devised the first mathematical theory of genetics by taking a quantitative approach (Mendel, 1951). There are examples of these approaches in all fields of cell biology, ranging from the forces within and

between cells (Kekenes-Huskey et al., 2016; Javanmardi et al., 2021; Bidhendi et al., 2019), direct quantification of gene expression profiles (Bakstad et al., 2012), to the precise turnover rates and lifespans of proteins within mitochondria ((Huang et al., 2020; Bomba-Warczak et al., 2021), again in mice). There are also estimates of the specific number of individual proteins with a single plant cell mitochondrion (Fuchs et al., 2020; Hildebrandt et al., 2021). By quantifying the world of the cell, we can measure uncertainty, variability, noise and feedback, lending statistical power to our hypotheses or inspiring further experiments. Quantitative approaches are important across all fields of biology, and studies on mitochondria are no exception. These approaches are necessary for studying cellular interactions and emergent behaviours of a large number of individuals. The cycle of hypothesising, quantifying, theorising, modelling, experimenting and inferring gives us a rigorous frame in which to account for the dependencies of the system we are studying, while being able all the while to account for uncertainty (Howard, 2014; Autran et al., 2021).

1.2.1 The expanding picture – from individual interactions to social organelles

In contrast to reductionist arguments and focus only on individual components of a system, a less reductive, more integrative approach to thinking about the busy intracellular environment is appearing. The communities of interacting organelles within the cell can be described as 'social' – with individual organelles cooperating to facilitate metabolic functions, isolate damaged individuals and forming membrane contact sites for interorganellar biomolecule transfer (Silva et al., 2020). The connections between organelles within cells are numerous, heterogenous and dynamic. Valm et al. (2017) took a systems approach to imaging the organisation of the diverse eukaryotic cell. They found many two- up to five-way connections between six different organelles, and that each organelle has a characteristic dis-

persal and distribution pattern within the cell– leading to the connectivity of these organelles to be referred to as the 'interactome' (Valm et al., 2017; Cohen et al., 2018). Organelles as dynamic, interacting, integrated communities share many features with networks of social agents, and mitochondria in particular have many features of sociality (Picard and Sandi, 2021). In communicating with each other, responding to external stresses, self-maintaining through fission and fusion cycles, synchronising their behaviour, forming groups and having functional specialisation, the mitochondrial population within a cell shows itself as social, and should be evaluated as such to quantify an overall state and identify perturbations (Picard and Sandi, 2021). If sociality emerges from the complex interactions between individuals in a population, we state throughout this thesis that this concept is even more applicable to plant mitochondria as collective impermanent interactions of separate entities than reticulated *physical* mitochondrial networks.

1.2.2 Quantifying connectivity

Complex systems are made from the interactions of many different components. One way we begin to explain the collective behaviour of the system is by quantifying the connectivity of the individual components (Barabási, 2016). Network science is used as a tool to analyse connectivity across a wide range of fields, from sociology, physics, ecology, electronics, computing and biology. It has been used to map non-physical networks such as the cell-type specific interactome– intracellular networks of protein interactions in different cell types (Huttlin et al., 2021). Network science has been used to quantify physical structures, such as the structural network and physical topology of fungal networks (Fricker, Heaton, Jones, and Boddy, 2017). It has also been used to quantify the structure and functionality of physical cellular connectivity in plants and development of multicellular structures (Jackson et al., 2017).

When it comes to mitochondria, the networks of reticulated structures can be mapped in a similar way to fungal networks, or the endoplasmic reticulum (Pain et al., 2019). Reticulated structures are the common mitochondrial form found in yeast and animal cells (Rafelski, 2013; Viana et al., 2020; Zamponi et al., 2018). Sukhorukov, Dikov, et al. (2012) and Sukhorukov and Meyer-Hermann (2015) used network science to effectively map the connectivity of reticulated mitochondria as nodes and edges. Junctions of connected elongate mitochondria become nodes, with four-way connections being rare, and the edges are elongate bodies of these organelles. The steady-state morphospace of these networks has also been mapped (Sukhorukov, Dikov, et al., 2012). A spatial component can also be introduced to factor in the length of edges, or the mitochondrial volume of the cell (Rafelski et al., 2012). However, the mitochondrial form in plants is mostly as individual organelles, and has not previously been quantified using network science and graph theory.

1.2.3 Large-scale biological data and ideas

The past 20 years has seen an explosion in the amount of data available to science (Manzoni et al., 2018). For example, since the first genome sequences of hCOV-19 were made available on the 10th Jan 2020, 5,122,766 genome sequences have been submitted to GISAID, an open-access database tracking pandemics ((Shu and McCauley, 2017), correct as of 13/11/21). Great genomic detail of model organisms is also available, such as *A. thaliana*; including geographical distributions of genetic diversity (Alonso-Blanco et al., 2016). But to take advantage of the diversity of the tree of life and the different mechanisms, inheritance patterns and lifestyle traits of a broader range of species, a view beyond well-established models is needed. The number of genomes available for non-model organisms is increasing and diversifying as sequencing technologies improve and become more affordable (Tagu et al., 2014; Fonseca et al., 2016).

But how do we gain knowledge from these sheer volumes of data? Nurse (2021) discusses the need for ideas and theories as well as data, and the necessity but insufficiency of data alone. Theoretical frameworks are needed to both build upon and verify to, as well as 'sanity checking' against known quantities or well-established theories (Milo and Phillips, 2015; Nurse, 2021).

1.3 Aims

In order to quantify connectivity across the disconnected chondriome, we proceed as follows; we develop a pipeline imaging and tracking mitochondria in a single plant cell. We build networks of close encounters and quantify connectivity across the mitochondrial population. To uncover the priorities of the cell, the ability to maintain the organellar genome and continue to address energetic needs, the unique dynamics and sociality of plant mitochondria are investigated. The pipeline and modelling framework developed here will enable us to address *why* the plant maintains such a dynamic chondriome.

Across the chapters of this thesis, we use single-cell imaging and network science to investigate a trade-off the cell navigates between a well-spread chondriome and the capacity to communicate and transfer signals and biomolecules across the population. To investigate how the priorities of the cell change when this trade-off is provoked, both mitochondrial physical spacing and genetic stability are challenged. From this, the mitochondrial connectivity network will form the basis of a theoretical framework to investigate the emergence of the mitochondrial 'metagenome'. Finally, the genetic stability of mitochondria was further investigated using bioinformatic tools to identify mitochondrial recombination ability across the tree of life, and its potential correlation with lifespan. Throughout, the importance of this bioenergetic organelle upon the function of the cell and the links between the physical

dynamics and genetic dynamics are highlighted, taking a new perspective to the field of plant bioenergetic organelles with a view to crop improvement and a fundamental understanding of *why these fascinating organelles move the way they do*.

Chapter Two

Mitochondrial dynamics as social encounter networks

2.1 Introduction

Mitochondrial dynamics have been previously well-characterised in plants, with the physics of this motion revealed by staining, fluorescent plant lines, and modern imaging techniques, but do not often consider the entire population of cellular mitochondria. These works demonstrated heterogeneity in size, shape, speed and distribution across the mitochondrial populations (Logan and Leaver, 2000; Logan, 2003; Logan, 2006b; Arimura, Yamamoto, et al., 2004; Scott and Logan, 2008; Arimura, 2018). These organelles vary genetically (Lonsdale et al., 1988; Kmiec et al., 2006; Arimura, Yamamoto, et al., 2004; Preuten et al., 2010) and functionally (Nakamura et al., 2021; Collins et al., 2002) across eukaryotes. The mitochondrial proteome also varies across cell types within the plant (Lee, Eubel, et al., 2012). Overall, plant mitochondria are pleomorphic, highly dynamic and form a 'discontinuous whole' of individuals.

The use of cytoskeletal strands by mitochondria has also been demonstrated, with

long distance travel and positioning occurring via actin filaments and –to a lesser degree– anchoring through the use of microtubules (Van Gestel et al., 2002; Boldogh and Pon, 2006; Doniwa et al., 2007; Romagnoli et al., 2007; Avisar et al., 2009; Wang and Hussey, 2015; Breuer et al., 2017). The speed of mitochondria varies across cell types (Table 2.1). When mitochondria are not being transported on actin filaments, they move diffusively, with a wide range of speeds. High speeds can cause cytoplasmic streaming, a motive force causing cytoplasm to flow around larger cellular compartments such as the vacuole/nucleus– another method by which organelles such as mitochondria are transported around the cell (Shimmen and Yokota, 2004; Ekanayake et al., 2015; Peremyslov et al., 2015; Tominaga and Ito, 2015).

Speed	Cell type	Reference
0.6–3.4 μms^{-1} (up to 10 μms^{-1})	*Arabidopsis thaliana* Root hair	(Zheng, Beck, et al., 2009)
0.1–0.5 μms^{-1}	*Nicotiana tabacum* BY-2 cells	(Watanabe et al., 2007)
1.42 $\pm$ 0.85 μms^{-1} (as low speed) 7.1 $\pm$ 1.5 μms^{-1} (as high speed)	*Picea wilsonii* Pollen tubes	(Zheng, Wang, et al., 2010)
0.3–5.4 μms^{-1} (Mean 1.44 $\mu ms^{-1} \pm S.D.0.89$)	*Arabidopsis thaliana* Leaf epidermal cells	(Doniwa et al., 2007)

Table 2.1: Speed of mitochondria varies across cell types within plants.

As these organelles move around the cell, they can localise to each other, for between lengthy amounts of time down to only transient associations. This motion and intermitochondrial connectivity within the cell leads to complex emergent behaviours (Williams and George, 2019; Giannakis et al., 2021). Mitochondria can therefore be conceptualised as 'social organelles'– with interactions between individuals as links in a dynamic 'social' network, and consequent emergent behaviours as the 'social dynamics' of the system. Viewing or-

ganelles as social has gained traction recently– allowing a more integrated understanding of the communication and contact (direct or indirect) between individuals and how it impacts the normal function of the cell (Cohen et al., 2018; Picard and Sandi, 2021), and has been applied particularly to the reticulated structure of fused mitochondria (Sukhorukov, Dikov, et al., 2012; Sukhorukov and Meyer-Hermann, 2015).

However, we argue that the social organelle concept is even more applicable to the plant system. Plant mitochondria exist as individual organelles with 'quasi-fixed' identities of their own, and the impermanent interactions between them are less inherently structured or dictated by the physical structure of a connected network (Picard and Sandi, 2021), making the perspective of social mitochondrial even more applicable to this system. Social networks built from the transient interactions of these mitochondria can therefore genuinely correspond to the connectivity between individuals, leading us to understand the chondriome as a whole, as well as any emergent behaviours. Tracking the interactions of individuals throughout time can lead us to insights otherwise inaccessible. Mitochondrial motion within the cell is not a wholly random process, but is under the control of the cell, and tightly regulated (Logan, Scott, et al., 2003; Okamoto and Shaw, 2005; Frederick and Shaw, 2007; Pan and Hu, 2015). This suggests that there may be benefits to the cell through emergent collective behaviours of dynamic mitochondrial motion.

The term mitochondrial dynamics is used within this thesis to describe the general movement of mitochondria within the cell, including their speed, direction, area travelled and how they are navigating the cell, captured using localised fluorescent proteins (see Section 2.3.1). Mitochondrial dynamics can also be used to describe the cycles of fusion and fission that these organelles undergo (in that context it is mostly used by those studying reticulated mitochondrial structures). Fission and fusion cycles are not directly captured within these following experiments, but are inherently reliant on the movement of mitochondria, and the variability in closeness to each other that this motion provides. This spatial proximity is a

prerequisite and a necessity for the fusion of individual mitochondria (Arimura, Yamamoto, et al., 2004), and photoconvertible probes have been used to demonstrate that mitochondrial mixing can occur within 3s, preceded by a period of close mitochondrial colocalisation (~20s) (Arimura, Yamamoto, et al., 2004). Many processes are monitored through intermitochondrial communication, discussed in Chapter 1. Altogether, these processes demonstrate the impact of mitochondrial influence on the cell, even without direct fusion between adjacent individuals.

Interactions between mitochondria are beneficial to overall cellular health, but so too is a controlled distribution of these organelles within the cell. There are many reasons for this, discussed in Section 1.1.4. Taking these observations into account, we hypothesised that the cell has dual and conflicting priorities– to keep mitochondria evenly spread throughout the cell, yet facilitate 'social connections' between them. These are physical encounters between individuals that allow the build-up over time of networks describing the connectivity across the whole organelle population. An ideal resolution to this tension would be a cellular system that could utilise mitochondrial motion to avoid local oxidative damage and respond swiftly to environmental fluctuations. An ideal system would be responsive to local energy demands, while also maintaining a healthy population of bioenergetic organelles. This maintenance would occur through the exchange of biomolecules, metabolic interaction, and genetic complementation– and also allow maintenance of quality control mechanisms. By utilising a population of motile bioenergetic organelles, we argue that the cell is suited to addressing a variety of problems and priorities in order to remain functional and healthy (Chustecki, Gibbs, et al., 2021).

One method of delving into cellular priorities is through the use of mutants – in this case one that interferes with the mitochondrial dynamics within the plant cell. FRIENDLY is a fusion protein, and when it is perturbed mitochondria demonstrate reduced levels of mitochondrial fusion, spend a longer time associated with one another, have an increase in

intermitochondrial matrix mixing, form mitochondrial clusters within the cell, demonstrate a wide range of metabolic behaviours and also have a perturbed growth phenotype ((El Zawily et al., 2014), Figure 3.5.D). It is a member of the clustered mitochondrial superfamily of genes (CLU), found across eukaryotes (Ayabe et al., 2021). FRIENDLY has recently been implicated in the process of mitophagy, localising to depolarised mitochondria (Ma et al., 2021; Nakamura et al., 2021). Mitophagy is an organelle-specific form of autophagy where damaged mitochondria are removed from the population. This removal will also degrade any mtDNA within that organelle, implying that *friendly* may present genetic implications for the population as well as physical perturbations.

Here, we embrace the changing perspective on dynamic organellar interactions in order to conceptually and experimentally capture these organelles as entire populations (Valm et al., 2017; Cohen et al., 2018; Picard and Sandi, 2021), and seek out the guiding principles and mechanisms behind social and physical dynamics of plant mitochondria. We use a mixture of experimental single-cell time lapse imaging, distributional mutants, and social encounter networks to investigate this hypothesised trade off.

2.2 Methods

2.2.1 Plant growth

In order to visualise mitochondria *in planta*, we used mitochondrial-targeted mtGFP (green flourescent protein) *Arabidopsis thaliana* seeds kindly provided by Professor David Logan (Logan and Leaver, 2000; El Zawily et al., 2014). These seeds were surface sterilized with 50% (v/v) household bleach solution for 4 minutes with continual inversion, rinsed three times with sterile water, and plated onto $\frac{1}{2}$ MS Agar. Plated seeds were then stratified in the dark for 2 days at 4°C. Seedlings were grown in 16hr light/8hr dark at 21°C for 4-5 days. Seed stocks were maintained through self-pollination of existing lines. A kanamycin resistance gene within the mtGFP construct can be used for detection of fluorescence presence, and $50\mu g/ml^{-1}$ kanamycin $\frac{1}{2}$ MS plates were sometimes used to select for seedlings with strong mtGFP for growth or imaging.

2.2.2 Imaging

Prior to mounting, individual seedlings were taken carefully from agar plates and stained with 10µM Propidium Iodide (PI) solution for 3 minutes ((stored as 1mg/mL in water) Sigma-Aldrich #P4864; CAS: 25535-16-4). Following a protocol modified from Whelan and Murcha (2015), seedlings were mounted in water and a cover slip placed on top. Various mounting techniques were experimented with, including mounting on agar or with a barrier of surgical tape below the cover slip to provide a buffer against mechanical force. However, movement of the field of view with these methods prevented clear images from being taken, and agar mount prevents a good focus upon a single cell in this case. Imaging within living biological systems

is a constant balance between spatial and temporal resolution and maintaining physiological conditions for the sample. To avoid hypoxic stress upon the seedling, we imaged dynamics at low laser powers, and only imaging within as much as 10 minutes after sample mounting, following personal communication with Prof. Markus Schwarzländer.

A Zeiss 710 laser scanning inverted confocal microscope was used to image seedlings, capturing time lapse images. To capture mitochondria we used excitation wavelength 488nm, with detection range 494-578nm for GFP (peak emission 535.5nm). For the PI stain, we used excitation wavelength 543nm, detection range 578-718nm for PI (peak emission 648nm) as well as chlorophyll autofluorescence (peak emission 679.5nm). We also used a Zeiss 900 with Airyscan 2 detector to independently validate identically prepared samples. These gave no difference in summary statistics beyond natural variability. See section 2.4 for further discussion of imaging techniques and choices.

2.2.3 Video analysis and tracking

From the field of view, single cells were cropped from each time lapse, using the PI stain as a marker for the outside of each cell. Videos were all adjusted to 5 pixels/µm resolution, and any with a different frame interval were excluded. Single mitochondria were tracked using Trackmate (Tinevez et al., 2017) on ImageJ (Fiji) 2.0.0. Typical settings are described here. Detection of individuals was done using the LoG detector, set with a blob diameter of 1µm, and a threshold of 2-7. Quality filters were used on spots if deemed necessary. Tracking was done using the simple LAP tracker, with a linking max distance of 4µm, a gap closing distance of 5µm, and gap closing maximum of 2 frames. The accuracy of detection and tracking was assessed visually, and manual editing was done of spots and tracks where necessary. We independently verified the robustness of this tracking technique using alternative tracking software (Mosaic Particle tracker (Sbalzarini and Koumoutsakos, 2005)).

2.2.4 Independent video analysis

We tested our technique upon previously published time lapses of mitochondrial motion. We used the same analysis techniques and network construction tools as described in this methods section. Independent video 1 shows mitochondria with Kaede fluorescence in the cotyledon of *A. thaliana* (Arimura, Yamamoto, et al., 2004), via the POD3 database (Mano, Miwa, et al., 2008; Mano, Miwa, et al., 2009; Mano, Miwa, et al., 2011; Mano, Nakamura, et al., 2014). Independent video 2 shows TMRM stained mitochondria from the hypocotyl of wild-type mtGFP *A. thaliana* (El Zawily et al., 2014). These videos were adjusted to the same resolution of 5 pixel/µm, making them comparable to the time lapse videos taken for this study. Comparisons between the two videos were done at frame times equivalent to 4, 12, and 24 seconds.

2.2.5 Network construction

Physical colocalisations of mitochondria were represented as an undirected network, with each node being an individual mitochondrion and edges being the colocalisation, or encounter, events. We defined an encounter as mitochondria at a distance $\leq$ 1.6µm away from one another (a characteristic length of one mitochondrion). Colocalisation events are not necessarily fusion events. We then used custom code in Mathematica 11.3.0.0 to analyse the networks and compute summary statistics, that has now been reconfigured into R to avoid proprietary software.

2.2.6 Agent based physical simulation

The model was constructed by Prof. Iain G Johnston, University of Bergen (Chustecki, Gibbs, et al., 2021). The mechanistic simulation is made of simulation space X x Y, modelled after sampled hypocotyl cell lengths as 30 x 100 µm in size. n_{mito} mitochondrial agents are randomly positioned within the cell, as well as N_{cyt} straight cytoskeletal strands randomly placed. Attachment and detachment of mitochondrial agents to these strands can happen according to Poisson processes at rate k_{on} and k_{off} respectively, and when agents are within distance d_{cyt} of the strand. When not attached to a strand, mitochondria move diffusively with diffusion coefficient D, although the simulation can also be used to model Lévy flight type movement (not used within this study). It is possible for agents to switch strands at cytoskeletal intersections. Diffusion coefficient scaling by parameter K_{mito} (k_{mito} = 1: no effect) occurs when mitochondria come within d_{mito} distance of each other- this is to model mitochondrial slowing upon colocalisation. Nearby agents can also influence each other with hydrodynamic force F_{hydro}, which is scaled by the reciprocal distance to another mitochondrion ($1/d_{mito}$), modelling cytoplasmic streaming within the cell as an additive contribution from proximal agents, and not intended to solve real fluid equations of motion. Movement out of the field of view during imaging was modelled by creating a boundary region (diameter 4µm) around the edge of simulation space. Agents disappear from within this boundary region at rate k_{out}, and when an agents disappears, a new agent is created within the boundary region- in order to keep n_{mito} constant. In the "closed" case, where k_{out} = 0 physical steps that would remove agents from the cell are truncated. Simulations were ran for 10^3 iterations before data capture began, in order to initialise the system behaviour and determined with preliminary investigation to be sufficient to remove influence of initial conditions. Figure 2.7 summarises the model.

2.2.7 Theoretical models

Theoretical models were used to simulate a wide range of behaviours, and were used in the network analysis. All parameterisations for these models can be seen in Table B.1. Each related group was given a shorthand reference name, shown in parentheses. Here the most prominent parameters for model behaviour are discussed, and models were chosen to highlight the different influence of parameters on the system.

Models **ST** (stripped down) and **NM** (null models) had n_{mito}=100. **NM** simulations were the simplest, with changes only within edge loss k_{out}, diffusion rate D and hydrodynamic force F_{hydro}, except NM11 where cytoskeletal strand use was introduced. **ST** simulations were simple models without cytoskeletal strands, and **ST** 3-8,10,13,14 had a low diffusion rate D= 0.086µm^2/s, and the remaining **ST** models had D ranging uniformly from 0-0.85µm^2/s. **R** (random) simulations were models generated from between the values set as uniform priors with completely random parameterisations (generated using the runif function in R (stats package 4.0.1)). **R** models had varied parameterisation with for example: n_{mito} between 9-191, D between 0.152-0.705µm^2/s, n_{cyt} between 0-13, all based in part on experimental observations. **BM** (biological model) simulations all used cytoskeletal strands, with n_{mito}=198 mitochondrial agents, to better reflect mitochondrial number in the cell. They were based on a single simulation with random parameters (generated as **R** models above) and diffusion rate was altered. Across **BM** models, diffusion rate differed (BM1-4,7,9 had values between D=0-0.85µm^2/s) as did hydrodynamic force (BM5-8,10 had D=0.52µm^2/s and ranging F_{hydro}=0-0.8). **S** (simulation) models were deliberately chosen as their behaviours reflect informative limits of possible dynamics. S1 had polar clustering of agents at each end of simulation space, due to high k_{cyt} and 'strand-like' formations within the network structure- and many agents round the cell perimeter appearing and disappearing. S4 made heavy use of cytoskeletal strands, and had a high k_{on} and low k_{off}, forming

waves of continuous motion for agents as a strong streaming effect arose. Agents in model S5 barely moved, having a low diffusion rate and not using cytoskeletal strands. S6 formed a well-connected network despite only an intermediate diffusion rate and no strand use. S7 formed a very dense network, due to a high diffusion rate, although no strand use- but leading to a system where agents moved about very quickly, increasing encounters.

2.2.8 Further model behaviour under different parameterisations

In order to explore the model further, and the direct effect of specific parameter alterations, we generated further models with only one or two parameters different from an arbitrary default. Parameter alterations and statistics can be seen highlighted in Table B.2, and model outcomes and networks can be seen in Figure 2.9. Results from this parameter sweep are discussed in Section 2.3.4. In each case, these models are generated to describe a range of potential behaviours of the system, not to give exact values nor solve a specific inference problem.

2.2.9 Defining and quantifying of summary statistics

Both physical and network statistics were used to analyse mitochondrial motion across simulations and experimental sample cells.

Physical statistics included speed (μms^{-1}) calculated as distance each trajectory moved per frame, averaged over all mitochondria in all frames. Angle of motion (degrees) was calculated as $180 - \left(\frac{180}{\pi}\cos^{-1}\frac{a \cdot b}{|a|\,|b|}\right)$ with $\boldsymbol{a}$ and $\boldsymbol{b}$ being vectors between three coordinates over three frames. Distributions of angles are all mitochondria over all frames. Area was calculated as the area (μm^2) within a polygon (convex hull) traced around all the furthermost points in a trajectory of frame length ≥ 3, representing all mitochondria

within all frames, unless otherwise stated. Convex hull rate is the convex hull divided by the length (in seconds) each trajectory has spent travelling the cell. Diffusion rate was calculated from the slope of Mean Squared Displacement (MSD) over time, taken from $n = 9$ mitochondria seen to be moving not linearly (i.e. not on cytoskeletal strands), across a small area in cellular space and not colocalising with any other mitochondria. Calculation of colocalisation time was the length of time in seconds for which two mitochondria were consecutively paired within adjacency matrices- taken over all mitochondria and all frames unless otherwise stated.

The networks of encounters described were built from adjacency matrices of mitochondria that had colocalised, and were historical, building upon previous encounters to collect edges and nodes as time went on. There were also singletons, mitochondria that never localised with another, and these were included in the connectivity statistics. The statistics described below were taken for the networks at the final frame of each video, unless stated otherwise. Connected component number quantifies the number of internally connected graphs, not externally connected with other graphs, and describes the state of global connectivity. Degree gives the number of immediate neighbours each node has, and is more a measure of local connectivity. Network efficiency is the reciprocal sum of the shortest distance between all nodes in the network, and is calculated as $E(G) = \frac{1}{n(n-1)} \sum_{i \neq j \in G} \frac{1}{d(i,j)}$ with G the network of interest, n the number of nodes in the networks, and $d(i,j)$ the distance between nodes i and j. This statistic can help describe the ease of information transfer across a graph. The average number of connected neighbours is the number of other nodes each single node in a connected component can reach, averaged over all nodes in all connected components (including singletons). This statistics described the "social circle" of mitochondria. Percolation threshold is the frame time at which the size of the largest connected component becomes 50% bigger than at the previous frame- describing when and if long range connectivity happens across the system. Degree drop is the difference in the degree

value from the highest degree node to a node 5 steps (random walks) away- this value is taken for 200 random walks from that highest degree node, normalised by n (node number), and averaged. The number of individual cells or models used in each experiment can be seen in the relevant figure legends.

2.2.10 Time-dependant behaviour of summary statistics

Summary statistics are gathered from networks that have an inherent time dependency, as they are built from encounters between agents over time. The changes, or lack of, in summary statistics are discussed in Section 2.3.5. These changes in statistics over time are worth noting as they reveal the nature of the system as we captured it.

2.3 Results

2.3.1 Physical mitochondrial dynamics in single *Arabidopsis* hypocotyl cells are revealed through experimental characterisation

Characterisation of mitochondrial dynamics within living cells can be achieved by confocal imaging of mtGFP *A. thaliana*. The hypocotyl cells of 4-5 day old seedlings were imaged over time to capture mitochondrial dynamics and cropped to a single cell. Often multiple cells were found in the same field of view, in which case they are cropped and analysed separately, and are classed within statistical analyses as independent samples. Hypocotyl cells were chosen as they provide a quasi-planar field of view, due to the vacuole compressing cytoplasmic contents towards the cell surfaces of their roughly cuboidal structure. This view provides a clear two dimensional capture of a subset of cytoplasmic space. Implementation of confocal microscopy allows control of the amount of signal captured from the sample, and allows a tight field of view across the cell. Therefore mitochondria captured in these samples are within close proximity depth-wise. Within wild-type mtGFP cells, the mean number of mitochondria seen over the video time ranges from 22 - 207 across samples collected. The hypocotyl is also green photosynthetic tissue, allowing for occasional capture of chloroplasts alongside mitochondrial motion over time. This single cell type was used continuously across this study; other cell types within the same organism can have varying mitochondrial dynamics (see Chapter 1). Snapshots of mtGFP hypocotyl cells used in the analysis can be seen in Figure 2.1.

Quantification of mitochondrial dynamics was achieved by tracking these organelles over time, using TrackMate plugin for Fiji (ImageJ) (Tinevez et al., 2017). By tracking spots of intensity within the video, paths of motion and positions of individual mitochondria over time were collected (see Section 2.2). From these coordinates over time, a number of

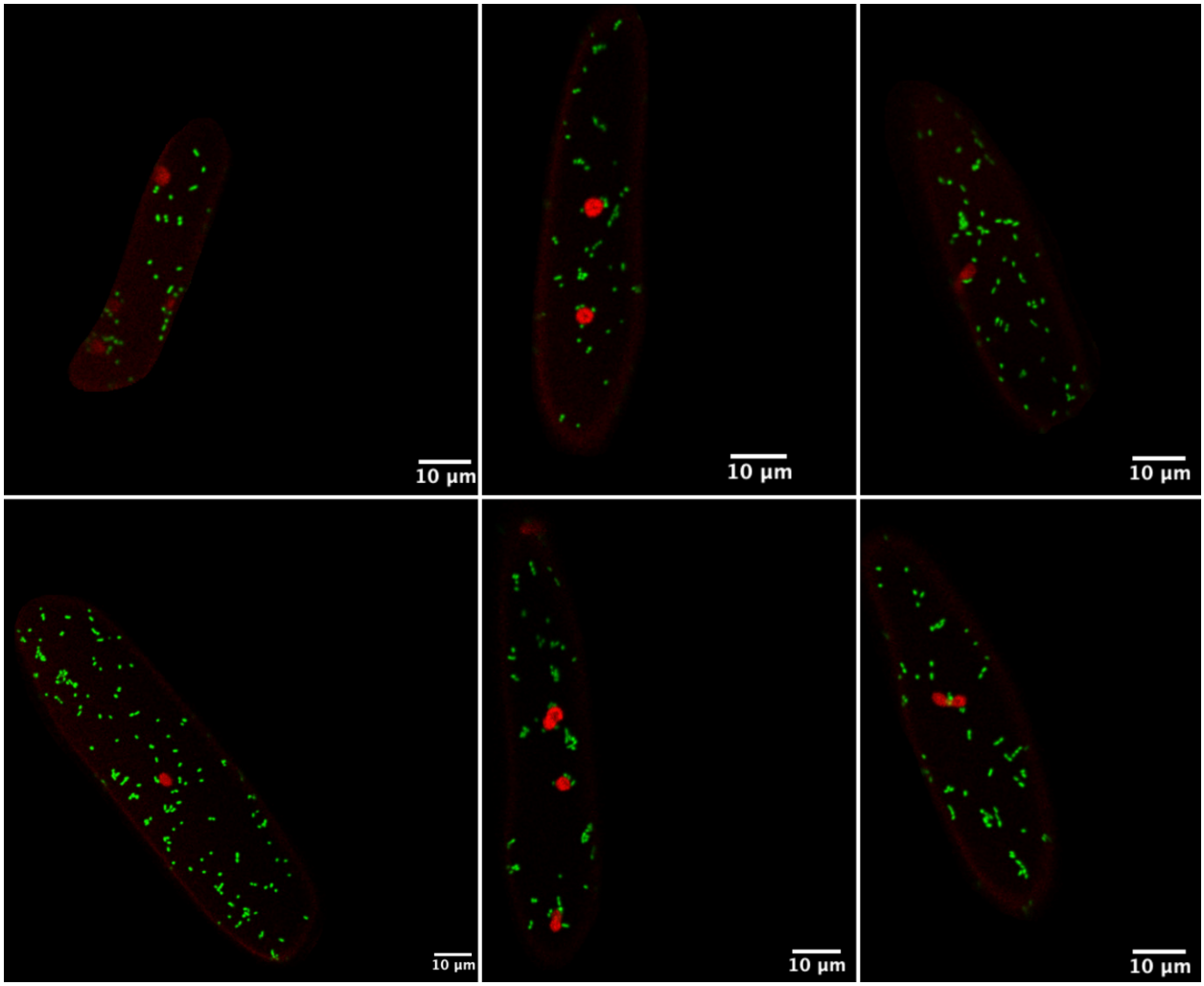

Figure 2.1: Fluorescent mitochondrial *Arabidopsis* lines can be used to characterise mitochondrial motion. Gallery of single cell confocal micrographs of mtGFP, green = mtGFP tagged mitochondria, red outline = propidium iodide stained cell walls, dense red spots = chloroplasts. Scale bar = 10µm.

physical statistics can be taken. These include instantaneous speed, angle of motion, inter-mitochondrial distance, area travelled, association time between individuals and diffusion constant. Physical statistics for a sample mtGFP hypocotyl cell can be seen in Figure 2.2

A range of speeds from 0.0-2.5µm/s were captured in the mtGFP lines, with a repre-

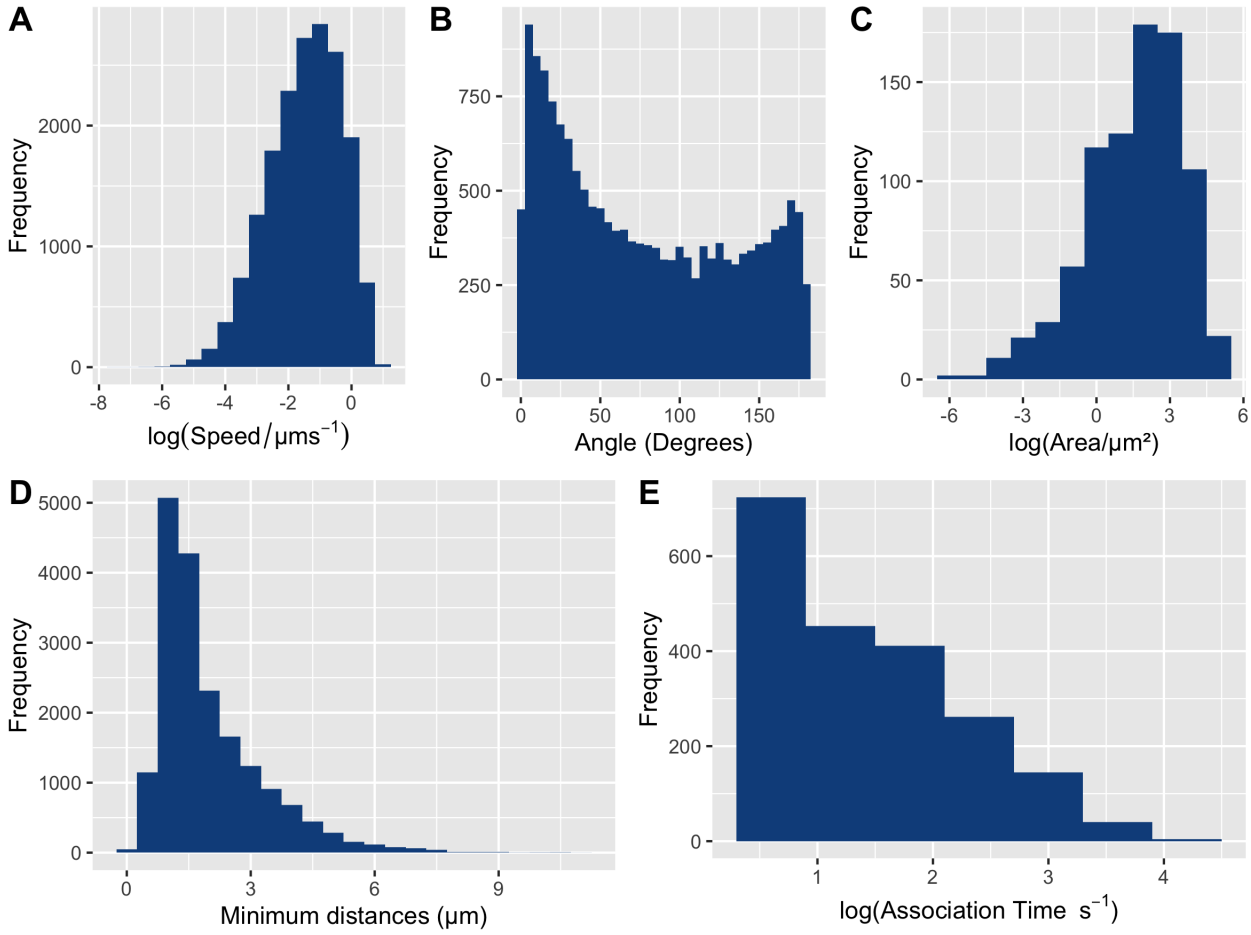

Figure 2.2: Physical statistics of mitochondrial motion demonstrate heterogeneity. Frequency plots of physical statistics for a representative single mtGPF hypocotyl cell (GFP3). (A) Instantaneous speed of all mitochondria across all frames. (B) Angle of motion, 0 = straight ahead, 180 = reverse motion, for all mitochondria from all frames. (C) Total area travelled by each trajectory, for all mitochondria. (D) Minimum Euclidean distances between all mitochondria across all frames. (E) Association times between any pair of colocalising mitochondria (seconds) based on an encounter distance of 1.6μm, across all frame time and all mitochondria. Part A-D reproduced from Chustecki, Gibbs, et al. (2021).

sentative distribution shown in Figure 2.2.A. Heterogeneity in speed has been well demonstrated previously (see Section 2.1). High speeds are reached when mitochondria are actively transported along actin filaments within the cell (2.5 - 10µms^{-1}) (Breuer et al., 2017; Van Gestel et al., 2002; Doniwa et al., 2007; Avisar et al., 2009; Wang and Hussey, 2015; Oikawa et al., 2021), and diffusive motion when not using the cytoskeleton has a wide range of observed speeds (0 - 2.8µms^{-1}, (Oikawa et al., 2021)). Instantaneous speeds were measured and average speed at each time frame did not show a systematic difference over time (Figure 2.3). This result demonstrates that the imaging method did not cause a consistent speeding up or slowing down of mitochondria, across all videos, as well as demonstrating mean speed does not depend on history (time-independent).

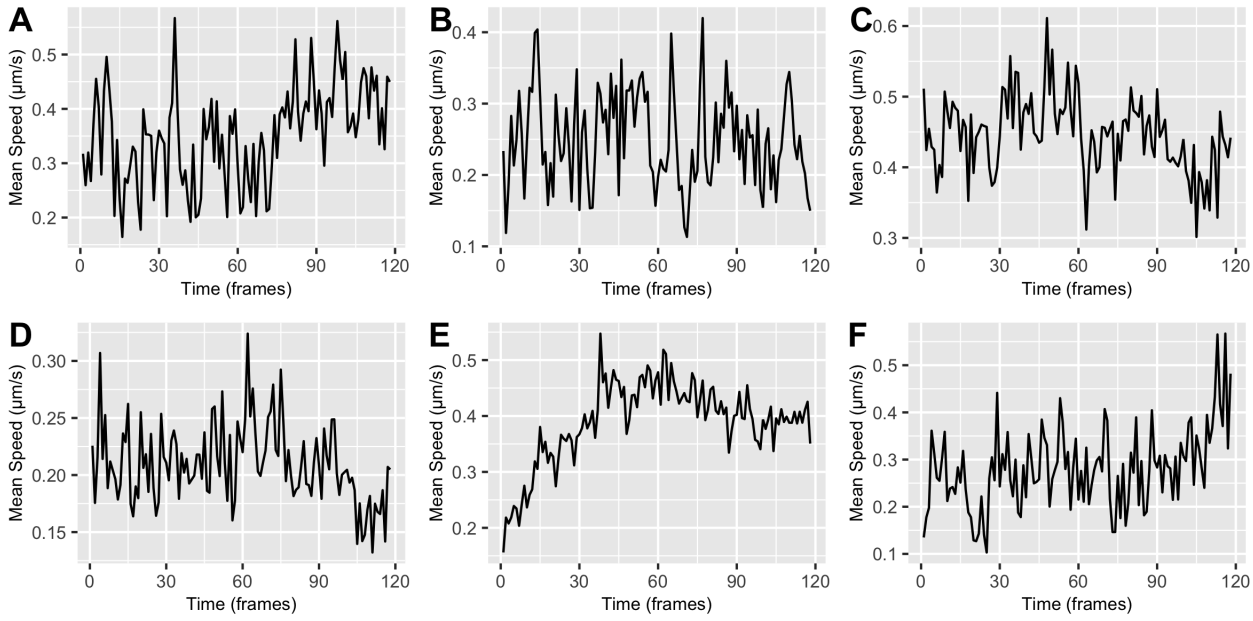

Figure 2.3: Mean speed of mitochondria over time demonstrates no systematic difference over time for all videos. Mean speed for each frame, over frame time, from a selection of 6 mtGFP videos.

The use of cytoskeletal strands can be inferred from the angle of motion of mitochondria. The U-shaped distribution of Figure 2.2.B demonstrates mitochondria either moving

at a constant angle (near to, or 0 degrees, i.e. straight line motion) representative of motion along a cytoskeletal strand, or at a complete reversal (180 degrees, see Section 2.2 for calculation). All mtGFP samples reported this characteristic distribution. The centre of the distribution demonstrates diffusive motion, with a large proportion of mitochondria moving at a wide range of angles.

Minimum inter-mitochondrial distance is the minimum Euclidean distance between each mitochondrion and its nearest neighbour. There are few large distances between individuals (Figure 2.2.D). A large proportion of mitochondria at smaller distances approximately 1µm from each other demonstrate close associations between mitochondria, through encounters, transient clustering or close association on cytoskeletal strands. The remaining mitochondrial population are varied in their distances from each other, a result of a dynamic and heterogeneous system.

This dynamic motion is also captured in the area traversed by each mitochondrion (Figure 2.2.C). Area is calculated using the convex hull of each trajectory (see Section 2.2). Area travelled predictably increases with sampling time (Chustecki, Gibbs, et al., 2021). Most mitochondria move within an area of between 0-10µm^2, dependant on the length of their trajectory (median area traversed is 6.48µm^2, range is 0.002µm^2 - 233.7µm^2). Trajectory lengths for the sample in Figure 2.2 ranged from two frames to full video length (~4secs - 231 secs, mean ~40secs). We also take time into account, by calculating the rate of increase in convex hull size with time– the convex hull rate. The average convex hull rate for this sample was 0.3µm^2/s ± 0.28 (SD), with the maximum rate at 1.8µm^2/s. Overall, the average area traversed (convex hull) is 16.7µm^2 ± 26.8 (SD), with each trajectory present for an average of 40 seconds, traversing on average 0.3µm^2 per second. There also exists a proportion of the population travelling much larger areas throughout video capture time. Maximum area traversed in the sample is 233.7µm^2 (from a trajectory travelling for 188 seconds), and there are 19 trajectories that travel >100µm^2 within the video capture. These mitochondria

may benefit from active transport on cytoskeletal strands, to reach distant areas of the cell– although status of whether individual trajectories were on/off the cytoskeleton was not collected experimentally. These individuals also demonstrate the ability of the capture method to track either fast moving individuals, or over long frame times.

This flexibility is also apparent in the speed distribution discussed above (Figure 2.2.A), and physical spread afforded by variation in distances between mitochondria (Figure 2.2.D) provides the system with a wide range of options for response. Speed may be limited for organelles that are responsible for localising to a particular region or organelle (e.g. the endoplasmic reticulum), and increased for individuals heading towards, or utilising the scaffold highways of the cytoskeleton. We therefore can begin to build a picture of the population of mitochondria as a whole, taking into account the variation amongst individuals that make up the chondriome.

2.3.2 Characterisation and quantification of the mitochondrial "social networks" of single *Arabidopsis* hypocotyl cells reveal parallels to physical heterogeneity

Characterisation of collective behaviours of individuals can be achieved using social networks (see Section 2.1). Within the majority of plant cell types, mitochondria move as individual organelles, interacting with each other while travelling throughout cellular space. To uncover the driving principles behind this motion, the connectivity across the population of individuals is quantified.

When we begin to look at the entire population of mitochondria within a sample, we see not only variation within their motion but also variation in their interactions. Proximity to other mitochondria offers opportunity for exchange of information (See Section 1.1.4).

Association time is a quantification of how long pairs of mitochondria spend in close proximity to each other. For the sample given in (Figure 2.2.E), we see a large proportion of encounters lasting only a short amount of time (1 - 2 frames). These are transient encounters, either through mitochondria passing each other at a very close distance, or only colocalising for a very short amount of time. Interestingly, there is also a proportion with extended association times. The maximum association time for this sample was 78 seconds. Quantitative analysis of this sample association time shows us that 2% of mitochondria that interact with another do so for >20 seconds, a period of direct adjacency demonstrated pre-fusion by Arimura, Yamamoto, et al. (2004). Subsequent exchange of mitochondrial content can occur within 3s (Arimura, Yamamoto, et al., 2004). However, direct fusion is not necessary for a wide range of intermitochondrial signalling to still occur (see Chapter 1), and it is not length of proximity, but previous fusion events and local sites that determine fusion probability (Twig, Liu, et al., 2010).

To build a social network of encounters between individual mitochondria, an encounter distance of 1.6µm was imposed, and adjacency matrices were built from pairs of mitochondria coming within this threshold of each other. From this, a network builds up over sampling time, as demonstrated for three samples in Figure 2.4 and another in Figure 2.5.A.i-iii. 'Singletons' are also collected alongside the adjacency matrix; these are mitochondria that have not yet encountered other individuals in the system.

Once a network has been built from encounters between individuals, methods and statistics from network science/ graph theory can be applied for the quantification of connectivity across the mitochondrial population. One such statistic is degree, simply a measure of the number of immediate neighbours an individual node has. There is a heterogeneity associated with the degree values of these networks, shown by the heavy-tailed distributions for each time frame shown in Figure 2.5.A.iv. We note that these are not exact power-law degree distributions, although describing them as scale-free-like may help describe the pat-

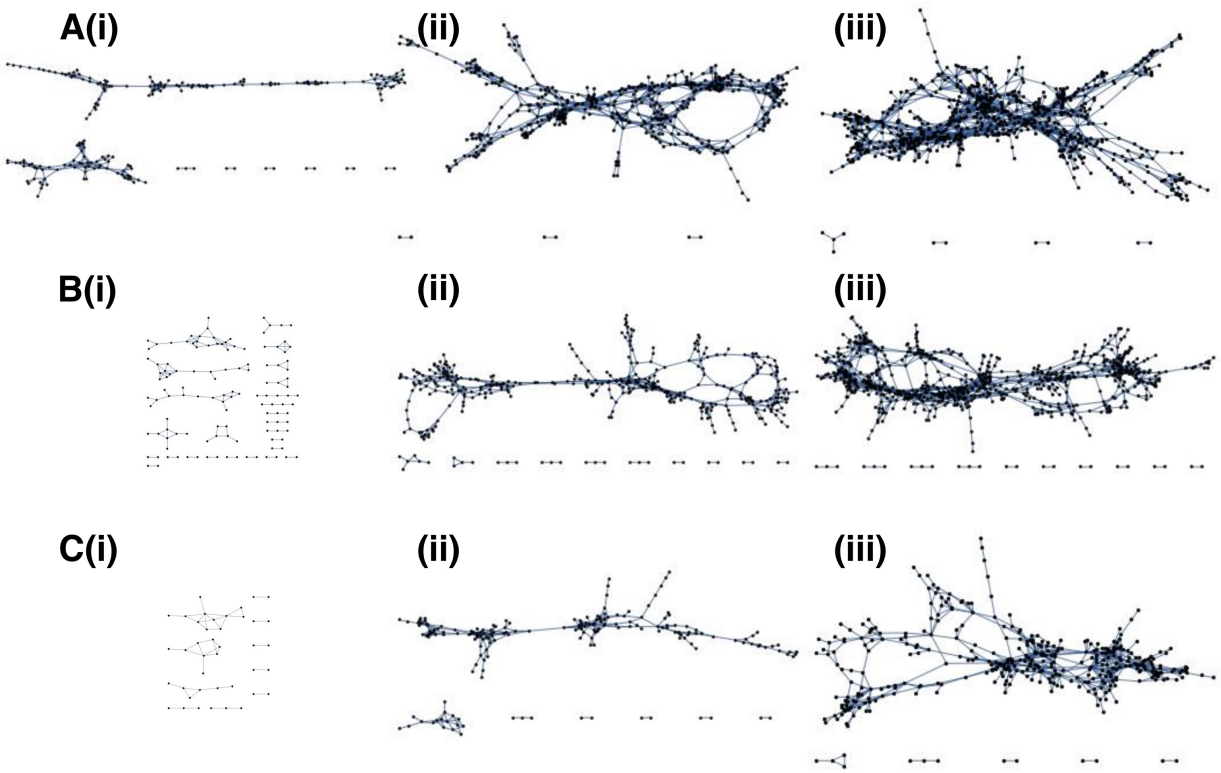

Figure 2.4: Mitochondrial encounters as 'social' networks show characteristic build-up over time. (A-C) Build-up of an encounter network over time (edges = encounters, nodes = mitochondria) for three mtGFP Samples (GFP5,8,4), at (i) 19, (ii) 93 and (iii) 193 seconds. Singletons (disconnected nodes) are not included in these plots.

terns of connectivity at least at early time frames. The highest degree nodes are found at final frame times (shown in grey in Figure 2.5.A.iv). The mean degree increases throughout frame time, levelling off towards the final frames as the network builds (Figure 2.5.A.v), giving a generalised read out of how well-connected the system is. The coefficient of variation for degree is also calculated (Figure 2.5.A.v (inset)). This statistic is time-dependent for this system, as a dampening effect is seen in the variation of degree over time, particularly apparent at early time frames as singletons encounter other mitochondria. The pattern of the degree distribution shows the system of encounters as it is collected over 120 frames.

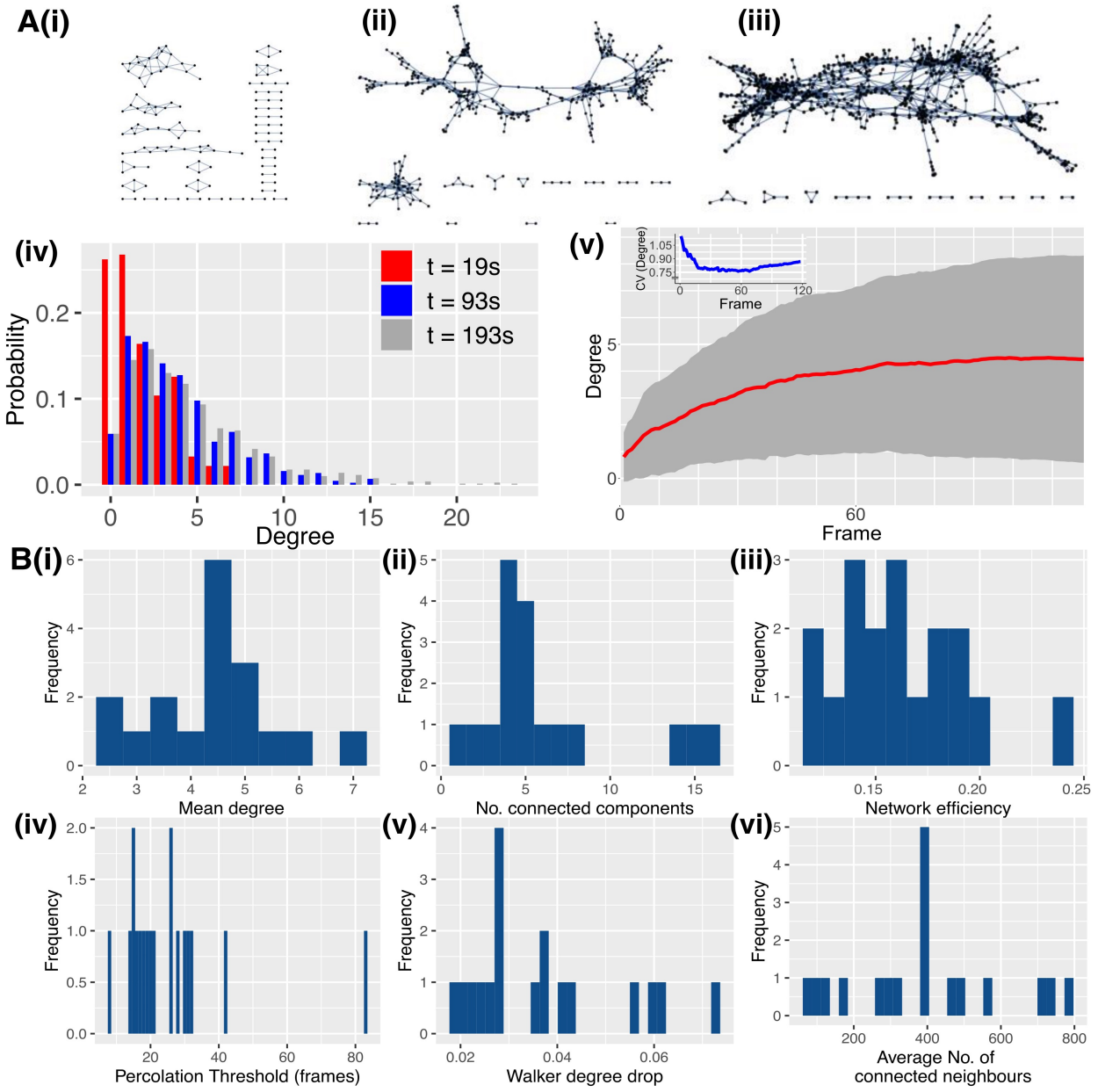

Figure 2.5: 'Social' networks of mitochondrial encounters show connectivity and heterogeneity. (A(i-iii)) Build-up of encounter networks (edges=encounters, nodes=mitochondria) over (i) 19, (ii) 93 and (iii) 193 seconds. Singletons (disconnected nodes) not plotted. (iv) Degree distributions at corresponding time point. (v) Degree mean (red) and standard deviation (grey), with coefficient of variance (blue, inset) over time. Plots labelled (A) (reproduced from Chustecki, Gibbs, et al. (2021)) correspond to one mtGFP cell sample, GFP3. B(i-vi) network summary statistics for final frames (230s) of 18 mtGFP cell samples. See Chapter 2.2.9 for summary statistic descriptions.

Network build-up over time can also be demonstrated by connected component number, a measure of the number of disconnected subgraphs (Figure 2.5.A.i-iii). Across mtGFP videos, we see separate components joining up into one main connected component. Separate connected components at early time frames illustrate mitochondria in a similar physical proximity, but over time, links occur between these components, and the entire system tends towards connectivity. In mtGFP videos there remain some small connected components not connected by the end of frame time, due to mitochondria coming into frame only at the final time points, or never encountering more than one or two other individuals (Figure 2.5.B.ii). The shape of the networks is informative, with the heterogeneity in degree reflected as some nodes are located on the tips of thin protrusions from the main connected component (Figure 2.5.A.iii), some are located in tighter clusters of nodes, and some appear as connections along edges connecting two or more clusters. The exact shape depends on the plotting method, but the topology of these networks reflect the variation across the chondriome in terms of number of encounters per individual. This topology has also been informative when theoretically testing information transfer across the chondriome (See Section 4, (Giannakis et al., 2021)).

2.3.3 Robustness of approach as demonstrated by independent video analysis

So far, the use of a 'social' lens through which to examine mitochondrial motion has demonstrated variability across social statistics, mirroring the previously described heterogeneity we see within the physical movement of mitochondria (see Section 2.3.1). Measuring local connectivity using degree, and the more global measurement of connected component number has shown the patterns of encounters between individual mitochondria, and the extent to which, in the experimental time frames, a well-connected scale-free-like community of

individuals forms.

In order to demonstrate the applicability and scope of quantifying chondriome connectivity using encounter networks, we analysed two independent video samples both from *A. thaliana*, taken from (Arimura, Yamamoto, et al., 2004; El Zawily et al., 2014) (see Section 2.2 for further source information). The same tracking methods were applied to these videos and networks were built using the same encounter distance (1.6µm) and methods as in Section 2.2. Results are shown in Figure 2.6. Both independent videos show an increase in the size of their largest connected components over time, and overall similar mean degree values, despite independent video 1 (Figure 2.6.A) having more connected components and higher degree nodes. Independent video analysis demonstrates how our approach can be applied to different experimental set-ups.

2.3.4 Individual-based modelling identifies different cellular control signatures and priorities/potential movement regimes

Following analysis of physical and social characteristics of experimental samples, we next sought to use these statistics to compare hypotheses for the mechanisms underlying mitochondrial motion within the cell. For this, a predictive individual-based simulation of mitochondrial motion was built. The model was built by Prof. Iain Johnston (University of Bergen), and I provided qualitative guidance. We directly used measurements and observations of mitochondrial motion from experimental samples to inform us of some parameters such as number of mitochondria, simulation area size (length and width), and time frame (see Section 2.2), with other factors influencing motion able to be varied arbitrarily (cytoskeletal strand use, diffusion rate, hydrodynamic force etc.). This *in silico* system allows us to uncover which of the range of physically possible behaviours resemble biological reality, by allowing us to impose constraints upon different aspects of the system, and uncover which

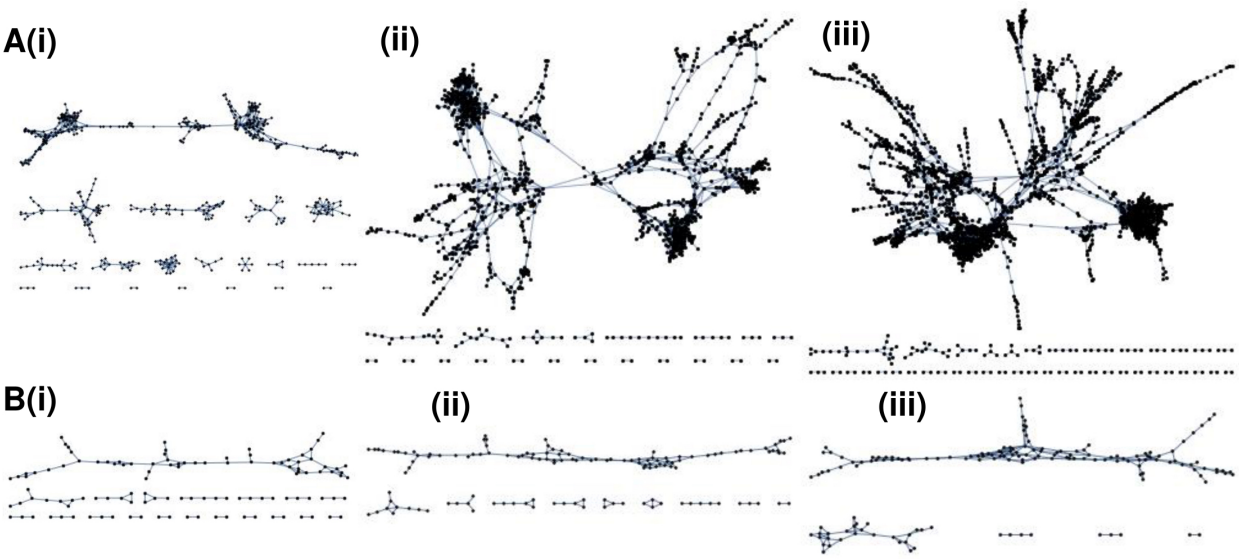

C	logMeanDegree (at 24 seconds)	InterMitoMean (at 24 seconds)	MeanSpeed (0–24 seconds)	DegreeCV (at 24 seconds)	Network Efficiency (at 24 seconds)
Independent Video 1	1.34	1.86	4.84	1.15	0.0918
Independent Video 2	1.31	1.39	0.178	0.585	0.108

Figure 2.6: Independent videos of mitochondrial motion yield quantitatively similar network structures. Networks built from mitochondrial interactions in independent video 1 (A) and 2 (B) shown at frames equivalent to (i) 4 seconds; (ii) 12 seconds; (iii) 24 seconds. (C) shows network physical and networks statistics taken at stated time, with singletons omitted. Glossary; logMeanDegree, logged value of mean number of immediate neighbours of each node; InterMitoMean, mean minimum Euclidean distance between each mitochondrion (µm); MeanSpeed, in $\mu m/s^{-1}$; DegreeCV, coefficient of variation in degree; Network Efficiency, average "closeness" (reciprocal of shortest path length) between pairs of nodes. Independent video 1 shows mitochondria with Kaede fluorescence in the **cotyledon** of *A. thaliana* (Arimura, Yamamoto, et al., 2004), via the POD3 database (Mano, Miwa, et al., 2008; Mano, Miwa, et al., 2009; Mano, Miwa, et al., 2011; Mano, Nakamura, et al., 2014). Independent video 2 shows TMRM stained mitochondria from the **hypocotyl** of wild-type mtGFP *A. thaliana* (El Zawily et al., 2014). Reproduced from Chustecki, Gibbs, et al. (2021).

physical principles hold regardless of control mechanism. There is also scope for adjustment to other cell types and species. The structure of the cell and factors influencing mitochondrial motion within this model can be seen in Figure 2.7.

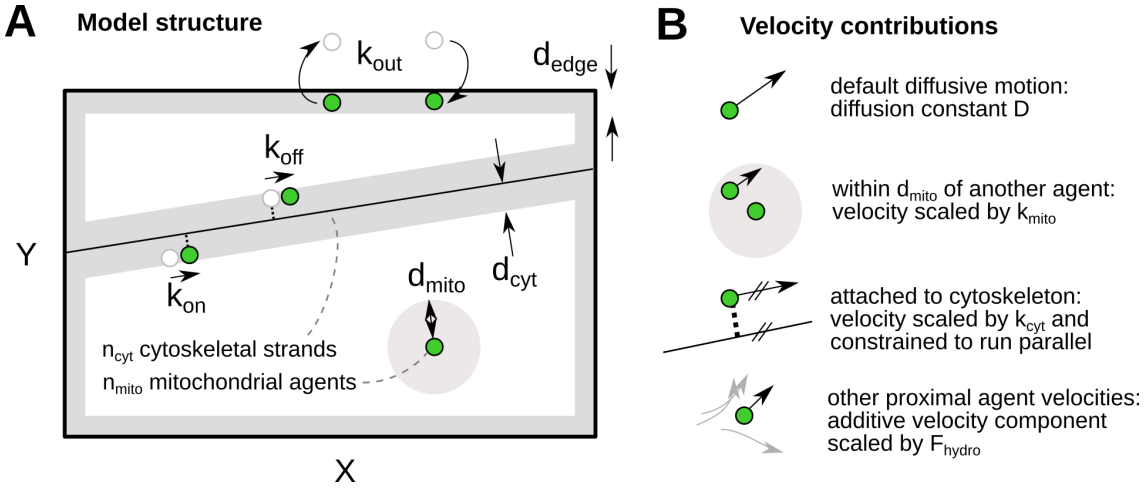

Figure 2.7: Individual based model of mitochondrial motion reveals a wide range of physical mechanisms of dynamics. (A) Summary of model structure. A cell of size X × Y is filled with n_{mito} mitochondrial agents. The cell contains n_{cyt} linear cytoskeletal strands, randomly placed. Agents can attach to the strands when within a distance d_{cyt}, with a rate k_{on}, and are removed with rate k_{off}. Mitochondrial motion can be scaled upon other agents being within distance d_{mito}. Movement of mitochondria out of the field of view when collecting time-lapse images is modelled using rate k_{out} when agents are within d_{edge} of the edge of the cell, and these are replaced by new agents randomly positioned within the cell boundary. (B) Factors influencing mitochondrial motion. Mitochondrial agents move by default with a diffusion constant D. Any proximal agents have their velocity scaled by k_{mito} when they come within distance d_{mito} of another ($k_{mito} = 1$: no effect). When attached to a cytoskeletal strand, mitochondrial agents can only run parallel to the strand, with a velocity of k_{cyt}. This can contribute to cytoplasmic streaming, modelled as an additive contribution from proximal agents, scaled by d_{mito} and F_{hydro} ($F_{hydro} = 0$: no effect). Reproduced from Chustecki, Gibbs, et al. (2021).

Within the earliest iterations of the model, we used very few parameters to describe mitochondrial motion, only cell size, frame time, number of agents and the 'step type'- a parameter specifying if mitochondrial motion should be built from steps from a Gaussian distribution where the step type is a diffusion coefficient, or a long-tailed Lévy distribution, where the step type is the exponent for calculating step length. After preliminary analysis of the network results, and careful observation of our experimental video data, it was decided that mitochondrial motion was best described as Gaussian, random diffusion, when not using cytoskeletal strands. In some way, Lévy flights are appropriate for describing the diffusive motion of mitochondria with occasional ballistic motion, but this is a pre-defined motion lasting more than a single step due to mitochondrial implementation of the cellular cytoskeleton. Therefore, moving forward we used an extended model, introducing the cytoskeleton, as well as further parameters during the continuation of model development.

Different modes of motion were explored using the individual based model. A range of different movement regimes were generated, using some parameters taken from prior experimental estimates, and some using random numbers from using uniform distributions within a pre-set range. It must be noted that within this study, this model was not used to solve an explicit inference problem (for example, for finding parameters at which the population was performing best at a particular outcome, or the 'fitness peak' of the system was found), although it could be implemented in this way. Neither was the model used to generate the most accurate simulation of mitochondrial motion in a plant hypocotyl cell. Instead, it was used to explore parameter space, and the control, dynamics, and priorities of this system, to then compare these quantities to experimental data. It was also used to explore limitations of the system, such as:

• Whether it is possible to generate the same connectivity as experimental data using only cytoskeletal strands for movement.

• Whether only diffusive motion could capture the same connectivity as experimental data.

• To uncover how much cytoplasmic streaming contributes to or contends with even spread across the cell.

We also directly question our hypothesis- is it possible to generate a model in which mitochondrial agents can be both well connected and evenly spread across the cell without having to sacrifice either?

The full range of parameters used for the models seen throughout this chapter are quantified in Table B.1 and B.2, and described in Section 2.2. For each model, both the physical and encounter network statistics were examined and compared. To directly test our hypothesis that a combination of connectivity between mitochondria (1), and even spread throughout the cell (2) helps the experimental plant cell outperform theoretical configurations, we generated four scoping models. These scoping models can be seen in Figure 2.8 [1] [2].

Here in Figure 2.8, models A, B and D are "null models", where motion is purely diffusive. Each of the four models have the same k_{out} parameter, mimicking field of view loss and gain of mitochondria. Null **model A** has a low diffusion rate, and does not have cytoskeletal strands to utilise, and so mitochondria diffuse mainly on the spot, as seen in Figure 2.8.A.i. Being static in space keep these agents at a spread configuration through the cell, fulfilling part (2) of our hypothesis. However, because they barely move, their encounters with other agents are very low, as seen in the degree distribution and mean (Figure 2.8.A.ii, E), which does not fulfil (1). Null **model B** has a high diffusion rate, and does not utilise cytoskeletal strands. In contrast to A, the agents cover cellular space well in the time given (see the dense traces in Figure 2.8.B.i), giving ample opportunities to

[1] Models in Figure 2.8 correspond to parameterisations NM9-12 in Table B.1.

[2] Dynamic representation of the models can be viewed as part of the 'Activity' section of mitochondri-amove.com – although the parameterisations are not the exact NM9-12 quantities – they are representative of the ranges in dynamic motion available to the model cell.

encounter other agents- resulting in higher degree values and larger connected components (Figure 2.8.B.ii, B.iii, E). Theoretically, this would support both parts of our hypothesis, with agents travelling far and wide throughout the cell and maintaining a relatively even spread (Figure 2.8.E), while being well connected. However, the diffusion rate for this model (D = 0.85μm^2/s) is much higher than that characterised within this study (0.15μm^2/s, see A.6), or within other studies (0.091μm^2/s, (Zheng, Beck, et al., 2009)), and so represents a rate of motion either physiologically inaccessible to the plant cell, having other detrimental consequences, or being unsustainable for the cell. So, a greatly increased diffusion allows both mitochondrial connectivity and even spacing, but is not deployed in nature.

To assess the performance of models with a biologically reasonable diffusion rate, we generated models C and D with rate D = 0.15μm^2/s. **Model C** made use of cytoskeletal strands while **D** did not. Directly comparing both, we see that the use of cytoskeletal strands by model C facilitates encounters across cellular space, leading to an increase in degree value (Figure 2.8.C.ii,D.ii,E), and connecting separate connected components; This can be thought of as connecting separate cliques or communities of mitochondrial agents, that otherwise may not be connected. The use of cytoskeletal strands increases the probability and density of mitochondrial agent encounters, by limiting their motion to strand-adjacent areas. It also allows higher magnitude of displacement across the available space. Therefore, we see that the implementation of cytoskeletal strands in the model system facilitates connectivity (1), and reduces intermitochondrial mean (2), as agents can be better linked due to this efficient transport method (Figure 2.8.E). Model C goes some way to provide a regime where both aspects of the hypothesis can be met.

This increased connectivity also provides a network that is more efficient at passing information between socially connected agents. We quantify network efficiency as the reciprocal shortest path lengths between nodes in the network, which gives a read out of how close the social connection between pairs of mitochondria is (see Section 2.2). The higher the

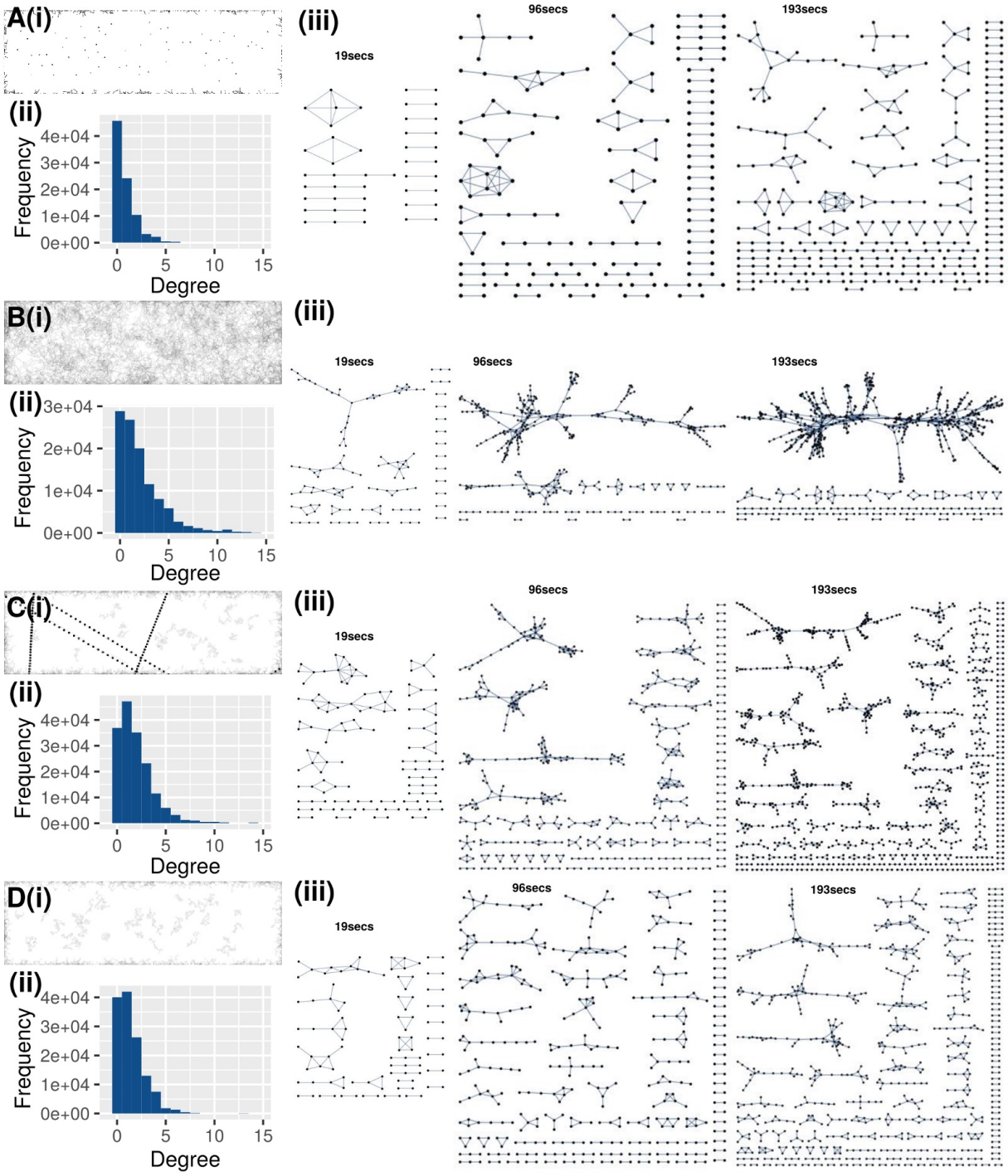

E

	logMeanDegree (final frame)	InterMitoMean (overall)	logMeanCH (overall)	DegreeCV (final frame)	Network Efficiency (final frame)
network (A)	−0.161	3.36	−2.64	1.27	0.00161
network (B)	0.755	3.04	3.14	1.22	0.0465
network (C)	0.674	2.64	−0.00767	0.936	0.00393
network (D)	0.414	2.92	−0.108	0.975	0.00289

Figure 2.8: (See next page)

Figure 2.8: Individual based models capture a wide range of mitochondrial motion under different cellular mechanisms. Four different systems are described (A) Low diffusion rate, D = 0.009µm^2/s, k$_{out}$ = 0.086s^{-1}. (B) High diffusion rate, D = 0.85µm^2/s, k$_{out}$ = 0.086s^{-1}. (C) Intermediate diffusion rate, D = 0.15µm^2/s, k$_{out}$ = 0.086s^{-1}, using n$_{cyt}$ = 5 strands, with k$_{on}$ = 0.85s^{-1}, k$_{off}$ = 0.43s^{-1}, kcyt = 0.85µm/s. (D) Intermediate diffusion rate, D = 0.15µm^2/s, k$_{out}$ = 0.086s^{-1}. For each, illustrations show (i) model space with motion of agents over time (grey traces), cytoskeletal strands as black dots (ii) Degree distributions for all agents across all frame time (230 seconds) (iii) Historical encounter networks of proximal connections between agents at 19, 93, 193 seconds. (E) Table of physical/social statistics collected either at the final frame or across frame time (230 seconds) (stated). Glossary; logMeanDegree, logged value of mean number of immediate neighbours of each node; InterMitoMean, mean minimum Euclidean distance between each mitochondrion (µm); logMeanCH, logged value of area travelled throughout time (µm^2); DegreeCV, coefficient of variation in degree; Network Efficiency, average "closeness" (reciprocal of shortest path length) between pairs of nodes. See 2.2.9 for summary statistic descriptions. Reproduced from Chustecki, Gibbs, et al. (2021).

network efficiency, the closer the social connection and the better the ability to pass information across the system. Model C has an increased network connectivity compared to model D (Figure 2.8.E), demonstrating that cytoskeletal strands can help increase communication across the network, compared to diffusive motion alone.

We next asked: what effect does altering each parameter have on the system? Each parameter was altered specifically, to judge the effect on agent behaviour (Figure 2.9, Table B.2). This scoping showed that a broad range of model behaviour was preserved under a range of k_{out} values (Figure 2.9, Table B.2). Also shown is that a high k_{on}:k_{off} ratio (rate of attachment or detachment to the cytoskeleton) leads to an increase in motility, connectivity and ultimately network efficiency (Figure 2.9.C-H, Table B.2.C-H). The ratio of these two rates has more impact than their absolute values. High hydrodynamic interactions controlled by F_{hydro} also showed comparably less ballistic movement on cytoskeletal strands and more aligned mitochondrial trajectories (Figure 2.9.I), compared to a model with low F_{hydro} (Figure 2.9.J). Other parameters had less of a drastic effect at the ranges chosen for this scoping.

Overall, we demonstrate the ability of this individual based model to generate a range of mechanisms describing mitochondrial motion, including those outside of biologically feasible ranges, and a whole variety of those within.

2.3.5 A trade-off between physical and social priorities is revealed through characterisation of theoretical and experimental mitochondrial dynamics

After establishing and characterising our *in silico* model of mitochondrial motion, we next investigated the hypothesised tension between even spread and organellar social encounters.

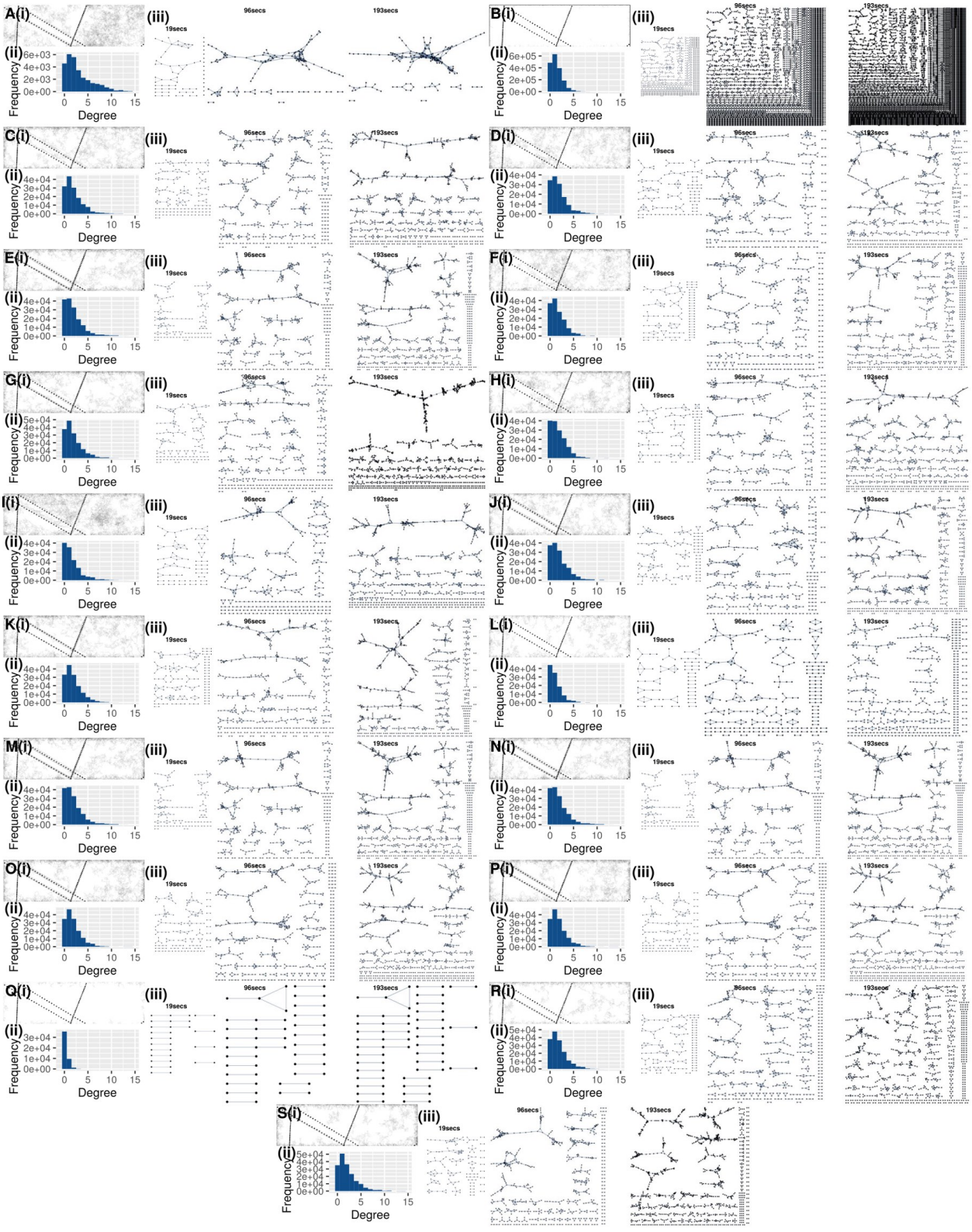

Figure 2.9: (See next page)

Figure 2.9: Simulation results of 'model sweeps' to assess the influence of individual parameterisations at a time. Systems A-S demonstrate model parameterisations differing by one parameter from an arbitrary default state. Parameters and physical/social statistics of these models are shown in Figure B.2, with each altered parameter highlighted. In brief; (A,B) are high and low k_{out}, (C-H) are varied k_{on} and k_{off}, (I,J) are high and low F_{hydro}, (K,L) are high and low k_{cyt}, (M,N) are high and low k_{mito}, (O,P) are high and low d_{mito}, (Q-S) are high d_{mito} and varying k_{mito}. Reproduced from Chustecki, Gibbs, et al. (2021).

We asked to what extent this tension exists in theory, and also how experimental systems (real plant cells) may go about resolving this tension. In order to do this, we simulated a further set of different behaviours with our physical model. Implementing these behaviours, very different networks were produced and this highlighted potential strategies the cell may in theory employ. We tracked the performance of these models with respect to the even spread/social connectivity trade-off with various physical and network statistics. Model parameterisations used here can be seen in Table B.1, and described in Section 2.2.7.

Comparing these theoretical systems reveals a trade-off between physical spread and social connectivity, illustrated by a negative correlation across mean degree and intermitochondrial mean (Figure 2.11.A). Without mitochondrial dynamics, these organelles would either be clustered or spaced from each other, with very little opportunity to do both. Therefore, if mitochondria are static, it is impossible to resolve this tension. Plant mitochondria adopt dynamics that help them overcome this tension, forming a new Pareto front with more opportunity to resolve the tension (visualised in Figure 2.10). Experimental results plotted alongside theory demonstrate that when plant cells face this tension, they adopt dynamics that allow a high intermitochondrial connectivity, at the expense of even spread throughout the cell. This means the particular dynamics adopted by the wild-type plant cells favour connectivity more than other theoretical options do. So how do they do this? Plant mi-

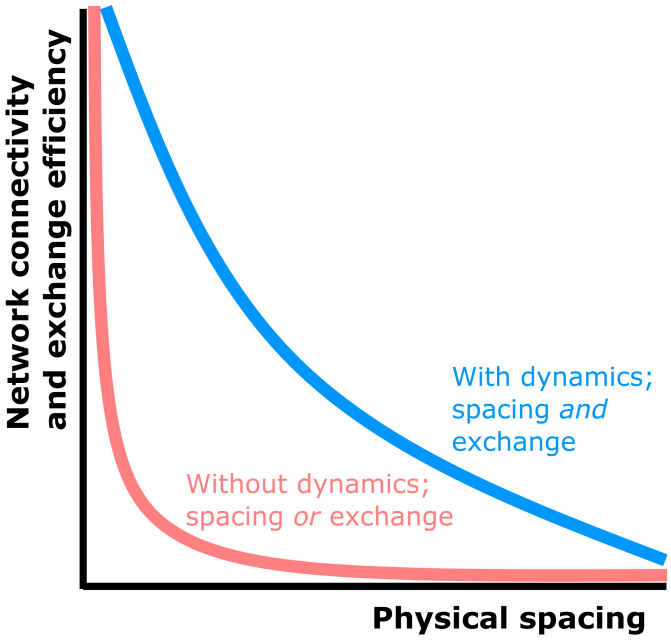

Figure 2.10: Mitochondrial dynamics offer the system more opportunity to resolve the connectivity-spacing trade-off. There exists a trade-off between a well-spaced chondriome (x-axis), and network connectivity and potential for exchange (y-axis). Mitochondrial dynamics offer the system more opportunity to have both (blue line) than they would without (red line). Adapted from Chustecki, Etherington, et al. (2021)

tochondria maintain a moderate association time when they colocalise, which allows them to build networks that are well connected, have a small number of connected components (Figure 2.11.B), and a reasonably high degree (Figure 2.11.C).

The motion exhibited by mitochondria within the plant cell emerges as a mechanism allowing mitochondria to maintain a high level of connectivity, while remaining evenly spread throughout the cell. Intuitively, an increased speed allows increased area to be travelled (Figure 2.11.D). An increased area travelled is correlated with an increase in connectivity to other mitochondria (Figure 2.11.E). However, an increase in area is not the only way to increase connectivity, as moving ballistically in a straight line (being constrained with others

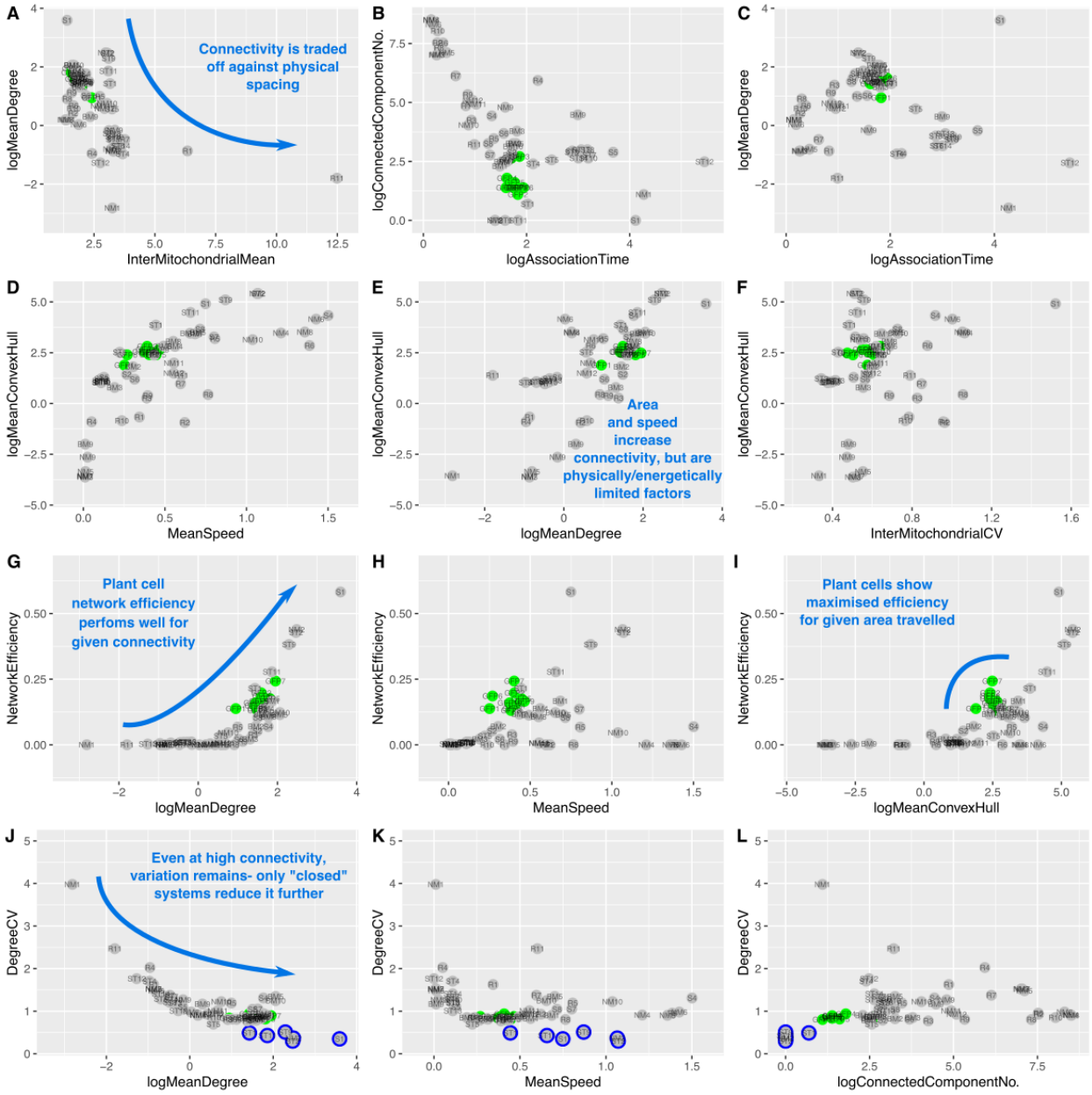

Figure 2.11: Comparison of physical and social statistics between theoretical and experimental systems reveals a trade-off between even spacing and chondriome connectivity. Points illustrate experimental (green, n=10) and theoretical (grey, n=54, different parameterisations) systems over 230s. Statistics are from both networks (at the frame corresponding to 230s of video time) and physical dynamics. Datapoint labels represent individual experiments (GFPn = 1-10), from single hypocotyl cells) and simulations (e.g. NM1 (null model 1), all simulation names and parameters can be seen in B.1). Simulations of interest are highlighted in blue. Reproduced from Chustecki, Gibbs, et al. (2021).

to the 2D cytoskeletal strand) or being part of a more static cluster could also increase connectivity and interactions to other mitochondria, as could other factors such as association time. Within our theoretical model, there are no restraints placed upon the amount of energy each mitochondrion uses travelling (for example on cytoskeletal strands). There are also few restraints on where they can move and diffusion rate and cytoskeletal speed are consistently defined. However, in the plant cell, there are more constraints, such as the amount of ATP spent for each step along cytoskeletal strands, other organelles to navigate as well as the viscous cytoplasm limiting speed of travel. We see that the models with the largest areas and highest speeds travelled (Figure 2.11.D,E) lie above the experimental samples, likely as they are not limited by the physical and energetic constraints described. These are also the models that reach the highest levels of connectivity as measured by mean degree. Models that indeed do travel the largest areas and have the highest connectivity may be using the wide reach of each agent to connect to many other mitochondria, increasing connectivity in those situations. This may ensure connectivity of the chondriome while enabling an even, if very wide, spread of individual agents, going some way to address the trade-off described in Figure 2.11.A. However, as they outperform the experimental agents in terms of their increased connectivity, there must be other factors at play in the experimental system that can still lead to a chondriome able to face the tension of even spacing versus connectivity.

This may, for example be realised by a highly physically constrained case such as in model S1. Here, all agents are found within the two polar ends of the cell, with only one or two agents moving between these clusters. The individuals within the clusters are diffusing rapidly, forming a topology similar to that of a random graph, but not tested for quantitative similarities. We see that model S1 has a high efficiency and high mean degree (Figure 2.11.G), which we might expect from a random graph, as well as being able to cover on average a large area even without leaving the confines of the two polar ends due to their high diffusion rate (Figure 2.11.D,E).

This increase in connectivity as measured by degree demonstrates that itinerant mitochondria travelling larger areas throughout the cell contribute to global connectivity throughout the chondriome. Theoretical systems allow a very broad range of speeds and area travelled to be realised, showing that systems with the fastest agents can reach very high levels of connectivity. This would allow a compensatory mechanism to arise, allowing a high connectivity poise while maintaining what even spread they can. However, plant cell mitochondria are physically and energetically constrained, meaning that this is not a strategy for overcoming this trade-off that is available to them (Figure 2.11.E). Therefore, these mitochondrial dynamics observed by us and others are used to allow interactions between individual mitochondria, while remaining evenly spread and at the same time limited by physical constraints.

Theory also demonstrates that there is an inevitable level of heterogeneity in intermitochondrial distance, emerging from this resolution of tension in these complex and multi-agent systems. We see that when variation in intermitochondrial distance is much below experimental levels, the area travelled throughout the cell is greatly reduced (Figure 2.11.F), and hence also reduces the mean connectivity across the chondriome (Figure 2.11.E). Therefore, in order to increase connectivity and also be evenly spread, there is a level of heterogeneity in the motion of mitochondria that must be met for this resolution to be facilitated.

One surprising result is that experimental networks are almost as efficient (reporting how close the social connection between pairs of mitochondria is) as the best theoretical models for a given connectivity (Figure 2.11.G), lying closer to the upper bound of network efficiency than the majority of theoretical systems. Network efficiency, as described is the average of the reciprocal shortest distance between all nodes in the network (see Section 2.2), meaning it measures the accessibility between nodes. It will be higher should paths across the network be shorter, and so here can give a quantification of how dense the network is, or

how easy it is to pass information throughout the system. This relates, in the case of plant mitochondria, the potential of the mitochondrial network to exchange genetic information and protein machinery (Arrieta-Montiel, Shedge, et al., 2009; Mouli et al., 2009; Hyde et al., 2010; Patel et al., 2013; El Zawily et al., 2014; Welchen et al., 2014; Giannakis et al., 2021). These exchange events are vital for the maintenance of a healthy chondriome through complementation of damage proteins and genomes, therefore we hypothesise a high network efficiency is a desirable characteristic of these networks (Logan, 2010b). Experimental results also demonstrate an efficiency approaching and exceeding theoretical values at a given speed (Figure 2.11.H), and area travelled (Figure 2.11.I). This demonstrates that the speed and area travelled by dynamic mitochondria in plant cells are *near optimal* for information transfer across the organellar population.

These relationships as compared across wild-type and simulated mitochondrial encounter networks demonstrate key features of these biological networks. In order to define these encounter networks against classical networks from graph theory, a further investigation into the relationships across well-defined network models was undertaken. Results of this can be seen in Section A.0.2.

To further investigate network efficiency and whether network weighting has an effect on these results, experimental networks were weighted by 1/association time, revealing a strong correlation between the efficiencies of the 10 unweighted vs weighted networks (see Section A.0.1, Figure A.1). In Figure 2.11.B-C experimental cells have a moderate association time in comparison to some theoretical models. Using these association times as network weightings, we concluded that unweighted networks can sufficiently capture the underlying behaviours of the system and support the results discussed here.

The level of physical heterogeneity required for a well-spread chondriome and increased areas travelled described earlier is mirrored by an unavoidable level of heterogeneity

within connectivity, that is adopted by plant cells when seeking resolutions to the connectivity/spacing trade-off. Our theory suggests a negative correlation between variation in degree (degree CV) and mean degree (Figure 2.11.J), showing that the less connected a network is, the noisier the connectivity will be. This noise, however, never decreases to 0- the most well connected theoretical networks retain a degree CV of 0.25-0.5, in comparison to the other theoretical networks of 0.75-4. This variation cannot be avoided by even the fastest moving systems of agents with speeds that are biologically unattainable, or for the most well-connected networks with only one connected component (Figure 2.11.K,L). There are, however a small collection of theoretical models that come close to reducing this required heterogeneity. They are encircled in blue (Figure 2.11.J,K,L) and also shown in Figure 2.12, and are the only potential mechanisms showing that a modest reduction in social heterogeneity can potentially be achieved without sacrificing a resolution to the connectivity/spacing trade-off. However, what sets this small collection of theoretical systems apart is that they represent "closed" systems ($k_{out} = 0$), where the agents cannot leave or enter the cell. The agents also travel large areas throughout the cell (Figure 2.12.A), move at high speeds (Figure 2.11.K), and are never stationary (Figure 2.12.C). These systems do not reflect the experimental observations made (in which mitochondria can move in and out of the imaged area), but do reflect another potential mechanism for resolution of the connectivity/spacing trade-off- by restricting the space in which organelles can travel.

It is also worth noting the time-dependent behaviour of the summary statistics used. Physical summary statistics are not dependent on history, meaning they remain consistent over sampling time, so statistics such as mean speed (Figure 2.11.D, 2.13.iv) and inter-mitochondrial distance (Figure 2.11.A, 2.13.i) retain the same patterns over time. Some physical statistics predictably increase over time, such as the mean area travelled by mitochondria (Figure 2.11.E, 2.13.v). In terms of social statistics, as networks build over time, the connected component number consistently decreases across sampling time (Figure 2.11.B,

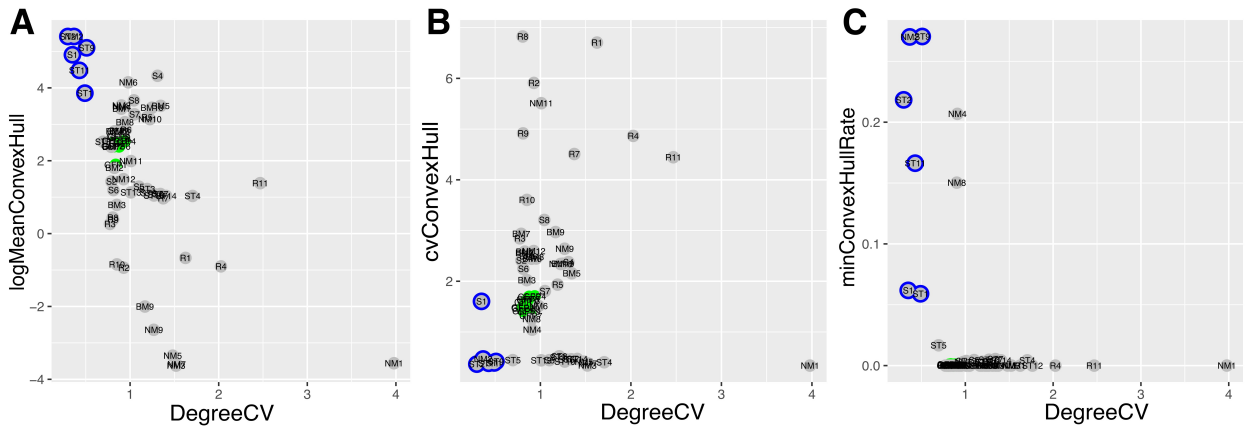

Figure 2.12: Networks exempt to the rule of increased heterogeneity being a requirement of connectivity display outlying motion. A) mean area travelled; B) variation in area travelled; C) minimum area travelled. Experimental results; mtGFP ('GFP' green, n=10), theoretical results (Grey, n=54), here name labels represent similarities in parameter grouping. Blue circles denote theoretical simulations of interest.

2.13.ii), and this increase in connectivity is reflected in increased mean degree over time (Figure 2.11.J, 2.13.x, 2.5.A.v). Conversely, variation in degree decreases over time, which occurs as the more extreme degree values are averaged out and dampened as the network becomes more connected over time (Figure 2.11.J,L, 2.13.x,xii, 2.5.A.v (inset)). Model S1 continues to be an outlier, with a low variation in degree matched to a high degree values throughout frame time (Figure 2.11.J, 2.13.Ax,Bx). Stable speed and intermitochondrial distance alongside changing network statistics reflect the nature of the system as it is captured, and the ability of the chosen statistics to describe this reality.

It is also worth noting that reducing the distance used to define an encounter between individuals does not change the overall connectivity trends across experimental data or models (see Section A.0.3).

Overall, these results demonstrate the dynamic mitochondrial motion we observe in plant cells allows both the spread and connectivity between individuals, while being subject

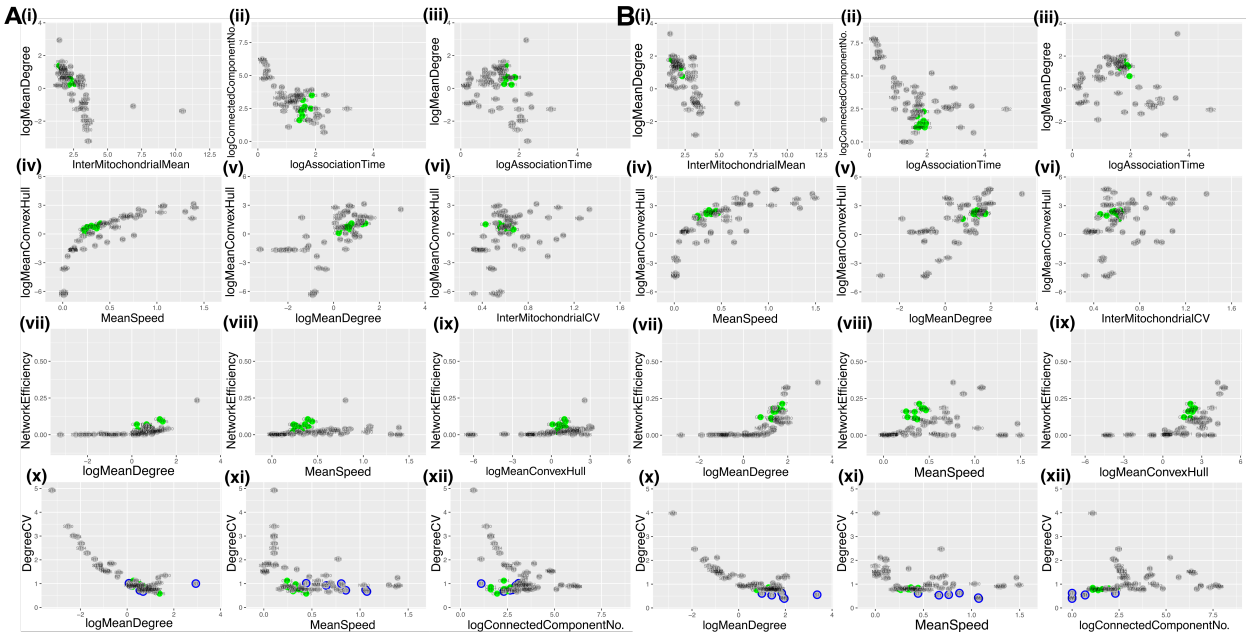

Figure 2.13: Physical and social statistics at different time-points reveal any time-dependent relationships. (A) Statistics taken at 1/10 of video time, representing 22 seconds. (B) Statistics taken at 1/2 of video time, representing 115 seconds. Datapoints represent individual videos/simulation, green = mtGFP (n=10), grey = theoretical (n=54). Blue highlights simulations of interest. Glossary; logMeanDegree, logged value of mean number of immediate neighbours of each node; InterMitoMean, mean minimum Euclidean distance between each mitochondrion (µm); MeanSpeed, in µm/s^{-1}; DegreeCV, coefficient of variation in degree; Network Efficiency, average "closeness" (reciprocal of shortest path length) between pairs of nodes. Reproduced from Chustecki, Gibbs, et al. (2021).

to a broader set of rules governing energetic expenditure, required level of heterogeneity and the cellular space itself. Given these requirements and restrictions, we demonstrate that plant cell mitochondria offer a near-optimal, efficient foundation for information transfer across the dynamic chondriome.

2.3.6 A mutant with disrupted cellular mitochondrial distribution poses a temporal challenge to the physical-social trade-off

After establishing there is a trade-off between physical spacing and "social" connectivity across theoretical space as defined by our scoping models (Figure 2.11.A), and that wild-type mitochondrial motion does surprisingly well at efficient information exchange compared to the different regimes set out by theoretical models (Figure 2.11.G-I), we next sought to understand how the mitochondrial system addresses this trade-off when challenged. In order to challenge mitochondrial dynamics, we used the mtGFP-*friendly* mutant, where mitochondrial distribution is disrupted due to a mutation in the *FMT* gene, responsible for mitochondrial fusion and a role in mitophagy (El Zawily et al., 2014; Ma et al., 2021). Impacting these fusion mechanisms leads to formation of large clusters of *individual* organelles, as can be seen in (Figure 2.14.A), which are capable of moving as a unit along the cytoskeleton and within the cell, and forming larger clusters when meeting at cytoskeletal junctions. Disruption of the cytoskeleton in *friendly* by latrunculin B arrests movement of mitochondria, as in the wild-type (El Zawily et al., 2014). There is also no current evidence of a general cytoskeletal disruption in the *friendly* mutant, as peroxisome (another cytoskeletal-dependant organelle) motion is not disrupted in these plants (El Zawily et al., 2014). The disruption caused by *friendly* leads to a detrimental plant phenotype in *Arabidopsis* (reduced growth phenotype of mtGFP-*friendly* can be seen in Figure 3.5), as well as reduced photosynthetic performance, more dead cells in the root, shorter roots overall, shorter etiolated hypocotyls, reduced biomass and increase in organelle-level stress (El Zawily et al., 2014) .

This increased clustering of mitochondria leads to compromised even spread throughout the cell, and could lead to an increase in local connectivity between these individuals. We hypothesised that this would lead to a corresponding shift on the identified trade-off (between even spread and intermitochondrial connectivity). In order to address this hypothesis,

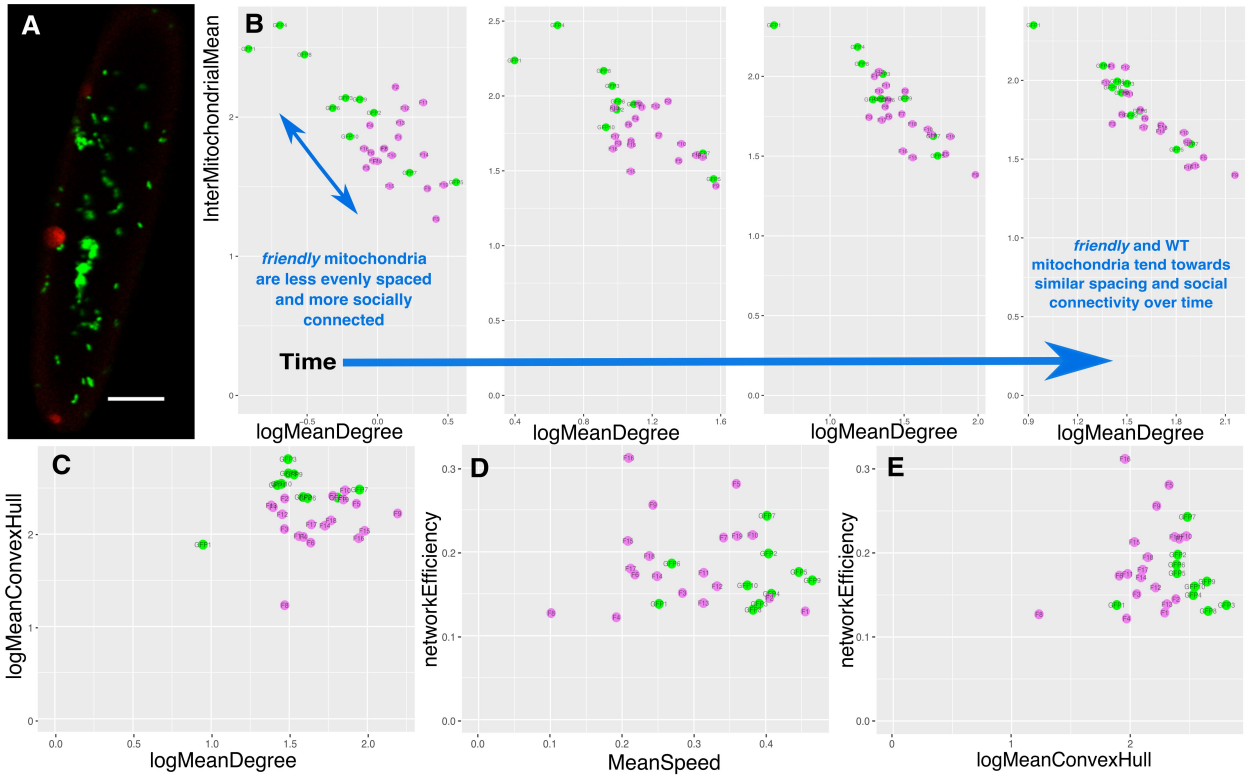

Figure 2.14: Physical and social statistics of the mtGFP-*friendly* mutant compared to wild-type. (A) Snapshot of mitochondria (green) within the mtGFP-*friendly* mutant, demonstrating characteristic clustering of discrete individuals, scale bar = 10 µm. (B) Mean degree versus mean inter mitochondrial distance (µm) in mtGFP-*friendly* (violet, $n = 19$) and mtGFP (green, $n = 10$), calculated across different time windows, L-R: 2, 39, 97, and 193 seconds. (C-E) Further social and physical statistics calculated across full frame time, or at final frame (as in Figure 2.15). Modified from Chustecki, Gibbs, et al. (2021).

we used a *friendly* line with GFP localised to the mitochondrial matrix (El Zawily et al., 2014), using the same technique of staining, imaging and tracking to gather time-dependent mitochondrial dynamics within single *Arabidopsis* cells (see Section 2.2), and build "social" encounter networks from close interactions of these individuals.

Initial scoping of the differences between wildtype mtGFP and mtGFP-*friendly* revealed a similar location in the simulated theoretical space for both genotypes (Figure 2.15). There were similarities within social and physical statistics, however there was separation of the two genotypes across axes comparing association time and connected component number (Figure 2.15.B), as well as mean speed and network efficiency (Figure 2.15.H). These differences are driven by alterations in physical statistics. mtGFP-*friendly* samples have an increased association time between individual mitochondria, which may contribute to the lower speeds observed due to the clustering phenotype restricting motion in the cell (Figure 2.16).

In order to address the hypothesis of mtGFP-*friendly* shifting the trade-off resolution between even spacing and connectivity, we look at the mean degree versus mean intermitochondrial distance axes. We first observed a trade-off at early time frames (Figure 2.14.B). mtGFP-*friendly* mitochondria are less evenly spaced at early time frames and more socially connected. This demonstrated that the disrupted distribution of mitochondria within this mutant brings about a shift in the previously identified trade-off. However, over time, this difference between mtGFP and mtGFP-*friendly* diminishes, with both genotypes converging towards similar mean degree (connectivity) and intermitochondrial mean (spacing). This is surprising, as it shows *friendly* does not completely compromise the cells' ability to reconcile this trade-off. What it does is challenge this trade-off in the short-term, perhaps providing a clue as to why disruption of *friendly* is clear within the whole-plant phenotype, but not fatal.

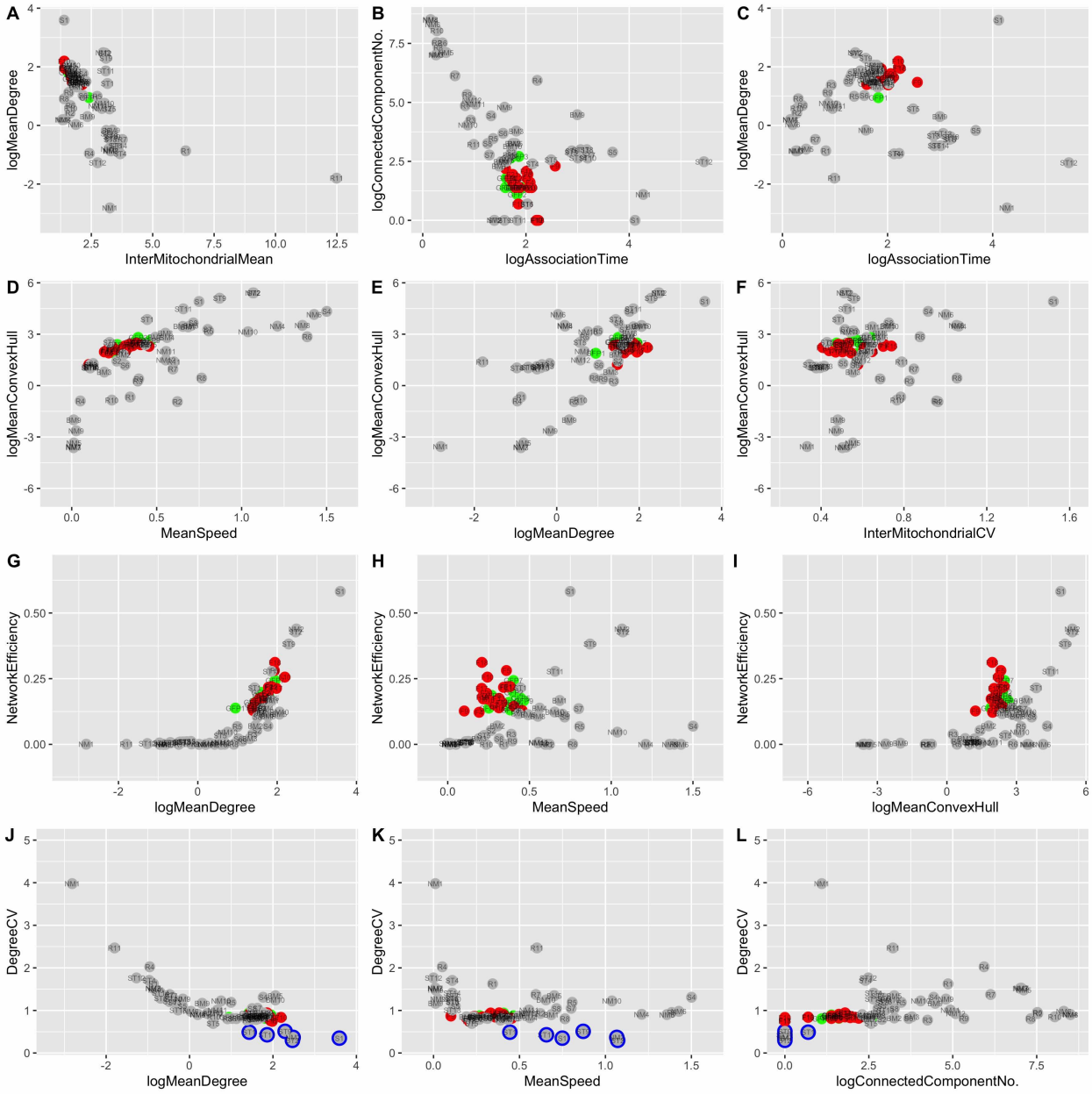

Figure 2.15: Comparison of physical and social statistics between theoretical and experimental systems including the mtGFP-*friendly* mutant. Same data as Figure 2.11, with the addition of mtGFP-*friendly*. Points illustrate experimental (mtGFP (WT), green, n=10 and mtGFP-*friendly*, red, n=19) and theoretical (grey, n=54, different parameterisations) systems over 230s. Statistics are from both network (at frame corresponding to 230s of video time) and physical dynamics. Labels represent individual experiments (GFP n = 1-10, FR n = 1-19), from single hypocotyl cells and simulations (e.g. NM1 (null model 1), all simulation names and parameters can be seen in Table B.1). Simulations of interest are in blue.

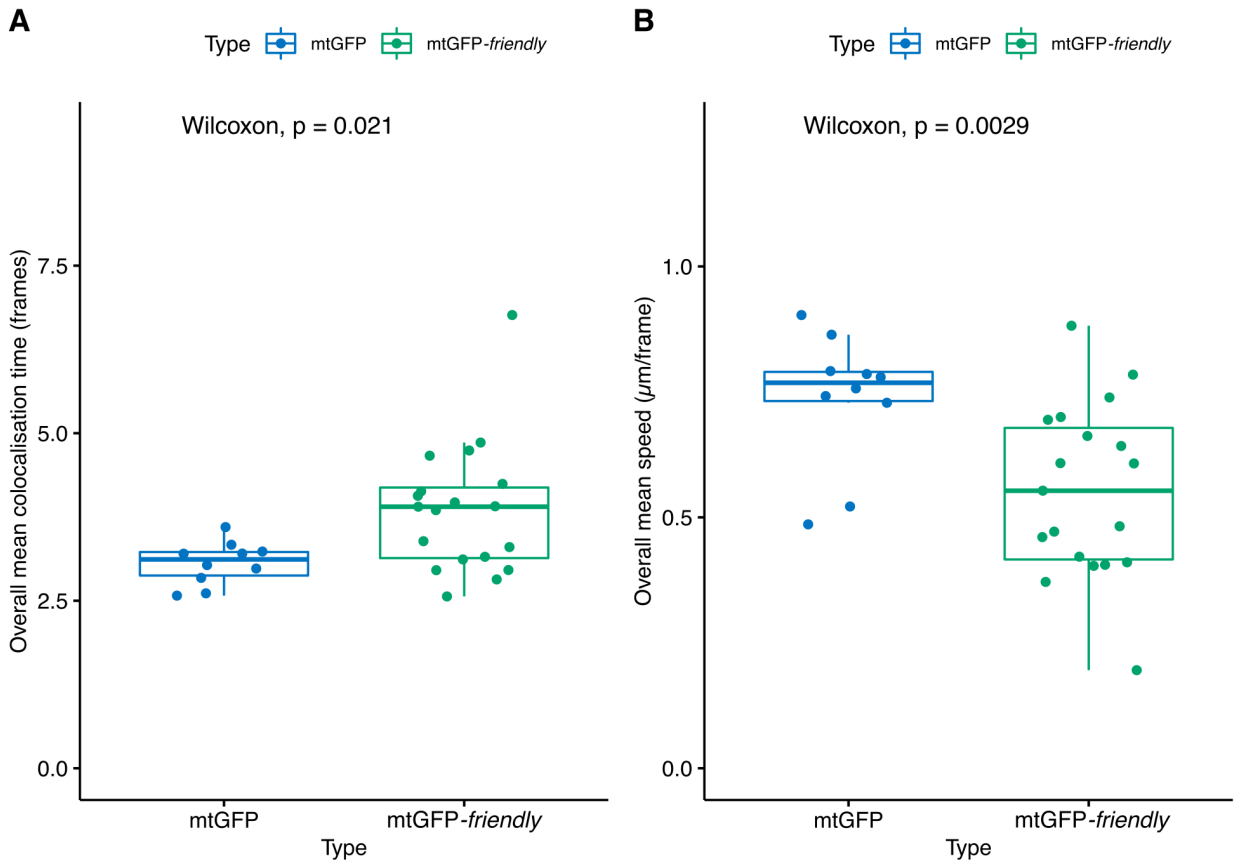

Figure 2.16: Colocalisation time (frames) and speed (µm/frame) differ between mtGFP and mtGFP-*friendly*. Each datapoint represents the overall mean of speed values and colocalisation time over all frame time (230 seconds). Note that mtGFP $n = 10$, mtGFP-*friendly* $n = 19$. Boxplots represent the median and 25th/75th percentile, with whiskers showing the smallest/largest value within 1.5x the interquartile range. P-values represent Wilcoxon test outcomes across both genotypes.

In order to assess this temporal challenge to the trade-off in more statistical detail, MANOVA analysis was performed upon the mtGFP and mtGFP-*friendly* samples (Figure 2.17). This analysis attempts to pick apart which response variable (mean degree or inter-mitochondrial mean) has the biggest influence on the genotypes becoming more 'similar' over time. Note mtGFP video (single-cell) samples n=18 here. Genotype samples were

compared across the intermitochondrial distance and mean degree axes, with the overall difference between the two remaining beneath a significance threshold of $p \leq 0.05$ for all frame times examined. Across Figure 2.17.A-E, the response in comparison across mean degree values remains beneath a $p \leq 0.05$ threshold, however response across the intermitochondrial distance axes fails to pass this significance threshold after 93 seconds of frame time. This demonstrates that although the trade-off overall is challenged as the two genotypes are different across these axes especially at earlier frames, they become more alike in values for these statistics as time goes on, mainly led by intermitochondrial distance becoming more alike between mtGFP and mtGFP-*friendly* as time goes on. This is supported by plotting the magnitudes in changes when the overall mean of these values are taken (Figure 2.17.F-G). The difference between the genotypes in terms of mean degree does become bigger as time goes on, but the two genotypes do not diverge completely– both trend towards a flattening of mean degree. It may be speculated that although this is not a closed system, we would see a steadying of mean degree value over time for these historical networks. In terms of intermitochondrial mean, the values start very diverged, and become more similar over time, supporting intermitochondrial distance being the driver for converging similarities between the genotypes over time.

This leads to the question of how *friendly* reconciles these differences with mtGFP in the long-term. Figures 2.14.C-E illustrate reduced area travelled and mitochondrial speed in mtGFP-*friendly*, but comparable network efficiency and degree between the two genotypes. This shows that the global network structure across the *friendly* chondriome is comparable, and maintained even in the face of physical perturbation. How does the cell manage this? Mitochondrial clusters have been shown to move around the mtGFP-*friendly* cell (El Zawily et al., 2014), and we have observed itinerant mitochondria moving from cluster to cluster (Figure 2.18).

These mitochondria are therefore physically constrained, and in networked cliques.

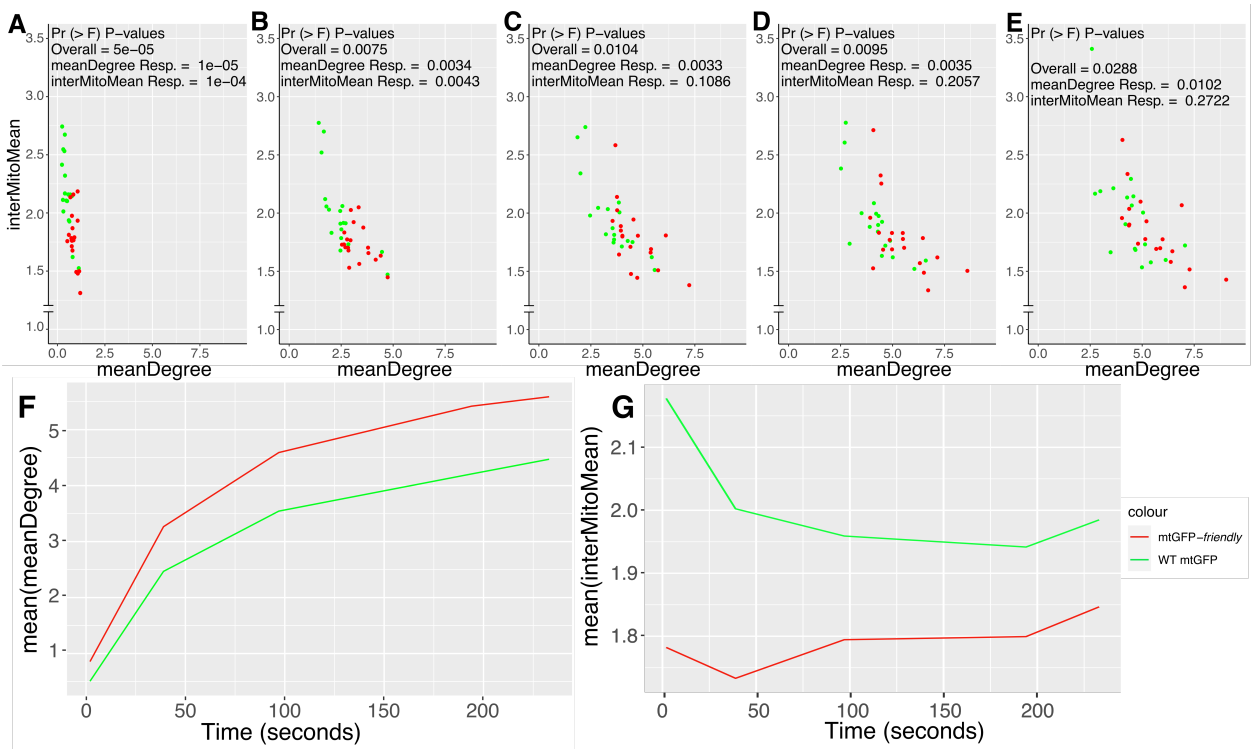

Figure 2.17: Differences across the physical-social trade-off change over time. (A-E) Relationship between overall (up to and including specified frame time) intermitochondrial mean (µm) and mean degree values (from network at specified frame time) across L-R 2, 39, 97, 193, 230 seconds. P-values are the result of multiple analysis of variance tests across the two genotypes at each time point, given for the overall comparison, and response by each variable. Each data point is a single cell sample. mtGFP (green) n= **18**, mtGFP-*friendly* (red) n=19. (F, G) Overall mean values of mean degree (F), and mean intermitochondrial distance (G), for the data points displayed in (A-E) demonstrating magnitude of change between the two genotypes over time.

However, these clusters are motile, or can have itinerant mitochondria moving between them. Therefore they still have an opportunity to be interlinked, building a global network structure. However, because clusters are slower moving and there are less itinerant mitochondria within mtGFP-*friendly* than the wildtype, this global connectivity is not built as swiftly, resulting in the slower timescale of the resolution to this connectivity/spacing trade-off.

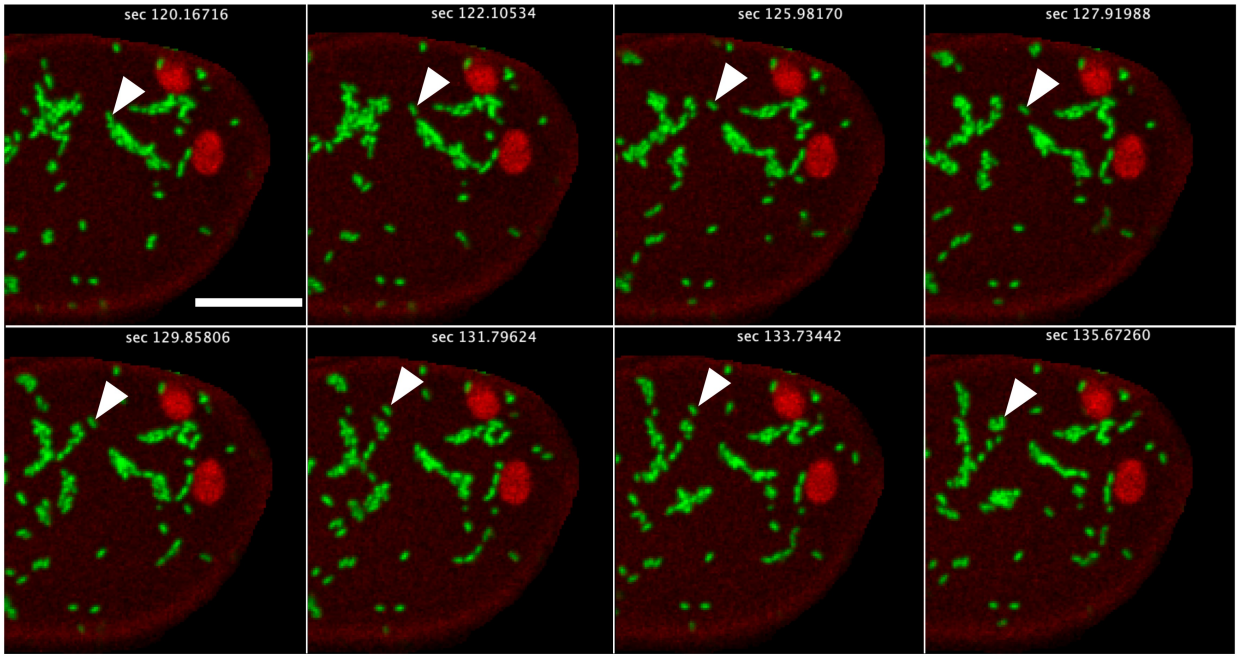

Figure 2.18: Itinerant mitochondria move between clusters within the *friendly* mutant may contribute to later-frame similarities with wild-type networks. Highlighted individual (arrow) over time moves between clustered mitochondria (green). Chloroplasts and cell area (red) are also seen. Scale bar= 10µm. Panel 1, 5, 8 reproduced from Chustecki, Gibbs, et al. (2021).

2.4 Discussion

Throughout this work, experimental characterisation and mechanistic modeling have been used to demonstrate that mitochondria in plant cells face a tension between intermitochondrial connectivity and even spread. Notably, plant cells have evolved a resolution to this trade-off, and efficiently manage their mitochondrial populations to get 'the best of both worlds'. Previous work has used network theory to quantify mitochondrial connectivity (Sukhorukov, Dikov, et al., 2012; Rafelski, 2013; Zamponi et al., 2018; Picard and Sandi, 2021), encoding large networks constructed through mitochondrial strands as edges and the junctions that join them as nodes. We take a different but complementary approach, more

analogous to human social networks, using the individual nature of plant mitochondria to represent each organelle as a node and close proximity between them as an edge. This builds a network that is less reliant on an underlying physical structure to dictate network connectivity, and allows dynamic interactions across a whole system of individuals to be quantified. To do this we use physical statistics and concepts from graph theory to calculate spread, connectivity, association, the potential for information transfer as well as demonstrating cellular priorities of energetic organelles in model plants.

From our findings, we predict that this balance of even spread and transient organellar connectivity underlies mitochondrial dynamics and organisation within the plant cell. It is known that cell geometry changes across cell types and dynamically through time (Bassel and Smith, 2016)- our hypothesis would add that similar physical behaviours would be observed and network structures formed across these cell types, given appropriate imaging technologies, and that even differential mitochondrial positioning in varied cell types would be facing a trade-off between spacing and connectivity. Some cell types within plants (e.g. the SAM), and many other species such as mammalian and yeast cells commonly have reticulated network structures (Hoitzing et al., 2015). There remains an open question about the structures of these networks- do they manage to achieve through reticulated structures what plant cells achieve through dynamics? That is, are the reticulations evenly accessible across the cell? As well as, are the network connectivity statistics describing *physical* connectivity in physically constrained reticulations similar to our encounter network statistics? Does inflexibility at mitochondrial junctions ensure mitochondrial strands cannot bunch up, and is efficient information transfer established by these structures? Network analysis and our flexible model can be modified and extended to whole cell and three dimensional mitochondrial dynamics, enabling further investigation into these questions. Our model can be used for inference work to uncover, based on priors about the system, how the plant cell would respond to different challenges or stresses, based around a desirable outcome (increased spread, con-

nectivity, efficiency, speed, to name a few). It is also extendable to other cell geometries, and other organelles. Research across reticulated network structures has been well characterised (Fricker, Lee, et al., 2008; Pain et al., 2019), but an individual based connectivity model is more broadly applicable to organelles and organisms that don't form extensive physical networks. Our open-source (see Section 2.2) model generation and analysis pipeline provides opportunities for transfer to other systems.

Throughout the imaging of young *Arabidopsis* seedlings, care was taken to maintain physiological conditions while retaining steady positioning of the sample for time-lapse imaging. Mitochondria are very sensitive to changes in cellular oxidative and redox states, and so care needs to be taken to not image for too long, lest diluted oxygen in mounting medium become unavailable (see section 2.2). Care was also taken to limit laser power and exposure time, while still using fluorescence microscopy for the clearest view of each individual mitochondrion. Perfused media can be used to keep intracellular oxygen supplies constant for much longer time frames (Schwarzländer, Fricker, et al., 2008). Mechanical stress also should be avoided, as the cytoskeleton can rearrange upon externally applied forces (Robinson and Kuhlemeier, 2018). In this case, imaging using whole seedlings in cuvettes can be used to avoid gravitrophic effects of not being upright, and external mechanical forces (Baesso et al., 2018). In our experimental set-up, time of imaging was kept to a minimum in order to collect time lapses long enough to gather enough encounters to quantify the system, but not put the seedling under undue stress or long enough for mechanical reshaping of the cytoskeleton to impact mitochondrial dynamics. Ongoing improvements to imaging technologies will allow systems like these to be viewed in even more detail in the future (Valm et al., 2017).

The work within this study offers quantitative illumination upon the question of why the plant invests energy in keeping the chondriome dynamically moving throughout the cell. Our conclusions suggest that this dynamic motion allows the plant to resolve a trade-off between physical spacing (that could be achieved by having mitochondria remain static, but

could not by only clustering), and the necessary capacity for communication and exchange (which cannot be achieved by remaining static and spread within the cell). There is evidence that this communication and exchange is important for normal functioning of the plant cell (Arrieta-Montiel, Shedge, et al., 2009; Mouli et al., 2009; Xu, Arrieta-Montiel, et al., 2011; Patel et al., 2013; El Zawily et al., 2014). We have also shown however, that this resolution is not without cost to the cell- there must be a level of heterogeneity induced, and even spread of mitochondria is compromised to favour connectivity. The specific influence of these encounters and exchange of proteins and the sparse mitochondrial genetic material (Preuten et al., 2010) between individuals is an exciting question, forming a connection between physical and genetic dynamics of these organelles within the cell- does the chondriome alter its physical dynamics to address genetic needs or damage? How do physical mitochondrial dynamics shape the genetic (mtDNA) population (Johnston, 2019b)? This is the focus of Chapter 3 using network characterisation of mutant lines, as well as ongoing modelling and theoretical work.

The observed dynamics in the cell are likely a combination of many mechanisms influencing behaviour, as is the case for many complex systems. Within this study, we do not claim that the proposed trade-off between even spacing and connectivity is the only driver of mitochondrial motion, as there are key factors such as interorganellar colocalisation to consider. Mitochondria interact with a great number of other organelles, such as chloroplasts, peroxisomes and the endoplasmic reticulum (Raghavendra and Padmasree, 2003; Scott, Sparkes, et al., 2007; Mueller and Reski, 2015; Shai, Schuldiner, et al., 2016; Van Dingenen et al., 2016; Barton et al., 2018), with these interactions changing dynamically depending on environmental conditions and cellular requirements. Exploration of mechanisms of motion using our general physical model have revealed the influence of using cytoskeletal strands, moving purely diffusively or implementing a mixture of both has on the system and the efficiency and connectivity of encounter networks. The spread of organelles has been

quantified here, using the mean minimum distance between each mitochondrion. Measuring the variance in distance values, or normalising by cell size would also give insight into population spread. Closer physical details of these encounters will be useful to uncover finer-grained connections. Imaging of this system under various stress conditions may also illuminate how the priorities of the chondriome alter to cope and respond to heat shock, cold treatment or hypoxia. Motion on cytoskeletal strands is also dependant on ATP, and its provision and availability will influence mitochondrial motion- which is where detailed ATP sensors can be of use to understand the drivers and mechanisms influencing this dynamic system (De Col et al., 2017). Of interest also are probes allowing individual mitochondrial states to be assessed across the population, such as mitochondrial pH, metabolite availability, membrane depolarisation and even mtDNA amount per mitochondrion (Wagner et al., 2015; Preuten et al., 2010; Lim et al., 2020; Prole et al., 2020; Ma et al., 2021)– all of these could be correlated with and driving dynamic mitochondrial motion, from individual interactions to cell-to-cell variability with a range of different mutants that could used for investigations such as these.

Chapter Three

Physical and social mitochondrial dynamics in an *msh1* recombination surveillance mutant

3.1 Introduction

Having established a pipeline for the imaging and quantitative analysis of social connectivity across a mitochondrial population ((Chustecki, Gibbs, et al., 2021), Chapter 2) and explored the effects of physical perturbations to mitochondrial dynamics, we next explored collective dynamics using the *msh1* mutant, known among other effects to impact the stability of mtDNA.

In plants, mtDNA is greatly expanded in size due to non-coding introns and repeat sequences, and is also recombinatorally active (Woloszynska, 2010; Klucnika and Ma, 2020). Therefore, through the dynamic syncitium of the mitochondrial population, exchange and recombine mtDNA molecules between individuals can occur (Rose, 2021). This makes up an important element of the trade-off identified in the previous chapter, linking connectivity

between mitochondria and their genetic properties upon encounters.

This was explored using social networks as a measure of intermitochondrial connectivity, demonstrating that mitochondrial dynamics allow the cell to address this dilemma; allowing transient encounters and intermitochondrial exchange of information while also retaining even physical spacing in the cell. We also showed that a physical fusion mutant named *friendly* posed a temporal challenge in shifting the cells' resolution to this connectivity/spacing tension. However, the question of if and how the plant alters this behaviour in response to a genetic challenge still remains. The relationship between mitochondrial genetics and physical dynamics is what we set out to explore within this chapter, hypothesising that a perturbation to the genetic state of these organelles may, alongside other effects, influence their physical state. This investigation will be a direct application of our previous work on the tension between and resolution of cellular spacing and intermitochondrial connectivity using encounter 'social' networks.

In order to investigate this relationship, we used a mutant of a key nuclear gene involved in the repair of cytoplasmic genomes - MutS HOMOLOGUE 1 or *MSH1.* First characterised by George Redei (Rédei, 1973; Rédei and Plurad, 1973), what was originally known as the chloroplast mutator gene (*CHM*), due to its strong variegated phenotype, is now recognised as a recombination surveillance gene, with the nuclear-encoded *MSH1* protein being targeted to both mitochondria and chloroplasts (Abdelnoor, Yule, et al., 2003; Abdelnoor, Christensen, et al., 2006; Shedge et al., 2007; Fukui et al., 2018). It is a homologue of bacterial MutS, but is not involved in mismatch repair as in bacteria (Davila et al., 2011; Wu et al., 2020; Christensen, 2014; Maréchal and Brisson, 2010). It contains a MutS-like mismatch recognition domain, an ATPase domain, and a unique GIY-YIG endonuclease, forming a compact protein with the ability to recognise, bind and cut mismatched double stranded DNA (Figure 3.1) (Abdelnoor, Christensen, et al., 2006; Fukui et al., 2018; Maréchal and Brisson, 2010; Wu et al., 2020). There is estimated to be just one dimer of

MSH1 within each mitochondrion in *Arabidopsis* cells (Fuchs et al., 2020). Although the full molecular mechanism of *MSH1* has yet to be fully elucidated (including whether the GIY-YIG domain has active endonuclease activity) (Fukui et al., 2018; Wu et al., 2020), several recent studies support the role of *MSH1* in double-strand break homology-directed repair (Davila et al., 2011; Christensen, 2014; Wu et al., 2020), and limiting ectopic recombination at small repeats (Davila et al., 2011; Abdelnoor, Yule, et al., 2003; Xu, Arrieta-Montiel, et al., 2011). Upon disruption of mitochondrial-targeted *MSH1* there is an increased level of insertion-deletion mutations and single nucleotide variants (Wu et al., 2020); disruption can also lead to substoichiometric shifting within the mitochondrial genome (Martínez-Zapater et al., 1992; Sakamoto et al., 1996; Abdelnoor, Yule, et al., 2003) and altered mitochondrial transcript profiles (Sakamoto et al., 1996; Arrieta-Montiel, Shedge, et al., 2009). These studies demonstrate that disruption of *MSH1* can compromise genetic integrity and pose a genetic challenge to mitochondrial DNA.

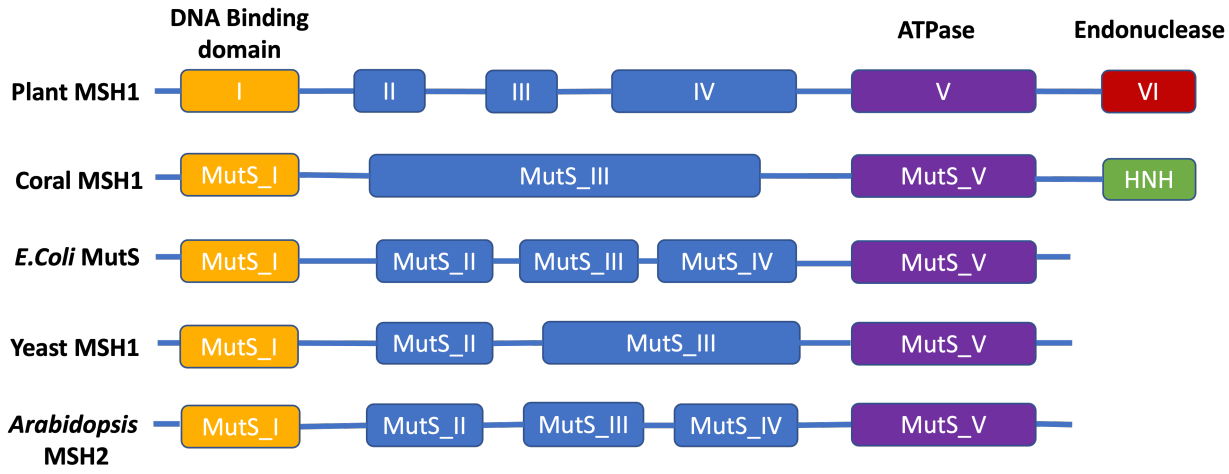

Figure 3.1: Protein domains of *MSH1* and related MutS across species. Plant *MSH1* domains are generalised across *Arabidopsis*, rice, soybean, common bean, tomato, and maize (Abdelnoor, Christensen, et al., 2006). Figure modified from (Abdelnoor, Christensen, et al., 2006).

There are other effects upon the plant from *MSH1* disruption other than mitochon-

drial genome instability. The chloroplast genome is also disrupted (Xu, Arrieta-Montiel, et al., 2011; Wu et al., 2020). When *MSH1* is mutated in *Arabidopis*, a variegated leaf phenotype appears, due to the perturbed development of chloroplasts (Martínez-Zapater et al., 1992; Sakamoto et al., 1996; Yu, Fu, et al., 2007). This corresponds to a low frequency plastid genome alteration in the white sections of *Arabidopsis msh1* leaves (Xu, Arrieta-Montiel, et al., 2011; Hofmann, 2011). There is also plastid genome instability upon *MSH1* mutation in the moss *Physcomitrella patens* (Odahara et al., 2017). Mitochondrial and chloroplast morphology and internal structure were altered within the white sections of leaves (Xu, Arrieta-Montiel, et al., 2011). Mitochondrial motion is also qualitatively reduced in green sections of leaves, and almost stationary within white sections (Xu, Arrieta-Montiel, et al., 2011). *msh1* disrupting the function of mitochondrial and chloroplasts has a metabolic influence on the cell, depending on the severity of the phenotype and offspring generation (Shao et al., 2017). Pathways impacted include redox regulation, circadian rhythms, environmental responses and plant immunity (Shao et al., 2017). *MSH1* disruption can also have transgenerational effects and demonstrated epigenetic reprogramming, such as hypermethylation (Virdi et al., 2016).

In order to compromise mitochondrial genetics, we used a mutant line with disrupted *MSH1*. With any effects outside of mtDNA stability in mind, we hypothesised that upon compromising the genetic stability of mtDNA using this mutant, the cell would respond by altering its mitochondrial dynamics and chondriome connectivity. This would happen through an increased level of intermitochondrial connectivity, which in turn would allow increased sharing of genetic material between mitochondria, allowing them to access different genomic sequences and template strands– compensating for this loss of genetic integrity. Increased connectivity may also allow the increased sharing of metabolites between these organelles, supporting normal function even with compromised ability to encode the most bioenergetically necessary protein subunits, and overcome metabolic and other stresses upon

the cell from the disruption of *MSH1*.

In order to characterise mitochondrial dynamics and connectivity, we crossed mitochondrially-localised GFP into *msh1 A. thaliana*, and used single-cell confocal imaging, tracking, computational analysis and network science to analyse mitochondrial behaviour. We compared the results to wild-type mtGFP, and also to the physical mutant mtGFP-*friendly*, to evaluate where *msh1* mutants reside on the Pareto front between intermitochondrial connectivity and even cellular spacing (Chustecki, Etherington, et al., 2021).

3.2 Methods

3.2.1 Plant growth and crossing

Arabidopsis thaliana msh1 mutant seeds were ordered from NASC http://arabidopsis.info/StockInfo?NASC_id=3372 reference number CS3372. The line contains the *chm1* and *gl1* polymorphisms, with the *chm1* mutation within the *MSH1* gene locus (AT3G24320), and homozygous recessive. The point mutation causes a null allele of *MSH1* (Wu et al., 2020; Abdelnoor, Yule, et al., 2003). This line was developed by George Redei (Rédei, 1973; Rédei and Plurad, 1973) and subsequently used in (Wu et al., 2020; Xu, Arrieta-Montiel, et al., 2011; Martínez-Zapater et al., 1992; Abdelnoor, Yule, et al., 2003). Seeds of *Arabidopsis thaliana* with mitochondrial-targeted GFP were kindly provided by Prof. David Logan (Logan and Leaver, 2000).

msh1 and mtGFP seeds were surface sterilized in 50% (v/v) household bleach solution for 4 minutes with continual inversion, rinsed three times with sterile water, and plated onto $\frac{1}{2}$ MS Agar. Plated seeds were stratified in the dark for 2 days at 4°C. Seedlings were grown in 16hr light/8hr dark at 21°C for 4-5 days, before transferal to 4:2:1 compost-vermiculite-perlite mixture, and grown until first buds developed.

Crossing technique followed the Browse et al. (1993) protocol, with mtGFP plants as the pollen donor and *msh1* accepting. Pollinated stigmas were wrapped gently in plastic wrap and siliques left to develop. F1 seeds from successful crosses were plated and sown to soil as above, leaf samples collected for DNA extraction, and F2 seeds harvested. F2 seeds were sown onto 50µg/ml^{-1} Kanamycin $\frac{1}{2}$ MS plates, selecting for individuals carrying the fluorescence construct (Logan and Leaver, 2000), and grown on soil as before. Leaf samples were not taken from F2 samples due to laboratory access restrictions during the COVID-19 pandemic. F3 and F4 seeds were grown in the same way, with leaf samples taken.

3.2.2 DNA extraction

Quick DNA extraction was performed on young leaf samples (2-3 weeks old, age dependant on growth rate, slower in *msh1* line). Leaf samples were macerated with a pipette tip in 40µl Extraction Buffer (2.5mL 2M Tris-HCl, 500µL 1M EDTA, 6.25mL 2M KCl, made to 50mL with ddH_2O). Samples were then incubated in a heat block for 10min at 95°C. 40µl Dilution buffer was then added (3% BSA (1.5g in 50mL), filter sterilised), and samples spun down at 13000rpm for 60s before storing at -20°C.

3.2.3 Primer design

The loss of proper function of the *MSH1* gene comes from an ethyl methanesulfonate-derived mutant allele *chm1-1* in the 4th exon of chromosomal region At3g24320. The single nucleotide change comes at a Gln codon CAG → stop codon TAG. Using the dCAPS protocol laid out in Neff et al. (1998), careful primer design was used to introduce a novel restriction site based around the SNP in this region. BsrGI cuts at the restriction site pictured in Figure 3.2.A.

A reverse primer (RP1) (5'AAACTTCGCGTGGAAACCTTGACTTAATGT 3') designed to run into the SNP site was designed using dCAPS finder 2.0 (Neff et al., 1998), and the forward primer (FP1) (5'CATCTCACCTTCTAGATGTCAGCCTTT3') was designed within a 100bp region 200bp upstream of the restriction site (Figure 3.2.B). By design, BsrGI will cut a region of 30bp from the 293bp element, producing one larger (260bp) and one smaller (∼30bp) fragment compared to the WT single fragment.

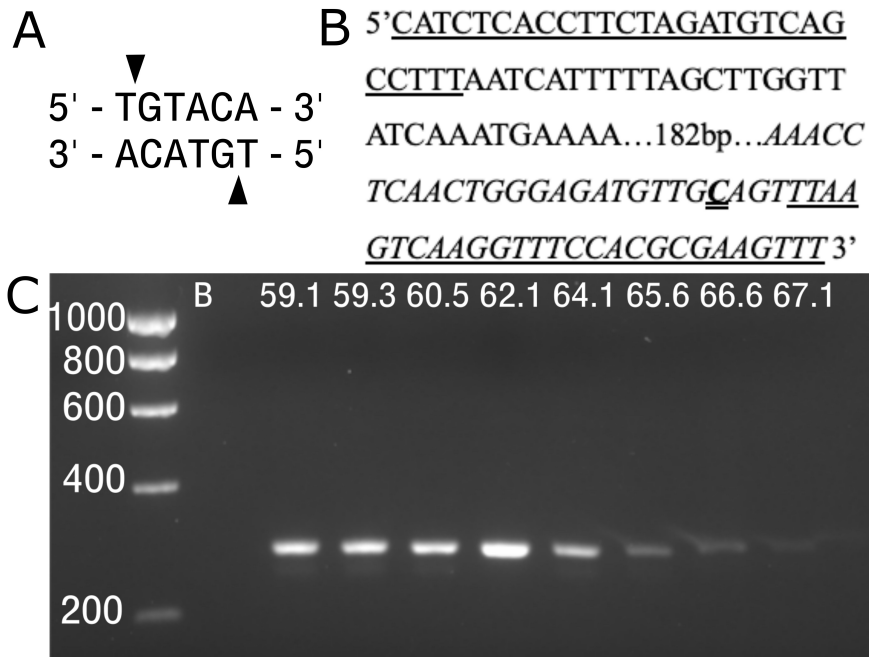

Figure 3.2: Technique summary for genotyping *msh1* lines. (A) Cut site for restriction enzyme BsrGI. (B) Genotyping primers in situ with single base pair mutation site (double underline), forward and reverse primers (underlined) within introns (italics) and exons of chromosomal region AT3G24320. (C) Agarose gel image showing the 8 temperatures (°C) tested for optimising primer annealing temperature, on Col-0 samples.

3.2.4 PCR and restriction digest

Samples for PCR were prepared with 6.25µL DreamTaq Green PCR Master Mix [ThermoScientific], 4.5µL nuclease-free H_2O, 0.75µL each forward and reverse primers (at 10µM working stock), and 1.0µL DNA suspension. Blank samples and a control of Col-0 DNA were always included. PCR was carried out with an initial denaturation stage of 95°C, 30-35 cycles of denaturation (95°C, 30sec), annealing (62.1°C, 1min, calculated using a gradient PCR, Figure 3.2.C), and extension (72°C, 1:30min) with a final elongation hold of 72°C (5min). Product stored a 4°C until used.

Restriction digest directly used half (5µL) of PCR product for each sample, added

to 1.5µL Cutsmart buffer [NEB], 0.2µL BsrGI restriction enzyme [NEB], 8.3µL nuclease-free H_2O. Samples were then incubated at 37°C overnight.

Gels were prepared with the desired agarose percentage dissolved in 1x TBE, and EtBr added as 1/30 (v:v) to the agarose mixture before pouring. Samples were loaded for gel electrophoresis by using alternating undigested (~5µL)/digested samples (10µL), and ladders of 100bp [NEB, 500µg/ml], and 1kb HyperLadder [Bioline].

3.2.5 Sequencing

Sequencing work was undertaken by my colleague Ross Etherington (Chustecki, Etherington, et al., 2021). Sequencing of candidate line 11.9.2 used one F3 sample, and three offspring F4 samples. The region of interest was flanked by FP2 (5'TTGGACCCTAGCTTGAGGAA 3') and RP2 (5'ATCGAAGACCACCAAAAGGA 3'), and amplified using PCR with Phusion high-fidelity DNA polymerase (NEB CATNO.M0530S). PCR products were then purified using QIAquick PCR Purification Kit (Qiagen) and sequenced from primer FP2 using am ABI 3730 capillary sequencer (Applied Biosystems). Sequences were aligned using ClustalW alongside the TAIR references genome for *A. thaliana*.

3.2.6 Cell morphology quantification

Area (µm^2), length and width (µm) of individual cells were measured using ImageJ (Fiji), by manually outlining the cell using the free selection tool, or drawing using the straight line tool. Individual mitochondria were counted within the cell using the Trackmate tracks output (Tinevez et al., 2017). By collecting the number of trajectories frame by frame throughout video time, a mean number of tracked mitochondria was calculated, as well as the standard deviation.

3.3 Results

3.3.1 Construction and validation of mtGFP-*msh1*

In order to image mitochondrial dynamics of *msh1* plants in real time, mutant plants were crossed with those carrying the mtGFP transgene (see section 3.2). This crossing followed the schematic illustrated in Figure 3.3. The first generation (F1) post-crossing seeds were collected and grown up on ordinary 1/2 MS agar, with F2 seeds collected and named line 1,2,3..etc. F2 seeds were grown up on Kanamycin selection plates (selecting for mtGFP transgene construct (Logan and Leaver, 2000)), as seen in Figure C.5, and transferred to soil. No samples could be taken for these plants due to laboratory access restrictions, due to the COVID-19 pandemic. F3 seeds were again grown on selection plates and can be seen in Figure C.6. Samples were taken for DNA extraction, results of genotyping of this generation can be seen in Figure C.3. Candidate lines from the results of this sampling were 11.1.3, 11.2.3, 9.2.2, 11.9.2, 15.1.3 and 15.1.1. Line 11.2.3 did not develop fully enough to produce viable seeds.

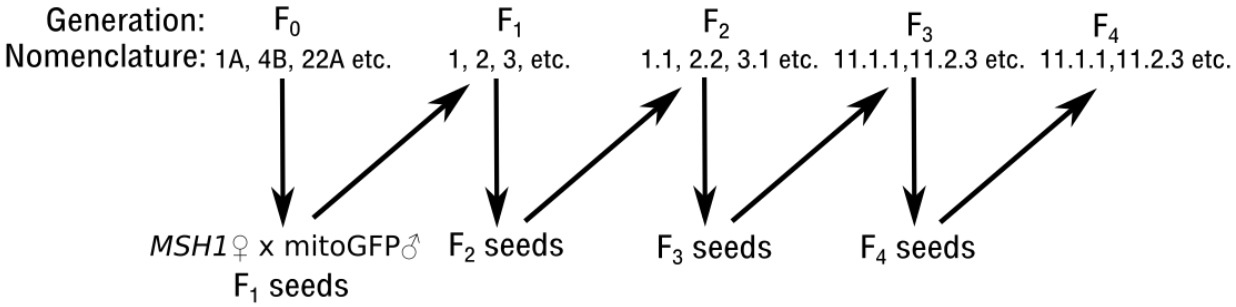

Figure 3.3: Schematic of generations following initial cross and labelling of samples and seeds.

All other candidate lines were taken forward to the F4 generation, keeping the same line reference. These lines were grown on selection plates (Figure C.7), and phenotyped. The

msh1 mutation confers upon the plant a variegated phenotype, due to its dual localisation to mitochondria and chloroplasts, where it disrupts chloroplast development (phenotypes of all three lines used and Col-0 can be seen in 3.5). Rosette images can be seen in Figures C.8, C.9, C.10, C.11, C.12, and Col-0 control can be seen in C.13. These F4 plants were also genotyped, and this can be seen in Figure C.4. Based on these results, the lead candidate line was 11.9.2, looking to be homozygous for *msh1*, all individuals at this generation being variegated, as well as carrying the mtGFP fluorescence construct.

To further validate the candidate line, sequencing was performed on one 11.9.2 F3 sample (see section 3.2). This confirmed the presence of the SNP within the fourth exon of genomic region AT3G24320, leading to a nonsynonymous glutamate → stop codon change (Figure 3.4). Three F4 offspring samples of this line also had the same SNP at the same position, validating the genetic makeup of the mtGFP-*msh1* candidate line.

3.3.2 Mitochondrial dynamics are altered in mtGFP-*msh1*

After validating the genetic makeup of the mtGFP-*msh1* cross, the dynamics of fluorescent mitochondria were imaged under the confocal microscope (Figure 3.6).

Not all cells within each field of view had motile populations of mitochondria, although the occurrence of these non-motile mitochondria were not quantified between wild-type and *msh1* cells. As with the set of wild-type cell samples, often multiple cells were found in the same field of view, in which case they are also analysed and are classed within statistical analyses as independent samples.

Applying the same principles and methods as in Chapter 2, the physical dynamics of mtGFP-*msh1* were quantified. Comparisons were made between this recombination surveillance mutant and wild-type mtGFP. To begin with, the number of discrete mitochondria

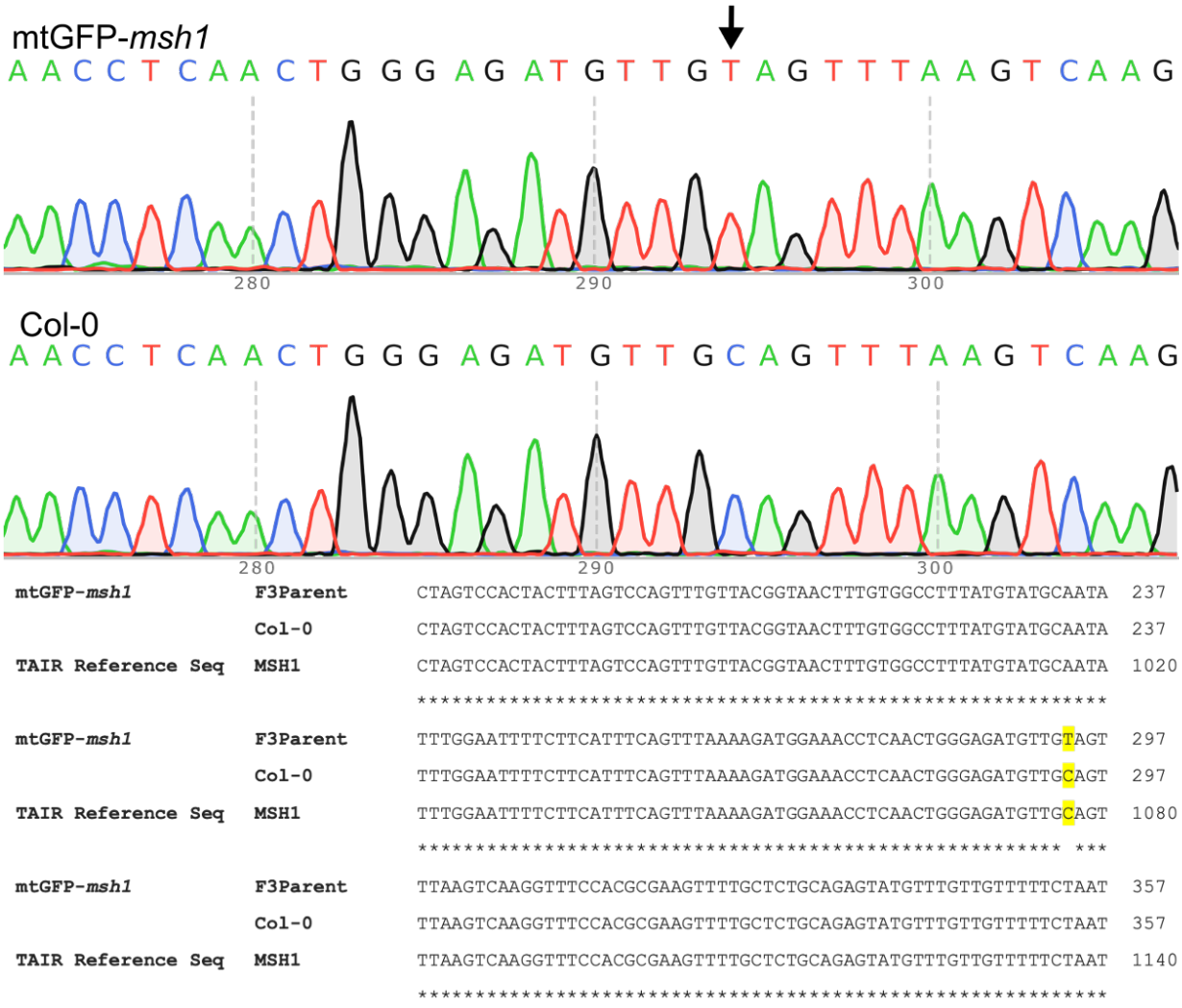

Figure 3.4: Sequencing alignment of candidate line 11.9.3 F3 sample. Upper panel alignment peaks demonstrate the presence of homozygous C→T nucleotide change (arrow). This SNP leads to CAG (glutamate) to TAG (stop) change. Single peaks at each base demonstrate homozygosity. Lower panel shows alignment of base pair reads of mtGFP-*msh1* F3 parent, Col-0 sample, and the TAIR reference genome at the *MSH1* gene. SNP position highlighted in yellow. Reproduced from Chustecki, Etherington, et al. (2021).

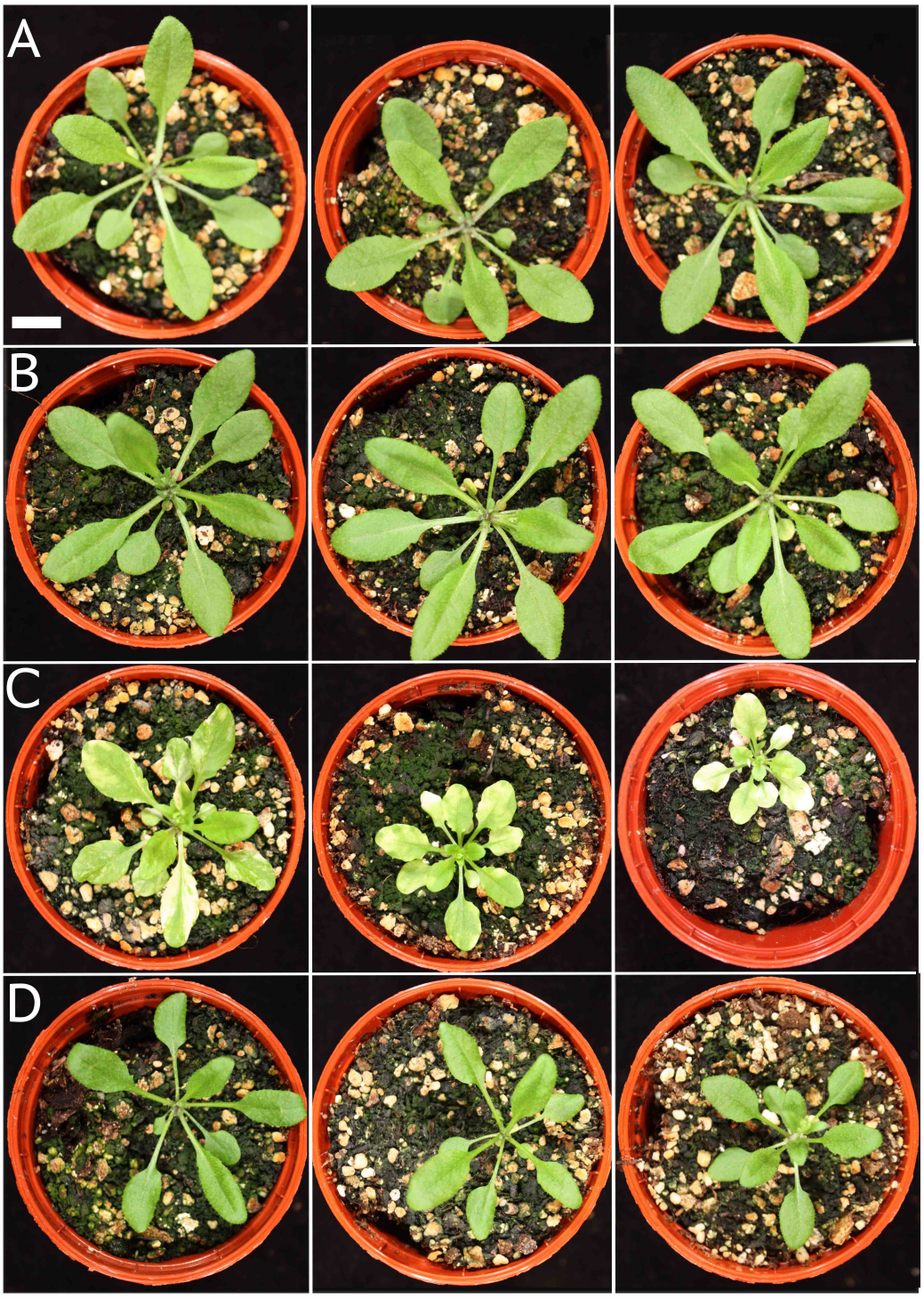

Figure 3.5: Rosette images of the different genotypes demonstrate the extent of the whole-organism alteration for both mutants affecting genetic or physical states of mitochondria. From top to bottom; (A) Col-0, (B) mtGFP wild-type, (C) mtGFP-*msh1*, (D) mtGFP-*friendly*. Scale bar = 1cm. Reproduced from Chustecki, Etherington, et al. (2021).

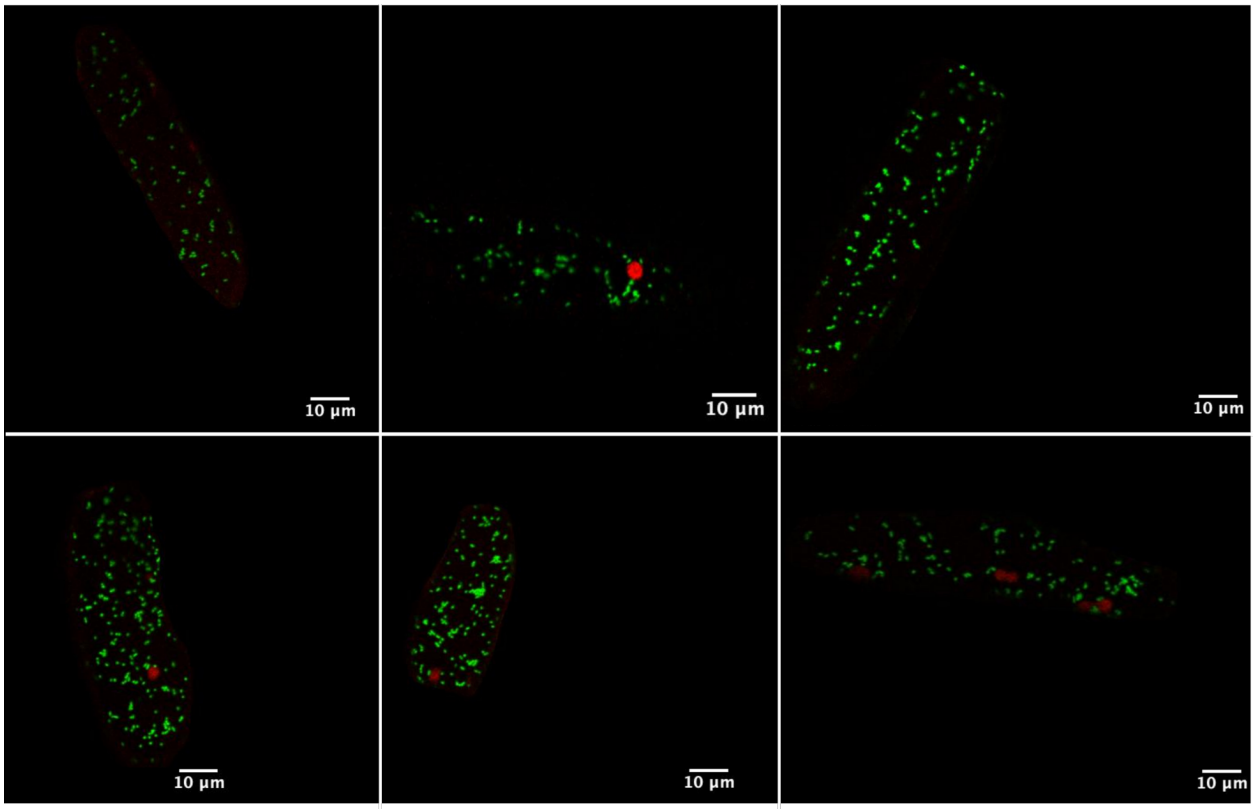

Figure 3.6: Fluorescent mitochondria in the mtGFP-*msh1* cross as viewed under the confocal microscope. Gallery of single cell confocal micrographs of mtGFP-*msh1*, green = mtGFP tagged mitochondria, red outline = propidium iodide stained cell walls, dense red spots = chloroplasts. Scale bar = 10µm

within each cell, as well as cell area, were measured (Figure 3.7, see section 3.2). Comparisons across the three genotypes (mtGFP, mtGFP-*msh1*, mtGFP-*friendly*) showed no significant difference in number of mitochondria or cell size (Kruskal-Wallis test, $p>0.05$)).

Looking to the dynamic motion of these organelles, when the physical statistics of mitochondrial motion are compared between wild-type mtGFP and mtGFP-*msh1*, the perturbation of the *msh1* mutation to the system becomes apparent. Overall intermitochondrial distance, representative of how evenly spread mitochondria are throughout the cell, is significantly reduced in mtGFP-*msh1* cells (Figure 3.8.A) (Wilcoxon test, $p<0.05$). The median

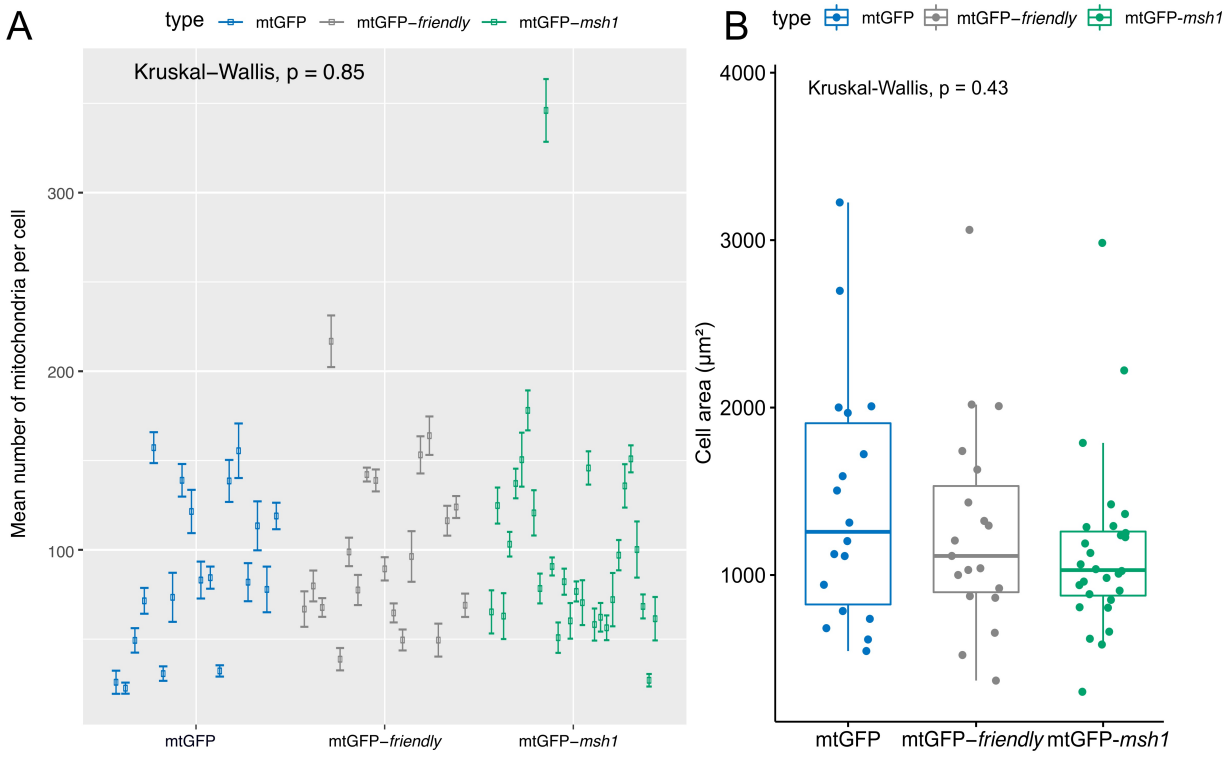

Figure 3.7: Quantification of number of mitochondria and cell area across all samples for all genotypes. A) Number of discrete mitochondria within the cell, averaged over all frames in each sample (mtGFP n= 18, mtGFP-*friendly* n= 19, mtGFP-*msh1* n= 28), with error bars representing standard deviation. B) Comparison of two-dimensional cell area (µm^2) between the three genotypes using the Kruskal-Wallis test. Boxplots represent the median and 25th/75th percentile, with whiskers showing the smallest/largest value within 1.5x the interquartile range. P-values of both plots represents Kruskal Wallis test outcome across all three genotypes. Part B reproduced from Chustecki, Etherington, et al. (2021).

values for overall mitochondrial mean speed is also lower for mtGFP-*msh1*, but this didn't reach significance using a conservative non-parametric test (Figure 3.8.B). Mean colocalisation time is increased in mtGFP-*msh1*, meaning mitochondria within this mutant spend a longer time associated with each other over frame time (Figure 3.8.C). There is no significant difference between the mean area travelled by mitochondria across video time (Figure 3.8.D).

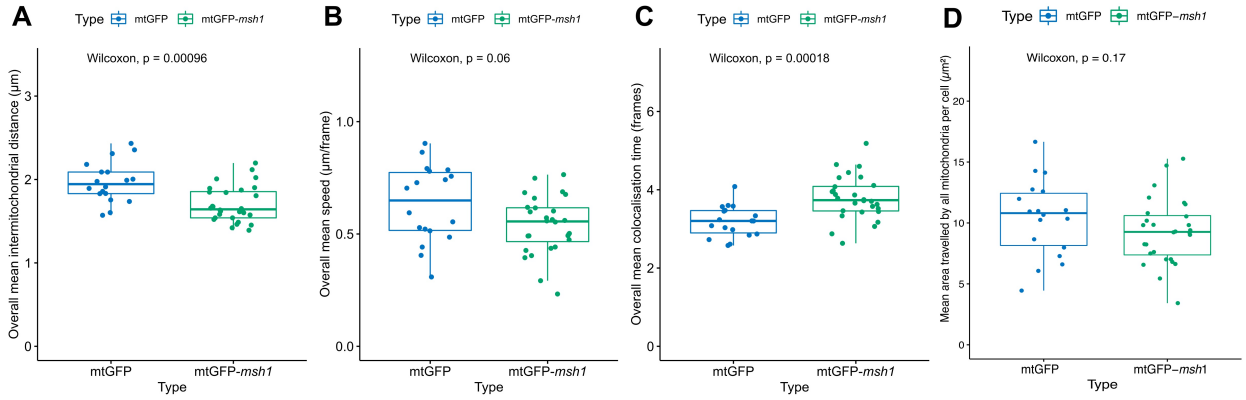

Figure 3.8: Physical statistics (A-D) compared between mtGFP and mtGFP-*msh1*. (mtGFP n= 18, mtGFP-*msh1* n= 28), Boxplots represent the median and 25th/75th percentile, with whiskers showing the smallest/largest value within 1.5x the interquartile range. P-values of both plots represents Wilcoxon test outcome between genotypes. Parts A-C reproduced from Chustecki, Etherington, et al. (2021).

3.3.3 Alterations in physical dynamics within mtGFP-*msh1* affect social dynamics of mitochondria

We next asked, do the perturbed physical dynamics of mtGFP-*msh1* mitochondria described above facilitate social connectivity? To investigate this, encounter networks tracking inter-mitochondrial connectivity were built. Using the same methodology laid out in Chapter 2, encounters of close proximity between individual mitochondria are stored, and can be used to build-up historical networks of connectivity across the mitochondrial population, much like social networks. As previously, proximity here is not fusion between individual mitochondria, but a close colocalisation between mitochondria– a prerequisite for fusion and sharing of metabolites or even genetic material. Here the network statistics gathered can be used to inform of any differences in the connectivity patterns between mtGFP wild-type mitochondrial dynamics and those within mtGFP-*msh1*.

One method of measuring large-scale network connectivity is through the quantification of separate connected components, the number of disconnected subgraphs (see Section 2.2)

The number of connected components across frame time within mtGFP-*msh1* does not differ from that of the wild-type across frame time (Figure 3.9.A). There is no statistically detectable difference in node or edge number at those time frames, shown in Figure 3.10, except for the edge number at frame 10, where the samples from mtGFP-*msh1* show an increased edge number (Figure 3.10.B.i). mtGFP-*msh1* also shows an increase in the mean size and maximum size of connected components at this early frame 10 (Figure 3.9.B.i, C.i). This higher connectivity is visible in three randomly selected samples of *msh1* cells at frame 10 in Figure 3.11.B.i, compared to the same for mtGFP wild-type, Figure 3.11.A.i. This increased connectivity defined by connected component size demonstrates that at least at very early time frames, the reduced intermitochondrial distance and increased colocalisation time of mtGFP-*msh1* increases the number of encounters between individual mitochondria. However, this relationship does not stand over longer frame times, and at frames 50, 100, and 120 of the videos we see little difference across these connectivity values for both genotypes (Figure 3.9, 3.10). The build-up of networks over time can be seen in (Figure 3.11, with mtGFP wild-type as 3.11.A, and mtGFP-*msh1* as 3.11.B.). This similarity looks to be driven by the increase in size of the wild-type components, and as the number of components between the genotypes did not differ at the early time frame suggest mtGFP-*msh1* had a similar number, but larger connected component set before the full effect of dynamics over time allowed a similar build-up between these genotypes.

Alongside connected component size and number, node degree and network efficiency were quantified. These statistics can be seen for the final frame of each video in Figure 3.12. Mean degree, the average number of immediate neighbours each node within the network has, is significantly higher for mtGFP-*msh1* encounter networks (Figure 3.12.A).

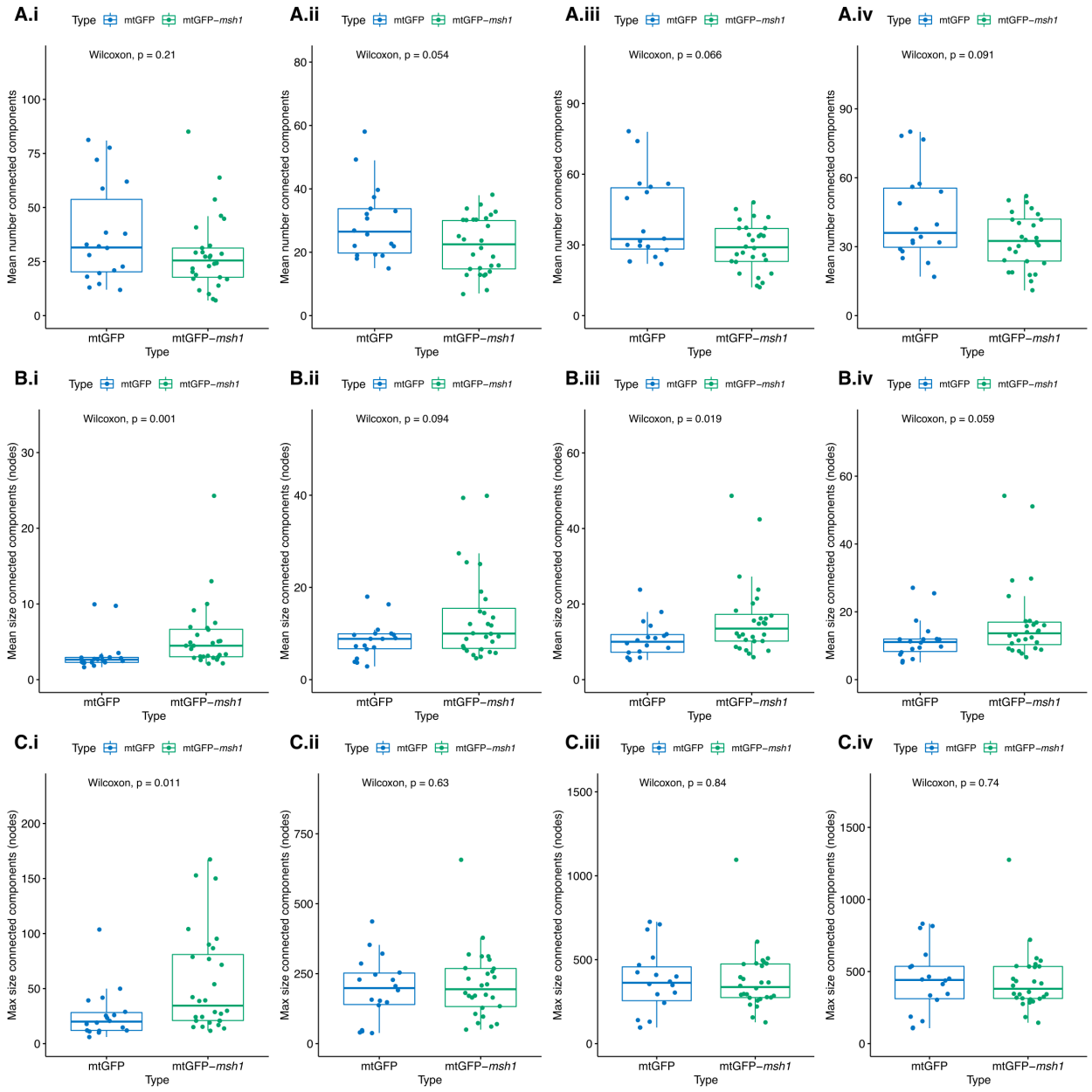

Figure 3.9: Mean number, mean size and maximum size of connected components over time (A-C) compared between mtGFP and mtGFP-*msh1* show little difference across frame time. Each value is taken from snapshots of networks at frame times (i) 10, (ii) 50, (iii) 100, (iv) 120 (232 secs). (mtGFP n= 18, mtGFP-*msh1* n= 28), Boxplots represent the median and 25th/75th percentile, with whiskers showing the smallest/largest value within 1.5x the interquartile range. P-values represent Wilcoxon test outcomes across both genotypes.

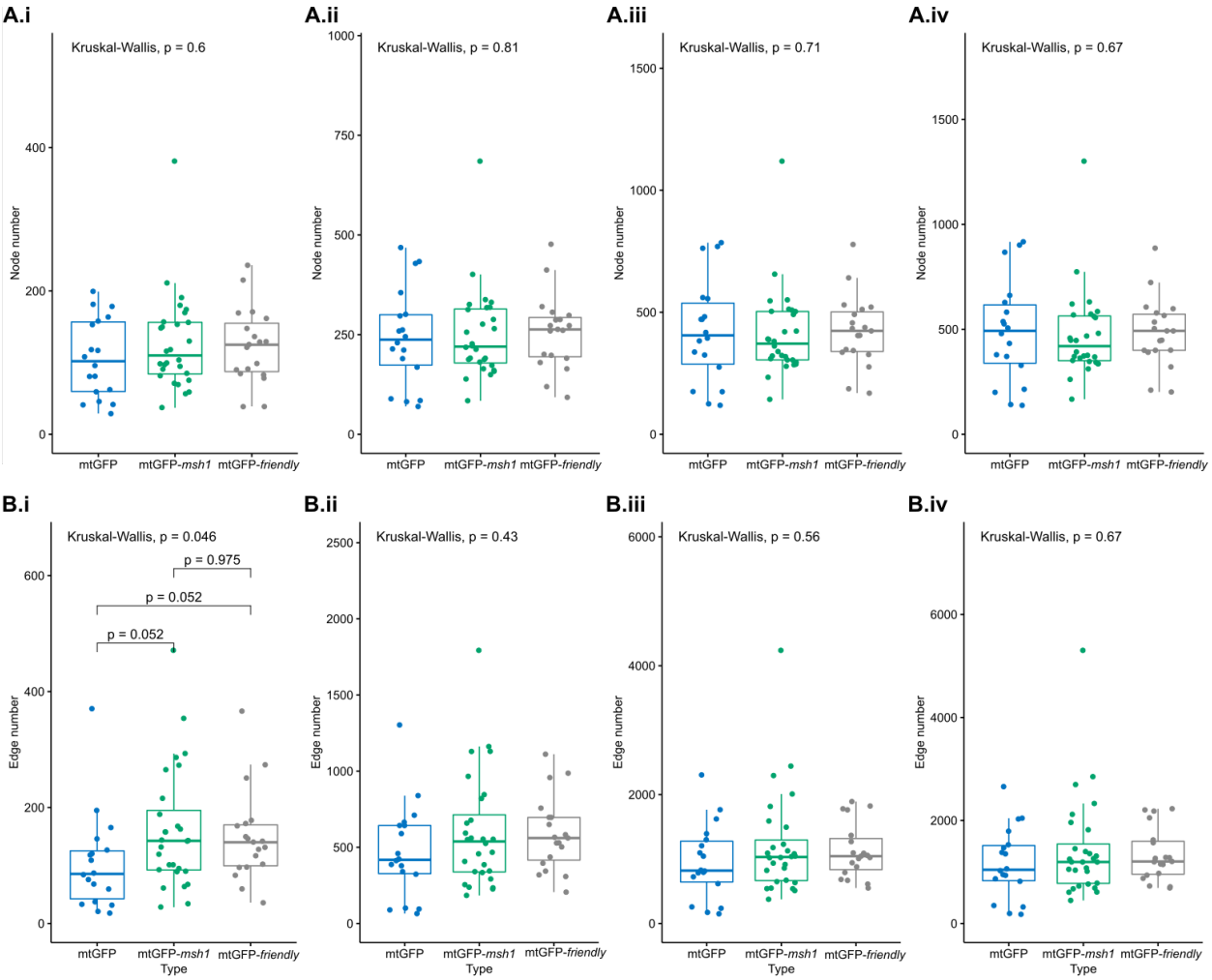

Figure 3.10: Node (A) and edge (B) number between mtGFP, mtGFP-*msh1* and mtGFP-*friendly* show little difference. Edge and node number are taken from snapshots of networks at frame times (i) 10, (ii) 50, (iii) 100, (iv) 120 (232 secs). (mtGFP n= 18, mtGFP-*msh1* n= 28, mtGFP-*friendly* n= 19) Boxplots represent the median and 25th/75th percentile, with whiskers showing the smallest/largest value within 1.5x the interquartile range. P-values of both plots represents Wilcoxon test outcome between genotypes and pairwise p-values are false discovery rate adjusted outcomes of a Post-hoc Dunn test, without multiple hypothesis correction across statistics. Reproduced from Chustecki, Etherington, et al. (2021).

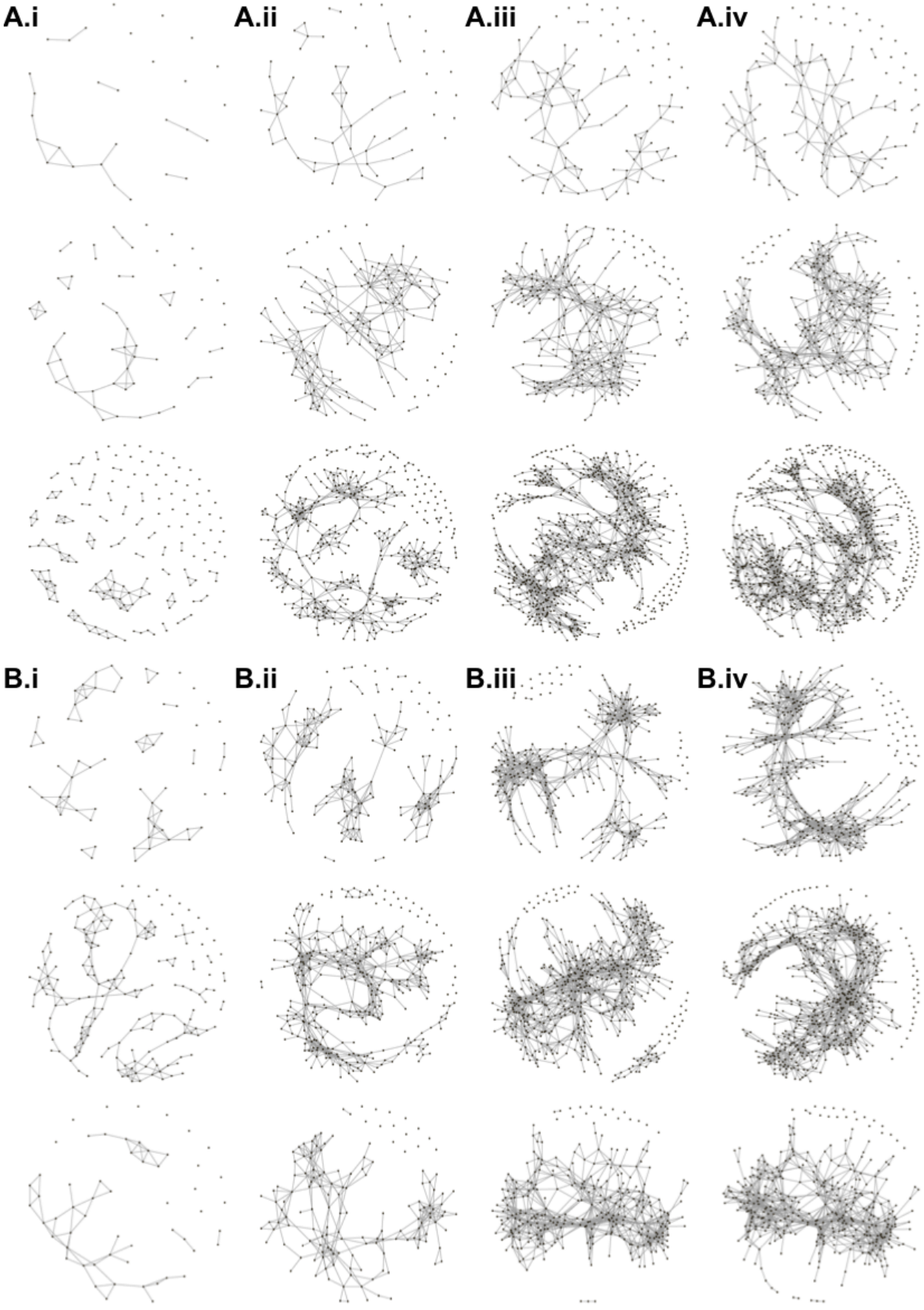

Figure 3.11: (See next page)

Figure 3.11: Representations of networks over time demonstrate build-up as encounters occur. Representations of networks over time demonstrate build-up as encounters occur. Encounter networks of (A) mtGFP (B) mtGFP-*msh1* build-up over frame times (i) 10, (ii) 50, (iii) 100, (iv) 120 (232 secs). 3 (2 A.iv, 1 B.iv) networks reproduced from Chustecki, Etherington, et al. (2021).

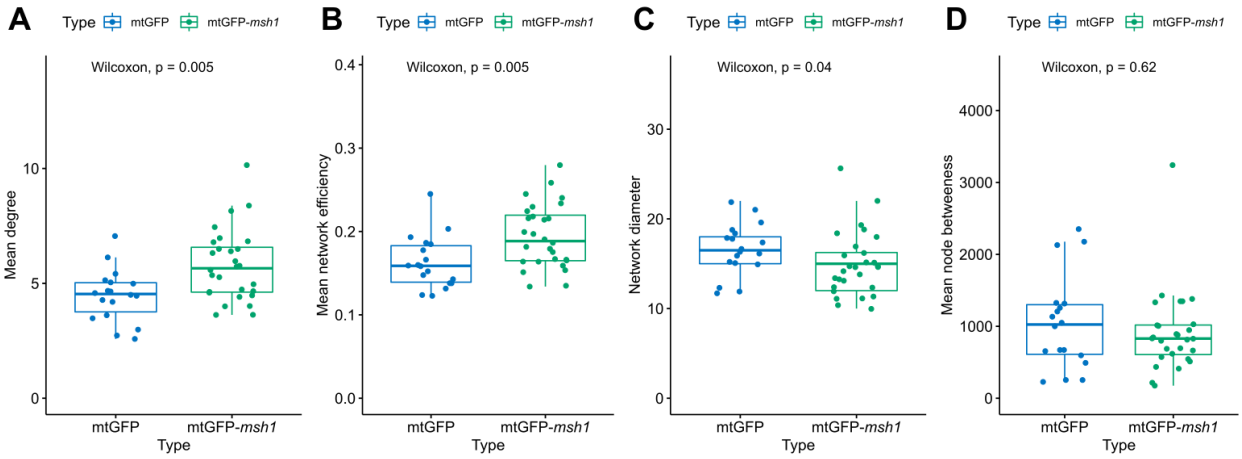

Figure 3.12: Social statistics reveal increased connectivity across mtGFP-*msh1*. Each point represents a summary statistic (A-D) for one cell (mtGFP n= 18, mtGFP-*msh1* n= 28). Boxplots represent the median and 25th/75th percentile, with whiskers showing the smallest/largest value within 1.5x the interquartile range. P-values represent Wilcoxon test outcomes across both genotypes. Each individual point is from a network corresponding to an observed time window of 233 seconds. Reproduced from Chustecki, Etherington, et al. (2021).

Therefore, the mitochondrial population within mtGFP-*msh1* samples share more encounters across the same frame time than those in the wild-type mtGFP. Network efficiency is also increased in mtGFP-*msh1* (Figure 3.12.B). This value describes the ability of the network to exchange information. It is a quantification of the average reciprocal lengths of the shortest paths between each pair of mitochondria in the network. If paths between mitochondria

(nodes) are short, the network efficiency is high, and if the paths are long, or the network is disconnected, the network efficiency will be low. Therefore, the increased network efficiency, alongside increased mean degree supports our hypothesis that mtGFP-*msh1* prioritises the sharing of contents between mitochondria. This could be in order to mitigate damage to the mtDNA through increased sharing of mitochondrial contents.

Other useful network statistics for quantifying connectivity are network diameter and betweenness centrality. The first of these is the length in edges of the longest route across the network. For networks of a similar size, a shorter diameter may mean the network is more compact, and there are shorter routes from one side to the other. For networks with a larger diameter this may mean a less locally well-connected network, or a forced path due to only a few edges joining large clusters. For these experiments, we found that mtGFP-*msh1* had a significantly decreased network diameter (Figure 3.12.C). However, it must be noted that this significant difference was not retained after multiple hypothesis testing. For the final social summary statistic, we looked at mean node betweenness centrality, the number of times the shortest path between any two nodes passes through the node of interest, averaged over all nodes in the network [1]. For this data there was no significant difference found between betweenness centrality for mtGFP and mtGFP-*msh1* (Figure 3.12.D).

These networks are readouts of dynamic motion of organelles over time, and so build-up over time as more encounters occur. This means that network summary statistics such as those described here alter with time (as explored in Chapter 2). Here we explore changes in statistics over time between mtGFP-*msh1* and wild-type mtGFP (Figure 3.13). The increased degree of mtGFP-*msh1* networks is consistent over time (Figure 3.13.A), with network efficiency increasing at later time frames (Figure 3.13.B). Network diameter is similar

[1] This statistic only reports how many shortest paths a node is situated on, and so is not heavily implemented in this project. For this statistic to report information transfer across the network, an assumption that information travels only on the shortest path would be made.

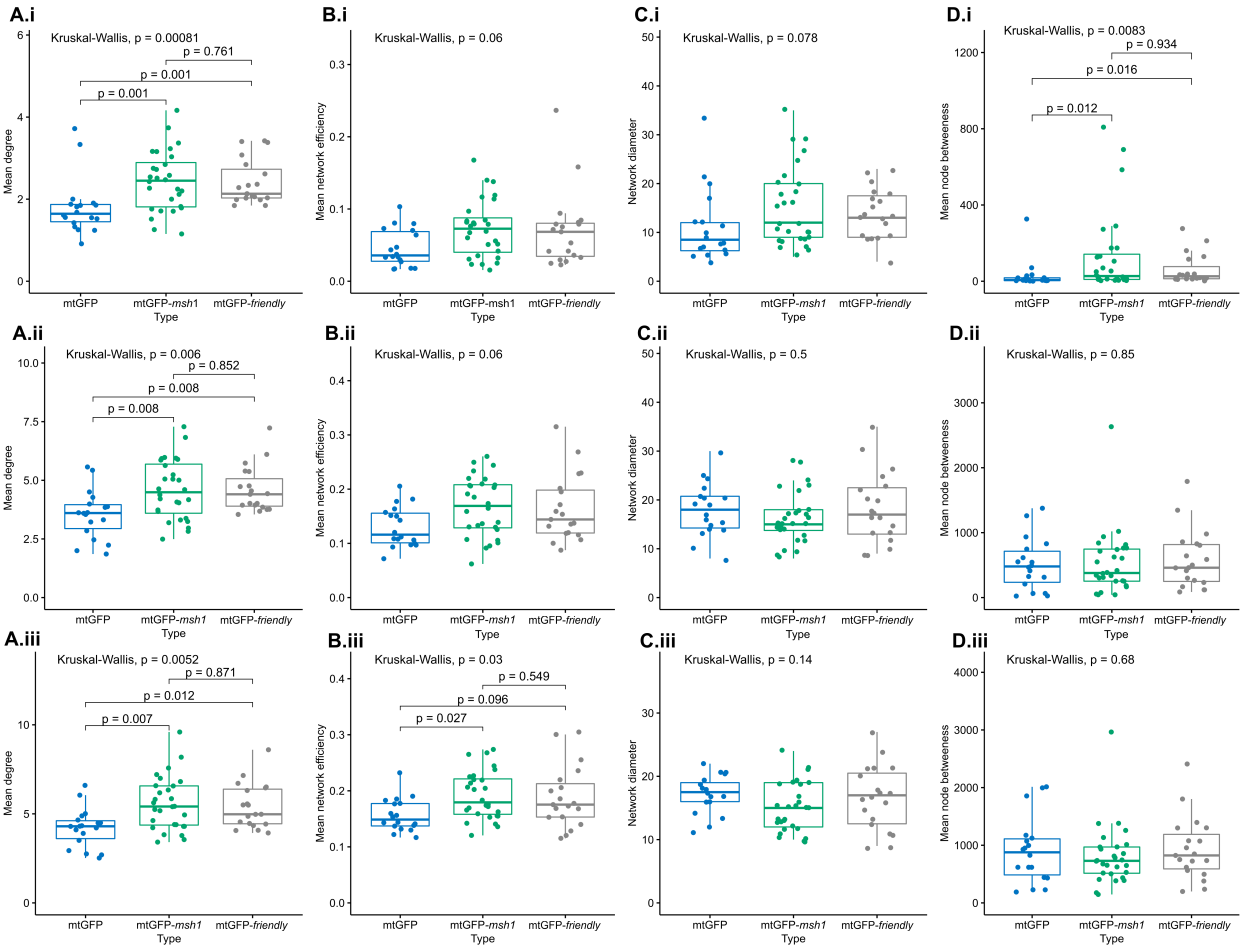

Figure 3.13: Social statistics are time-dependant. Each point represents a summary statistic (A-D) for one cell (mtGFP n= 18, mtGFP-*msh1* n= 28, mtGFP-*friendly* n = 19), and values are shown over frames (i) 10 frames, (ii) 50 frames, (iii) 100 frames. P-values represent Kruskal Wallis test outcomes across all three genotypes, and pairwise p-values are false discovery rate adjusted outcomes of a post-hoc Dunn test, without multiple hypothesis correction across statistics. Boxplots represent the median and 25th/75th percentile, with whiskers showing the smallest/largest value within 1.5x the interquartile range. Frames correspond to 19, 97 and 194 seconds, respectively. P-values are for individual experiments. Reproduced from Chustecki, Etherington, et al. (2021).

between genotypes across time (Figure 3.13.C), with only the previously mentioned final frame being significantly different between mtGFP and mtGFP-*msh1* (Figure 3.12.C). It is interesting to note that at the early time frame, betweenness centrality (defined above) is significantly increased in mtGFP-*msh1* versus mtGFP wild-type, although this could be due to the three high betweenness outliers in this sample cell population (Figure 3.13.Di).

Overall, these social summary statistics are quantifications of network features that allow for exchange of mitochondrial contents. Finding an increased degree, increased network efficiency and reduced network diameter for mtGFP-*msh1* shows increased potential for the system to compensate for damage caused by the *msh1* mutation. The affected physical dynamics, where even spread is sacrificed for more time spent together benefits the social connectivity across the population of mitochondria, therefore increasing the potential for contents sharing and opportunities for mtDNA exchange.

3.3.4 The collective dynamic response of mitochondria within a genetic mutant resembles that of a physical mutant

After analysing the physical and social response of mitochondria in a mutant whose mitochondrial genetics are compromised, we explored whether this resembles the response of a physical mutant where mitochondrial dynamics are perturbed. For this, we looked in more depth at the mtGFP-*friendly* mutant. This mutant has been shown to pose a transient challenge to the physical-social trade-off demonstrated in Chapter 2 and Chustecki, Gibbs, et al. (2021). We ran multiple comparisons across the mtGFP wild-type, mtGFP-*msh1* and mtGFP-*friendly* mutants. Remarkably, there was no significant difference between the physical and genetic mutants in either their physical or social dynamics (Figure 3.14). This lack of significance does not necessarily rule out a difference in effect on mitochondrial dynamics from these two mutants, however the moderate sample sizes (mtGFP n= 18, mtGFP-*msh1*

n= 28, mtGFP-*friendly* n = 19) and change compared to wild-type give confidence in the similarities of these physical and genetic mutants. When compared to wild-type mtGFP, both genotypes demonstrated a reduced intermitochondrial distance, increased colocalisation time and increased mean degree, demonstrating two systems that (for different mechanistic reasons) are aiming for increased connectivity between their energetic organelles.

In an earlier section a difference between intermitochondrial mean and mean degree was shown to diminish between mtGFP and mtGFP-*friendly* as video time went on. Between that conclusion and this particular analysis, there are n = 8 more mtGFP samples being used, and here the comparison is one-dimensional in that we are looking at one statistic at a time, rather than upon an axis of two statistics. The temporal diminishing of a difference between degree for mtGFP and mtGFP-*friendly* is still supported here (Figure 3.13), but this does not stand for other network statistics such as network efficiency where the difference between mtGFP and the mutants is more stable - if not increasing - for the mutants over time. Overall, for *friendly* and *msh1*, the magnitude and temporal dynamics of changes to mitochondrial dynamics were similar, hinting at a similar strategy or influence of physical and genetic perturbations upon the mitochondrial population within plant cells.

3.4 Discussion

We investigated the alterations in physical dynamics upon perturbation to a mtDNA recombination surveillance mutant (mtGFP-*msh1*). Our hypothesis that the cell increases the physical connectivity of mitochondria upon genetic perturbation in order to increase exchange of important biomolecules and compensate for this mtDNA disruption is supported by the findings set out in this chapter and in Chustecki, Etherington, et al. (2021). The dynamics and connectivity had a surprising similarity to a physical mutant (mtGFP-*friendly*),

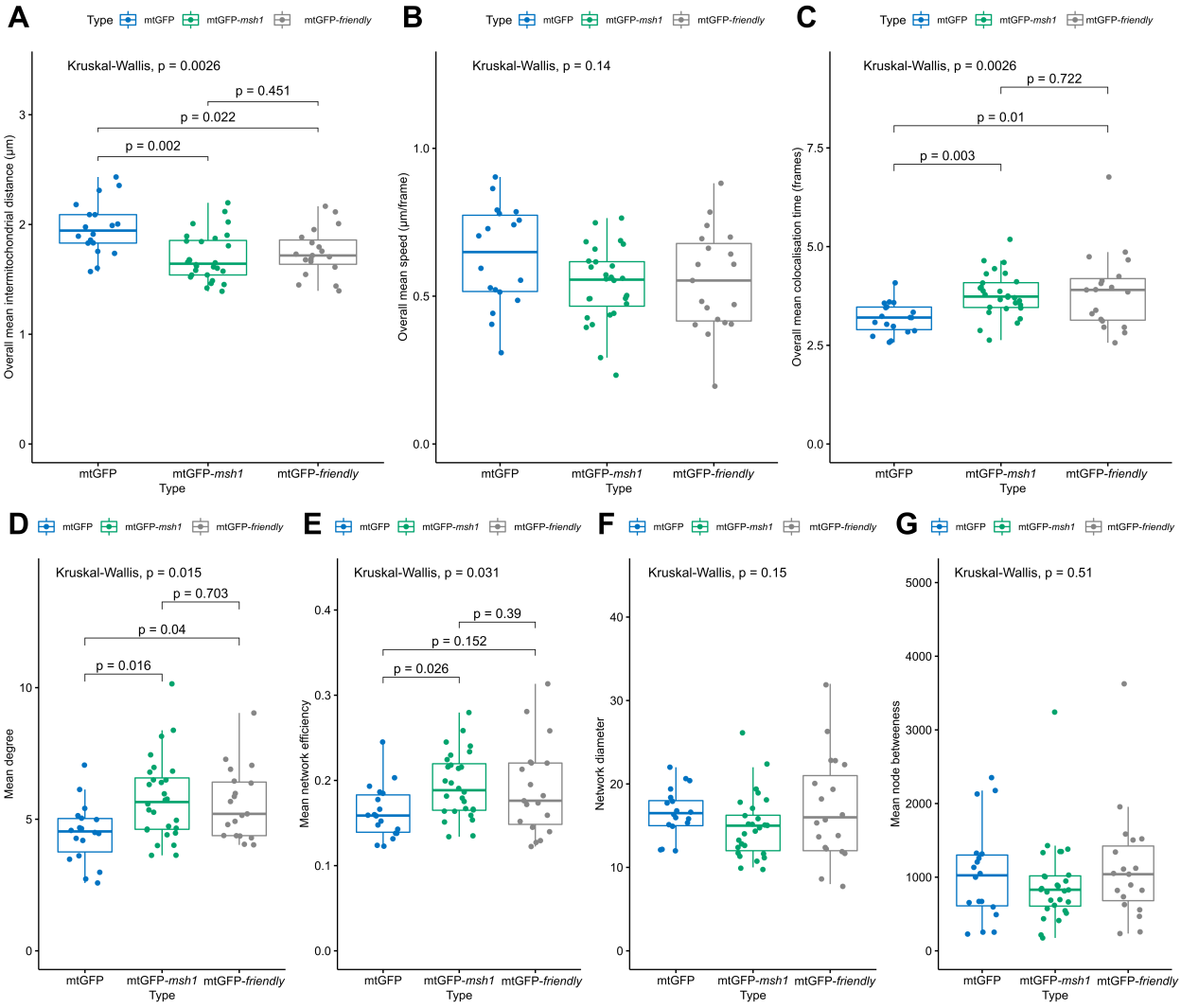

Figure 3.14: Physical and social statistics of mitochondria dynamics in wild-type, a physical mutant and a genetic mutant. Upper plots show overall means of physical statistics taken over all frames of video time, lower plots show social statistics of networks at the final frame of each video, representing 233 seconds. Each point represents the statistic taken from one cell (mtGFP n= 18, mtGFP-*msh1* n= 28, mtGFP-*friendly* n = 19). P-values represent Kruskal Wallis test outcomes across all three genotypes, and pairwise p-values are false discovery rate adjusted outcomes of a post-hoc Dunn test, without multiple hypothesis correction across statistics. Boxplots represent the median and 25th/75th percentile, with whiskers showing the smallest/largest value within 1.5x the interquartile range. P-values are for individual experiments. Reproduced from Chustecki, Etherington, et al. (2021).

even across frame time– highlighting the link between genetic and physical chondriome dynamics.

Overall, mtGFP-*msh1* reduces the even distribution of mitochondria within the cell. This lends some support to our hypothesis that in order to mitigate damage to mtDNA, exchange of genetic material and contents between these organelles is prioritised, even at the detriment of a well-spread mitochondrial population. However, the effects of MSH1 disruption are numerous, trans-organellar, trans-generational and conditional on disruption method used (Shao et al., 2017). These effects include the implications of oDNA disruption, leading to metabolomic effects and influence from dysfunctional chloroplasts and mitochondria. These may differ from cell to cell, and so cell choice is an important factor at play for the detailed network analysis. A broad approach to rectify this would be to characterise the cell-cell difference in mitochondrial motility *from the same seedling*. However, a finer grained approach would be to characterise the cell-cell heteroplasmy in oDNA mutations to characterised the variation between cells of the same sample. Experiments controlling for mitochondrial-specific effects using a complementation line could also be used, maintaining the plastid form of MSH1 (Xu, Arrieta-Montiel, et al., 2011). Or, independent treatments or disruption to mtDNA by mutation could specifically affect mtDNA status, offering useful controls.

Subtle transgenerational effects of mtDNA mutations, and nuclear DNA methylation also should be considered (Xu, Arrieta-Montiel, et al., 2011; Virdi et al., 2016; Wu et al., 2020). Seedlings of the F4 generation were imaged, and as the *msh1* line was used as the pollen acceptor, cytoplasmic mutations may accumulate. Testing the mitochondrial mutations of the generation and line used, as well as quantifying the network statistics across generations would be suitable controls for these effects. However, our lead-order investigation was designed as a scoping experiment to uncover any differences in physical/social dynamics within this particular mutant, so these control experiments are suitable for fur-

ther investigation now we have uncovered these effects upon physical dynamics and social connectivity.

We note the similarity in summary statistics between mtGFP-*msh1* and mtGFP-*friendly*. In each case, we hypothesise on the effect of each mutant as a response to the specific perturbation each puts upon the system. However, to some extent there is overlap. mtGFP-*friendly* has been implicated in autophagy (Ma et al., 2021; Nakamura et al., 2021), which would, in theory remove mtDNA from the chondriome gene pool, linking this protein to genetic dynamics. mtGFP-*msh1* has been implicated in metabolic effects upon plastid/mitochondrial disruption, which could impact the physical dynamics of the chondriome. Therefore there is crossover and links between physical and genetic dynamics of the chondriome, the 'dynamic syncitium'. There is also the possibility of the increased connectivity and reduced dynamic motion of both genotypes (Figure 3.14) being a generalised stress response of the mitochondrial population.

Throughout this chapter, we put forward evidence for the hypothesis that mitochondrial dynamics (as defined by speed, colocalisation time and intermitochondrial distance) in a recombination surveillance mutant *msh1* line are not incompatible with a compensatory response of the organelle to increase connectivity across the chondriome. This is supported by increased connectivity (as defined by node degree, network efficiency and network diameter) across the 'social' network of organellar interactions. This would allow mtDNA recombination and contents mixing, provision of more template strands for repair via homologous recombination and monitoring of mitochondrial health (Christensen, 2014; Edwards et al., 2021; Rose, 2021). A compensatory response can occur at the cellular, organelle and molecular level, with mitochondrial-targeted and motility related proteins encoded by the nucleus, organelle interactions influencing mitochondrial positioning under stress, and alterations in intra-mitochondrial organization and size (Labbé et al., 2014; Eisner et al., 2018). However, other effects of this fascinating mutant need to be further examined in the future with re-

gards mitochondrial dynamics, following from this scoping investigation into the effect on chondriome connectivity.

Chapter Four

Spatial and genetic priorities of bioenergetic organelles

4.1 Introduction

Within plant cells, bioenergetic organelles (mitochondria and chloroplasts) exist as populations. The individual organelles are key energy providers for the cell, and also have their own genomes. They have been shown to interact, and colocalise between themselves and other organelles. Previous results have demonstrated the social and physical priorities of dynamic motion of mitochondrial populations, revealing trade-offs between the two (Chapter 2). The studies described here aim to examine further the social (linking to genetic) priorities of these collective mitochondrial movements, as well as physical priorities, particularly in relation to another bioenergetic organelle, the chloroplast.

Plant mitochondrial physical structure and dynamics (previously described in Chapter 2) are coupled to the genetic structure of mitochondrial DNA (mtDNA) (Chapter 3). Each individual mitochondrion within plant cells carries only a subgenomic molecule of mtDNA i.e. less than the full range of genes encoded by mitochondria. Some carry no mtDNA at all

(Preuten et al., 2010; Takanashi et al., 2006; Johnston, 2019a). mtDNA encodes genes that are vital for bioenergetic function (Johnston and Williams, 2016), meaning that it is essential each mitochondrion has access to either the protein products, mRNA or DNA needed for provision or repair of encoded electron transport subunits. So how do these organelles maintain their full complement of proteins without a full local genome? **One possibility is the exchange of mtDNA upon close physical encounters**. This would allow access to the full complement of mtDNA, and help to maintain mitochondrial proteostasis. Over time, close encounters and exchange of genetic material between individuals would lead to the build-up and emergence of an 'effective' genome. Transient colocalisations can and do occur between the individual mitochondria of plant cells (Chapter 1, (Liu, Weaver, et al., 2009; El Zawily et al., 2014; Chustecki, Gibbs, et al., 2021)). Tracking of close encounter events between individuals can be achieved by using time lapse imaging and network science to build historical encounter networks (See Section 2.2).

The emergent behaviour of these mitochondria is therefore greater than the individual behaviours alone, as the collective dynamics can theoretically allow the build-up of a full effective genome (Giannakis et al., 2021)– something individual, or even pairs of mitochondria could not do alone. In addition, the mitochondrial population interacts with other cellular components. One important process within plants is photorespiration, vital for supporting photosynthetic pathways and removal of phosphoglycolate (2PG) when Rubisco utilises O_2 in high oxygen environments. In order for these processes to occur, metabolites must be exchanged between these organelles, as well as with peroxisomes (Takagi et al., 2011; Bauwe et al., 2010). This exchange is helped by the close colocalistion of these organelles (Jaipargas, Mathur, et al., 2016; Takagi et al., 2011). Close colocalisation can be measured qualitatively (Jouhet et al., 2004) and quantitatively, by for example– sectioning the cell into inner/outer periclinal walls and anticlinal walls, (Islam, Niwa, et al., 2009; Islam, Van Nguyen, et al., 2020), or using the distance (µm) between the chloroplast centroid and the centroids of

surrounding mitochondria (Oikawa et al., 2021), or with the use of photoconvertible colour-changing probes (Baillie et al., 2020).

Currently, it is not clear by how much colocalisation is influenced by the organisation of the cystosol, as an epiphenomenon of the cytosolic structure. For example, the presence of chloroplasts expands the cytosol and disturbs the potential positions mitochondria can occupy. In this preliminary work, we sought to apply a quantitative approach to colocalisation specifically for mitochondria and chloroplasts on a whole cell level, looking at the entire population of mitochondria visible within our imaging field of view and measuring colocalisation to visible chloroplasts. By quantifying mitochondrial position in the whole field of view, we take into account distributional alterations due to cytosolic structures when considering colocalisation. Our approach for investigating evidence for mitochondrial colocalisation to chloroplasts was to ask: given the positions that mitochondria can occupy in cytoplasmic space at any given time, are they more likely to be found per frame in the regions surrounding the chloroplast? Therefore we can control for any expansion of the cytosol and focus on active mitochondrial-chloroplast colocalisation. This method also mitigates the use of additional probes on top of our current imaging setup (subsection 2.2.2).

Using the approaches described here, we aim to further investigate the social, genetic and physical coordination of these organelles, and describe routes of inquiry for uncovering more answers as to why plant mitochondria move the way they do.

4.2 Executive summary

4.2.1 Emergence of effective mtDNA genomes from collective mitochondrial dynamics

Previous work in Chapter 2 has demonstrated the ability of plant mitochondria to form efficient, well connected encounter networks given physical limitations and the need to remain well-distributed within the cell (Chustecki, Gibbs, et al., 2021). We took these characterised wild-type *Arabidopsis* encounter networks forward, and applied a theoretical framework to investigate emergence of an effective genome structure from the physical collective dynamics of these organelles (Giannakis et al., 2021) (Figure 4.1). Our framework shares similarities with other research efforts into dynamic networks in other domains (Moore and Newman, 2000; Cao et al., 2018; Flajolet et al., 1992; Vasudevan et al., 2009).

The theoretical framework was created and analysis undertaken by Dr. Konstantinos Giannakis and Prof. Iain Johnston (University of Bergen) (Further details of the methodology of synthetic encounter network generation and coupon collectors equations can be found in Giannakis et al. (2021)). Firstly, the emergence of effective genomes on the mitochondrial encounter networks of *Arabidopsis* was framed as a network science problem, as seen in Figures 4.2 and Box 1.

A subset of experimental encounter networks were taken from the study in Chapter 2, and were collected as shown in Section 2.2. Each node represents a single mitochondrion, and the edge between them is an encounter, formed when two individuals come within a characteristic physical distance of each other (1.6µm). Within the theoretical framework, each node within the network has two vector labels- G (genome) and H (history). G describes the set of genetic elements each mitochondrion has. H describes the set of genetic elements

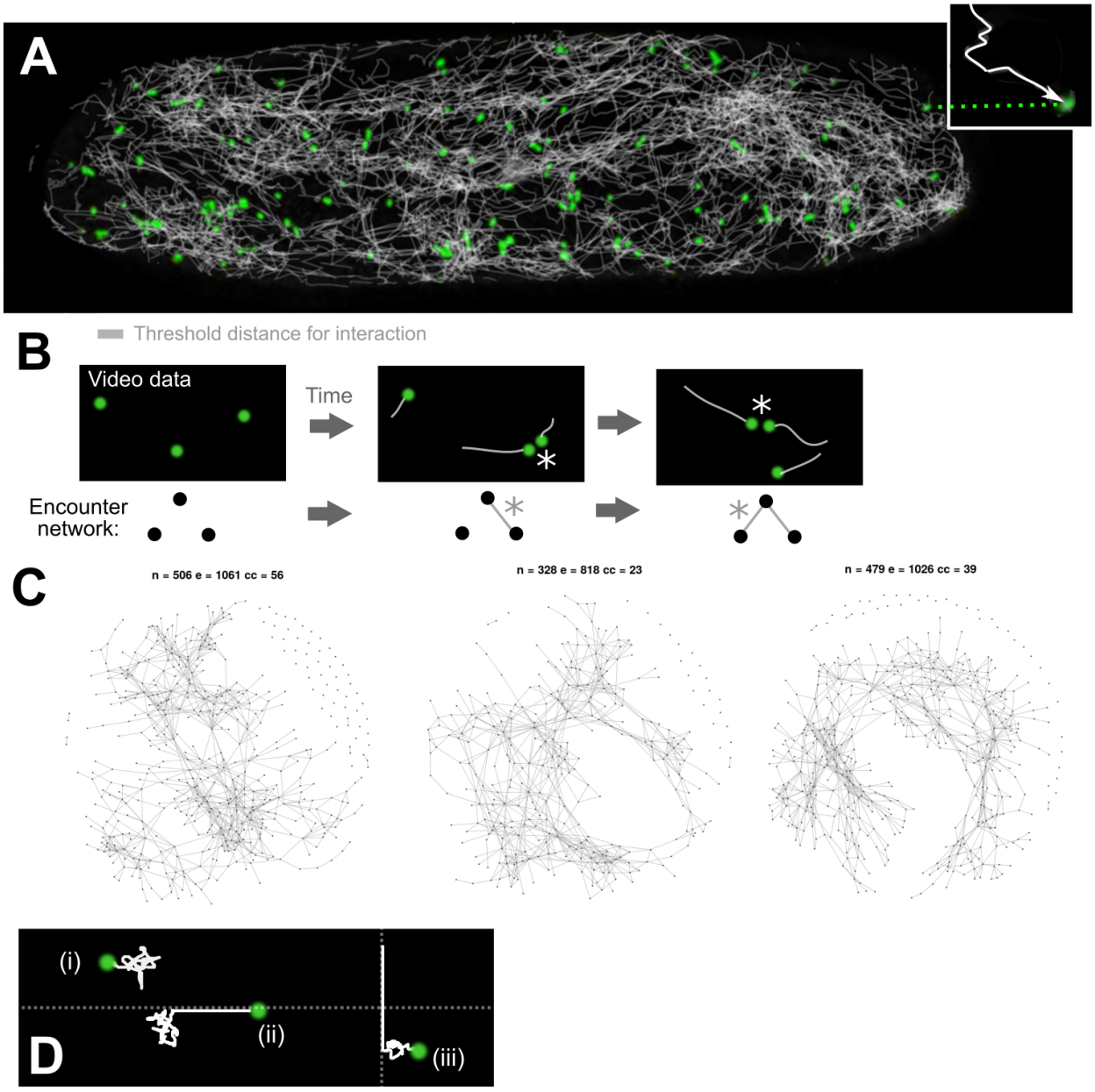

Figure 4.1: Characterisation of mitochondrial encounter networks and the emergence of effective genomes upon them. (See next page)

Figure 4.1: Simulation results of 'model sweeps' to assess the influence of individual parameterisations at a time. (A) Mitochondrial dynamics captured using mtGFP tagged mitochondria (Logan and Leaver, 2000; Chustecki, Gibbs, et al., 2021), with positional trajectories of travel shown over 231 seconds as grey traces. (B) Cartoon illustrating the potential for exchange of mtDNA sections when colocalisation between individuals occurs, and the build-up of effective genomes. (C) Three examples of encounter networks collected over 231 seconds from wild-type mtGFP *Arabidopsis* cells, including node number, edge number and connected component number. (D) Illustration of the simple physical model used to simulate mitochondrial dynamics showing mitochondria can move (i) purely diffusively with constant D; (ii) attach to cytoskeletal strands with rate k_{on} and move ballistically; iii detach from the cytoskeletal strand with rate k_{off}. This model is a simplified version of that seen in Chapter 2. Figure and Box 1 reproduced from Giannakis et al. (2021).

that the node has seen in the past. H and G are both vectors of length L, representing the number of genetic elements to 'collect', which can vary both in this theoretical framework (we looked at L between 2-10) as well as in mitochondrial gene count seen across eukaryotes. Exchange events are defined by the nodes' H vector gaining a 1 in the position of the genetic element that the G of the interacting node has, and vice versa (Figure 4.2). The aim of the individual node is to have seen the full complement of genetic elements, creating a full effective genome; We are interested in how the H labels of nodes changes as the number of encounters increases over time. We coined this network science problem the 'bingo' problem, as the individual node is attempting to collect as many bingo stamps (H vector 1s) as possible, with the bingo card size defined by L. The 'bingo score' of the node is the proportion of genetic elements it has been exposed to over time, and the node scores bingo when the mitochondrion has been exposed to all the genetic elements over time, and the 'bingo score' is 1. This problem, in the language of combinatorics and algorithmics, we

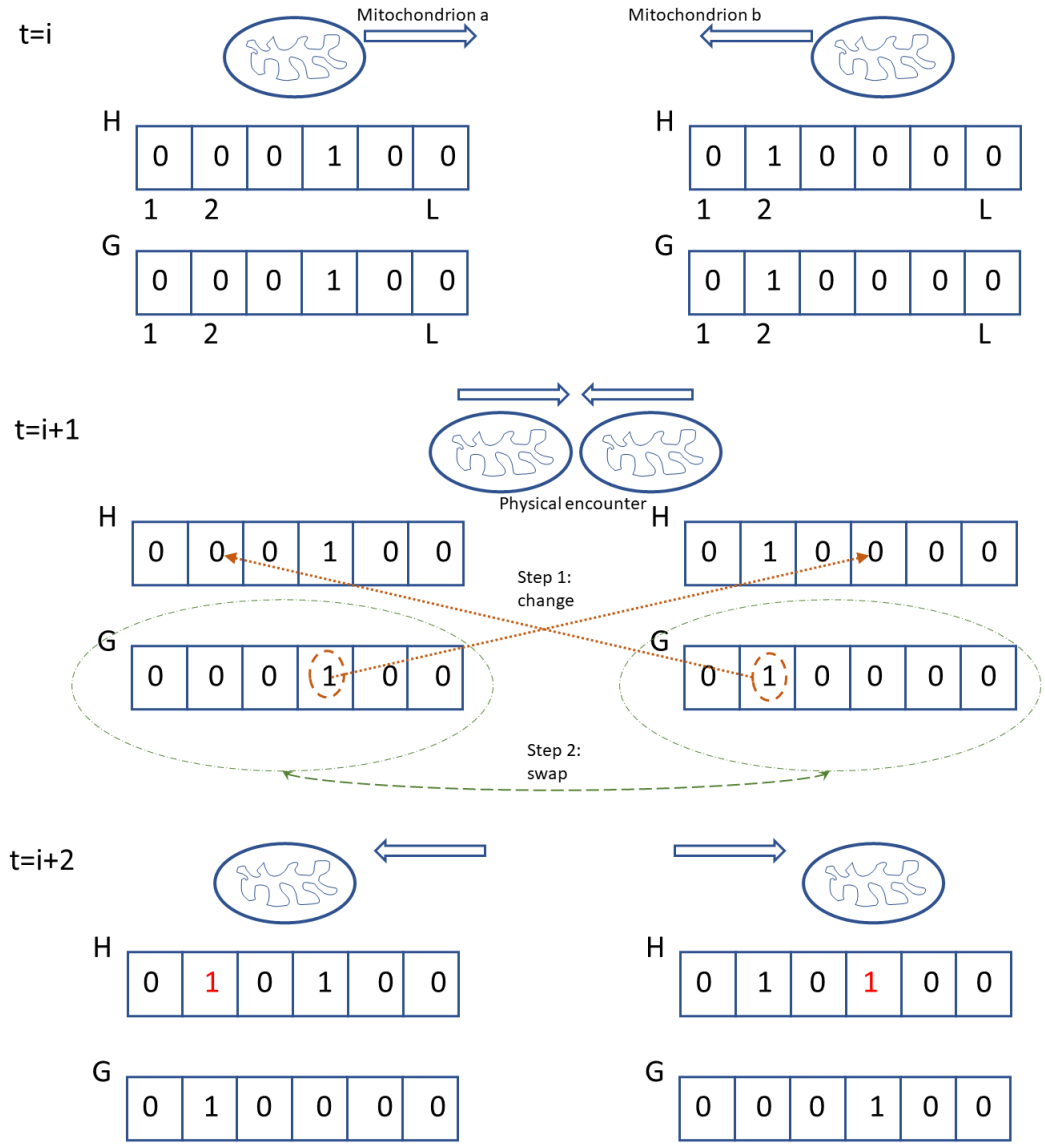

Figure 4.2: Emergence of effective genomes can be re-imagined as a network science problem. This cartoon and related Box 1 represent the algorithm used to build the 'bingo problem' framework onto experimental or synthetic encounter networks. Two mitochondria a and b encounter each other at $i+1$, exchanging genomes. H libraries are accordingly updated using G genomes. Reproduced from Giannakis et al. (2021).

Box 1: Our network phrasing is as follows. Allow each node to have two labels G (genome) and H (history), both binary vectors of length L. G describes the set of genetic elements within a node. H describes the set of genetic elements that have been within a node at some point in the past. When a node's H-label contains L elements of value 1, that mitochondrion has been exposed to every genetic element in the full set. Define an exchange event between two nodes a and b, connected by an edge, as follows. The H-label of a acquires a 1 value at every element where the G-label of b is 1. The H-label of b acquires a 1 value at every element where the G-label of a is 1. Then the G-labels of a and b are exchanged. Such an event corresponds to two mitochondria exchanging genetic information, with each being exposed to the genetic information currently in the other. A given instance of the problem is defined by initial conditions (G-labels for each node) and an adjacency matrix. We are interested in how the H-labels of nodes (the sets of genetic elements that mitochondria have been exposed to) change as the number of exchange events increases. Following the nomenclature in the main text, the bingo score of a node is the proportion of 1s in its $\sum_{i=1}^{L} H_i/L$, and a bingo is scored when this score is 1.

found corresponds to the coupon collector's problem- colloquially- how many cereal boxes with random type-n coupons do I need to collect to get the all the n types of coupons?

Using an experimental *Arabidopsis* network, we simulated the effective genome emergence at different values of L. We note that this experimental network was generated within 230 seconds of mitochondrial dynamics video time (Chapter 2). To measure the exchange of genomic material across encounters, the proportions (p) of nodes that had scored a bingo score was recorded, as a function of the proportion q of encounters that corresponded to an exchange. As the proportion of edges (encounters) that correspond to an exchange increased, so did the proportion of nodes that scored a bingo (gained a full effective genome) (Figure 4.3.A). However, this result relies on L, as if there are less genes to collect, fewer interactions are needed for a larger proportion of nodes to reach a full effective genome. For larger values

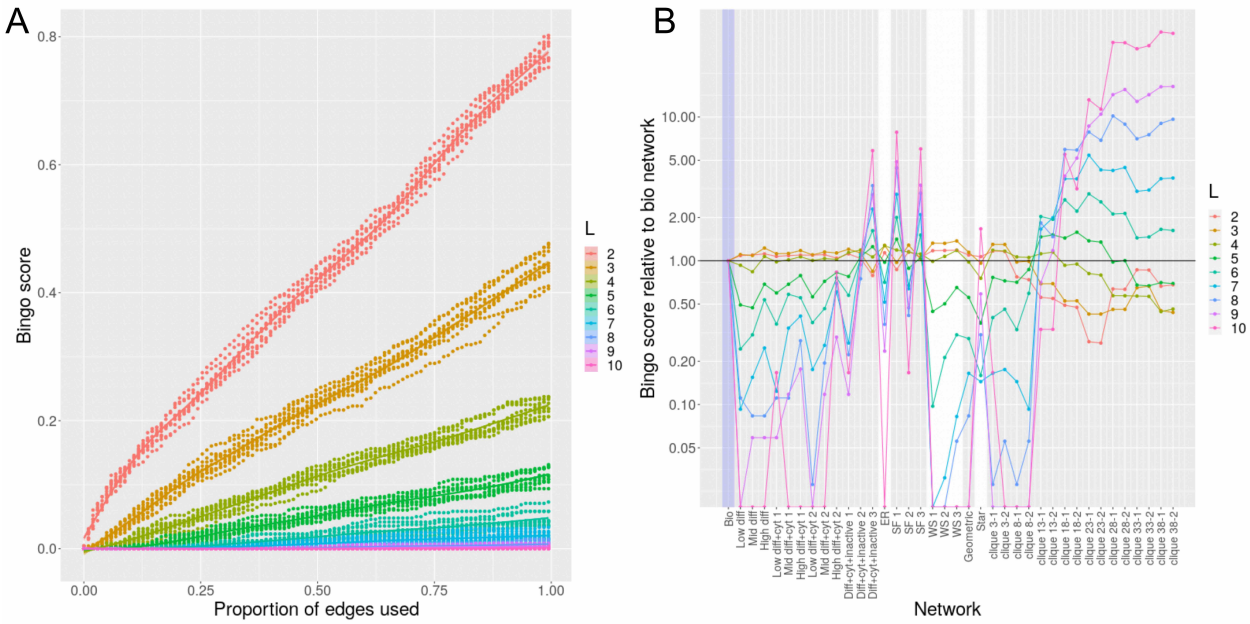

Figure 4.3: Genome emergence potential across encounter networks of both experimental or synthetic origin. (A) The proportion of nodes that have experienced a full effective genome, as a proportion of encounters that allow genetic exchange i.e. 'bingo score'. Ten simulations of the bingo game were performed upon an experimentally-characterised *Arabidopsis* encounter network, for each L value. (B) p^*/p_0 or final bingo score – the proportion of nodes that have experienced a full genome, normalised by the bingo score for a biological network. Connecting traces are for visualisation and do not represent relationships between the values. First grey section to the right of 'Bio' are simulations from the simple physical model, the rest are synthetic networks. Glossary: *diff* diffusion, *cyt* cytoskeletal motion, *inactive* switching the mitochondria between active and inactive states (stochastic inactivation, *ER* Erdős-Rényi, *SF* Scale-Free, *WS* Watts-Strogatz, *clique x-y* x being size of cliques, y = 1 denoting disconnected cliques, y = 2 denoting cliques joined by a single node. Reproduced from Giannakis et al. (2021)

of L, collecting the full genome becomes much harder, and at L=5 and q=1, only 10% of mitochondria manage to collect the full effective genome. Networks with high values of q – that is, more encounters leading to exchange – resulted in more nodes reaching full effective genome scores. This links biologically to the frequency of fusion and exchange events upon close encounters, perhaps aided by a more 'social' network and increased encounters. What might determine the timeframe for collecting a full effective genome? One factor would be fusion rate, estimated from various animal cells to occur every 15 minutes per mitochondrion (Twig, Liu, et al., 2010), and be dependant on contact rate and previous fusion events. Also, the need for effective genome build-up may be dependant on mtDNA mutation rate, slower in plants such as Spruce (2.2×10^{-9} mutations/base/year (Nystedt et al., 2013)) than in animals such as humans (1.28×10^{-8} mutations/base/generation (Rahbari et al., 2016)), or even longevity of the mitochondrial proteins they encode, varying in degredation rate from hours to days (Nelson et al., 2013; Bomba-Warczak et al., 2021). As our theoretical model is based on encounters with the potential for fusion and not fusion events themselves, more experimental and biological context is needed to predict the timeframe of effective 'bingo' in a wild-type system.

As well as experimental plant encounter networks, we generated a set of synthetic encounter networks– in order to ask how experimental encounter networks compared to synthetic alternatives in generating effective genomes. Our synthetic networks were generated using the same number of nodes and edges as the experimental networks, using well-characterised forms of network topologies, further details of their generation can be found in Giannakis et al. (2021). These were: Erdős-Rényi networks (randomly placed edges with uniform probability), Scale-Free topologies (randomly placed edges with probability proportional to degree), Watts-Strogatz networks (ring structure with rewiring to reduce distance across network), as well as star, random geometric graphs and two forms of cliquey graphs (Erdös and Rényi, 2011; Barabási and Albert, 1999; Watts and Strogatz, 1998; Moore and

Newman, 2000; Penrose, 2003). The two cliquey classes of graphs were included to address the hypothesis that cliques offer the chance for nodes to readily collect genes, as they are formed of nodes mutually connected, and not to outside nodes. One class was made with cliques of size n, and the other of cliques of size n connected by a single edge.

The performance of these different networks was measured by p if $q = 1$, i.e. the proportion of nodes with full genomes, if all encounters enable genetic exchange; which was normalised by the p score for the biological experimental network (p_0*), giving $p^*/p_0{}^*$. Performance of these networks was again dependant on L, with Erdős-Rényi, Watts- Strogatz, geometric and small clique networks performing best at $L \leq 3$ and poorly at ≥ 4, with large clique networks showing the opposite pattern (Figure 4.3.B). The main result was that both biological and scale-free networks performed consistently well over the different values of L, even if they were not the best performers for any given L.

The next step taken was to assess how the characteristics of mitochondrial motion within the biological system facilitates the emergence of an effective genome. To do this, a simplified version of the simulation seen in Chapter 2 was used (Figure 4.1). Parameters controlling diffusion rate, number of cytoskeletal strands, attachment and detachment rate to cytoskeleton strands and speed on these strands were used (motion is ballistic on strands). 12 different parameterisations of the model were generated, and encounter networks gathered in the same way as for experimental data, upon which the bingo performance was assessed using different L values. Diffusion and strand speeds were chosen as an order of magnitude higher, the same and lower than the average values for these found within Chapter 2 (Diffusion$\simeq 0.1\mu m^2 s^{-1}$ and Velocity$\simeq 1\mu m s^{-1}$ (Chustecki, Gibbs, et al., 2021)). Results demonstrated that overall, no simulated encounter networks could outperform the experimental biological networks for bingo performance ($p^*/p_0{}^*$), except those that had unreasonably high values for ballistic speed and diffusion (Figure 4.3.B). Following this, we introduced another parameter, with the ability to switch the mitochondria between active and inactive

states, effectively modelling individuals moving in and out of the region. In the biological system, this has been seen to contribute to intermitochondrial heterogeneity in dynamics, with some individuals remaining in a regions for a longer time than others. This contributes to how well each individual is connected to others, with those that remain longer being having more opportunity to encounter other individuals. By including a parameter that induces stochastic activity/inactivity, the resulting encounter networks (with high strand speed and diffusion) more closely resembled the bingo performance of biological networks, indicating that heterogeneous motion supports the resultant emergence of an effective genome.

Following from the previous results, the next question to ask was whether there are any summary statistics that correlate with good bingo performance for encounter networks. This would give an indication of any structural features that may be selected for within the cellular control of mitochondrial motion and encounter networks. For this, statistics such as global network efficiency, modularity and connected component number and size were calculated for the experimental, simulated and synthetic networks. It could be that structures enabling rapid spread of information through the networks could be an indicator of good bingo performance. Bingo performance was collected when $L = 2$ or 5. It was found that networks with high efficiency often did not perform well at bingo, and other network statistics did not show a strong correlation with bingo performance, or if they did, would show a strong correlation for a low L value and the relationship be reversed for a high L value. What was observed is that biological and scale-free networks, that perform consistently over L values, have a high range in degree values. In this work, degree range is defined as the number of values of k, for at which one node has value k. This suggests that the capacity of the system to accumulate information could be related to its 'scale-free' nature, and the wide range of degree values present. In order to consider a statistic or calculation predicting effective genome emergence, the theoretical framework of our bingo regime (Figure 4.2) was analogised to the coupon-collectors problem (CCP) (Ferrante and Saltalamacchia, 2014).

This problem considers the probability of collecting all L genes by an individual node given the number of encounters that have occurred. This spreading problem, and our analogy to CCP is a much simpler version of infection models such as SIR or SIS models (Ottino-Löffler et al., 2017). Further details of the CCP equation can be seen in Giannakis et al. (2021).

Using this framework, we were able to 'predict' the bingo performance of synthetic and biological networks, based on a simple scalar property involving the number of genes to collect (L), which closely correlated with the bingo performance calculated using our original theoretical framework. Therefore, we have shown it is possible to characterise the key properties and structures of these networks mathematically in order to predict how well they will perform at our bingo problem and efficient genome emergence. The work described here as in Giannakis et al. (2021) builds on the 'social' priority of mitochondrial dynamics characterised in Chapter 2, with the exchange of biomolecules including mtDNA between individuals benefiting and being prioritised by the cell. We have shown that the close encounters of individual mitochondria in plant cells can theoretically support the emergence of a full mtDNA genome, as individual genes are 'collected' within our bingo framework, with biological networks supporting this emergence more consistently than synthetic networks. This is because they – like scale-free networks – have a large degree range and a 'heavy-tailed' distribution of higher-degree nodes– helping them to perform well across a range of gene numbers (L), and demonstrating robustness (Liu, Zhou, et al., 2017). This scale-free property fits with these networks (Chapter 2) being 'social-like', similar to other social networks made of individuals with different features. It would be interesting to trace back to the dynamics or these individuals making up the heavy tails of degree distributions- what are the key behaviours of these individuals? It may also be hypothesised that in the plant system, they hold a larger amount of mtDNA than other individuals, acting as 'genetic libraries', but further investigations both theoretical and experimental are needed.

This theoretical framework does not consider other genetic dynamics at work within

the cell. These include recombination, replication and degradation of mtDNA (Johnston, 2019a). Our framework gives a range of possible behaviours and general principles without specifying parameters for replication and degradation which are to our knowledge uncharacterized, or giving specific rates or magnitudes of genetic exchange across these encounter networks, which here remain hypothetical. Population dynamics of the mitochondrial genome and the influence of physical motion on genetic dynamics is a topic of ongoing research (Albert et al., 1996; Arimura, Yamamoto, et al., 2004; Mouli et al., 2009; Poovathingal et al., 2009; Tam et al., 2013; Johnston, 2019a; Hoitzing et al., 2015; Edwards et al., 2021).

For the imaging experiments capturing the system in *Arabidopsis* seedlings (see Section 2.2), there are limitations and noise within the capture of these organelles. The time lapse images are taken over a finite time, and laser power is limited in an attempt to retain physiological conditions. A 2D plane of mitochondrial movement is captured, meaning mitochondria can disappear and reappear into the field of view. This may have the effect of reducing the values of nodes with the highest degree, as a motile mitochondrion moving throughout the cell may be lost from the field of view, becoming a 'new' node in the system upon re-entry, compromising the true degree value of that individual. These properties of the imaging protocol may affect the ability of the system to reach an otherwise expected steady state of all mitochondria having seen each other, and all nodes connecting with each other. However, a steady state could be unattainable as genetic information is 'forgotten' over time, and therefore our framework and conclusions represent a system within this finite time window and out of equilibrium.

We have shown that dynamics of mitochondria can facilitate the emergence of an 'efficient' mitochondrial genome, that allow individuals to 'collect' and see a full genome despite only carrying a subset. Performing better than many synthetic networks, we hypothesise that mitochondrial dynamics under cellular control may have evolved to support efficient genome emergence; representing a 'social' network fulfilling an important cellular function

under evolutionary control.

4.3 Investigations into preferential localisation of mitochondria to chloroplasts

4.3.1 Methods

Organelle positional data extraction from time lapse images

Time lapse videos captured using the method described in Chapter 2.2, cropped and adjusted to 5 pixels/micron were loaded back into ImageJ (Fiji) 2.0.0. For each video there are two channels, one capturing mitochondrial position using mtGFP, the other capturing chloroplast auto-fluorescence and Propidium Iodide (PI) staining. Channels were split, then exported as single-frame .tiff files.

Using Mathematica 11.3.0.0 (Wolfram, 2018), each frame was manipulated for background removal (Figure 4.4) and binarised. For chloroplast frames, an extra step of commonest feature filtering was used to remove any traces of the PI staining. From this, the positions of every pixel occupied by either mitochondria or chloroplasts could be extracted. Note that it is not the central point of each organelle that is extracted, but any coordinate where an organelle was present within each frame. From the positional data extracted, the Euclidean distance from every mitochondrial position to the centre of each chloroplast at that frame could be calculated. The central coordinate of each chloroplast was calculated using $((x_1 - x_2)/2) + x_2$ where x_1 is the maximum x coordinate for the chloroplast area at a given frame, and x_2 is the minimum, and the same for y.

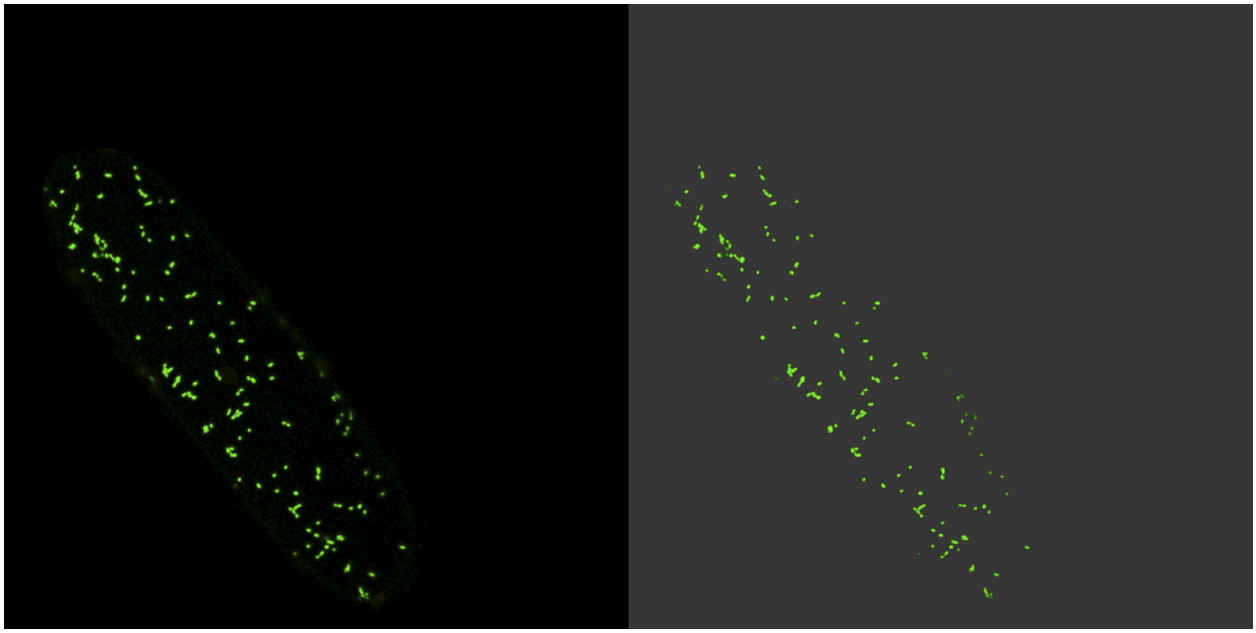

Figure 4.4: Demonstration of the background removal for a single frame of capture in a single *Arabidopsis* hypocotyl cell. To the left is the original image at one frame of the channel imaging mtGFP (capturing mitochondria), to the right is the same image with background removal, demonstrating the mitigated extent of information loss.

Autocorrelation analysis

Autocorrelation analysis was performed using the acf function in R (Package *stats* version 4.0.1). This computes an estimate (rho) of the autocorrelation function of a timeseries, between pairs of numbers for $lag(1...lag.max)$, with $lag.max$ defined as $10 \times \log_{10}(N/m)$ with N the number of observations and m the number of time series. The correlation was computed using x-coordinates (univariate, 2D), and is by default the Pearson correlation. Within each time series, the pairs of numbers compared were the x-coordinates of each mitochondrial trajectory (gathered using Trackmate (see Section 2.2)) and the position at the subsequent frame. The number of frames counted as correlated were those with an estimate above $1.96/\sqrt{n}$ with n as sample number, here the number of x-coordinate positions making up one trajectory, for a confidence limit of 95%. The median number of correlated frames was

then taken for all trajectories (Figure 4.8.B) and this number of frames was removed from the distribution of all mitochondrial positions, either side of the frame of interest for each "all versus frame x" comparison, going some way to render the two distributions independent.

Local mitochondria (heat-map) analysis to chloroplast

For the local analysis of mitochondrial positions within specified areas surrounding the chloroplast area, the maximum and minimum x and y values for all coordinate positions the chloroplast had been were calculated. From this, the radius (r) was calculated, and used to plot rings around the central circle ($A1 = \pi r^2$). Concentric ring areas (Ai) were calculated by adding 10 pixels to r, while subtracting the inner ring (i.e. $A2 = \pi(r + 10)^2 - A1$). For each of these areas, the mitochondrial pixel locations unique to each ring were found and totalled (Mi). The number of rings were limited to 6 to account for the geometry of the cuboidal hypocotyl cell.

4.3.2 A demonstration of preferential localisation of mitochondria to chloroplasts

Colocalisation of mitochondria and chloroplasts is key in exchange of signalling molecules and vital metabolites for processes such as photorespiration, as well as environmental responses such as high light (Jouhet et al., 2004; Islam, Niwa, et al., 2009; Islam and Takagi, 2010). To take a localised view of mitochondrial density around the chloroplast location and demonstrate colocalisation, the positions of mitochondria within 6 circular areas surrounding the chloroplast were calculated (Figure 4.5). These mitochondrial positions were calculated from pixel locations of mitochondria at any point in time, not trajectories (see Section 4.3.1). The number of mitochondrial positions within a ring (Mi) was then calculated in proportion

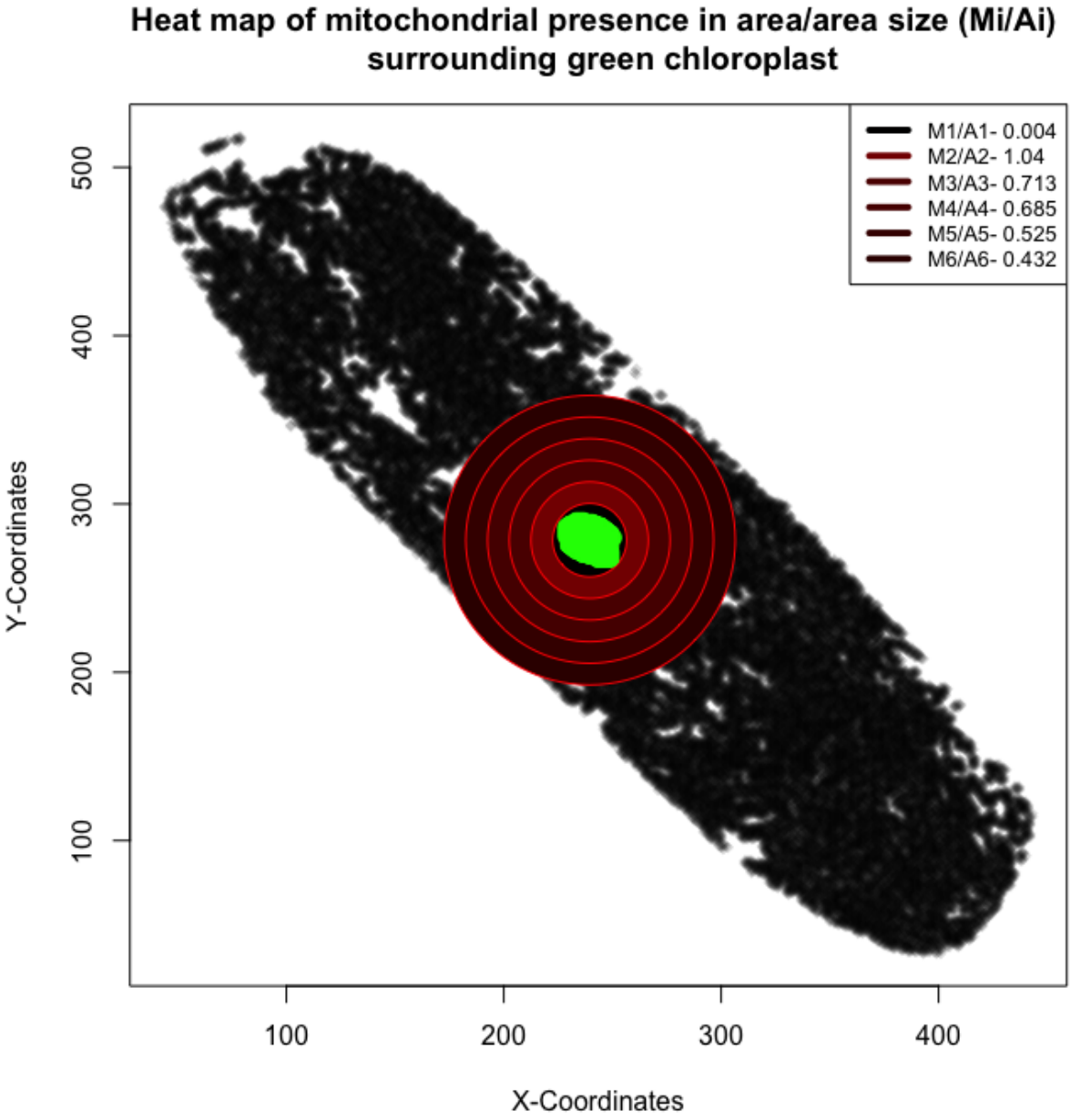

Figure 4.5: Local mitochondrial density relative to chloroplast position. Heat map demonstrating the number of mitochondrial coordinates found within areas denoted by rings, divided by the area of each ring ($pixels^2$), surrounding the chloroplast (green). Each black point is a coordinate at which mitochondrial presence has been found. Area rings are coloured in proportion to their Mi/Ai values.

to the area of the ring (Ai). The null hypothesis here is that all proportional values of Mi/Ai would be the same, indicating there is no preferential colocalisation between mitochondria and the chloroplast. However, what we find is the Mi/Ai for the ring directly adjacent to the outside of all chloroplastic positions over time is the highest. This evidences a larger number of mitochondrial 'sightings' within this region than any of the 5 other adjacent areas surrounding the chloroplast. This indicates that at least for this sample, there is evidence of *local* preferential positioning of mitochondria adjacent to chloroplasts.

4.3.3 A preliminary statistical analysis of mitochondrial colocalisation to chloroplasts

Having demonstrated that colocalisation does occur between these two organelles (see Section 4.3.2), we are interested in whether mitochondrial are *actively* preferentially localised to the chloroplast. In order examine this, we need to control for cytoplasmic structuring influencing the positions of mitochondria, to examine only whether mitochondria actively colocalise to chloroplasts. In order to do this, we need to take into account the positions of all individuals across the cell. For this, we asked two questions; is there any statistical evidence for a difference in distance to chloroplasts at a given frame versus all the places mitochondria can be present in the cell? As well as, is there any evidence for mitochondria being closely localised to the region directly adjacent to the chloroplasts position?

In order to address the first question, whether there is any evidence for statistically significant chloroplast-mitochondrial interactions, the cytoplasmic space mitochondria can occupy within a single sample was characterised. Taking the individual time lapse frames for a single hypocotyl cell with one visible chloroplast, the composite image in Figure 4.6 was built. Interestingly, the majority of cytoplasmic space has been covered by at least one mitochondrion, with empty spaces most likely occupied by other organelles, such as the

cellular vacuole, endoplasmic reticulum or nucleus. Also shown is a single central chloroplast, with the darker shade of red showing the cumulative previous locations before the final position is shown in the foreground. There are mitochondria underneath the chloroplast path, that have either been localised adjacent to the chloroplast as it has travelled throughout the cell, or passing across the chloroplast signal location (Figure 4.6, inset).

First, we asked whether there was a difference either way between the distance from all mitochondria over time to a chloroplast, and those distances in specific frames. The null hypothesis here is no evidence of a statistical difference between the distribution of distances to the chloroplast from any position mitochondria occupy and the distance distribution from any given frame. The distribution of distances from all mitochondrial locations to the central point of the chloroplast across all time points can be seen in Figure 4.7.A, with frame specific distributions in 4.7.B-D.

A slight left skew can be seen across these distributions, for distance values that are closer to the chloroplast. Using a quick non-parametric Mann-Whitney test between the distance distributions between all frames and each frame (1 to 119), 73 comparisons were below the significance threshold (≤ 0.05). The question arises as to whether the two samples are independent within this test, if the frame specific distances between mitochondria and chloroplast form part of the overall distance dataset. In order to address this, an autocorrelation analysis was performed, in order to investigate the number of frames before and after a particular timepoint, in which the positions of mitochondria are no longer correlated, or have been 'forgotten' (Section 4.3.1). We use the coordinate data of each mitochondrial trajectory to calculate the median frame time until the colocalisation value is under a significance cutoff (Figure 4.8). This is in order to remove these frames from the overall dataset for the independent comparisons.

The median number of frames showing strong autocorrelation were removed from

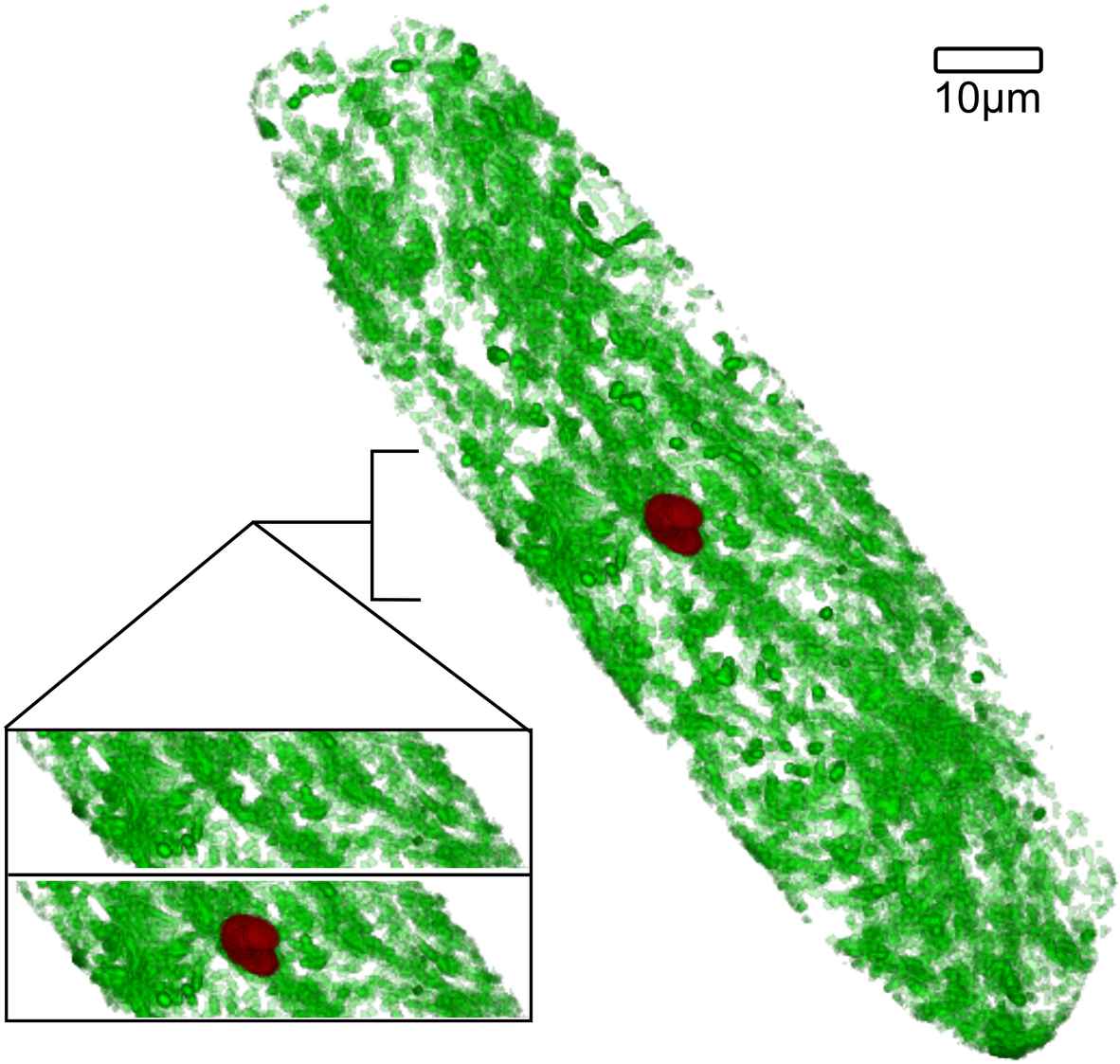

Figure 4.6: Positions of all mitochondria and a single chloroplast within a single *Arabidopsis* hypocotyl cell. Mitochondria (green) are extracted with background removed from images of each frame, and stacked on top of each other with reduced opacity, consistent across every frame. On top of these are stacked the positions of a single chloroplast (red) over time, with the most recent (end of frame time) in the foreground. Total frame time represented is 231 secs.

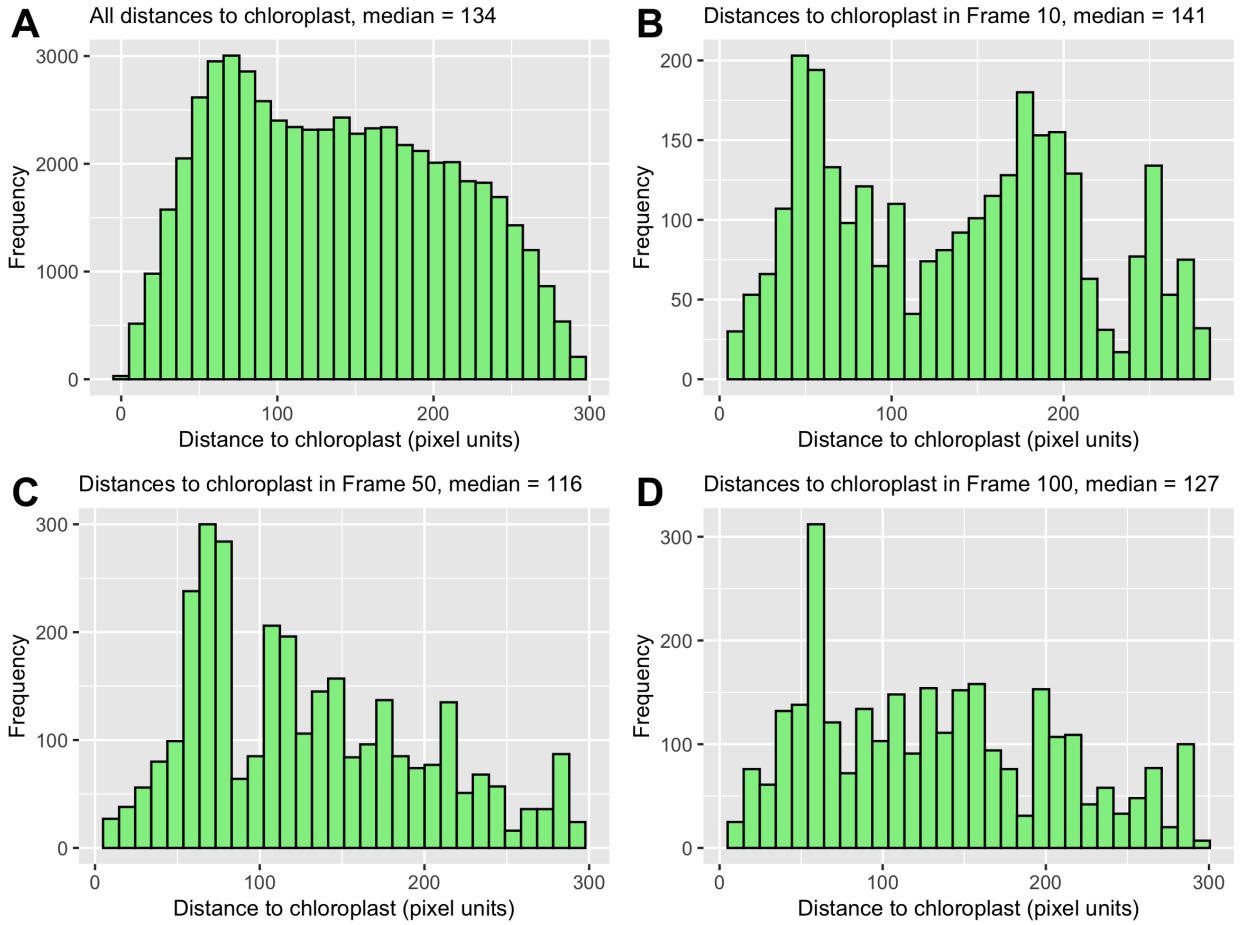

Figure 4.7: Distribution of distances of mitochondria to a single chloroplast within a single *Arabidopsis* hypocotyl cell. (A) The distributions of distances (in pixel units) to the central coordinate of the single chloroplast of the sample in Figure 4.6. (B-D) The distributions of all mitochondria captured in frame 10, 50 or 100 to the central coordinate of the chloroplast.

the total positional data, either side of the frame of interest. The same Mann-Whitney test was then re-run, with 75 out of 119 frames below the significance threshold (≤ 0.05). Therefore, when accounting for each mitochondrion to have 'positional memory' as it moves through cellular space, we conclude that using this method on one sample goes some way to demonstrate evidence of a statistical difference between the distance of mitochondria to the chloroplast and the position they may occupy at any given moment.

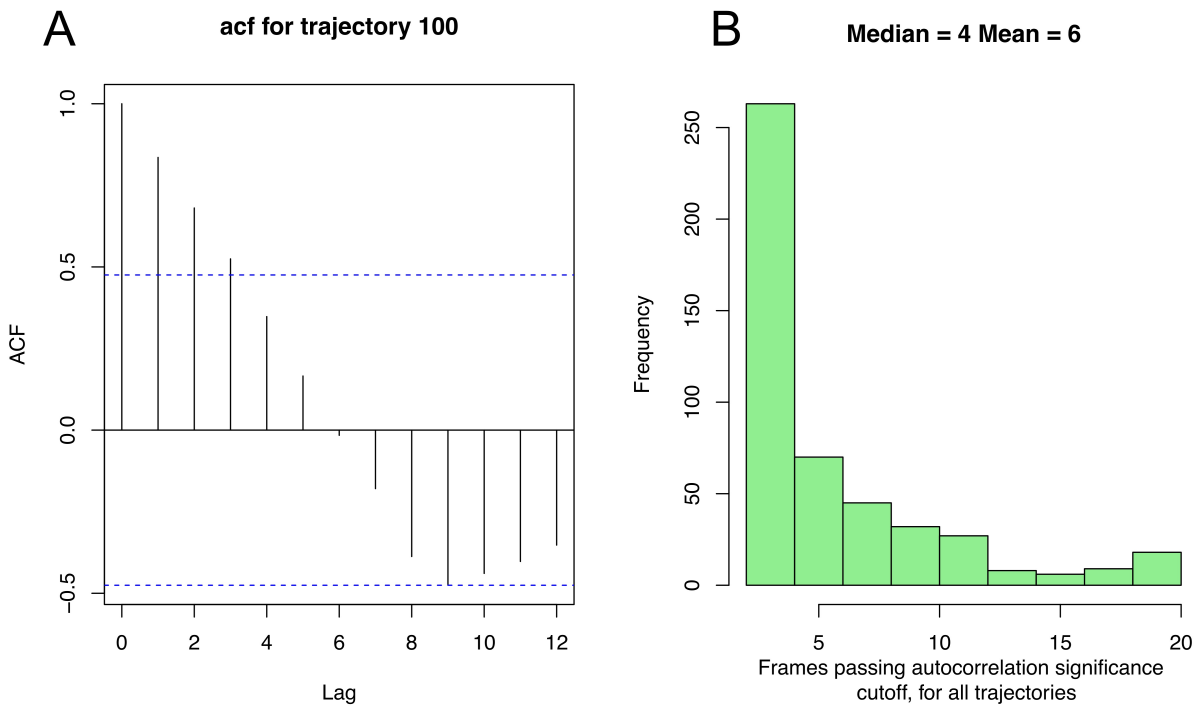

Figure 4.8: Autocorrelation analysis. (A) acf correlation values for $lag(1...lag.max)$ of the x-coordinates of a single mitochondrial trajectory. Blue line indicates the significance cutoff giving a confidence limit of 0.05 (see section 4.3.1). (B) The number of frames above the significance cutoff for all trajectories in the sample, with median and mean shown above.

4.4 Discussion

These two studies demonstrate further cellular implications of dynamic bioenergetic organelle behaviour. The particular connectivity of mitochondrial encounters in plant cells has shown to be well suited to allow the emergence of full effective genomes, helping these organelles to stay functional and healthy against continuous electron transport subunit damage, or proteotoxic stress. The plant mitochondrial genome is uniquely segregated into individual compartments, and the reasons for their dynamic movement have yet to be fully elucidated (Takagi et al., 2011; Hoitzing et al., 2015). Our theoretical framework offers a tantalising line of investigation- the emergence of a plant 'metagenome' controlled by short-term physical

dynamics and long term evolutionary pressures.

As with other models presented as part of this project (Chapter 2) the theoretical framework describing bingo performance of particular networks is extensible. Currently, the parameter q (proportion of encounters that allow genetic exchange) is increased (so that more encounters are used for exchange) in the order that these encounters occur biologically (Figure 4.3.A). Here, using experimental data, biological priors could be included. The q parameter would take the quantification, if calculated experimentally, of the proportion of close social encounters that are mtDNA transfer events (using tools such as antibodies, fluorescent nucleotide substitutes, fluorescent dyes (Prole et al., 2020)), and further illuminate the link between the physical and genetic dynamics of the mitochondrial chondriome, particularly in relation to plants (Gilkerson et al., 2008; Aryaman et al., 2019; Lieber et al., 2019; Prole et al., 2020). In comparison to synthetic networks, the experimentally-derived encounter networks of plant mitochondria have shown themselves to be particularly capable of efficient genome emergence, again validating the use of 'social' encounter networks, and not necessarily explicit fusion events for their ability to highlight cellular priorities.

Physical motion and spacing of mitochondria within the cell have, as demonstrated (Chapter 2), many different priorities within the cell. One of these is to colocalise with other organelles. Figure 4.6 shows mitochondrial positioning over an entire cell over 231 seconds. These organelles are well-distributed in the cell, and consistently over time too.

The colocalisation analysis discussed here provides good preliminary evidence for both the occurrence of colocalisation between mitochondria and chloroplasts in *Arabidopsis* hypocotyl cell, and also the potential of a purely statistical methodology for colocalisation studies, even without specifically imaging for these events. When comparing the distance from a chloroplast to every mitochondrial position in cellular space, there was evidence of a difference either way against the positions on a frame-by-frame basis. This demonstrates that

on a global scale, the chondriome is working to retain an even spread across cellular space, but that overall, mitochondria are often found colocalised to chloroplasts even when taking into account the cytosolic structure. Currently we are using a simple non-parametric test between distributions for all positions of mitochondria in the cell versus positions from each frame, but a different test for example of differences in skewness of the distributions would yield a more detailed comparison. This could be achieved for example by jackknife resampling of each to calculate skewness distribution, comparing these to a null model where the distributions have equal skewness. If, for example, the specific frame were to have mitochondrial distances overall closer to the chloroplast, this would be visible and go against the null hypothesis.

Another observation is the range of autocorrelation in mitochondrial positioning within the same trajectory. Even with analysis here showing only x-axis correlations, some trajectories show a high level of autocorrelation, in that they have an increased number of rho estimates above the significance threshold (Figure 4.8.B). These trajectories could well be mitochondria moving with only localised diffusion, staying predictably localised to a particular region. However, it is important with any abstracted correlation analysis to retain a 'geographical' knowledge of cell shape and structure, particularly when analysis is only done on one axis, for a rigidly cuboidal cell shape such as that of the hypocotyl.

On a local level where concentric areas surrounding the chloroplast are analysed, we see an increase in mitochondrial positions in areas closer to the chloroplast. Our method of local measurements in the region surrounding chloroplasts shows positive results for the sample used, and can be extended for > 1 chloroplasts within the field of view, or in 3D static images, or videos. The radius of concentric areas around chloroplasts can be adjusted for inter-chloroplastic spacing in different cell types (for example, chloroplasts are more numerous and tightly packed within mesophyll cells). This method shares similarities with the distance measurements taken in protoplasts of *A. thaliana* (Oikawa et al., 2021).

Chapter Five

A statistical investigation into organism lifespan and mtDNA recombination

5.1 Introduction

Due to their metabolic and energetic centrality, mitochondria are strongly implicated in organismal ageing. Having newly characterised some ways that cells maintain their mitochondrial populations, we next considered a related topic: the taxonomically broader link between mitochondrial maintenance and ageing.

The ageing of organisms is described using many definitions, that can often differ between studies. Here we use the terms: life expectancy, the average lifespan of a population of individuals; lifespan, the maximum amount of time any individual of a species can live (often maximum lifespan, but can be otherwise defined); senescence, the gradual deterioration of an organisms functional characteristics, or more commonly used on a cellular level, growth arrest and inability to complete the cell cycle as well as phenotypic alterations (McHugh and Gil, 2018). Ageing is a complex process, and on a cellular level, senescence can be caused through epigenetic factors, telomere shortening, as well as DNA damage and mitochondrial

dysfunction (McHugh and Gil, 2018). It is these latter two factors relating to our work on mitochondrial recombination that we carry forward in this chapter.

The link between ageing processes and mitochondrial function have been well studied, and mitochondrial dysfunction is one of the hallmarks of ageing (Harman, 1972; Dodig et al., 2019). Mitochondrial mtDNA mutations accumulate over the lifespan of organisms, mainly due to replication errors and unrepaired damage to double strand breaks (DSBs) (Krishnan et al., 2008; Chen, 2013; Lagouge and Larsson, 2013; Yui et al., 2003; Lakshmanan et al., 2018; Bender et al., 2006). Mitochondrial DNA damage can lead to mitochondrial dysfunction, disruption of the electron transport chain and the production of more Reactive Oxygen Species (ROS), which has led to the concept of a vicious cycle of damage, ROS production and ROS causing damage to mitochondrial DNA, also known as the free radical theory of ageing (Harman, 1956)– a concept that has since been critiqued over recent years as correlated, rather than causative of ageing (Chen, Hales, et al., 2007; Chen, 2013; Lagouge and Larsson, 2013; Kennedy et al., 2013). In order to uncover the selective forces and the genetic basis of extended lifespan across organisms with different genetic backgrounds and lifestyles, Kaya et al. (2021) examined phylogenetic, metabolomic and transcriptional differences of two yeast species. This was done using a phylogenetic generalized least-squares (PGLS) analysis of 76 related strains. Increased mitochondrial function was implicated throughout as an adaptation correlating with increased lifespan, as was a decrease in amino acid synthesis (Trp, Lys) and glycolytic activity. DNA repair was also implicated as an enriched term for strains with increased longevity. These results evidence the function and health of the mitochondrion as a key player in the longevity of an organism, which is itself influenced by mitochondrial health and genome stability. The function of the mitochondrion can in turn be influenced by genome stability.

An increase in mtDNA recombination can occur alongside mtDNA deletions and re-arrangements, increasing during ageing (Chen, 2013), which may lead to genetic instability.

However, it could also be that mtDNA recombination is increased as a protective mechanism against mtDNA damage, replacing damaged mtDNA. Evidence from the filamentous fungus *Neurospora crassa* has demonstrated that upon the mutation of a key recombination surveillance gene, *MSH1*, the organism demonstrated shortened life span, and mtDNA instability, with an increase in aberrant mtDNA mutations (Endo et al., 2020). This demonstrates that recombination surveillance genes such as *MSH1* may contribute to an organisms' lifespan, by protecting mtDNA from aberrant mutations (see Section 3.1). *MSH1* itself is an interesting gene with fascinating evolutionary origins. Forms of the gene are found across plants, sponges, placazoans and corals (Abdelnoor, Christensen, et al., 2006; Bilewitch and Degnan, 2011; Muthye and Lavrov, 2021). The latter are particularly interesting as corals not only live a long time, but are animals, the majority of which do not recombine their mitochondrial DNA except in rare cases (Chen, 2013).

It is worth noting the interesting evolutionary origins of coral mtMSH1 (mtMutS). Corals have a homolog of *MSH1* (Figure 3.1), encoded in the mitochondria, not in the nucleus as in plants. This mtMSH1 also contains an endonuclease domain, but not the same as plants– this is a HNH-type endonuclease domain, which has been shown in some cases to participate in single-strand nicking (Belfort and Roberts, 1997). It has been hypothesised that the presence of these two distinct endonuclease domains in both plants and coral mtMSH1 is an example of convergent evolution (Abdelnoor, Christensen, et al., 2006), where a MutS homolog has fused to an endonuclease, joining two proteins that are seperate in the bacterial MutS system (MutS for mismatch recognition, and MutH for endonuclease activity) (Mackenzie, 2018). Why is it interesting for our work that corals contain this gene? There are also other similarities between the mitochondrial genomes of plants and corals. Corals are the only known animal to carry introns in their mtDNA (Pont-Kingdon et al., 1998; Van Oppen et al., 1999), as well as have a very low mtDNA mutation rate like plants (Shearer et al., 2002). Bilewitch and Degnan (2011) Investigated mtMSH1 in octocorals, demonstrat-

ing that coral mtMSH1 has all the domains necessary for mismatch repair, as well as the endonuclease domain, supporting a functional role in DNA mismatch repair, which has not yet been shown for plant MSH1. The gene was also not of eukaryotic origin, meaning the gene had been horizontally transferred to coral, most likely from prokaryotic or viral sources, representing convergent evolution between *mtMutS* of corals, and nuclear *MSH1* of eukaryotic origin (Bilewitch and Degnan, 2011). It is likely that an early eukaryotic ancestor had all six *MSH* genes, which were subsequently lost in animals (Lin et al., 2007).

The presence of *MSH1* in both plants and corals, that both lack fixed body plans, led Edwards et al. (2021) [1] to consider the presence of recombination genes across taxa (Figure 5.1). BLASTx searches for 3 different recombination genes (Yeast *MHR1*, yeast *MGM101*, and yeast (nuclear encoded), *Arabidopsis* (nuclear encoded) and *Dendronepthya* (mtDNA-encoded) *MSH1*) revealed that the majority of organisms without fixed body plans retain recombination genes. This is one line of evidence leading to the conclusion that organisms that do not sequester a germline or use a genetic bottleneck (a reduction in mtDNA copy number in the germ line), can still generate variance across their organellar DNA. This is possible through the process of recombination and gene conversion, allowing the avoidance of Mullers' ratchet and deleterious mutational build-up (Christensen, 2014; Edwards et al., 2021). There are drawbacks to this variance- generating strategy, with structural alterations having the potential to disrupt bioenergetic capacities of these organelles, or generating highly proliferative selfish molecules (Johnston, 2019a). It is also interesting to note that searches in genomic repositories demonstrated that plant *MSH1* homologs with the GIY-YIG domain were present not only in Viridiplantae, but stramenophiles, alveolates, haptophytes, and cryptomonads (Wu et al., 2020), organisms without fixed body plans.

One genome maintenance protein found across fungi, slime molds and marine animals

[1] To this work, I contributed a literature review, helped develop theory on *MSH1* across eukaryotes and contributed bioinformatics support.

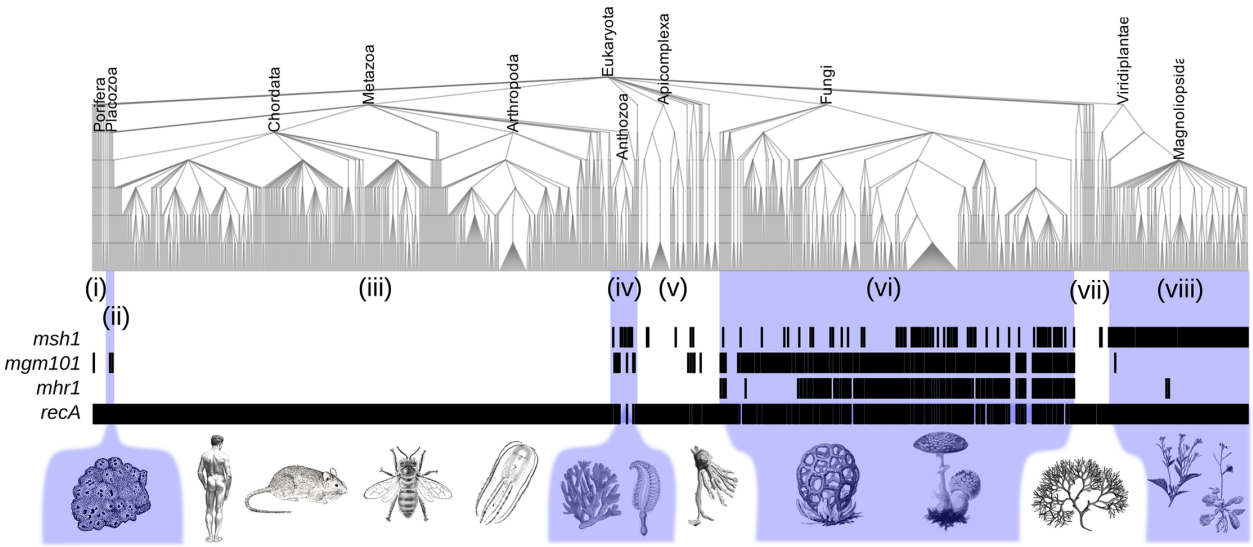

Figure 5.1: Presence of organelle DNA recombination genes across taxa. Barcode represents the presence/absence of recombination genes (black/white) across Porifera/Placozoa (ii), Metazoa with fixed body plans (iii), Anthozoa (iv), and other kingdoms without animal-like germlines (v-viii). Ctenophores, a basal metazoan, lacks recombination genes but does appear to have a more sequestered germline and fixed body plan (Reitzel et al., 2016). Reproduced from Edwards et al. (2021).

including cnidarians, placazoans and sponges is the recombination gene *MGM101*. In plants, *ODB1* (mitochondrial localising ODB) may represent a functional homologue of *MGM101* (Janicka et al., 2012). Alongside other repair proteins, *MGM101* ensures recombination-dependent double-stranded DNA repair after oxidative damage (Rendeková et al., 2016). It does this by forming nucleoprotein filaments around elongated ssDNA strands that can be directly annealed to donor sequences. The binding of *MGM101* has been suggested to be under redox control, responding to stress by conformational remodelling to bind and repair mtDNA (Nardozzi et al., 2012; Chen, 2013). Another player in the molecular machinery of mitochondrial recombination is *MHR1*. It is an ATP-independent DNA recombinase, binding ssDNA and dsDNA with comparable affinities. Its role is to mediate the strand invasion by ssDNA through homologous recombination by pairing to homologous dsDNA in D-loop

formations (Ling and Shibata, 2002). Both *MHR1* and *MGM101* were first characterised in yeast (Chen, Guan, et al., 1993; Ling, Makishima, et al., 1995; Ling and Shibata, 2002).

The longevity of plants, corals and other non-mammalian organisms with extended lifespans, and accumulation of mtDNA mutations during ageing led us to hypothesise a potential link between the presence of recombination surveillance genes, such as *MSH1*, and the extended lifespan of organisms. This link is touched upon by Møller et al. (2021), who suggests the root cause of extreme longevity amongst plants (such as the bristlecone pine *Pinus longaeva*) could be due to the high efficiency of mtDNA repair, mediated by homologous recombination (Davila et al., 2011; Christensen, 2014; Gualberto and Newton, 2017; Wu et al., 2020). The authors finish this review with the open question *"Why does plant mtDNA have such a low mutation rate? Is the low mutation rate connected with the extreme longevity of some plants?"*. We take this thinking and broaden it across the eukaryotic tree of life, to ask whether mtDNA recombination is correlated with long lifespan. In order to begin investigating this link, data was gathered for a broad range of organisms on both lifespan estimates and presence or absence of recombination genes. However, these datasets come with a metazoan bias, with theories of senescence based on animal model organisms, and demographic studies of lifespan have suffered similar biases, both of which are being addressed in the literature (Salguero-Gómez et al., 2013; Jones et al., 2013). Our aim was to take a preliminary approach to investigating the relationship between the presence of recombination genes, and organisms with extended lifespans.

5.2 Methods

5.2.1 Assembly of a broad eukaryotic tree using a common recombination gene RecA, and subsequent sister-cousin analysis

The following section is self-contained methodology for addressing our lifespan-*MSH1* hypothesis.

One method of generating a broad Eukaryotic tree uses a near-universal family of genes called the *recA* super-family (Hofstatter et al., 2016). This group is involved in the homologous recombination and repair of DNA, and is known as RecA in bacteria, and RAD51 in Eukaryotes. It is near-universal and provides an excellent candidate for a gene that many Eukaryotes have, and should the gene be annotated for a specific organism, the chance of other recombination genes of interest (e.g. *MSH1*) also being annotated increase. Organisms with the Gene label annotation RecA were found in NCBI's Gene database www.ncbi.nlm.nih.gov/gene/?term=reca. Gene label searches for mitochondrial recombination genes of interest *MSH1*, *MHR1*, and *MGM101* were also run www.ncbi.nlm.nih.gov/gene/?term=msh1ORmgm101ORmhr1. From this list, similarly named but unrelated genes were highlighted in model organisms known not to have these mitochondrial recombination genes; *Homo sapiens, Drosophila melanogaster, Mus musculus, Rattus norvegicus* and *Danio rerio*, these organisms were removed from the list. The remaining organisms within these search results were combined into one list, which was exported into NCBI's CommonTree, generating a taxonomy for a broad Eukaryotic tree based on Gene label searches.

A custom script was written (by Prof. Iain Johnston, University of Bergen) that takes a taxonomic tree and trims any tips that– in this case– do not have a lifespan estimate. It then

labels all nodes and node descendants (nodes are the points at which the tree splits, say from a genus to a species or a family to a sub-family) with a trait status (+/-), here a positive mark is a species or node with presence of a recombination gene from the *MSH1/MHR1/MGM101*-positive species/taxa list. If all descendants of a parent nodes are positive for the trait, the parent is labelled as positive for the trait. It then labels all tree tips with a lifespan estimate (lifespan estimates with no upper boundary, that had previously been labelled as infinity, were re-labelled as 1,000,000 yrs), and labels all parent nodes with an average of their children's lifespan estimate. As a result, we have a taxonomic tree with all internal and external nodes having a $+/-$ value for recombination genes of interest, and a lifespan estimate/average. Then, looking through the tree at any level, the script picks out any node that has descendants with different trait values, and records the ages of the two. Therefore, it builds up a list (depending on the n) of regions of interest where the hypothesis of mitochondrial recombination genes aiding extended lifespans can be tested.

5.2.2 BLASTx source data for *MSH1* presence across species

The following sections (5.2.2, 5.2.3, 5.2.4) are a broader analysis using protein and nucleotide sequence explorations of recombination gene presence.

Three parameters can be used to assess the success of BLAST searches: percent identity, how similar the query genomic sequence is to the target genomic sequence; E (expect) value, how many times you would expect a match given the size of the searched database (or, the number of alignments (sequence matches) expected by chance with the calculated score or better– for more significant alignments, the ET value should be close to 0); and query cover, how much of the query sequence is covered by the target sequence, which informs of how similar the two sequence lengths are to each other.

Accession Number	Query subrange	Species	Genomic location
NM_113339.4	(1..3819)	*Arabidopsis thaliana*	Nuclear encoded
NC_036022.1	(6348..9287)	*Dendronephthya putteri*	mtDNA encoded
NC_001140.6	(349574..352453)	*Saccharomyces cerevisiae*	Nuclear encoded

Table 5.1: Accession numbers and species used to query NCBI for *MSH1* presence.

Querying methods for *MSH1* were followed from Edwards et al. (2021). The BLASTx search function was used to query the non-redundant (nr, i.e. non identical proteins) protein database on NCBI, searching for 5000 maximum target sequences with an expect threshold of 1×10^{-51}. These results were not filtered for query cover or percent identity, and so some species with similar subdomains were included in these results. For example, *Tanacetum cinerariifolium* has a GIY-YIG nuclease domain similar to that of *A.thaliana MSH1.* Low query cover helped to find species such as soft coral *Xenia membranacea* with only 24% query cover similar to *Dendronephthya MSH1* for its partial *MutS* protein. The sequences of *MSH1* genes from 3 broad-taxa species were used to query the NCBI nr database (Table 5.1). Accession numbers are unique identifiers of a particular record in the database, most used here are NM entries for mRNAs that encode a specific protein.

All sequences producing significant alignments were exported, and sorted to filter for species names and TaxIDs. Hits for *Saccharomyces* were returned with a few MSH2 and MutS2 alignments– these were filtered out, and repeats of any species were removed. Species and TaxIDs were alphabetically interleaved for the three alignment results. The breadth of species collected were viewed with NCBI's CommonTree feature using TaxIDs of the species (Federhen, 2012).

5.2.3 Quick BLASTn searches for *MSH1* presence across various species

BLASTn was used to check for evidence of *MSH1* presence within specific species. The three *MSH1* accessions (Table 5.1) were separately used to search for nucleotide (bases making up DNA molecules, A,T,C,G) sequence similarity to the species-specific gene accessions. Parameters used were the default: 100 target sequences, expect threshold of 0.05, word size of 11, using no species-specific repeats filter. The version of BLASTn used was 2.12.0+ (Altschul et al., 1997).

5.2.4 Assembly of a broad eukaryotic tree with detailed genome annotation

Another method for generating a broad eukaryotic tree is to use assembly summaries from international genome databases. Assembly summaries were downloaded from GenBank using pre-defined keywords: fungi, invertebrate, plant, Protozoa, vertebrate_mammalian, vertebrate_other, and the same from RefSeq. GenBank is the comprehensive genome sequence database (Benson et al., 2013) from the National Institute of Health that is updated regularly with the most recent accessions and annotations (annotated genomes have had their gene locations, coding regions and probable gene functions labelled)– though some entries are unannotated. RefSeq (O'Leary et al., 2016) provides a more stable reference of well-annotated sequences, and are copies from selected assembled genomes available in GenBank. Other differences between these databases lie in where the information is collated from. Both of these databases have an assembly level assigned to each entry, defined as the highest level of assembly for any object in the genome assembly. Assembly summaries were filtered for the values 'complete genome' or 'chromosome'. 'Complete genome' is defined as all chro-

mosomes being gapless (i.e. no unknown or unsequenced regions), and having no runs of 10 ambiguous bases (nucleotides). There are also no unplaced or unlocalised scaffolds (sections of sequenced genome, made by joining several contiguous sequences of nucleotide bases (contigs) together), and all chromosomes expected are present. Genomes of organelles may or may not be present but if they are, they are gapless. 'Chromosome' assembly level is defined by sequence availability for one or more chromosomes, that can be either completely sequenced (no gaps) or containing scaffolds/contigs with gaps, and some scaffolds may be unplaced (within a sequences) or unlocalised (to a particular chromosome).

These are two levels of details chosen for the eukaryotic reference taxonomy. Using pre-defined levels of assembly gives a rigorous definition. An alternative method may be to use a common gene, such as *RecA* or Actin (*ActB*) to use as a reference, and should an NCBI entry hit for that gene, the rest of the genome is likely at a similar level of detail, as has been done in subsection 5.2.1.

5.2.5 Lifespan data collection

Data on species lifespan was collected from various sources. AnAge was used to collect maximum lifespan data on animals (Tacutu et al., 2018; AnAge, 2021). MitoAge was also used to gather maximum lifespan data on many animals (Toren et al., 2016; MitoAge, 2021). Data was collected from the Wikipedia list of longest-lived organisms (Wikipedia, 2021), it was noted whether these organisms are aquatic, live in colonies or are individuals. The Encyclopedia of Life (EoL) was a useful resource for varied species (Parr et al., 2014; Life, 2021) by searching for the 'Lifespan' attribute, both maximum lifespan and single measurement categories can be accessed for all measured species. Single measurements were treated the same as the span maximum, as they still carry useful data. Some EoL lifespan measurements were given in string 'high/medium/low' categories, so were transformed into

year ranges as defined by EoL (which uses data from plants.sc.egov.usda.gov, definition "For the Tree growth habit: Short: < 100; Moderate: 100 - 250; Long: >250. Life spans for other growth habits are not quantified"). Many annelid entries had >=5 years as their maximum lifespan estimates, so further investigation was taken for these species. All data was transformed into years, for continuity. For any species that had repeat entries, the maximum lifespan of all the repeats was taken. Subspecies and subgenuses were removed from EoL data. For all of these methods, if either only species name or TaxID was known, the online Tax Identifier tool (www.ncbi.nlm.nih.gov/Taxonomy/TaxIdentifier) was used, and in the case of EoL, NCBI's *preferred* species names were used instead of those found on the EoL site. For example, *Pseudobagrus ichikawai* is the 'preferred name' of *Coreobagrus ichikawai*.

5.2.6 Taxonomic tree generation and visualisation

Taxonomic trees can be visualised using NCBI's CommonTree (Federhen, 2012). For the most part, Taxonomic trees were generated using TaxIDs, rather than species name as it allows greater specificity, particularly for subspecies data. Taxomic trees were exported as .phy files. Age matching to taxonomic trees was done using species names. The phytools package was used in the visualisation of these trees (Revell, 2012).

5.3 Results

5.3.1 Self-contained approach for assessing the relationship between lifespan and presence of *MSH1* (sister-cousin analysis)

In order to address our hypothesis of a link between presence of mtDNA recombination genes and increased lifespans, we need to collect as many instances of close relatives with differences in traits as possible. We first took a self-contained approach where we generate a broad eukaryotic tree from a gene found across kingdoms (*recA*), as well as those with mtDNA recombination genes. We then search across this tree at multiple levels for pairs that have trait differences, collecting any and comparing lifespan data to address our hypothesis.

To begin, we generated a broad Eukaryotic tree from species with a 'RecA' Gene label. The *recA* super-family is a near-universal gene group involved in homologous recombination and repair of DNA (see section 5.2). Of the 13174 RecA Gene label results, 9045 were eukaryotes (including repeats), the rest viruses, bacteria and archaea. The same search for RAD51 (eukaryotic-specific *RecA* homologue) yields fewer, with 6862 eukaryotic results (including repeats). A search was also conducted for species marked with *MSH1/MGM101/MHR1*, to assess recombination gene presences. These results were combined with the RecA list and transformed into a taxonomic tree. With no repeats there were 1239 species in this tree. When species were matched to lifespan data lists, and species without lifespan estimates removed, 288 species remained.

For this remaining broad Eukaryotic tree, trait presence of *MSH1/MGM101/MHR1* $(+/-)$ was mapped onto both internal nodes and external tips (see Section 5.2). Trait presence can be seen as red boxes on the taxonomic tree in Figure 5.2. It can be seen that the majority of the species with these mitochondrial recombination genes are plants, and

they share in this particular tree, the parental node '*magnoliopsida*', with a median lifespan of 250 years. A region of interest for this study is amongst basal metazoa, as well as bivalves, in which some species have been shown to retain mtDNA recombination genes and live for long lifespans. Of the 288 species remaining to be used in this comparison, there were 17 plants, 3 bivalves, 1 budding yeast, 1 nematode and 1 sea urchin. Amongst these, only the plant species reported Gene labels with either of the three mtDNA recombination genes, with the remaining bivalve species (scallops and oysters) not positive for these genes, although bivalve species have been shown to recombine their DNA (Ladoukakis and Zouros, 2001; Burzyński et al., 2003).

Another node marked with mitochondrial recombination proteins was the yeast *Saccharomyces cerevisiae* with a lifespan estimate of 0.04 years. Working back up the tree towards the root, our analysis sought to find familial scenarios where one offspring group had the trait of interest, and the other did not. By this logic, the only comparison to come out of this sister-cousin analysis was the pairing between *magnoliopsida* + *Saccharomyces cerevisiae* vs *metazoa*, a very broad node (with an average lifespan of 20 years). We therefore conclude that although, given more data points, this analysis would provide a means to statistically investigate the lifespan of groups of organisms with or without a trait of interest (mitochondrial recombination genes), the data gathered did not provide more than $n = 1$ comparisons for this sister-cousin analysis.

While this sister-cousin analysis is simple and self-contained, it is not faultless, in that we know some organisms possess mtDNA *MSH1/MHR1/MGM101* that are not present in the Gene label database. This could be as genomes have not yet been annotated, or fully arranged. Therefore, we proceed by suggesting a more detailed and targeted pipeline to address these issues and although still a work in progress, provide a deeper level of detail on organisms with these genes.

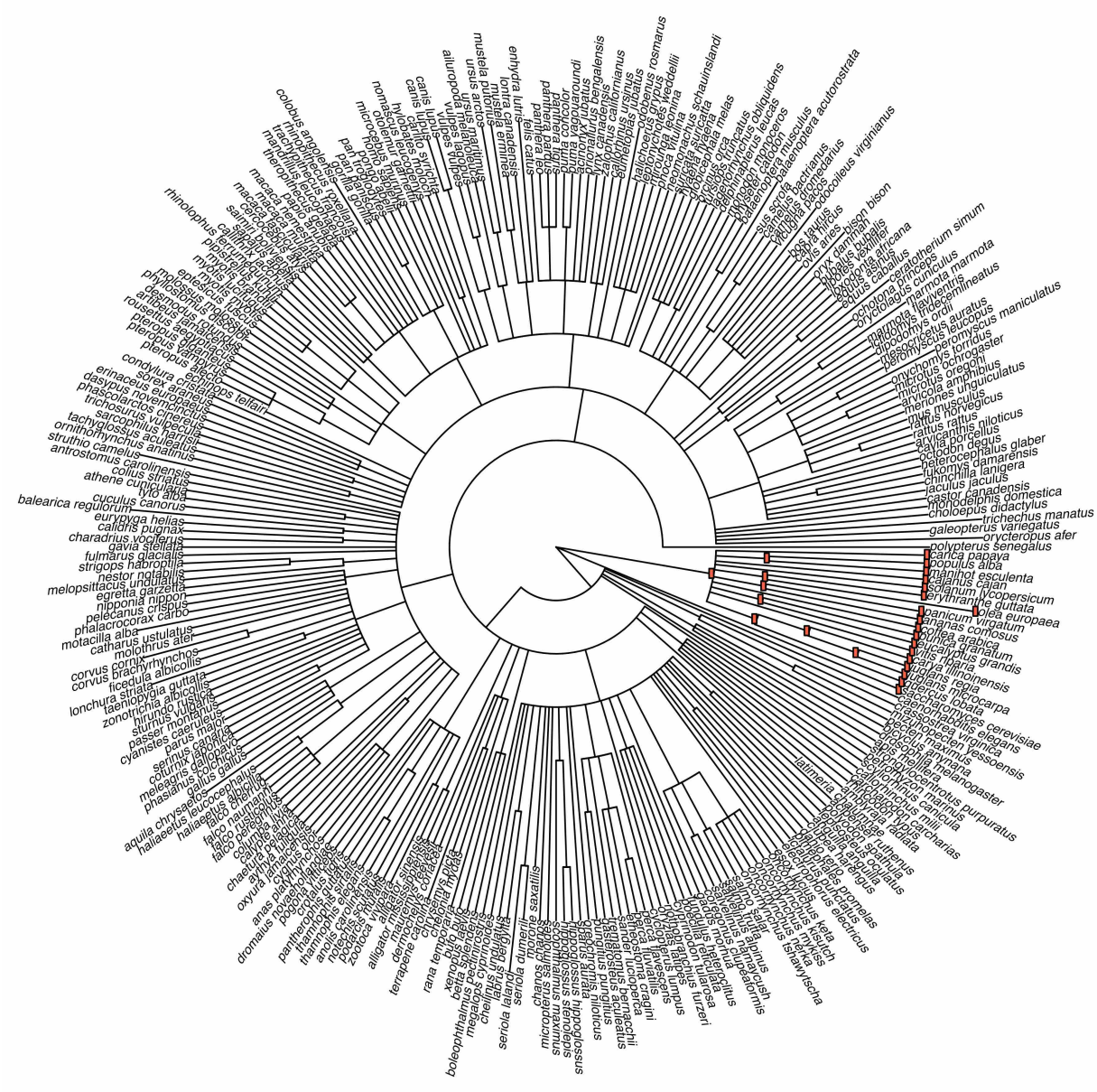

Figure 5.2: Broad Eukaryotic tree for sister-cousin analysis. The broad Eukaryotic tree is made from species given in both *RecA* and *MSH1/MHR1/MGM101* Gene label searches, that also have lifespan data available for them ($n = 288$). Nodes labelled with red boxes are the parent taxa and species with the presence of *MSH1/MHR1/MGM101* mitochondrial recombination genes.

5.3.2 Forms of *MSH1* found across broad taxa include corals, plants, and fungi

Data collection began for our broader approach with searching for species with similar nucleotide sequences to the *MSH1* gene (using three accessions of the gene (Table 5.1)). BLASTx was used initially, as a more specific search method than the Gene function in NCBI. Searches of protein databases using a translated nucleotide sequence allow for a more specific look at the accession available through the NCBI databases. Gene label can also be used as a search tool through the RefSeq database, but relies on genes having been annotated, and Gene records are not created for incompletely represented genomes (see Section 5.2).

Using the accession numbers of three species with different forms of *MSH1* (See Section 5.2), we collected 3652 distinct eukaryotic species (According to NCBI CommonTree, see Section 5.2). BLASTx hits are defined here as any accession in NCBI databases where the nucleotide sequences of available genomic information (tested in six reading frames) is similar enough to the search accession sequences to pass a low significance threshold (E value, here 1×10^{-51}, see Section 5.2). High level taxonomic groupings of these hits can be in Table 5.2.

5.3.3 Assessing presence and absence of a recombination gene across a broad taxonomic tree

We next wanted to produce a broad eukaryotic taxonomic tree, with which to gather examples of closely related species that have, or do not have, presence of MSH1 type recombination proteins. These examples can be used to test our hypothesis of whether there is a correlation between lifespan and presence of recombination genes. For this, we could use the

anthozoans	2185	ferns	1
placozoans	1	other green plants	5
bryozoans	1	diatoms	5
ascomycetes	907	oomycetes	2
basidiomycetes	230	cryptomonads	1
glomeromycetes	9	red algae	1
chytrids	2	other eukaryotes	2
other fungi	24	bacteria	2749
flowering plants	265	archaea	35
green algae	11	viruses	32
club-mosses	1	Other	1

Table 5.2: High level taxonomy groupings and the number of species within each group returned from BLASTx hits for *MSH1* like protein sequences (see accessions in Table 5.1, and Section 5.2). Red = animals, brown = fungi, green = plants, grey = various other eukaryotes.

NCBI Common Tree tool, which plots a broad taxonomic tree for all eukaryotic species with molecular data within the NCBI databases. However, the genomic detail of each of these entries is not provided, making it difficult to claim that any closely related species that does not have *MSH1* according to our BLASTx search does not have this protein at all. Therefore in order to claim a presence/absence of the gene– even to some extent– more genomic detail into each of the species is needed.

GenBank and RefSeq can provide this detail- see Section 5.2. Collecting taxonomic trees at two levels of assembly detail for both databases provides the basis to begin collecting instances of *MSH1* absence or presence across the tree of life (absence defined as a lack of *MSH1* for that species in BLASTx hits). *MSH1* hits from BLASTx searches were found

across an average $\sim\frac{2}{5}$ of species across both RefSeq and GenBank lists (Figure 5.4). Here, matches (blue, presence) are defined as the taxID being present in both the RefSeq/GenBank search and the BLASTx hits, and from this, pairs of closely related species (sisters) with one sister of *MSH1* presence and one with *MSH1* absence can be defined. However, we encounter a few issues described across the next sections and illustrated in Figure 5.3.

It must be noted that there are rare occasions where a certain strain may be found within BLASTx hits, which does not correspond to the species' TaxID in the RefSeq/-Genbank list- an example can be seen in Figure 5.3.A and 5.4.B, as *Hyphopichia burtonii* shows absence of *MSH1*, wheras the strain *Hyphopichia burtonii* NRRL Y-1933 appeared in BLASTx searches for *MSH1*. BLASTn searches against both the genome reference and the NRRL Y-1933 strain return results for the NC_001140.6 *S. cerevisiae MSH1* accession, however the genome reference does not appear in the constrained BLASTx search for this accession. This demonstrates the specificity of TaxID use, and potential differences between using translated nucleotide sequences in BLASTx and just nucleotide similarities on BLASTn.

There are also examples of where *MSH1* has been picked up in one sister species, but not another (Figure 5.3.B). The oak species *Quercus lobata* was hit by BLASTx searches, showing *MSH1* presence. However, its sister species *Quercus mongolica* was not picked up by the BLASTx search. Subsequent BLASTn searches on *Quercus mongolica* revealed a 74% percent identity with a 24% query length and a low E value of 2×10^{-62} to a whole genome shotgun sequence for the *Arabidopsis MSH1* accession, although it had not shown up on the BLASTx hits. This is compared to a 74% percent identity for *Quercus lobata* BLASTn with an 24% query coverage and a 1×10^{-59} E value. This result demonstrates the issue of false negatives, and the caution that should be demonstrated with the largest broad Eukaryotic tree generated with GenBank 'chromosome' assembly level data (Figure 5.4) - here *lobata* is *MSH1* present, but as *mongolica* has not been marked present by BLASTx,

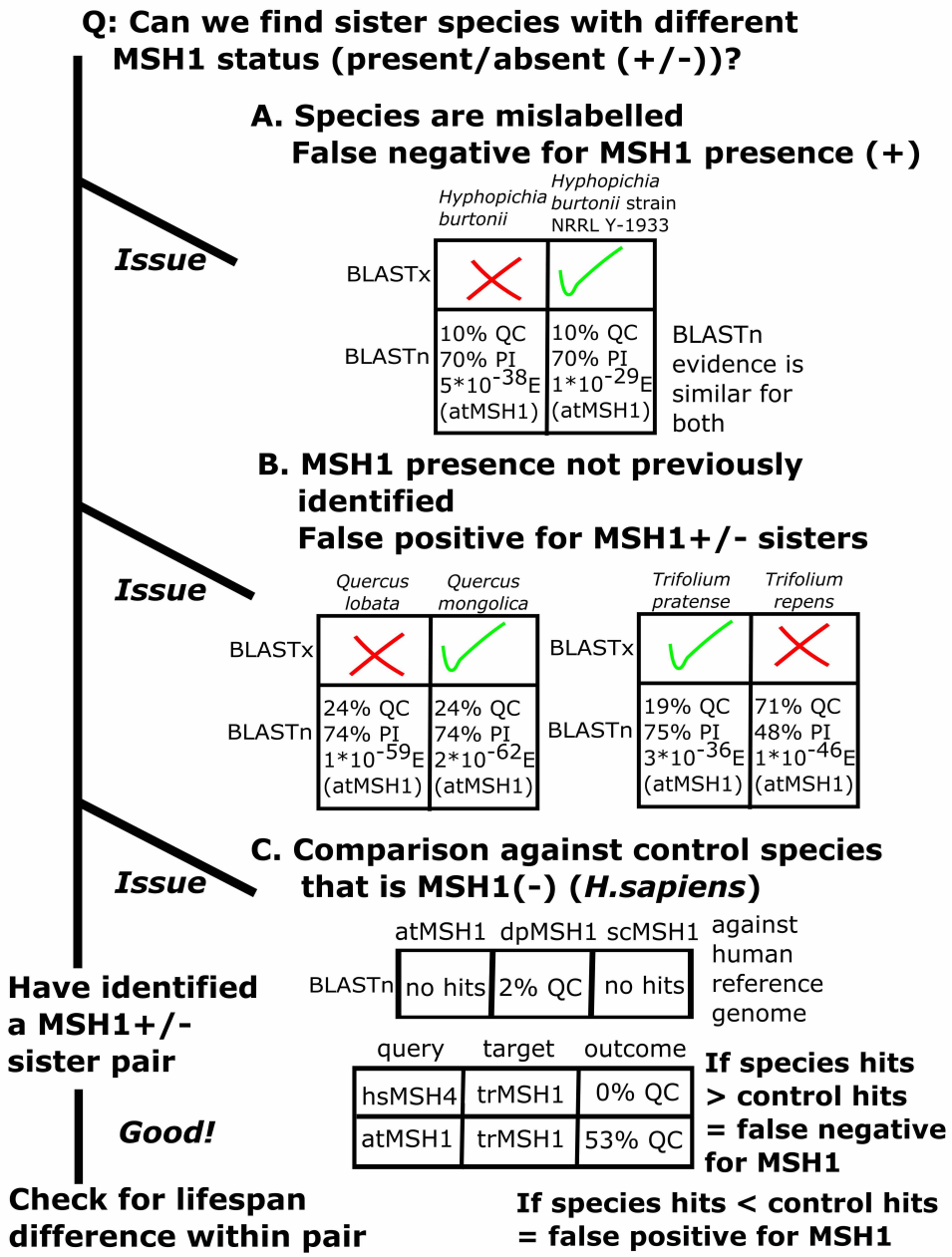

Figure 5.3: Issues with identifying true *MSH1* present/absent sister pairs using BLASTx sourced data. A decision tree laying out three (A-C) potential issues with analysis based on broad RefSeq/GenBank eukaryotic trees populated with BLASTx *MSH1* hits. Abbreviations: QC, Query cover; PI, percentage identity; E, expect threshold; hsMSH4, *Homo sapiens MSH4* accession; trMSH1, *Trifolium repens MSH1* accession; atMSH1, *Arabidopsis thaliana MSH1* accession; dpMSH1, *Dendronepthya putteri MSH1* accession; scMSH1, *Saccharomyces cerevisiae MSH1* accession;

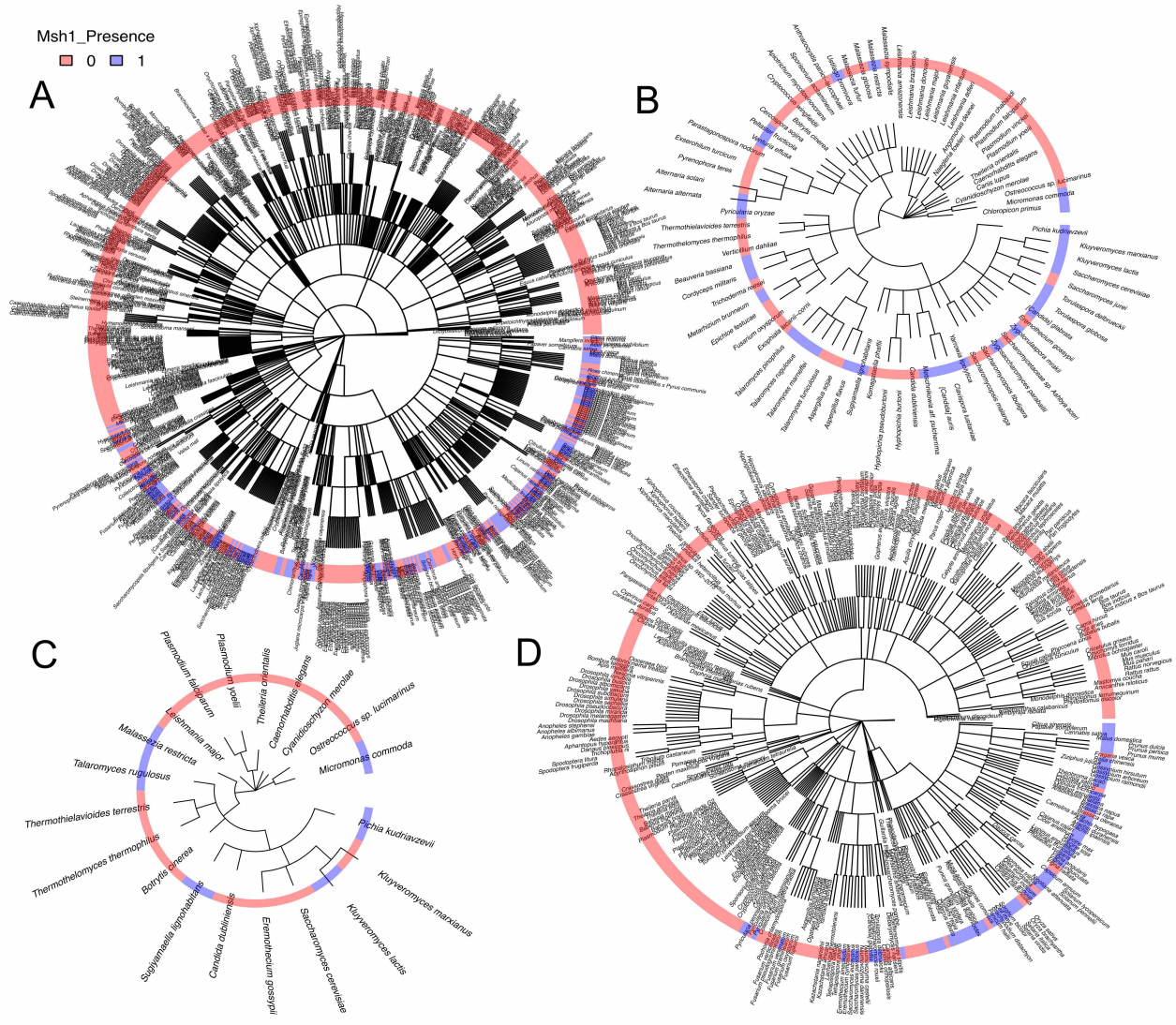

Figure 5.4: *MSH1* presence across four taxonomic trees of various detail. Taxonomic trees gathered from (A) GenBank data with 'chromosome' assembly level, (B) GenBank data with 'complete genome' assembly level, (C) RefSeq data with 'complete genome' assembly level, (D) RefSeq data with 'chromosome' assembly level. Blue highlight represents *MSH1* presence within BLASTx searches. Red represents *MSH1* absence within BLASTx searches.

it could be mistakenly taken forward as an example where close sisters vary in their *MSH1* gene presence, see Section 5.4.

It can be difficult to truly assess whether a species carries a gene based on nucleotide

similarity alone. The best evidence for gene presence would be to assess the protein product of the gene, create knockout lines that give expected phenotypes, and perform sequence similarity experiments across related species known to have the gene of interest. BLASTn gives us a good indication as to whether a certain species has a sequence with a high similarity to the gene of interest, and was used to assess the *Quercus* species above. However, there are other questions we can also ask. The first is what the sequence similarity looks like for our gene of interest (*MSH1*) in species we know lack it, but do have related genes (*MSH2/4/6*) (Figure 5.3.C)? One species lacking *MSH1* but that has *MSH2/4/6* is humans. A BLASTn search was performed for the three *MSH1* accessions (Table 5.1) against the recent *H. sapiens* accession GRCh38.p13. The search returned no hits against yeast and *Arabidopsis* accessions, but scored two hits with 88% and 80% sequence identity, 2% query cover with an E value of ~0.01 to the *Dendronephthya* accession. This means that any BLASTn hits using the *Dendronephthya* to look for *MSH1* should be viewed with caution, particularly when using the default parameters. We can apply this to an example from the BLASTx data. When looking for sister pairs with differences in *MSH1* presence (using the broad Eukaryotic trees 5.5.A), two *Trifolium* (clover) species were identified (Figure 5.3.B). *Trifolium pratense* was found to have *MSH1* presence according to methods in Section 5.2.2, wheras *Trifolium repens* was not. (*Trifolium subterraneum* and *Trifolium medium* were also found to have *MSH1* according to the BLASTx hits but were not in the broad Eukaryotic trees). It is unexpected that such a close relation of species that have shown evidence for *MSH1* presence would not have it, so *T. repens* was investigated further. BLASTn searches using the *Arabidopsis MSH1* accession turned out a 72% percentage identity, a 48% query cover and a low E value of 1×10^{-46} against *T. repens*. The presence of a hit at all is evidence of a sequence similar to *MSH1*, as a species without it (*H. sapiens*) would not give any hits for the *Arabidopsis* accession at least. The next step is to discern that the hits found correspond to *MSH1*, and not any other *MSH* gene.

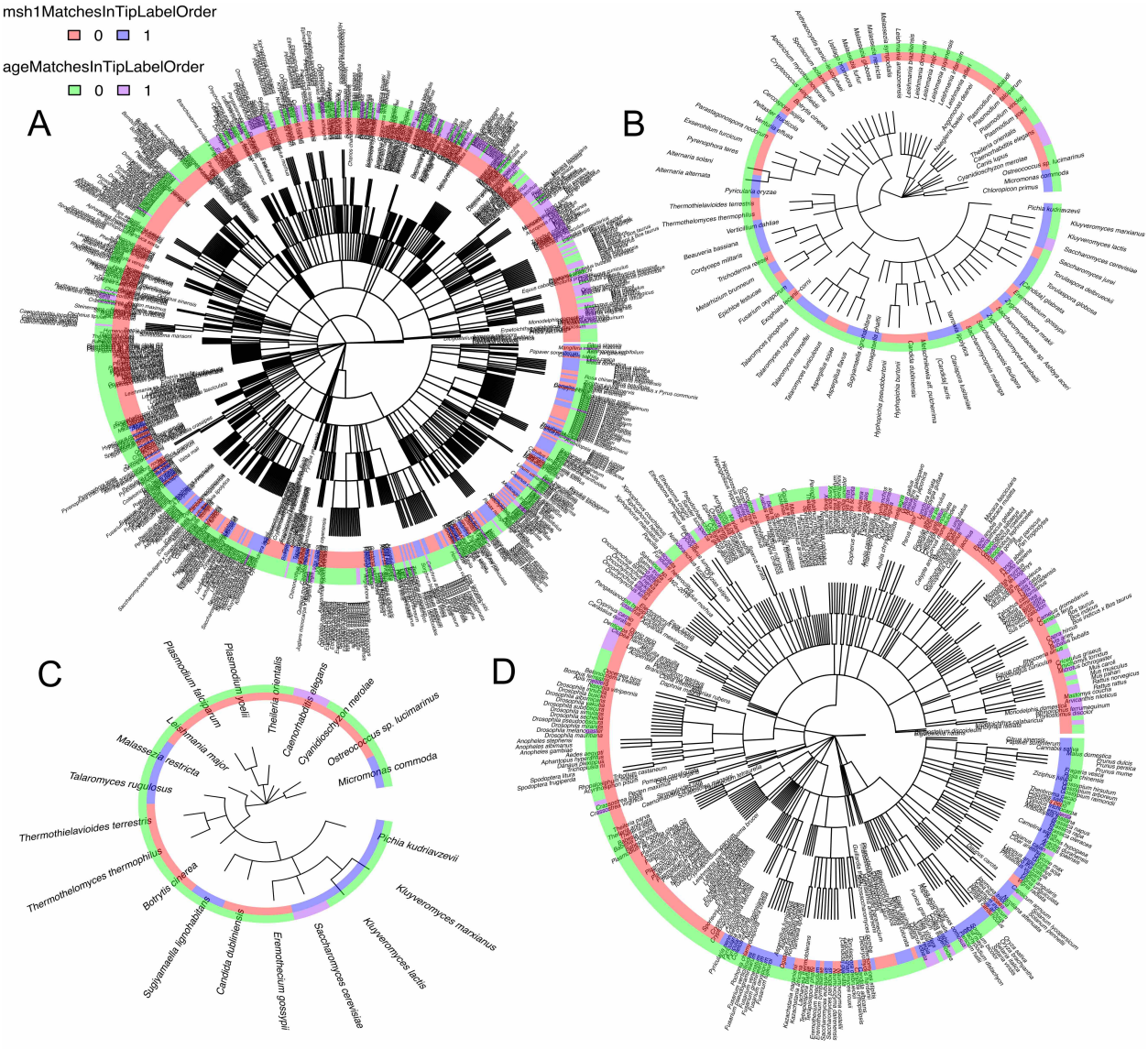

Figure 5.5: *MSH1* presence lifespan data availability across four taxonomic trees of various detail. Taxonomic trees gathered from (A) GenBank data with 'chromosome' assembly level, (B) GenBank data with 'complete genome' assembly level, (C) RefSeq data with 'complete genome' assembly level, (D) RefSeq data with 'chromosome' assembly level. Blue; *MSH1* presence within BLASTx searches. Red; *MSH1* absence within BLASTx searches. Green; species without associated lifespan data. Purple; species with associated lifespan data

.

For this, we can ask whether the highest percentage identity contig (a single section or overlapping sections of genomic DNA used to map the full sequence of a chromosome/region) found in the BLASTn hit had a higher sequence identity with *MSH1* or with other MSH genes (Figure 5.3.C). This is as the *MSH* sequences can be similar, as they are thought to all be descended from bacterial *MutS* (*MSH1*) early in eukaryotic evolution, but their protein products have different locations and functions within the cell. For this the BLASTn suite tool for comparing 2 sequences against each other were used. First, Human *MSH4* [1] was used as the Query sequence, and *T. repens MSH1* candidate [2] was used as the Subject sequence. The comparison had to be done in 10 million base chunks of the subject sequence at a time, across the 95 million bases of *T. repens MSH1* candidate. Comparison to *MSH4* gave lots of very low query cover hits, wheras comparison to *Arabidopsis MSH1* gave good sized query cover, with good percent identity. The same was seen for *MSH2/4*. We can conclude that the *T. repens MSH1* candidate is more likely to be *MSH1* than other *MSH* genes.

Detail of taxonomic levels can also be seen in Figure 5.6, with animals well represented within this tree. Some species that have *MSH1* presence in certain taxons may not be represented within the RefSeq data, as it is a subset of organisms available in NCBI databases. Gathering instances of sister species with differences in traits, here the presence or absence of *MSH1* is a key step towards testing our hypothesis of mtDNA recombination influencing organism lifespan.

5.3.4 Lifespan data across a broad taxonomic tree

Lifespan data was collected from various sources, from monitored databases to webpages, and collated into a list of organisms with maximum lifespan estimates (see Section 5.2.5). This

[1] Accession number NC_000001.11 (positions 75796882..75913242)

[2] Accession number CM019101.1 (72% identity to *Arabidopsis MSH1*)

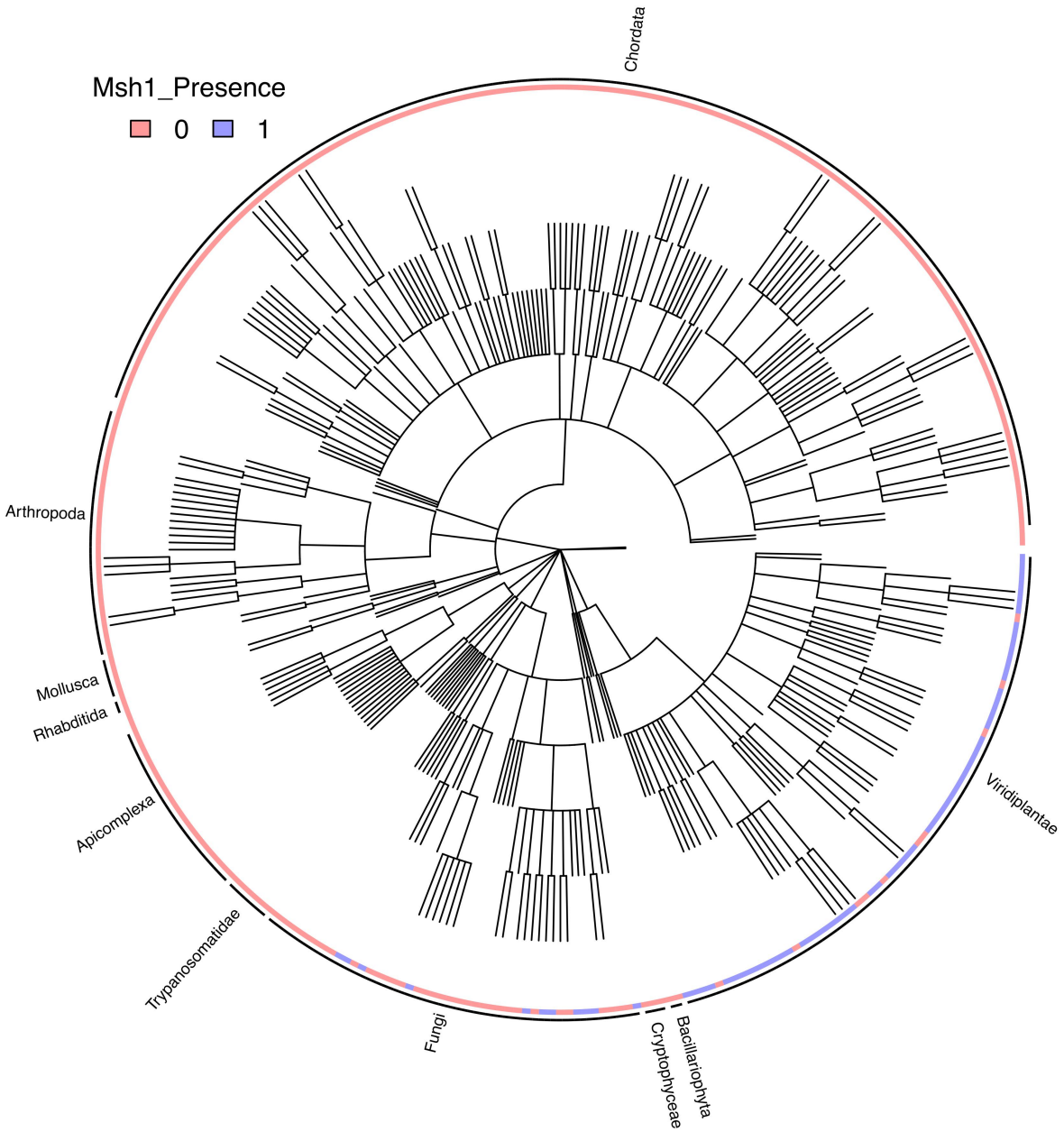

Figure 5.6: *MSH1* presence across 'Chromosome' level assembly of a eukaryotic tree. High-level taxonomy labels are marked around outside of tree. Blue highlight represents *MSH1* presence within BLASTx searches. Red represents *MSH1* absence within BLASTx searches. This taxonomy is also seen in Figure 5.4.D.

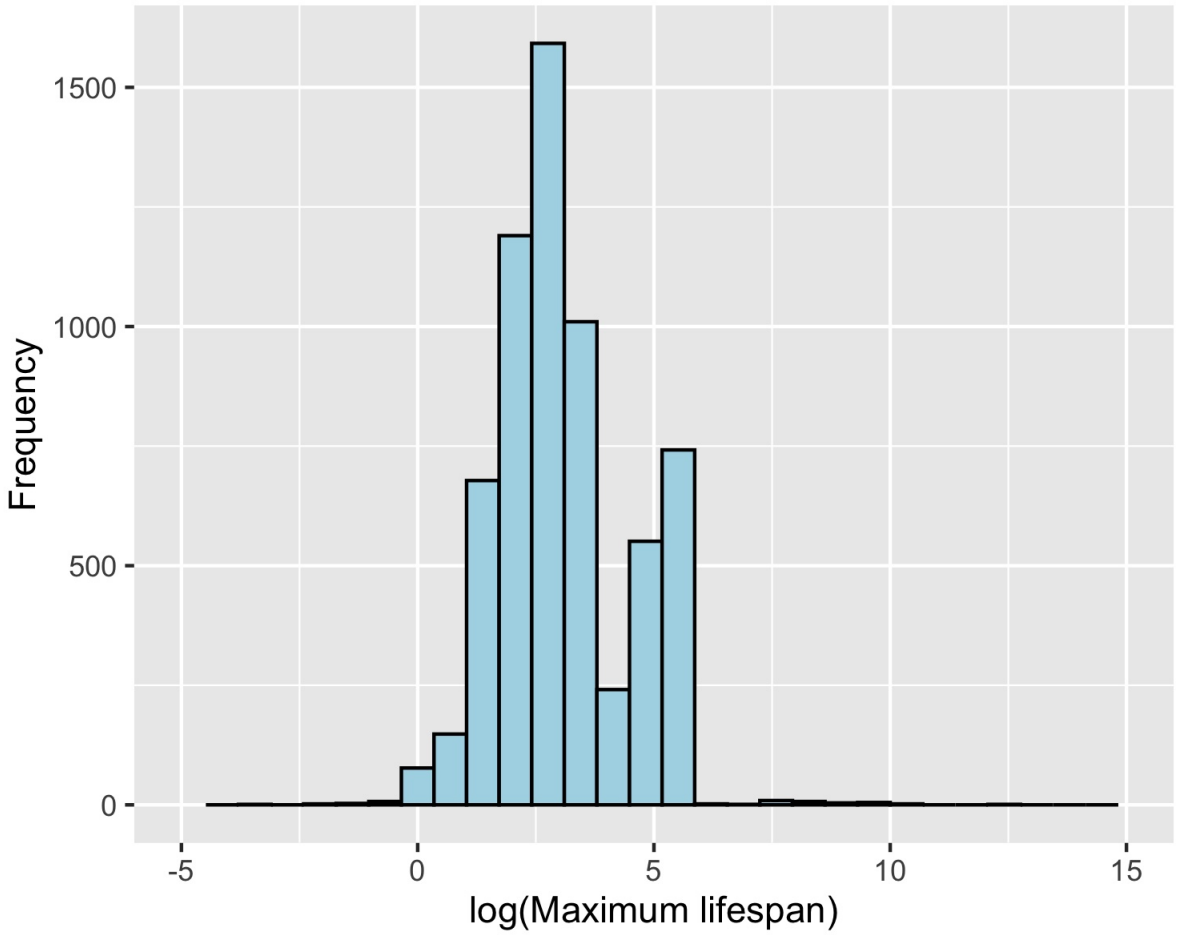

Figure 5.7: Range of values for maximum species lifespan data (years). Values where predicted lifespan maximum are undefined or infinity are excluded.

list covers a broad range of species, and again metazoa are well-represented. Exact values for maximum lifespan range from 0.04 (*Saccharomyces cerevisiae*)- 200,000 yrs (*Posidonia oceanica*, a clonal seagrass) (Figure 5.7). Some organisms were noted as having infinite lifespans, mostly as they were designated $n+$ years in databases used.

Across Metazoans, we see very few long-lived organisms, with only a few exceptions such as some reptiles like Tuatara (*Sphenodon punctatus*, 111 yrs) and European pond turtle (*Emys orbicularis* 120 yrs), fish such as the Greenland shark (*Somniosus microcephalus*, 512 yrs) and some bivalves (*Margaritifera margaritifera*, 250 yrs and *Arctica islandica*, 507

yrs) (Figure 5.8). Polychaetes are consistently short lived with the exception of *Escarpia laminata*, a tubeworm (1000 yrs). Streptophytes (land plants and some green algae) have consistently long lifespans, with species such as *Lomatia tasmanica* (43,600 yrs), *Quercus palmeri* (30,000 yrs) and *Picea abies* (9550 yrs) being some of the longest lived examples. Overall, 6824 varied lifespan entries for unique species were collected, spanning the broad taxonomic range (Figure 5.8).

It is worth briefly mentioning how maximum lifespans are estimated for these organisms. For tree age estimates, cores can be taken from living individuals and dated based on ring number. The oldest bristlecone pines in California, US have even been used to calibrate radiocarbon timelines (Damon et al., 1974). Estimates can be verified against continuous historical records or extrapolations based on regressions of size and age. A comparable method is used in dating the incremental depositions of bivalve shells (Butler et al., 2013). For long-lived fish such as the greenland shark, radiocarbon dating from eye nuclei of unintended bycatch has been undertaken (Nielsen et al., 2016). Some mammals can be observed in captivity, such as laboratory mice that are used in longevity studies and can be observed for their entire lifespan (Miller et al., 2002). Sea sponges, and their silicone-based skeletons made of spicules can be dated using the small amount of carbon stored in proteinaceous matrices of these structures to determine elongation rate (Fallon et al., 2010). Life span and growth estimates are often dependant of the species, for example the cushion-like Yareta plant found the Andes, South America has has its growth rate predicted by the digging of a central trench, and monitoring of the grow-back over the subsequent months (Kleier and Rundel, 2004).

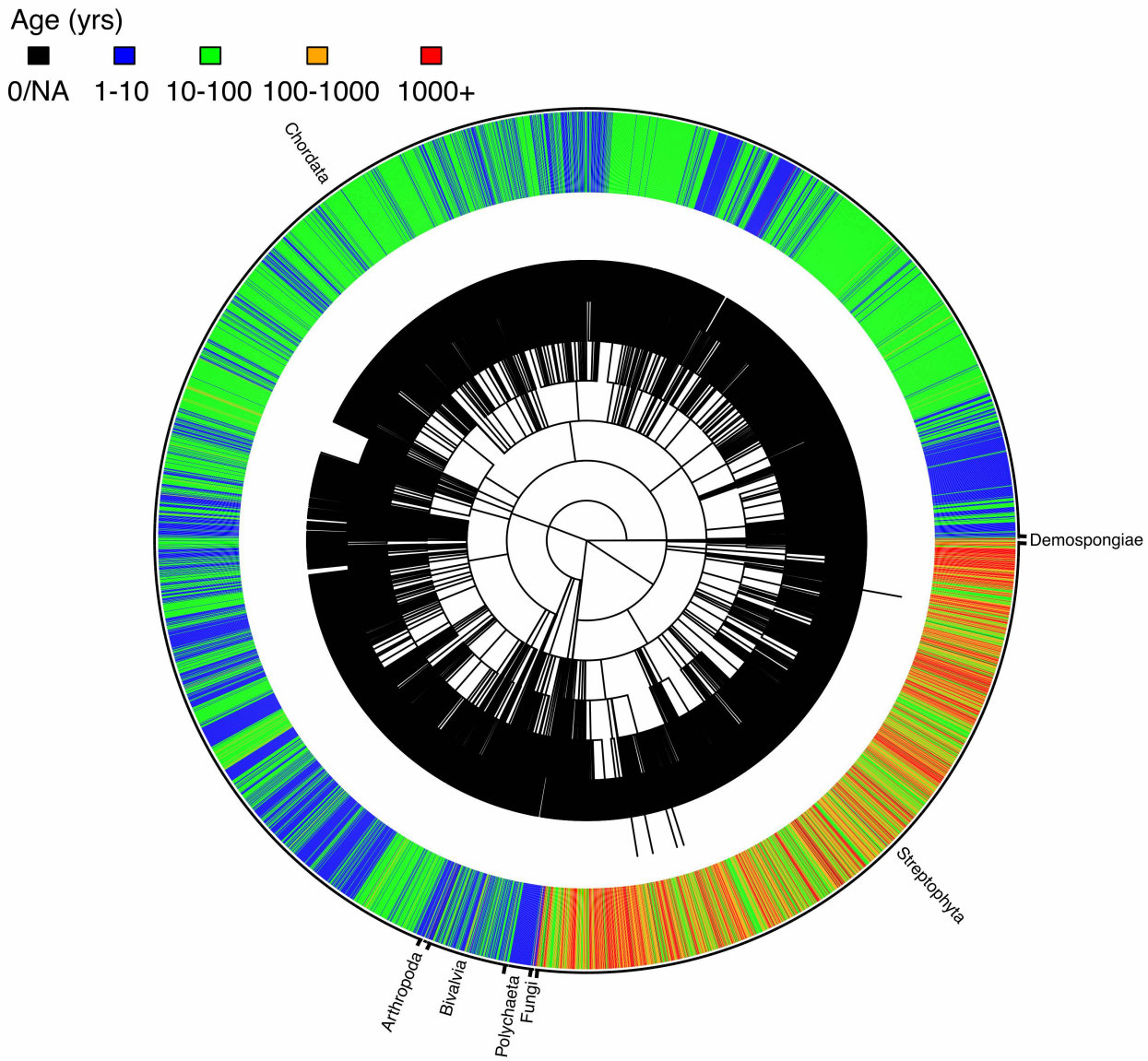

Figure 5.8: Maximum lifespan was collected for a broad range of taxa. Taxonomic tree has had single branches collapsed, resulted in reduced internal tree nodes such as phylum nodes. Groups of interest are labelled by the nearest sub-group node. Ages are colour coded according to legend.

5.3.5 Assessing the relationship between lifespan and presence of *MSH1*

Given that animals often tend to have short life-spans and no *MSH1*, and plants long lives and have *MSH1*, switching focus to species that are primitive animals, lack body plans, or early plants may reveal more diversity across traits of interest. We are interested in the link between lifespan and recombination gene presence. In order to quantify this, we need a range both lifespan and gene presence values, so that we can justify claims of changes in *MSH1* presence having an impact on lifespan. Most plants and animals don't have a range of recombination gene presence (*MSH1* presence/absence), as they either all have the gene, or do not– so we cannot quantify a link between traits. Therefore we focus our interest on basal animals and fungi, as they demonstrate a range in values for *MSH1* presence/absence. Figure 5.9 illustrates lifespan and *MSH1* presence across bivalves, arthropods, fungi, sponges, sea urchins and arthropods. Diversity in lifespan can be seen particularly for sponges, sea urchins and fungi. Conclusions in patterning are difficult to conclude due to a low n for these species based on which have lifespan data here, and which have *MSH1* as present.

For assessing the relationship between lifespan and *MSH1* presence, we began by aiming to collect as many sister (*genus/cousins/subfamily/family*) species as possible, with age data and with presence/absence of *MSH1*. This should allow us to automatically control for phylogenetic structure and differences across taxa, that otherwise might couple two variables of interest. For this, related pairwise comparisons can be performed. We note that absence of evidence is not evidence of absence, and absence is only defined according to our analyses: Absence is defined as no hit against the accessions used to BLASTx for *MSH1*, and that the broad taxonomic trees we are comparing to have enough assembly detail to give confidence that if BLASTx does not find the translated nucleotides within that sequence, then it most likely does not have *MSH1* (see *Quercus* discussion for false negative (section 5.3.3)).

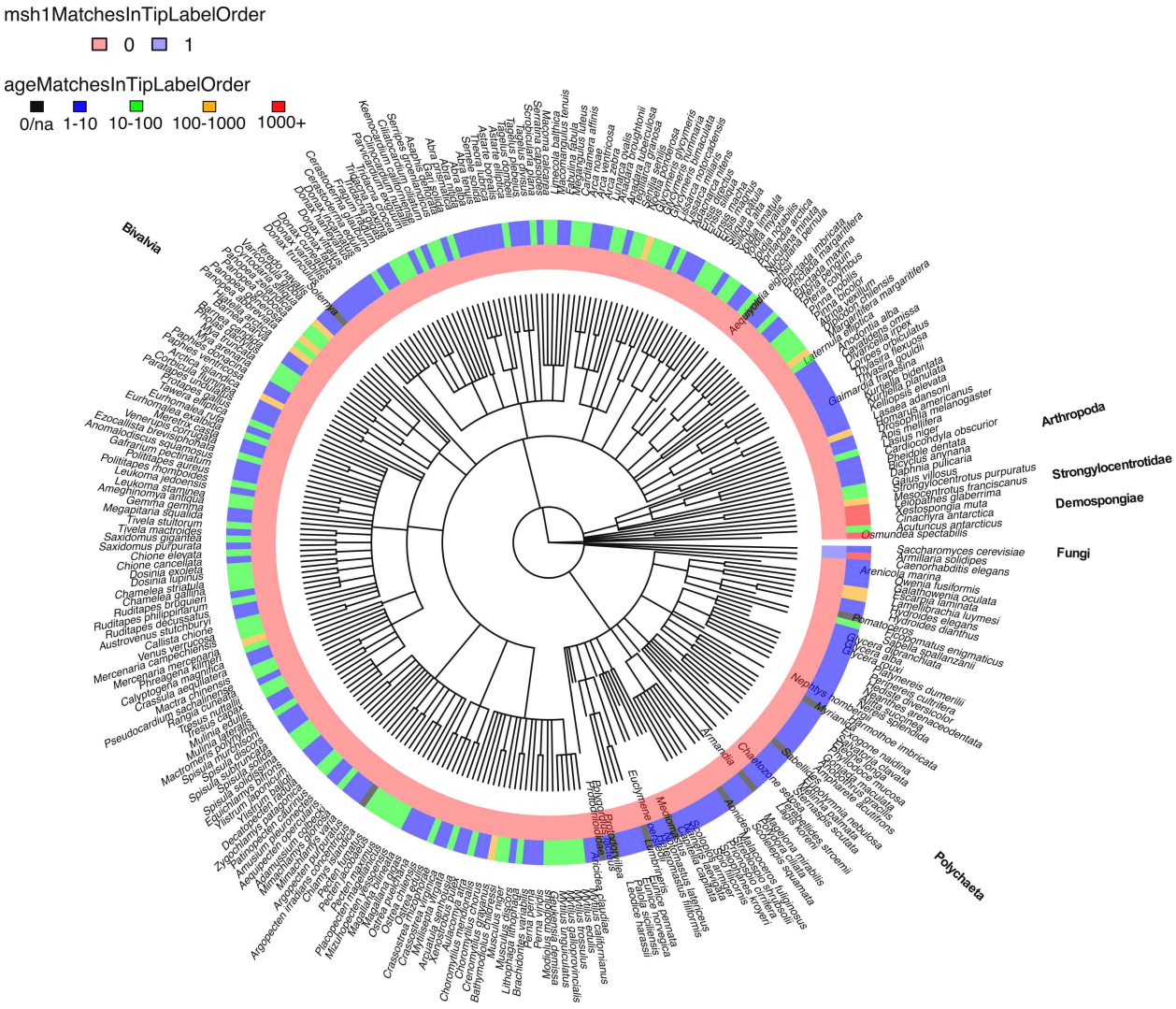

Figure 5.9: Lifespan and *MSH1* presence for a subset of species of interest. A taxonomic representation of species holding diversity in lifespan excluding chordates and Viridiplantae. Note that the structure is not built from a broad eukaryotic reference tree, but species within clade of interest with lifespan data. Tips of the tree are all at the same distance as nodes with only one tip have been collapsed. The colour black represents either species with negligible lifespans or species names that did not match between the two trait lists. Broad classes of species are shown in bold around the outside.

In order to get a broad look at the appropriate sisters/cousins with either/both of the traits of *MSH1* presence and lifespan estimate, both can be plotted against the Ref-

Seq/GenBank broad taxonomic trees (Figure 5.5). It can be seen that again, Metazoa are well-represented within the lifespan data across these trees, particularly in Figure 5.5.A. Our interest lies in sister pairs with lifespan estimates, with one sister with *MSH1* present, and another with *MSH1* absent. One paired example where both species have lifespan data and one has *MSH1* presence and the other absence is the grasses *Thinopyrum elongatum* (tall wheatgrass) which is noted as *MSH1* absent, and *Eragrostis curvula* (weeping lovegrass) that has *MSH1* present, according to our BLASTx searches. According to EoL (see section 5.2), *T. elongatum* has a moderate lifespan, and *E. curvula* a low lifespan. This pair does not correspond to our expected trend of *MSH1* presence increasing lifespan, as the grass with *MSH1* absence has the longer lifespan.

Another pair are two fruit trees, *Punica granatum* (pomegranate) which is *MSH1* present, and *Cocos nucifera* (coconut), which is *MSH1* absent according to our BLASTx searches. Both are shown to be of moderate lifespan (100-250 years) for trees. However, a quick search gave estimates for coconut of 70-100 years, and for pomegranate up to 300 years, but with best fruiting years very early on, which would demonstrate that species with *MSH1* presence have longer lifespans. However, since these BLASTx searches were run (Sept. 2020), a putative form of *MSH1* https://www.ncbi.nlm.nih.gov/protein/1954367237 in *Cocos nucifera* now appears in BLASTx searches using *A. thalaina MSH1*. This demonstrates again that is difficult to rule out *MSH1* absence completely, based on a static search.

Lack of sister pairs is not the only drawback to this approach. Ideally, comparing sisters, or even cousins in this way would count as an independent sample from a pair of unrelated sisters/cousins. However, if two pairs of sisters have the same mother, they are no longer unrelated. This is an issue, as we lose independence of these paired samples, and cannot claim that a difference in one pair is separate from any other effects.

5.4 Discussion

Using a broad taxonomic analysis across eukaryotic species, the possible link between recombination of mitochondrial DNA and extended organisms lifespan has been investigated. This preliminary analysis has demonstrated that organisms with long lifespans are often those with the presence of recombination surveillance genes. However, it has also revealed the difficultly in recruiting a large sample size of related species and taxa with differing gene traits, and reducing false negatives for these traits.

Factors affecting lifespans of organisms are numerous and complex (López-Otín et al., 2013; Dodig et al., 2019). It can often also be difficult to measure lifespan for organisms that have clonal life histories (Witte and Stöcklin, 2010; Arnaud-Haond et al., 2012). Amongst animals, basal metazoans have the longest lifespans, due in part at least to a simple body plan, and abundance of stem cells allowing– in some cases– regeneration even if the body is separated (Petralia et al., 2014). It has been shown that basal metazoa without fixed body plans often use mtDNA recombination genes as opposed to sequestering mtDNA early into a germline, as an alternative mechanism protecting against mtDNA mutation build-up (Edwards et al., 2021). Basal metazoa such as sponges, hydras, corals, placazoans, ctenophores and myxozoans hold a great diversity in terms of lifespan and mtDNA recombination gene traits (Muthye and Lavrov, 2021).

As expressed within subsection 5.3.1 however, our preliminary analysis currently does not include many datapoints for these basal metazoa, limiting the statistical power of our system to comparisons mainly between metazoa as a whole, and plants/fungi. It should be noted that our analysis of trait presence using a sister-cousin comparison, nominating trait presence to either tree tips or internal nodes is, by design, extensible. The relationships between clades of different traits can be examined, and organisms can have any continuous property, not just age data.

The data collected using NCBI databases are general searches, whether BLASTx searches against *MSH1* accessions or gene label searches for other recombination genes. Often, the level of detail available differs depending on the species, and this can have the consequence of offering false negatives. More specific BLASTn searches against nucleotide sequence data reveal similar results for two *Quercus* species for the same *MSH1* accession even though our BLASTx search hit only one. It would be unusual for one oak species to retain a recombination gene, and the other not, and so caution must be shown when describing 'absence' of the gene of interest.

Overall, however our preliminary analysis has shown that species with *MSH1* 'presence' are located in similar taxa (Figure 5.4) to taxa with extended lifespan (Figure 5.8). We can further examine which way the relationship is causative, do organisms with recombination genes retain these genes while they are useful, or is it these recombination genes that allow long lifespans? Further statistical support is necessary to back up our hypothesis of a positive link between the presence of mtDNA recombination surveillance proteins and a long lifespan.

Chapter Six

General discussion

6.1 Overview

This work has established a methodology for quantifying and characterising connectivity across the mitochondrial population of a single plant cell, and two pertinent physical distribution and mitochondrial genome surveillance mutants. Investigating the encounters of individual organelles over time, using network science and appropriate summary statistics for social and physical dynamics over time, we have identified a trade-off. This novel framework revealed that the cell must contend between a physically well-spread chondriome and a population with high connectivity between its individuals. The plant cell, in comparison to theoretical models, performs well at enabling 'the best of both worlds'. Connectivity across the chondriome carries genetic implications, investigated using a theoretical exchange framework and a bioinformatic investigation into recombination ability across eukaryotic organisms. These ideas contribute to open questions regarding longevity, genetic stability and the unique properties of the plant mitochondrial structure.

6.2 A new perspective on mitochondrial dynamics within plant cells

The pipeline demonstrated in Chapters 2 and 3 sets out a new approach to the plant chondriome. Graph theory has been previously used to describe the connectivity across reticulated intracellular networks (Sukhorukov, Dikov, et al., 2012; Sukhorukov and Meyer-Hermann, 2015; Fricker, Heaton, Jones, Obara, et al., 2018; Pain et al., 2019), but has not been used until now to quantify the transient encounters between individual mitochondria within plant cells. This approach has allowed an exploration into the priorities of the chondriome that, for most cells in the plant, is physically disconnected.

What is noticeable is the heterogeneity in area travelled by the individuals making up the chondriome within the cell (Logan and Leaver, 2000). There is a great deal of variety amongst these organelles, even within a single sample. This may partially be due to premature trajectory splitting by the tracking method, but is in part also caused by a sub-population of mitochondria moving diffusively, sticking to a local area, and another that utilised cytoskeletal strands to travel longer distances throughout the cell. Each sub-population represents a level at which the cell can respond to changes in metabolic or energetic needs. Sub-populations that move within smaller areas could be used for intra-organellar metabolite delivery, whereas mitochondria traversing further distances could be used for energy delivery to particular regions of the cell, depending on growth needs or environmental fluctuations. Heterogeneity in area travelled therefore provides the system with many levels at which to respond to changes in cellular requirements.

A level of social heterogeneity (as defined by the coefficient of variation of degree) was identified as necessary for network connectivity observed within the cell. However, the range of network topologies between cell types or of the same cell type from the same

seedling sample was not quantified. We hypothesise that the trade-off between even spacing and connectivity will remain across cell types of the plant, such as in the leaf/root tissues, but may lie further towards connectivity, or further towards even spread depending on the functional priorities, environmental pressures and internal organisation of the cell type. For example, in the leaf, the increased level of chloroplasts tightly packed at the surface of the cell decreases the space mitochondria can travel in, and colocalisation with chloroplasts may increase mitochondrial network connectivity by slowing motion upon association (Oikawa et al., 2021).

Timescales are also important to consider within the context of dynamic encounters. The encounter networks characterised are built over a specific timescale, reflected by the summary statistics and topologies. Over longer timescales, it is theoretically possible for a complete graph to be built. This would provide a network with a high propensity for information transfer. However, loss from the field of view, or over even longer timescales, autophagy of individual mitochondria may come into play, with mitochondrial turnover estimated as 9-24 days (from various organs in rats (Menzies and Gold, 1971)), with mitochondrial protein degradation rates (K_d) at 0-0.5 d^{-1} in *Arabidopsis* cells (Nelson et al., 2013). These factors would prevent a complete network graph or definition of the mitochondrial population as a 'closed system'.

6.3 Linking mitochondrial motion and encounters with genetic exchange and recombination

The link between genetic and physical dynamics is still being elucidated (Johnston, 2019b; Edwards et al., 2021). We have demonstrated that mitochondrial dynamics respond to both genetic and physical challenges, and predict that in the future, controlling mitochondrial

dynamics may help us exploit this relationship in the face of genetic perturbations within the cell, or even a local region. The use of encounter networks in linking physical interactions shows potential for genetic exchange (Chapter 3, 4, (Chustecki, Etherington, et al., 2021; Giannakis et al., 2021)), and highlights the quasi-2D plant cell as an excellent model for investigating the emergent collective behaviours of the chondriome.

Further investigation, however, is needed to understand the functional implications of mitochondrial encounters. The state of the mitochondrial network directly impacts the ability to share mtDNA, and controls the extent of mutations in the genome (Lieber et al., 2019; Aryaman et al., 2019; Giannakis et al., 2021). Direct imaging and quantification of nucleoids in individual mitochondria of the plant will give experimental evidence with which to test our theoretical framework of exchange upon mitochondrial encounter networks (Prole et al., 2020). The exact subcellular localisation of specific DNA sequences can be imaged using cloned or synthetic oligonucleotide fluorescent in-situ hybridisation (Beliveau et al., 2015). This would allow exploration of correlations between sequence and space. For example- is there anything specific about mitochondria localised to chloroplasts or to the nuclear envelope? Are the most social mitochondria in the cell being used as 'genetic libraries', providing sequences to others who need them? In-situ hybridisation has been used to demonstrate the removal of mutant mtDNA in the female germline of *Drosophila* by mitochondrial fragmentation, physical sequestration of mutant mtDNA and autophagy (Lieber et al., 2019). The drawback to this method is that samples must be fixed (Prole et al., 2020), so real-time transfer of specific mtDNA sequences between organelles would not be possible. However, cleverly designed sequences of recombination products may provide insight into the outcomes of any intermitochondrial mixing, and utilisation of fusion and fission mutants could help further investigate the link between physical and genetic mitochondrial dynamics in plant cells.

Quantification of the heterogeneity and recombination events between individuals'

mtDNA transfers could provide us with quantitative answers as to how the plant maintains such low mutation rates. This currently is not built into our theoretical model of exchange upon wild-type networks (the 'bingo' framework). There are certain regions of the mitochondrial genome that are more frequent sites of recombination (Arrieta-Montiel and Mackenzie, 2011; Davila et al., 2011). There can be alternate mtDNA forms generated through recombination, that may become predominant through a process called sub-stoichiometric shifting (Chevigny et al., 2020), which can result from preferential segregation or replication of certain mtDNA molecules. There is evidence from within cytoplasmic hybrids (where a cell has the nuclear genotype of one parent, but the cytoplasmic genome of both) that one form of mtDNA may be preferentially segregated and recombined (Bellaoui et al., 1998; Sanchez-Puerta et al., 2015; Garcia et al., 2019; Chevigny et al., 2020)– however, these are *sequence* variants rather than *structural* variants as in sub-stoichiometric shifting between mtDNA molecules. Sequence (base by base) repair is very efficient in plants, whereas in humans this can be a cause of mitochondrial disease as mutant allele types are propagated throughout the mtDNA population. In terms of structural variants, our model currently has no inbuilt preference for mtDNA transfer, an interesting future avenue. Including regions that overlap and cross over between the 'collected' genes in this framework would allow the modelling of damage recovery, and the recombination frequency that keeps nucleoids in the state we see them within the plant mitochondrial population i.e. not all mitochondria have nucleoids at any given time. It may be that the time frame within which our analysis is based needs to be extended in order to quantify a similar number of encounters if mtDNA transfer is required for an edge within the network. Imaging of nucleoids in plant mitochondrial populations is then subject to increasingly sophisticated experimental set-ups (perfusing mounting media, imaging within a cuvette) in order to maintain physiological conditions of an extended time period to collect enough functional encounters (Schwarzländer, Fricker, et al., 2008; Baesso et al., 2018; Prole et al., 2020).

6.4 Further investigation of mitochondrial dynamics

Static mitochondria pose an interesting question for our investigations on the chondriome. Their lack of movement may be the product of cellular stress, in which case a dynamic membrane potential indicator such as tetramethyl rhodamine methyl ester (TMRM) in non-green tissues would indicate the health status of individuals across the population, or mt-roGFP could indicate the level of oxidative stress across the population or individual (Schwarzländer, Logan, et al., 2012; Schwarzländer, Fricker, et al., 2008). As mitochondrial positioning and dynamics are so reliant on the cytoskeleton, static individuals could be present in cells where at that moment there is no cytoskeletal rearrangement and/or cell growth. Staining for the cytoskeleton during time lapses of mitochondrial dynamics would enable hypothesis testing here (Moore and Holzbaur, 2018; El Zawily et al., 2014). For cells where the majority of mitochondria are static, or at slow speeds, an investigation into how evenly spread they are may reveal another side of the identified spacing-connectivity trade-off. If mitochondria that are static are somehow 'satisfied' in terms of energy provision, mtDNA they carry, or the cell has low energy requirements, the mitochondrial population may find that even spread is favoured – compared to intermitochondrial connectivity facilitated by the dynamics we see across the cell space. Therefore the null hypothesis may be that mitochondria are static in an absence of stress. An example from neurons demonstrates that 'docked' mitochondria might serve as static energy providers for regions with high demands (Kang et al., 2008). A comparison of more static encounter network topologies and the network topologies made from a more dynamic system could reveal similarities between the two, producing a similar 'scale-free' like degree distribution despite different movement regimes. It is possible for networks with different structural properties (in terms of topology) to form scale-free networks (Grisi-Filho et al., 2013).

Comparison of encounter networks from plant mitochondrial dynamics and the spac-

ing of reticulated mitochondrial networks from animals is also an interesting point for future investigation. Structural distribution between the two mitochondrial population of animals and plants are very different. Why? It may be a protective mechanism on part of the plant (Johnston, 2019b). It offers a physically limited opportunity for mtDNA exchange, opportunity to rapidly degrade unhealthy individuals, and also respond rapidly to fluctuating environments (Johnston, 2019b), key for sessile plants. However, there may be comparisons with the spacing of reticulated structures in yeast, that are evenly spaced across the cell (Rafelski, 2013; Viana et al., 2020). Perhaps it is the case that animals and plants use two very different motion regimes to reach the same goal- efficient metabolite and energy provision across cellular space, while protecting mtDNA integrity and equal division of mitochondria into daughter cells. Cell geometry and its links to cytoskeletal organisation are cell-specific and dictate the paths upon which organelles are trafficked- microtubules and actin are involved in cell wall synthesis, and so animal/plant differences in organelle trafficking may also arise here (Kost and Chua, 2002; Paredez et al., 2006; Durand-Smet et al., 2020). However, there may even be a universal model dictating mitochondrial network structure across different species, mapped using physical networks or social networks of encounters.

6.5 Future directions and crop improvements

Overall, this thesis aims to quantitatively address the cellular priorities of plant bioenergetic organelles. Plant bioenergetic behaviour is recognised as a key target for further study and investigation in the face of environmental change (Budar and Fujii, 2012), with an aim to improve key crop species and address issues of food security (Budar and Roux, 2011). The importance of organelle positioning is particularly important for C4 photosynthesis. C4 photosynthesis is a strategy that has independently evolved 62 times (Sage, Christin, et al., 2011). In contrast to the majority of flowering plants using C3 photosynthesis, C4 increases

the photosynthetic efficiency of the plant by relocating the inefficient enzyme Rubisco to the bundle sheath cells and capturing carbon dioxide as 4C oxaloacetate. An extensive analysis of the evolution of C4 traits identified cellular organisation and mitochondrial and chloroplast positioning as three of the earliest steps on the way to becoming a C4 plant (Williams, Johnston, et al., 2013). Organellar position has also been shown to be a key step in this process (Sage, Sage, and Kocacinar, 2012; Williams, Johnston, et al., 2013), with mitochondrial relocalisation to the inner bundle sheath cell wall a key step to evolve efficient C4 photosynthesis. In rice, an intermediate step towards efficiency is taken within mesophyll cell. By having chloroplasts and their stromules form a barrier around the outside of the cell, and mitochondria positioned within the middle of the cell, the CO_2 released from photorespiration by cell-central mitochondria is re-fixed by chloroplasts (Sage and Sage, 2009; Sage, Sage, and Kocacinar, 2012). There are also differences in the number, size, and cell areas covered by mitochondria across three biochemical types of C4 photosynthesis (Fan et al., 2021). We ask: how can we use our knowledge of dynamic organelles to influence metabolism in crop plants? How can we increase efficiency by manipulating subcellular location for increased productivity? Having an understanding of the chondriome as a whole, as well as the priorities of positioning is needed when developing approaches for the improvement and bioengineering of more efficient photosynthesis in crop plants.

Appendix One

Results sections relating to Chapter 2

A.0.1 Robustness of unweighted networks describing plant mitochondria encounters

To further examine the quantification of connectivity through the use of encounter networks within this project, the impact of weighting encounters by association time between mitochondria was examined. To do this, edges were weighted by the reciprocal of association time between two colocalised mitochondria (in seconds). Network efficiency was then calculated (from the reciprocal of shortest path length between pairs of nodes, see Section 2.2), so longer association times contribute to shorter routes across the network. A close correlation between weighted and unweighted networks was reported, demonstrating that association time in seconds and the historical association reporting of the unweighted networks are closely linked (Figure A.1).

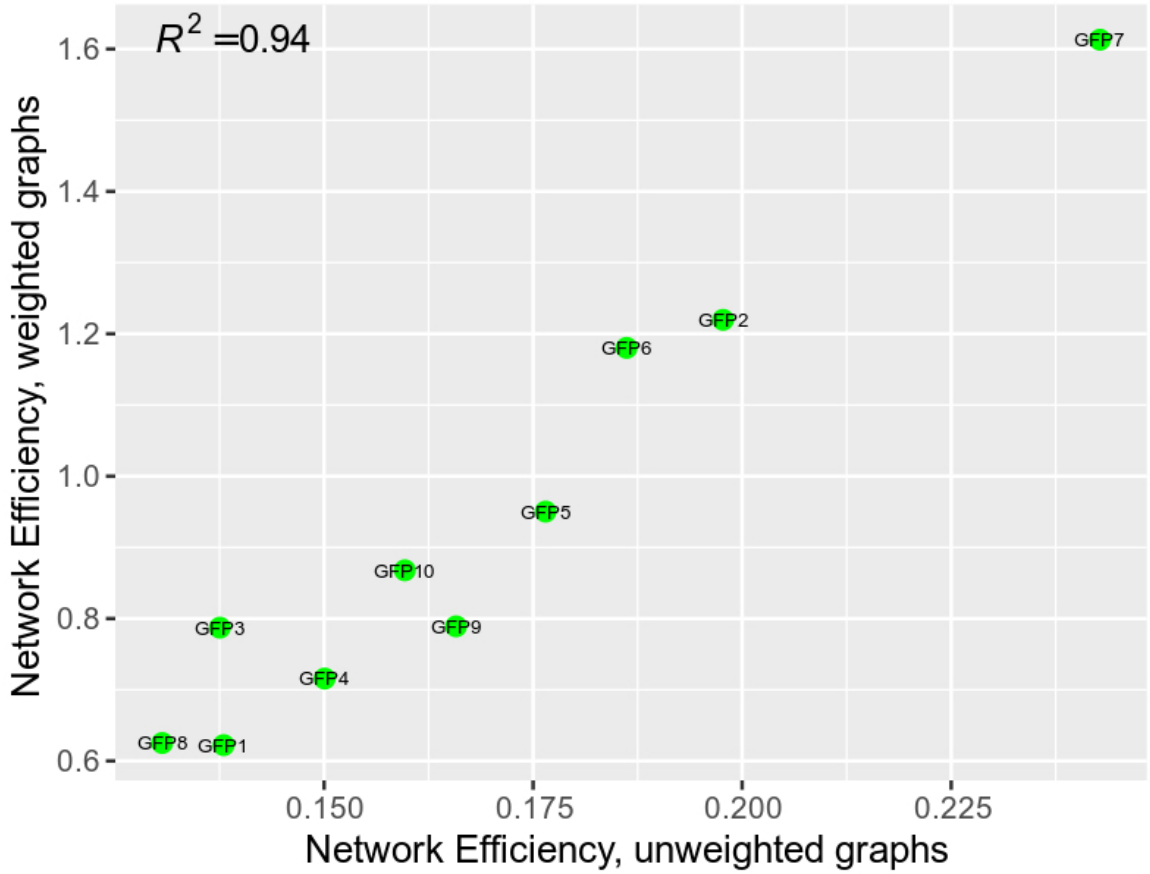

Figure A.1: Comparison between unweighted interactions networks and those weighted by association time show close correlation. Edges were weighted by 1/association time (in seconds), data points are from the final frame of WT (GFP1-10) experimental time lapse videos. Network Efficiency, average "closeness" (reciprocal of shortest path length) between pairs of nodes. See Section 3.2 for more details. Reproduced from Chustecki, Gibbs, et al. (2021).

A.0.2 Investigating relationships across summary statistics between mitochondrial encounter networks and classical graphs.

In order to get a better understanding of the characteristics of any network, it is beneficial to compare to a set of well-defined classical graphs such as random or scale-free networks.

This method has been used within Chapter 4 and we again apply this thinking to biological mitochondrial encounter networks from Chapters 2 and 3, in order to discern relationships we might expect from classical graphs to those we build from plant cell mitochondrial dynamics.

The classical graphs we use come from three models, briefly described here. Erdös-Rényi random graphs (Erdös and Rényi, 2011) can be constructed through one of two models: a defined number of edges placed uniformly and randomly between a defined number of vertices, or built up between a defined number of vertices with probability p, where each edge is independent from every other edge– degree values of both methods are summarised as Poisson distributions. Watts-Strogatz graphs (Watts and Strogatz, 1998) are built from a model of a basic lattice forming a ring structure of defined vertices and edge values, that are then rewired according to probability β. Scale-Free graphs according to the Albert-Barabasi model (Barabási and Albert, 1999) are built one node at a time, with each new node connecting to existing nodes with probability (p_i), based on the degree of the existing node– meaning that well-connected nodes become even more well-connected, and a power law degree distribution forms.

Looking across chosen summary statistics for mitochondrial encounter networks, we compare positioning of our 65 biological networks with those of a selection of classical graph models (Figure A.2). In Chapter 2 we noted a negative correlation between coefficient of variation of degree, and log(mean degree) (Figure 2.11). A negative relationship may be expected from a poisson degree distribution as defined by an Erdös-Rényi graph, where the mean (μ) is equal to the variance and the coefficient of variation is $1/\sqrt{\mu}$. In Figure A.2.A we see that this relationship holds true for all iterations of ER networks, whether based on vertex and node number of the 65 biological networks (grey) or the mean vertex number of all biological networks but chosen edge p values. But for biological networks (blue, green, pink) this relationship is not exact, in that they have an increased variation across degree values than would be expected for a purely random network.

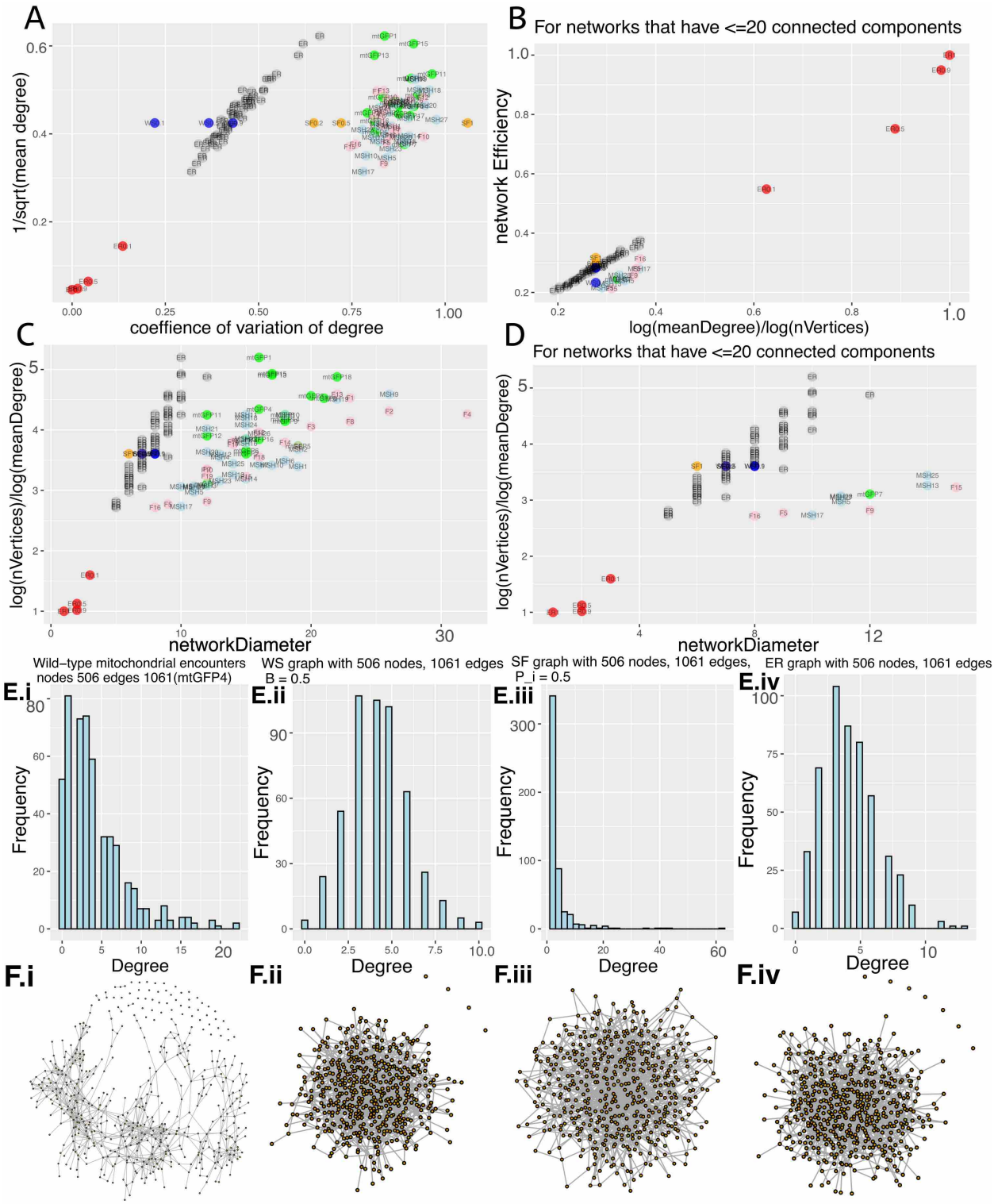

Figure A.2: (See next page)

Figure A.2: Relationships across summary statistics are not explained in whole by ER, SF or WS graphs. (A-D) Plots show all (or selected) biological networks (mtGFP (green) n = 18, mtGFP-*msh1* (pink) n =28, mtGFP-*friendly* (light blue) n = 19, total n = 65), alongside 65 ER networks (grey) based on the vertex and edge values of biological networks. SF (orange), WS (blue) and ER (red) networks had the mean vertex and edge values of all biological networks, with SF graphs having preferential attachment values of 0.2, 0.5, or, 1, WS having a rewiring probability β = 0.1, 0.5, or 0.9, and ER having an attachment probability of p = 0.1, 0.5, 0.9 or 1. Relationships shown are (A) 1/sqrt(mean degree) and coefficient of variation (SD/mean) of degree. (B) Network global efficiency and log(mean degree)/ log(vertices). Biological networks shown are those with less than or equal to 20 connected components, to approximate the main connected component that ER graphs form. (C) log(mean degree)/ log(vertices) and network diameter, and (D) the same plot but with those networks of less than or equals 20 connected components present. (E) Degree distributions over example networks from (i) Biological data, (ii) Watts Strogatz network with β=0.5, (iii) SF with P_i=0.5, (iv) ER networks. All networks have same edge and node number as example biological network (mtGFP4). (F) Network illustrations correspond to biological, WS, SF and ER graphs of (E).

We set out the calculation for network efficiency in Section 2.2. In connected random networks as defined by Erdös and Rényi, we might expect efficiency = log(mean degree)/log(vertex number) in the connected graph. We plot this relationship in Figure 2.11.B. This relationship was not calculated over only the largest connected component, although in most cases the ER networks are built of just one connected graph. Limiting the connected component number to 20 attempts to give an approximation for the biological networks of a connected graph. We see that the global efficiency is linear in the defined ER networks (grey, red), and roughly linear in the biological networks (blue, pink, green) although network efficiency is not exactly log(mean degree)/log(number of vertices).

We next compared the diameters of our mitochondrial encounter networks to those of connected ER networks. In the random graphs, we would expect diameter to equal log(number of vertices)/log(mean degree) ((Barabási, 2016), eq. 3.18), and while these values are not exactly equal over our random networks (grey, red), diameter does scale with the size and connectivity of the network. Our biological networks (green, blue, pink), either with all, or < 20 connected components, scale differently (Figure 2.11.C,D). For each size or connectivity across the network, their diameter is larger, roughly 1.5 but can be up to 3x larger than what would be expected from the denser random networks that have the same node and edge values (grey).

Finally, we ask whether the degree distributions of mitochondrial encounter networks are more similar to Scale-Free or Erdös-Rènyi networks. Scale-free networks typically have power-law degree distributions, characterised by long tails when plotted by frequency. We see this in our example SF graph, defined with the probability of connecting to another node is P_i=0.5 (Figure A.2.E.iii). We also see this long tail in our biological networks (Figure A.2.E.i), and it is this characteristic of few high degree nodes that makes mitochondrial networks efficient at exchanging information (such as in our bingo problem in section 4.2.1). This is in contrast to the more poisson-like distribution of the ER network, or even Watts-

Strogatz models (Figure A.2.E.ii,iv). Also, across the coefficient of variation (Figure A.2.A) SF networks are similarly variable in the degree values than WS or ER graphs. Overall, mitochondrial encounter networks could be described as more scale-free-like than random. Network representations of these models can be seen in Figure A.2.F.

A.0.3 Reducing distance needed for encounters between individuals retains connectivity trends across networks

The networks described so far have been built using an encounter distance of 1.6µm, (just over the length of one mitochondrion) to register as an interaction. When considering the potential for these individuals to fuse together, it is a prerequisite for mitochondria to be directly adjacent, in order for membrane fusion to occur. In order to quantify the connectivity of the chondriome for closer associations, the encounter distance was shortened to 0.8µm, in order to force a direct adjacency between individual mitochondria (Figure A.3).

When networks are built using the shortened encounter distance, we see a reduction in the number of edges formed at early frames (Figure A.4.E), and an increase in the number of connected components by later frames, meaning there are not as many encounters, or linking between connected components, happening across the cell as when using the increased (1.6µm) encounter distance (Figure 2.5). The absolute values of degree across the networks decrease when the encounter distance is reduced (Figure A.4.F). However, the degree value trends remain similar. There is an increase in the maximum degree values reached as the network builds up over time, and an overall increase in mean degree. One trend that does differ is the coefficient of variation for degree (Figure A.4.G (inset)). For the larger (1.6µm) encounter distance, this variation begins high and reduces to a constant of ~0.8 over time (Figure 2.5.A.v. (inset)). However, as the network starts so disconnected for an encounter threshold of 0.8µm, the variation in degree begins low and increases until ~0.6 by the final

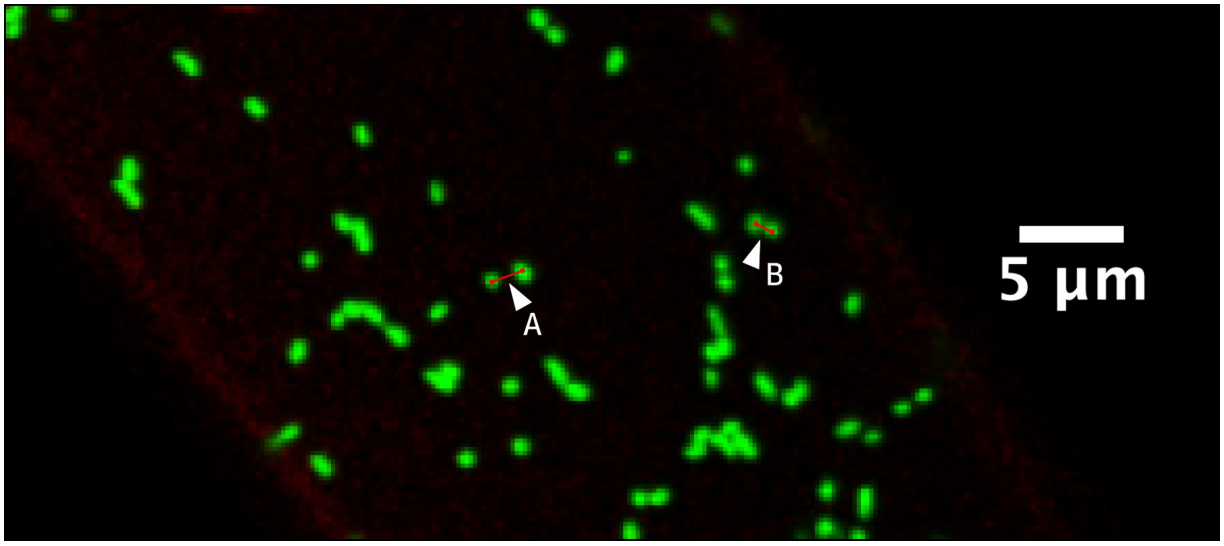

Figure A.3: Reducing encounter distance enforces direct adjacency between individual mitochondria. A micrograph of an *A.thaliana* hypocotyl cell, with increased magnification to demonstrate the difference in distance between two individual mitochondria (green) of (A) 1.602µm and (B) 0.805µm. Reproduced from Chustecki, Gibbs, et al. (2021).

frame, without plateauing.

Further social and physical statistics were generated for comparison between the reduced colocalisation distance networks (Figure A.5) and the distance used for all other networks (Figure 2.11). Even with a reduced colocalisation distance, there is a clear relationship between connectivity across the network as defined by degree and the even spread across the cell as defined by intermitochondrial distance (Figure A.5.A). Association time between mitochondria is consistently reduced across theoretical networks, with experimental data now retaining some of the longest association times of all networks (Figure A.5.B,C), due to the more stringent requirement on what 'association' entails. Networks efficiency is also reduced at this colocalisation distance, and experimental networks show a similarity to theoretical networks (Figure A.5.G-I), unlike in the original colocalisations distance (Figure 2.11.G-I). Although the ranges of values for social statistics and association time differ for reduced colocalisation distance networks, the remaining trends are consistent with networks

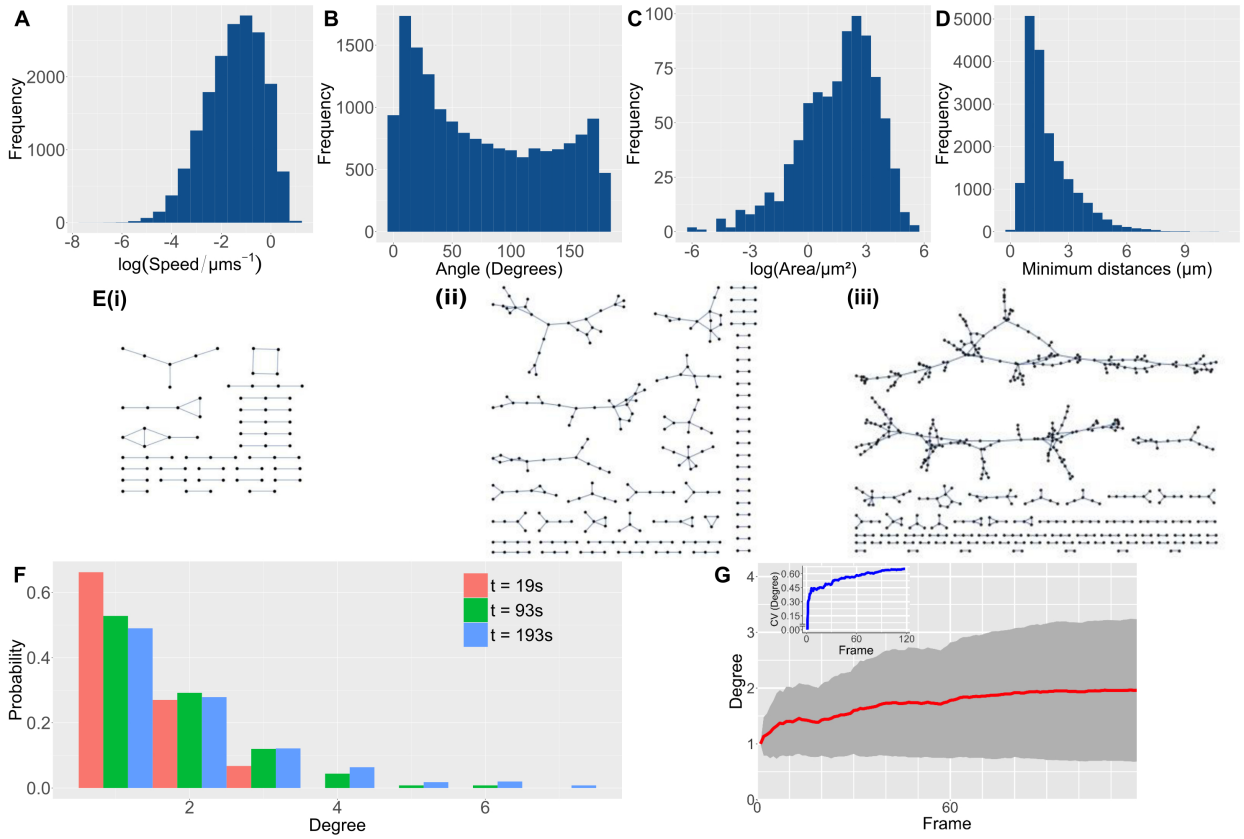

Figure A.4: Reducing encounter distances between individuals dampens connectivity, but patterns remain the same. Physical statistic distributions (A-D), network visualisations (E), degree distributions (F-G) of a sample analysed with reduced encounter threshold distance. Network visualisations (E) are at (i) 19 seconds, (ii) 93 seconds, (iii) 193 seconds. (F) depicts mean degree (red) over time, with standard deviation (grey) either side. The same individual cell was used for this analysis as in Figures 2.5 and 2.2. Note histogram bins differ in width for physical statistic distributions.

of an encounter distance 1.6μm.

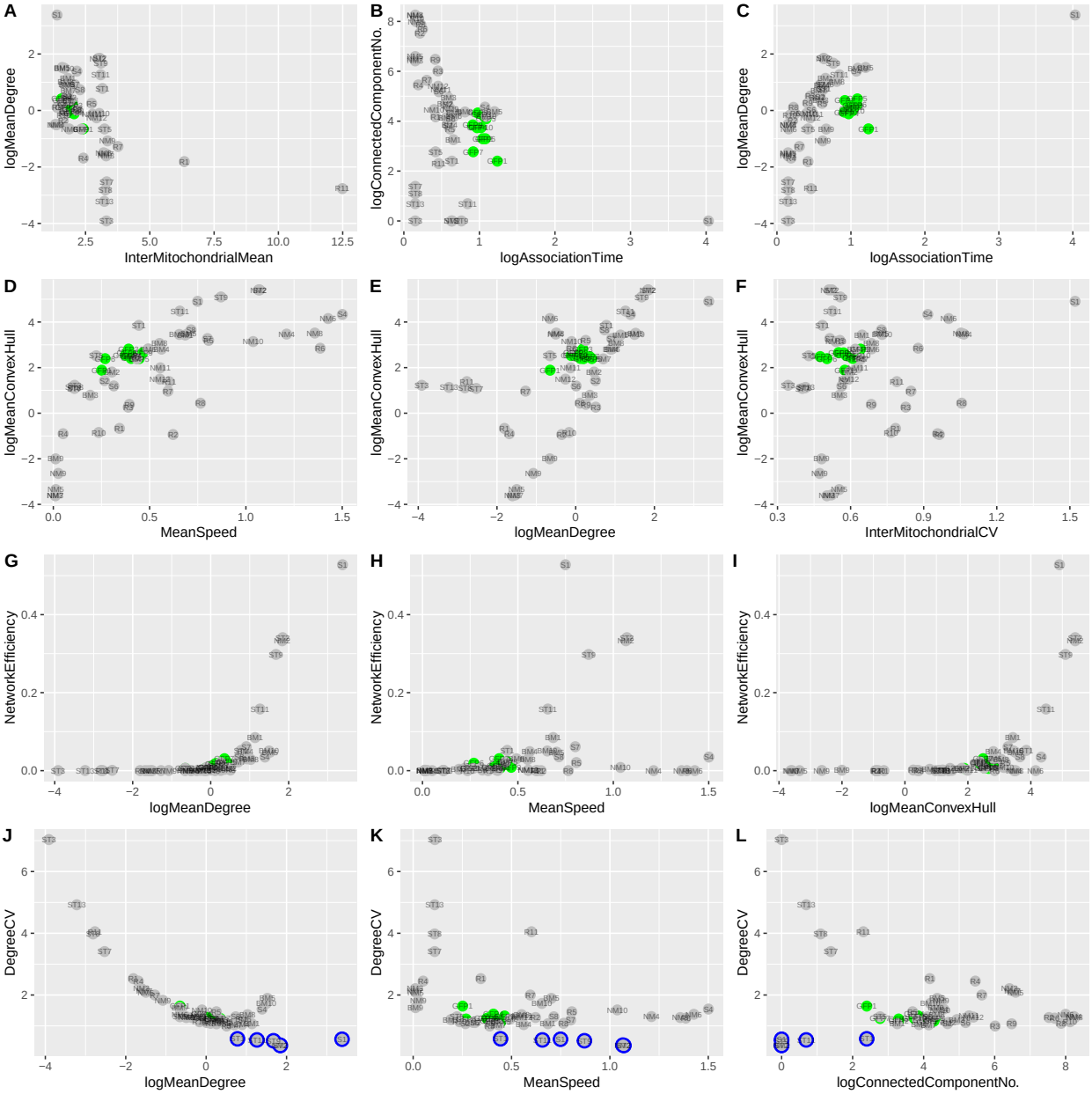

Figure A.5: Relationships between key physical and social statistics of reduced encounter distance networks remain. Statistics of wildtype ($n = 10$, green) and theoretical ($n = 47$, grey) networks at 230 seconds of video time. Networks are built with encounter distances of 0.8µm. Individual data point labels represent different experiments, (GFP 1-10), and simulations (different parameterisations shown in Table B.1, except S5, NM1, ST4, ST6, ST10, ST12, ST14). Reproduced from Chustecki, Gibbs, et al. (2021).

A.0.4 Analysis of diffusion constant of wild-type plant mitochondria

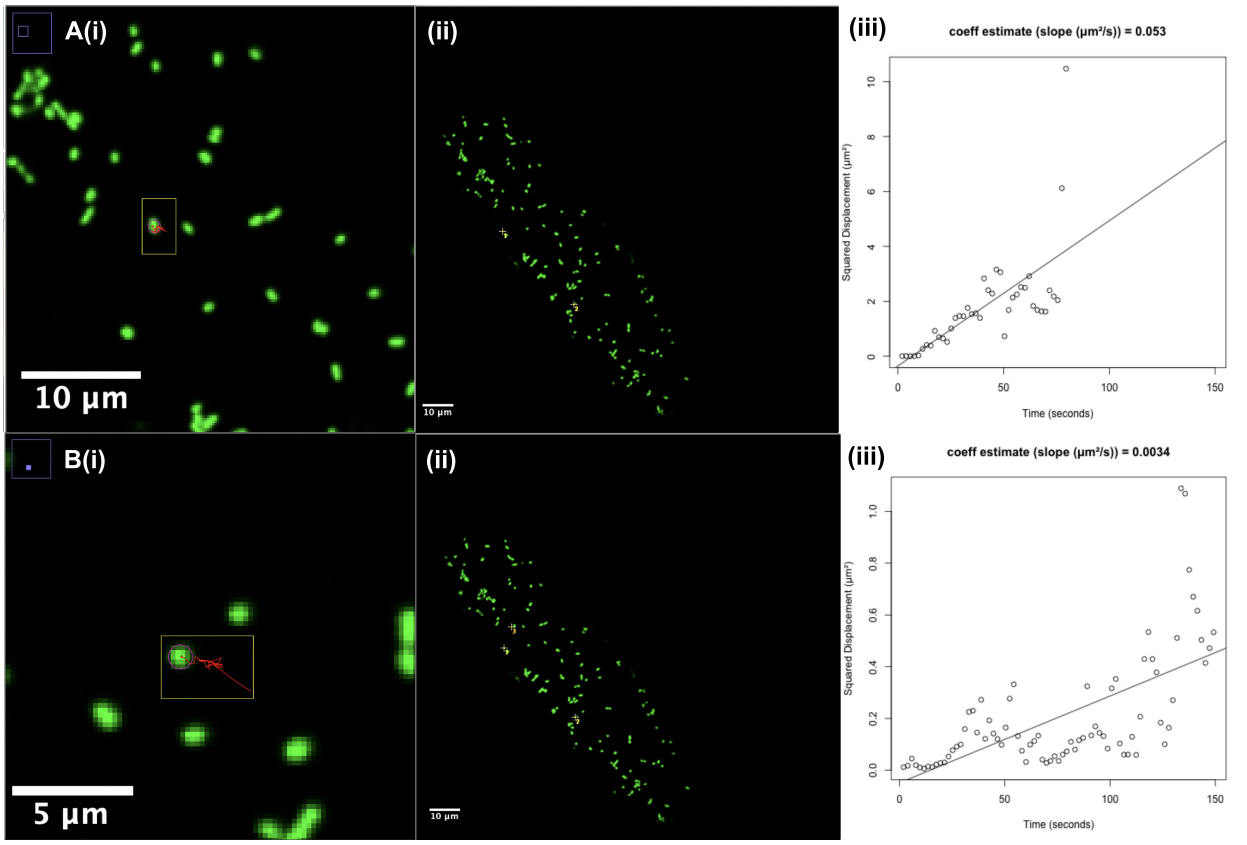

Figure A.6: Characterising diffusion rate from videos of mitochondrial motion. The process of diffusion rate characterisation begins with isolating trajectories (red) of diffusing mitochondria (green) (encircled by ROI (yellow)) (A(i)), from the whole cell (ii), and extracting squared displacement over time (iii). Two mitochondria from the same video shown.

Some mitochondria within cells imaged can be seen moving in a passive way within small regions of the cell, seemingly not using cytoskeletal strands or subject to strong cytoplasmic streaming forces. They could be said to be moving diffusively. In order to estimate the diffusion constant of mitochondria not using cytoskeletal strands, the mean squared displacement for sample mitochondria was calculated. Three sample mitochondria were chosen

from each of three wild-type mtGFP samples. Individuals not displaying the straight-line motion associated with cytoskeletal strand use, moving only within a small local region, and without associating with other mitochondria or chloroplasts were chosen. This helped to control for any influence of cytoplasmic streaming or slowing via inter-organellar encounters. From these, squared displacement over time was extracted (Figure A.6). The range of squared displacement varied from a minimum of 0.002 to a maximum of 0.15µm^2. Across all samples, the slope of mean squared displacement (the estimated diffusion rate) was 0.026µm^2/s (Figure A.7).

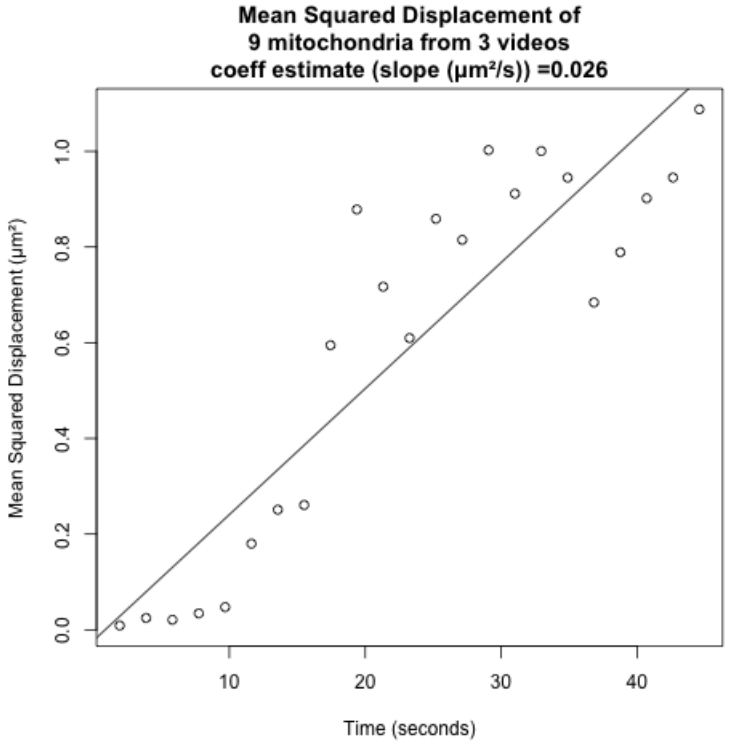

Figure A.7: Overall diffusion rate sample estimate. Mean squared displacement taken over n=9 diffusing mitochondria (3 videos, 3 mitochondria from each), over 44 seconds of frame time.

Appendix Two

Tables relating to Chapter 2

Simulation Label	N_{cyt}	N_{mito}	k_{out}	d_{cyt}	k_{on}	k_{off}	k_{cyt}	d_{mito}	k_{mito}	D	F_{hydro}
S1	4	128	0.000	6.008	0.809	0.479	6.412	8.339	0.770	0.754	0.000
S2	7	198	0.040	4.416	0.309	0.424	1.000	3.151	0.337	0.359	0.000
S4	16	123	0.098	4.860	0.945	0.234	1.300	0.252	0.620	0.851	0.526
S5	0	95	0.000	2.651	0.000	0.118	4.296	6.355	0.802	0.120	0.446
S6	1	154	0.050	7.079	0.000	0.706	9.341	5.627	0.408	0.431	0.000
S7	0	198	0.050	8.417	0.000	0.833	1.000	7.666	0.687	0.943	0.000
S8	12	124	0.056	1.630	0.441	0.343	5.014	3.176	0.490	0.441	0.000
NM1	0	100	0.000	0.000	0.000	0.000	0.000	0.000	0.000	0.010	0.000
NM2	0	100	0.000	0.000	0.000	0.000	0.000	0.000	0.000	0.990	0.000
NM3	0	100	1.000	0.000	0.000	0.000	0.000	0.000	0.000	0.010	0.000
NM4	0	100	1.000	0.000	0.000	0.000	0.000	0.000	0.000	0.990	0.000
NM5	0	100	1.000	0.000	0.000	0.000	0.000	0.000	0.000	0.010	0.990
NM6	0	100	1.000	0.000	0.000	0.000	0.000	0.000	0.000	0.990	0.990
NM7	0	100	1.000	0.000	0.000	0.000	0.000	0.000	0.000	0.010	0.010
NM8	0	100	1.000	0.000	0.000	0.000	0.000	0.000	0.000	0.990	0.010
NM9	0	100	0.100	0.000	0.000	0.000	0.000	0.000	0.000	0.010	0.000
NM10	0	100	0.100	0.000	0.000	0.000	0.000	0.000	0.000	0.990	0.000
NM11	5	100	0.100	1.000	1.000	0.500	1.000	0.000	0.000	0.174	0.000
NM12	0	100	0.100	0.000	0.000	0.000	0.000	0.000	0.000	0.174	0.000
BM1	7	198	0.040	4.416	0.309	0.424	1.000	3.151	0.337	1.000	0.000
BM2	7	198	0.040	4.416	0.309	0.424	1.000	3.151	0.337	0.400	0.000
BM3	7	198	0.040	4.416	0.309	0.424	1.000	3.151	0.337	0.200	0.000
BM4	7	198	0.040	4.416	0.309	0.424	1.000	3.151	0.337	0.800	0.000
BM5	7	198	0.040	4.416	0.309	0.424	1.000	3.151	0.337	0.600	0.800
BM6	7	198	0.040	4.416	0.309	0.424	1.000	3.151	0.337	0.600	0.200
BM7	7	198	0.040	4.416	0.309	0.424	1.000	3.151	0.337	0.600	0.000
BM8	7	198	0.040	4.416	0.309	0.424	1.000	3.151	0.337	0.600	0.400
BM9	7	198	0.040	4.416	0.309	0.424	1.000	3.151	0.337	0.000	0.000
BM10	7	198	0.040	4.416	0.309	0.424	1.000	3.151	0.337	0.600	0.600
ST1	5	100	0.000	0.000	0.000	0.000	1.000	0.000	1.000	0.400	0.000
ST2	5	100	0.000	0.000	0.000	0.000	1.000	0.000	1.000	1.000	0.000
ST3	0	100	0.000	0.000	0.000	0.000	1.000	0.000	1.000	0.100	0.000
ST4	15	100	0.000	0.000	0.000	0.000	1.000	0.000	1.000	0.100	0.000
ST5	5	100	0.000	0.000	0.000	0.000	1.000	0.000	1.000	0.200	0.000
ST6	20	100	0.000	0.000	0.000	0.000	1.000	0.000	1.000	0.100	0.000
ST7	2	100	0.000	0.000	0.000	0.000	1.000	0.000	1.000	0.100	0.000
ST8	6	100	0.000	0.000	0.000	0.000	1.000	0.000	1.000	0.100	0.000
ST9	5	100	0.000	0.000	0.000	0.000	1.000	0.000	1.000	0.800	0.000
ST10	4	100	0.000	0.000	0.000	0.000	1.000	0.000	1.000	0.100	0.000
ST11	5	100	0.000	0.000	0.000	0.000	1.000	0.000	1.000	0.600	0.000
ST12	5	100	0.000	0.000	0.000	0.000	1.000	0.000	1.000	0.000	0.000
ST13	8	100	0.000	0.000	0.000	0.000	1.000	0.000	1.000	0.100	0.000
ST14	10	100	0.000	0.000	0.000	0.000	1.000	0.000	1.000	0.100	0.000
R1	0	25	0.231	0.390	0.456	0.113	4.074	5.675	0.624	0.351	0.617
R2	1	92	0.585	0.363	0.685	0.040	1.945	5.062	0.417	0.820	0.537
R3	3	191	0.134	0.657	0.081	0.033	3.247	9.966	0.823	0.234	0.309
R4	2	90	0.718	0.637	0.712	0.796	9.271	5.810	0.044	0.318	0.136
R5	3	111	0.050	2.166	0.000	0.216	4.581	3.472	0.884	0.762	0.162
R6	13	159	0.565	0.796	0.985	0.366	4.181	4.870	0.879	0.413	0.642
R7	8	43	0.424	0.904	0.214	0.979	7.358	4.965	0.086	0.599	0.956
R8	3	161	0.526	0.340	0.440	0.735	3.929	0.422	0.423	0.673	0.411
R9	11	169	0.174	0.878	0.174	0.754	4.138	9.521	0.207	0.819	0.248
R10	0	183	0.745	0.313	0.259	0.964	4.211	6.884	0.571	0.177	0.609
R11	13	9	0.200	0.185	0.813	0.007	4.745	7.208	0.703	0.405	0.785

Table B.1: Simulation parameterisations for model exploration. Individual model parameters are labelled by similarity, rate units described here are per frame. Reproduced from Chustecki, Gibbs, et al. (2021).

Simulation Label	N_{cyt}	N_{mito}	k_{out}	d_{cyt}	k_{on}	k_{off}	k_{cyt}	d_{mito}	k_{mito}	D	F_{hydro}	logMeanDegree (final frame)	InterMitoMean (overall)	logMeanCH (overall)	DegreeCV (final frame)	Network Efficiency (final frame)
Model A	5	100	0.010	1.000	1.000	0.500	1.000	0.000	0.000	0.500	0.000	1.39	2.98	4.22	0.920	0.120
Model B	5	100	0.900	1.000	1.000	0.500	1.000	0.000	0.000	0.500	0.000	0.296	1.32	-1.73	0.905	0.000101
Model C	5	100	0.100	1.000	0.200	0.100	1.000	0.000	0.000	0.500	0.000	0.697	2.89	1.76	0.964	0.00773
Model D	5	100	0.100	1.000	0.100	0.200	1.000	0.000	0.000	0.500	0.000	0.591	2.90	1.63	0.960	0.00662
Model E	5	100	0.100	1.000	1.000	0.500	1.000	0.000	0.000	0.500	0.000	0.669	2.77	1.99	1.01	0.00764
Model F	5	100	0.100	1.000	0.500	1.000	1.000	0.000	0.000	0.500	0.000	0.537	2.91	1.60	0.948	0.00447
Model G	5	100	0.100	1.000	1.000	0.200	1.000	0.000	0.000	0.500	0.000	0.699	2.86	1.82	0.955	0.00780
Model H	5	100	0.100	1.000	0.200	1.000	1.000	0.000	0.000	0.500	0.000	0.634	2.85	1.44	0.960	0.00557
Model I	5	100	0.100	1.000	1.000	0.500	1.000	0.000	0.000	0.500	0.990	0.529	2.66	2.62	1.13	0.00547
Model J	5	100	0.100	1.000	1.000	0.500	1.000	0.000	0.000	0.500	0.010	0.694	2.85	2.03	1.00	0.00666
Model K	5	100	0.100	1.000	1.000	0.500	0.990	0.000	0.000	0.500	0.000	0.666	2.85	1.93	0.901	0.00705
Model L	5	100	0.100	1.000	1.000	0.500	0.010	0.000	0.000	0.500	0.000	0.125	2.83	1.05	1.10	0.00222
Model M	5	100	0.100	1.000	1.000	0.500	1.000	0.000	0.990	0.500	0.000	0.669	2.77	1.99	1.01	0.00764
Model N	5	100	0.100	1.000	1.000	0.500	1.000	0.000	0.010	0.500	0.000	0.669	2.77	1.99	1.01	0.00764
Model O	5	100	0.100	1.000	1.000	0.500	1.000	0.990	0.000	0.500	0.000	0.626	2.73	1.84	0.945	0.00511
Model P	5	100	0.100	1.000	1.000	0.500	1.000	0.010	0.000	0.500	0.000	0.626	2.73	1.84	0.945	0.00511
Model Q	5	100	0.100	1.000	1.000	0.500	1.000	5.000	0.000	0.500	0.000	-1.40	2.15	-0.0812	2.00	0.000794
Model R	5	100	0.100	1.000	1.000	0.500	1.000	5.000	0.200	0.500	0.000	0.654	2.40	0.669	0.944	0.00335
Model S	5	100	0.100	1.000	1.000	0.500	1.000	5.000	0.500	0.500	0.000	0.791	2.50	0.895	0.932	0.00548

Table B.2: Simulation parameterisations of 'model sweeps' to assess the influence of individual parameterisations at a time. Individual model parameters can be seen (left), alongside summary statistics for the models (right), taken either at the network of the final frame, or across the whole frame time (stated). Specific parameterisations varying from arbitrary default are highlighted in yellow. Modified from (Chustecki, Gibbs, et al., 2021).

Appendix Three

Figures relating to Chapter 3

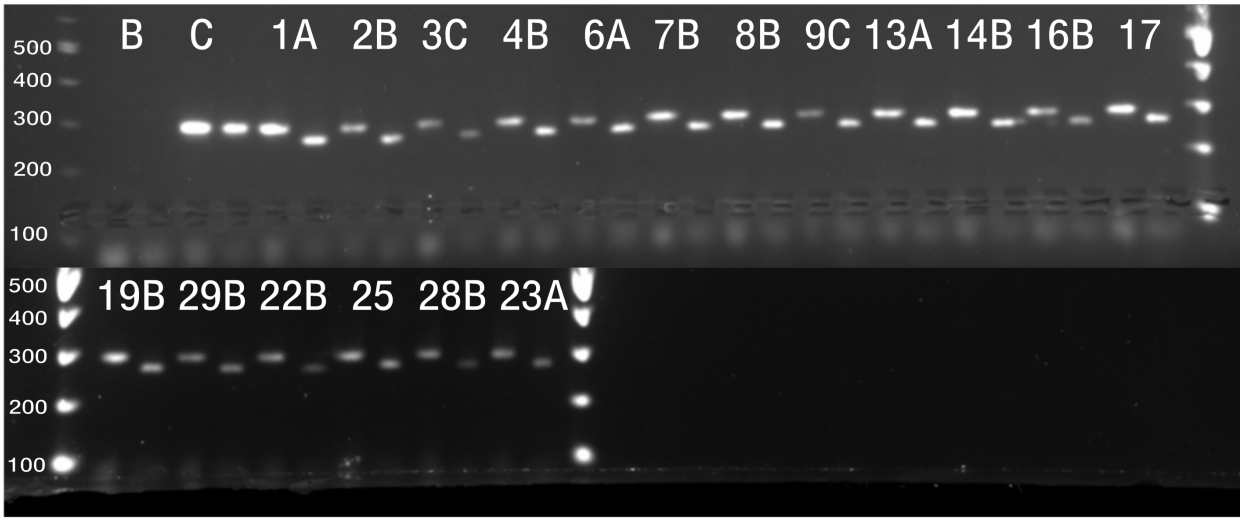

Figure C.1: Genotyping *msh1* seed stock. Agarose gel image showing a selection of *msh1* samples (CS3372). Each sample has two bands, the left being pre-digest, and the right post-digest.

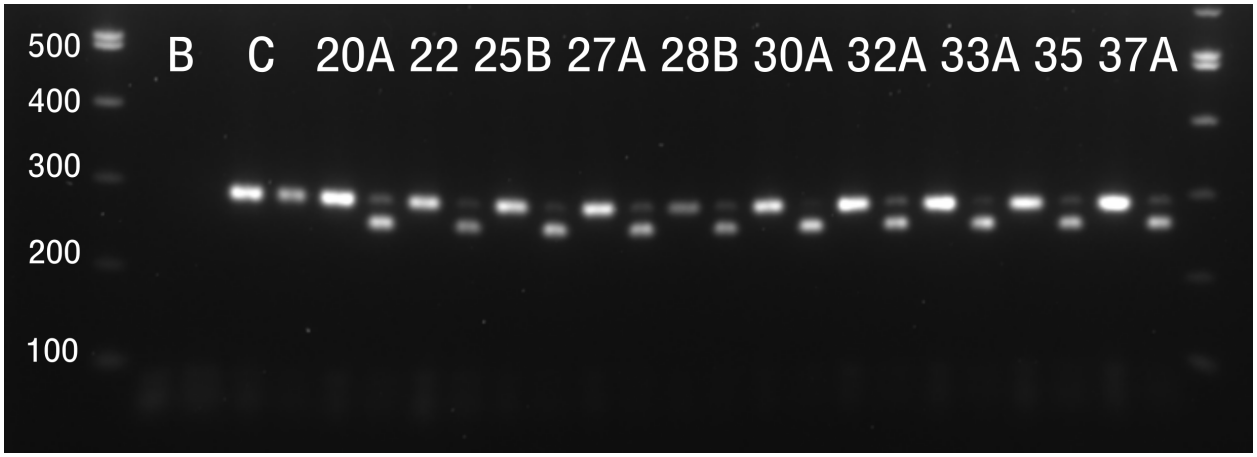

Figure C.2: Second check genotyping *msh1* seed stock. Agarose gel image showing a selection of *msh1* samples carried through for crossing. Each sample has two bands, the left being pre-digest, and the right post-digest.

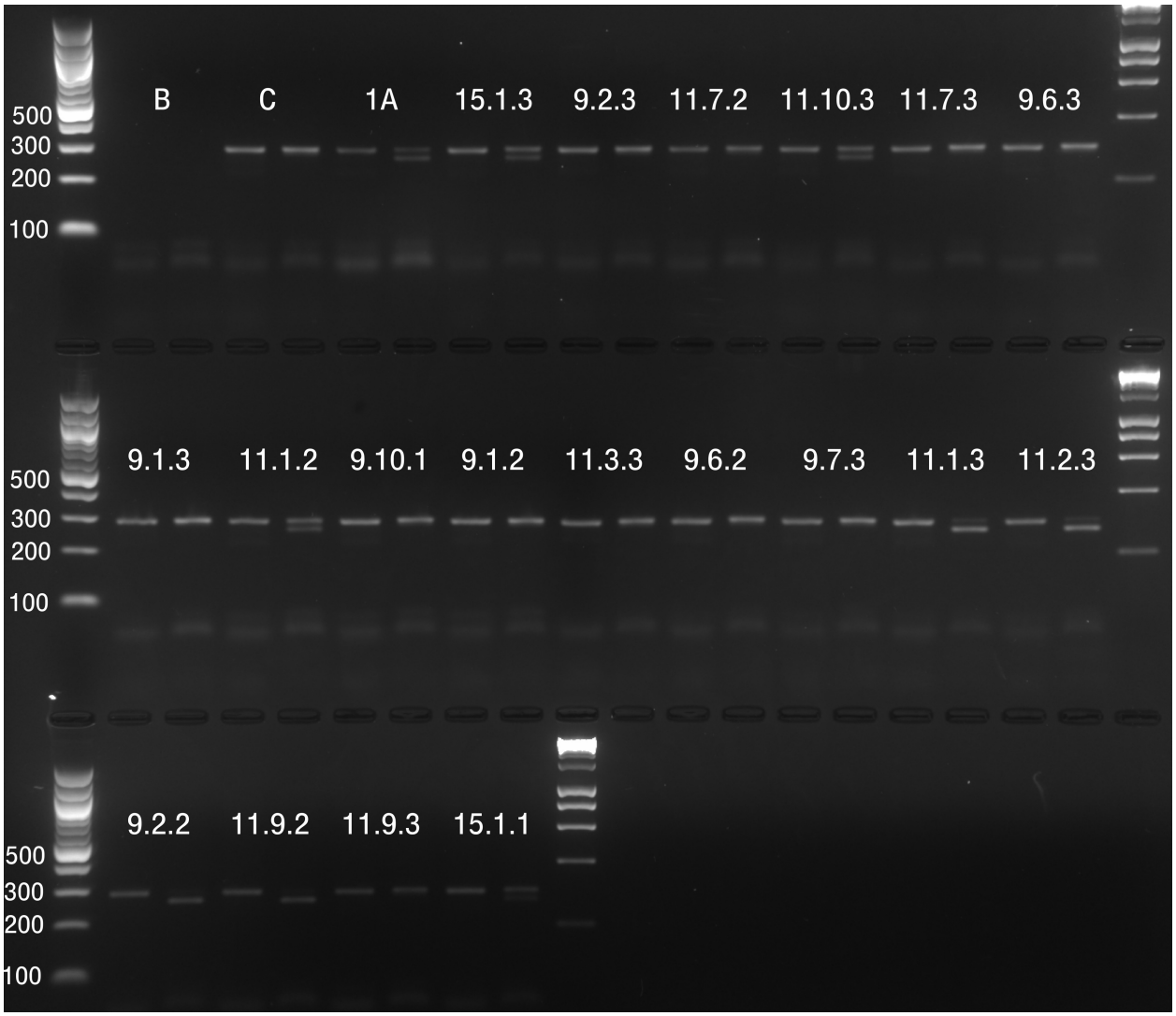

Figure C.3: Screening F3 samples for successful mtGFP-*msh1* homozygotes. Agarose gel image showing F3 samples of *msh1* x mtGFP crosses. Each sample has two bands, the left being pre-digest, and the right post-digest. Reproduced from Chustecki, Etherington, et al. (2021).

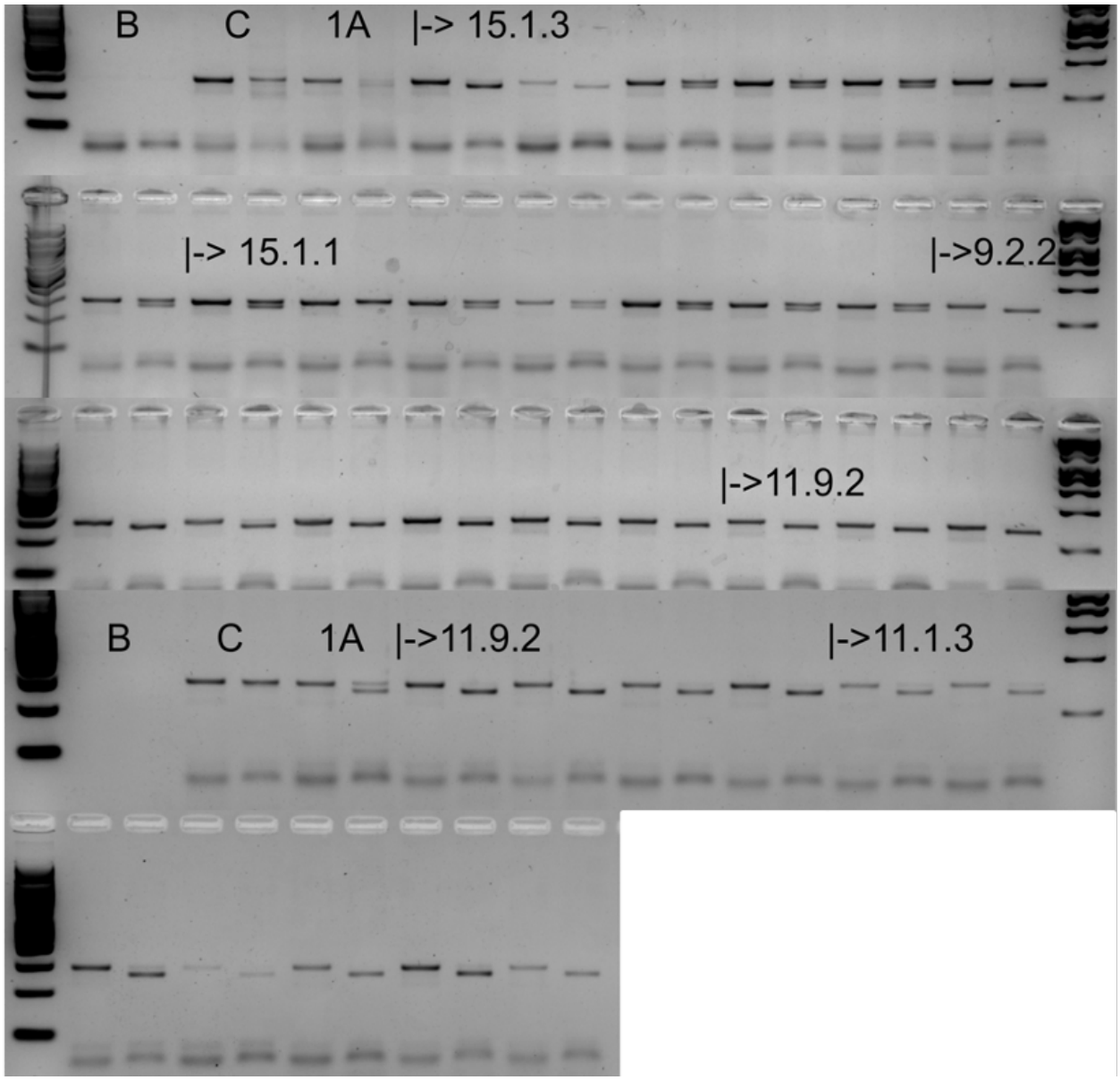

Figure C.4: Screening F4 samples for successful mtGFP-*msh1* homozygotes. Agarose gel image showing F4 samples of *msh1* x mtGFP crosses. Each sample has two bands, the left being pre-digest, and the right post-digest.

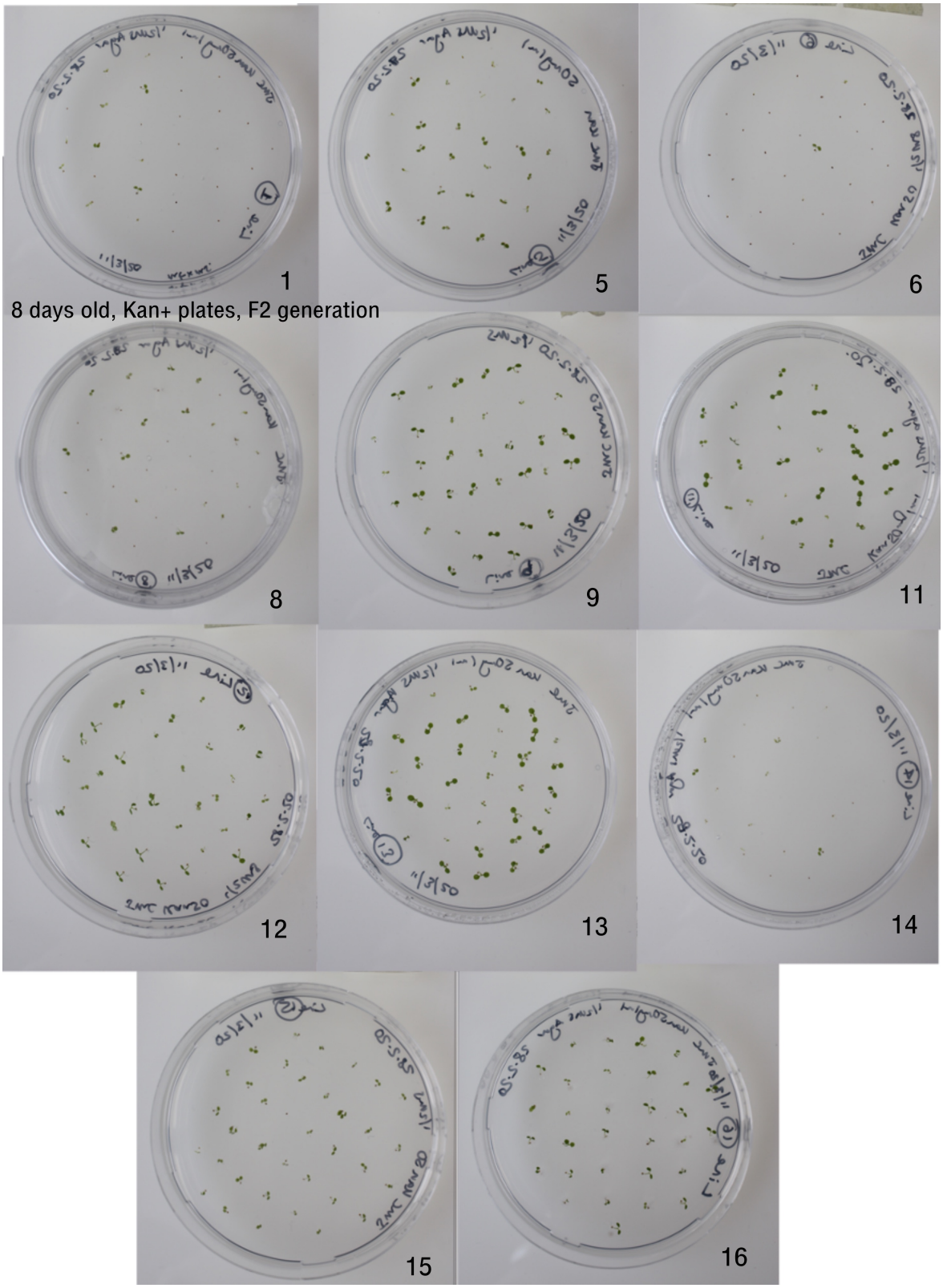

Figure C.5: Kanamycin selection plates of F2 individuals of *msh1* x mtGFP crosses.

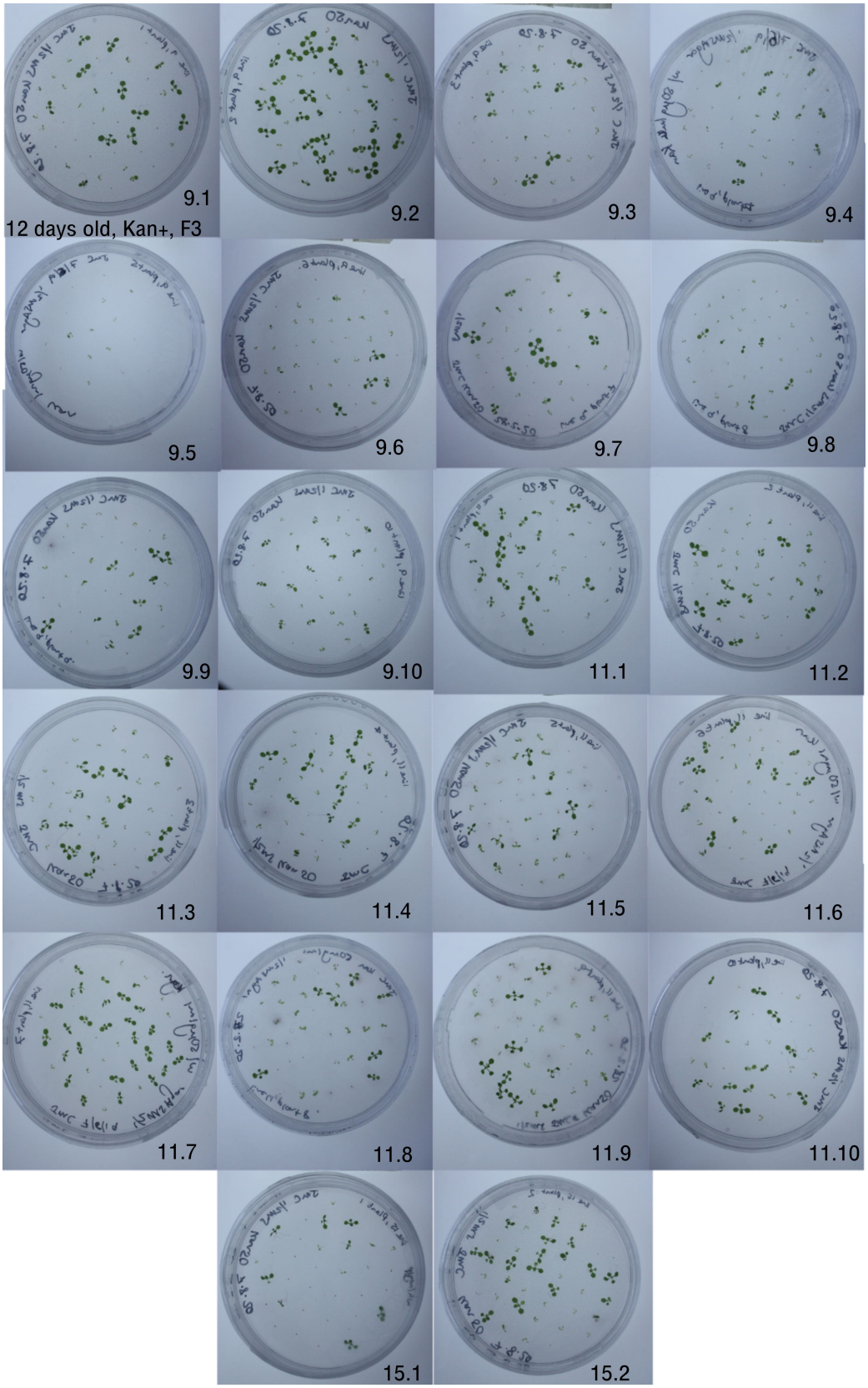

Figure C.6: Kanamycin selection plates of F3 individuals of *msh1* x mtGFP crosses.

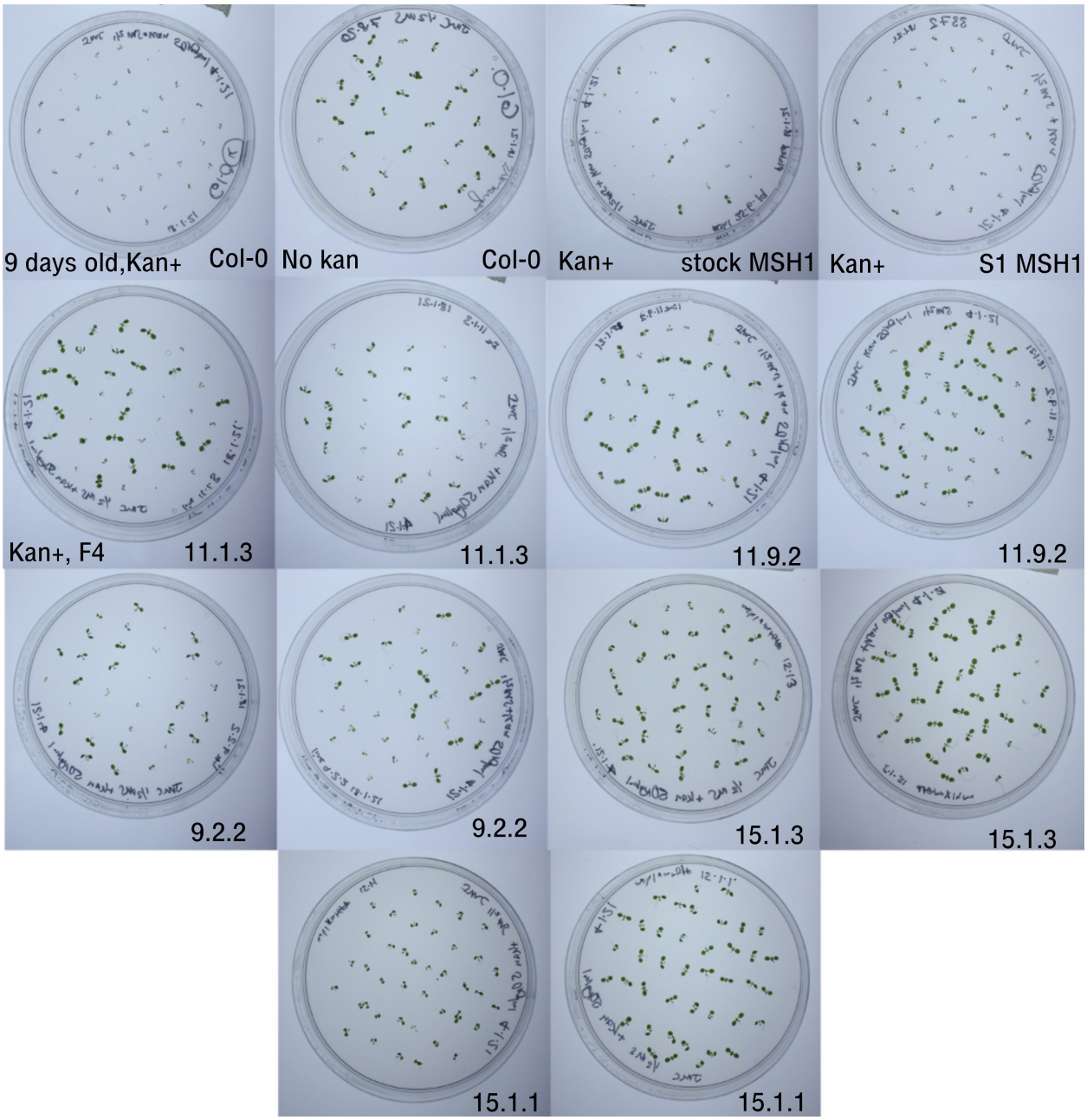

Figure C.7: Kanamycin selection plates of F4 individuals of *msh1* x mtGFP crosses, with controls (S1 - selfed *msh1* stock).

Figure C.8: 30 day old F4 individuals of line 9.2.2. Scale bar = 1cm.

Figure C.9: 30 day old F4 individuals of line 11.9.2. Scale bar = 1cm. Reproduced from Chustecki, Etherington, et al. (2021).

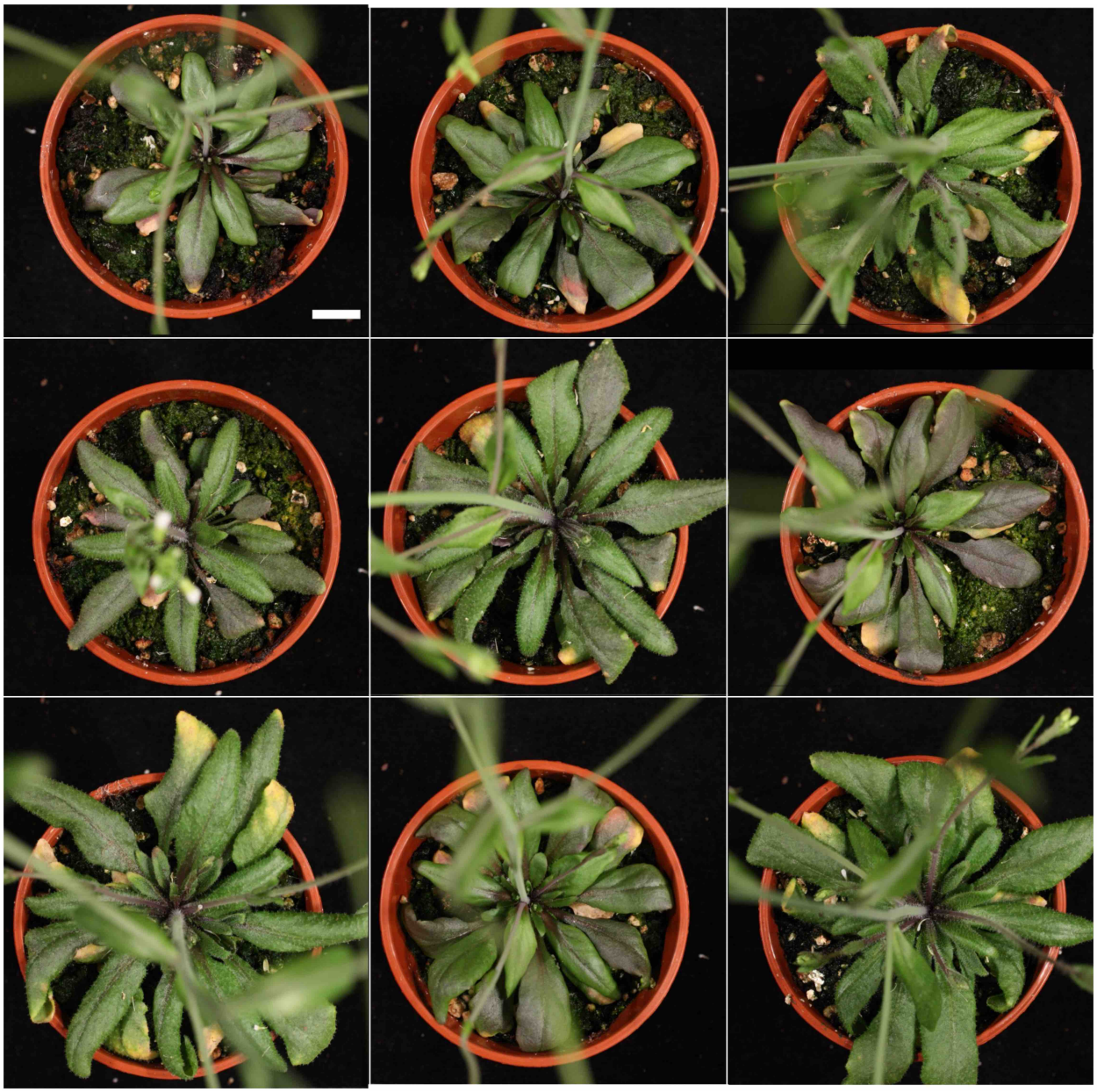

Figure C.10: 44 day old F4 individuals of line 15.1.1. Scale bar = 1cm.

Figure C.11: 44 day old F4 individuals of line 15.1.3. Scale bar = 1cm.

Figure C.12: 30 day old F4 individuals of line 11.1.3. Scale bar = 1cm.

Figure C.13: 30 day old individuals of Col-0. Scale bar = 1cm.

Appendix Four

Results relating to Chapter 5

D.0.1 Focusing on species of interest (long lifespans)

One fascinating group of organisms that have not appeared in either *MSH1* or lifespan lists are the Hydrozoa, to which the genus *Hydra* belong. *Hydra* are small (1cm) solitary freshwater Cnidaria, that have demonstrated negligible observable senescence in both a 4-year study by Martínez (1998) and a more recent 8-year study by Schaible et al. (2015), and constant mortality and fertility (although phenotypes associated with ageing have been observed in sexually reproducing *Hydra* (Yoshida et al., 2006)). This has been proposed to be for many potential reasons including *Hydra* not sequestering a germline separate to the soma, rapid cell turnover, many stem cells and a simple body plan (Schaible et al., 2015). We wanted to look into whether *Hydra* have the mitochondrial recombination surveillance protein *MSH1*. Therefore, the 5 species of Hydrazoan available on NCBI were found (Table D.1), and the *MSH1* accessions (Table 5.1) were blasted (BLASTn) against these entries, using defaults parameters. Of these 5, there are 3 *Hydra* species, but *MSH1* was searched for in all 5 Hydrozoan species, as we are interested in the variation between close familial species. All species except *Craspedacusta sowerbii* generated hits for one or more of the three *MSH1* accessions. *Clytia hemisphaerica*, *Hydra oligactis* (brown hydra) and *Hydra*

vulgaris (swiftwater hydra) all had hits >88% percent identity but only ~1% query cover for both the *Saccharomyces* and *Dendronephthya* accessions, but not the *Arabidopsis* accession. However, as these samples are taken from whole genome shotgun sequencing, the genomic fragments may be very large in comparison to the accession lengths, leading to a low query cover. *Hydra viridissima* (green hydra) has hits for all three, and all had at least one hit >90% sequence identity, with a 100% sequence identity against the yeast *MSH1* accession, all hits ~1% query cover and E value of 0.003 except *Dendronephthya* where the E value was 7×10^{-4}. These tiny query cover overlaps do not offer enough evidence of *MSH1* presence based on the *MSH1* accessions used against the three *Hydra* species.

Species Name	**Accession details**	**Size (Mbp)**	**Level**	**Year**
Clytia hemisphaerica	Clytia hemisphaerica genome assembly Reference GenBank: GCA_902728285.1	421.0	Scaffold	2020
Craspedacusta sowerbii	ASM368756v1 Reference GenBank GCA_003687565.1	673.2	Scaffold	2018
Hydra oligactis (brown hydra)	Ho_v1 Reference GenBank GCA_004118135.1	1,262	Scaffold	2019
Hydra viridissima (green hydra)	ASM1470644v1 Reference GenBank GCA_014706445.1	284.2	Scaffold	2020
Hydra vulgaris (swiftwater hydra)	Hydra_RP_1.0 Reference RefSeq: GCF_000004095.1	852.2	Scaffold	2009

Table D.1: Accession numbers and details for the 5 Hydrazoan species in NCBI databases. Note that for *Hydra viridissima* and *Hydra vulgaris* there were multiple accessions available, but the reference sequence was used.

References

Abdelnoor, R. V., R. Yule, et al. (May 2003). "Substoichiometric shifting in the plant mitochondrial genome is influenced by a gene homologous to MutS." In: *Proceedings of the National Academy of Sciences of the United States of America* 100.10, pp. 5968–73.

Abdelnoor, R. V., A. C. Christensen, et al. (Aug. 2006). "Mitochondrial genome dynamics in plants and animals: Convergent gene fusions of a MutS homologue". In: *Journal of Molecular Evolution* 63.2, pp. 165–173.

Adams, K. L. and J. D. Palmer (Dec. 2003). "Evolution of mitochondrial gene content: Gene loss and transfer to the nucleus". In: *Molecular Phylogenetics and Evolution* 29.3, pp. 380–395.

Agrawal, A., G. Pekkurnaz, and E. F. Koslover (Dec. 2018). "Spatial control of neuronal metabolism through glucose-mediated mitochondrial transport regulation". In: *eLife* 7.

Ahmad, N. and B. Nielsen (June 2020). "Plant Organelle DNA Maintenance". In: *Plants* 9.6: 683.

Albert, B. et al. (1996). "Dynamics of plant mitochondrial genome: Model of a three-level selection process". In: *Genetics* 144.1, pp. 369–382.

Alm, E. and A. P. Arkin (Apr. 2003). "Biological networks". In: *Current Opinion in Structural Biology* 13.2, pp. 193–202.

Alonso-Blanco, C. et al. (July 2016). "1,135 Genomes Reveal the Global Pattern of Polymorphism in *Arabidopsis thaliana*". In: *Cell* 166.2, pp. 481–491.

Altschul, S. F. et al. (Sept. 1997). "Gapped BLAST and PSI-BLAST: A new generation of protein database search programs". In: *Nucleic Acids Research* 25.17, pp. 3389–3402.

AnAge (2021). *: The Animal Ageing and Longevity Database* Date accessed 5 Oct 2020. URL: https://genomics.senescence.info/species/index.html.

Arimura, S. I. (Jan. 2018). "Fission and fusion of plant mitochondria, and genome maintenance". In: *Plant Physiology* 176.1, pp. 152–161.

Arimura, S.-i., N. Tsutsumi, et al. (Apr. 2002). "A dynamin-like protein (ADL2b), rather than FtsZ, is involved in *Arabidopsis* mitochondrial division". In: *Proceedings of the National Academy of Sciences of the United States of America* 99.8, pp. 5727–5731.

Arimura, S.-i., J. Yamamoto, et al. (May 2004). "Frequent fusion and fission of plant mitochondria with unequal nucleoid distribution". In: *Proceedings of the National Academy of Sciences* 101.20, pp. 7805–7808.

Arnaud-Haond, S. et al. (Feb. 2012). "Implications of Extreme Life Span in Clonal Organisms: Millenary Clones in Meadows of the Threatened Seagrass *Posidonia oceanica*". In: *PLoS ONE* 7.2, E10, e30454.

Arrieta-Montiel, M., A. Lyznik, et al. (2001). "Tracing Evolutionary and Developmental Implications of Mitochondrial Stoichiometric Shifting in the Common Bean". In: *Genetics* 158.2, pp. 851–64.

Arrieta-Montiel, M. P. and S. A. Mackenzie (2011). "Plant Mitochondrial Genomes and Recombination". In: *Plant Mitochondria*. New York, NY: Springer New York, pp. 65–82.

Arrieta-Montiel, M. P., V. Shedge, et al. (Dec. 2009). "Diversity of the *Arabidopsis* mitochondrial genome occurs via nuclear-controlled recombination activity". In: *Genetics* 183.4, pp. 1261–1268.

Aryaman, J. et al. (Aug. 2019). "Mitochondrial network state scales mtDNA genetic dynamics". In: *Genetics* 212.4, pp. 1429–1443.

Autran, D. et al. (2021). "What is quantitative plant biology?" In: *Quantitative Plant Biology* 2.

Avisar, D. et al. (June 2009). "A comparative study of the involvement of 17 *Arabidopsis* myosin family members on the motility of Golgi and other organelles." In: *Plant physiology* 150.2, pp. 700–9.

Ayabe, H. et al. (2021). "FMT, a protein that affects mitochondrial distribution, interacts with translation-related proteins in *Arabidopsis thaliana*". In: *Plant Cell Reports* 40, pp. 327–337.

Baesso, P., R. S. Randall, and G. Sena (2018). "Light sheet fluorescence microscopy optimized for long-term imaging of *Arabidopsis* root development". In: *Methods in Molecular Biology* 1761, pp. 145–163.

Baillie, A. L. et al. (2020). "It Started With a Kiss: Monitoring Organelle Interactions and Identifying Membrane Contact Site Components in Plants". In: *Frontiers in Plant Science* 11.

Bakstad, D. et al. (Feb. 2012). "Quantitative measurement of single cell dynamics". In: *Current Opinion in Biotechnology* 23.1, pp. 103–109.

Barabási, A. .-. and R. Albert (Oct. 1999). "Emergence of scaling in random networks". In: *Science* 286.5439, pp. 509–512.

Barabási, A.-L. (2016). *Network science*. Cambridge University Press.

Barton, K. A. et al. (Jan. 2018). "Chloroplast behaviour and interactions with other organelles in *Arabidopsis thaliana* pavement cells". In: *Journal of Cell Science* 131.2, jcs202275.

Bassel, G. W. and R. S. Smith (Feb. 2016). "Quantifying morphogenesis in plants in 4D". In: *Current Opinion in Plant Biology* 29, pp. 87–94.

Bauwe, H., M. Hagemann, and A. R. Fernie (June 2010). "Photorespiration: players, partners and origin". In: *Trends in Plant Science* 15.6, pp. 330–336.

Belfort, M. and R. J. Roberts (Sept. 1997). "Homing endonucleases: Keeping the house in order". In: *Nucleic Acids Research* 25.17, pp. 3379–3388.

Beliveau, B. J. et al. (May 2015). "Single-molecule super-resolution imaging of chromosomes and in-situ haplotype visualization using Oligopaint FISH probes". In: *Nature Communications* 6.1, pp. 1–13.

Bellaoui, M. et al. (1998). "Low-copy-number molecules are produced by recombination, actively maintained and can be amplified in the mitochondrial genome of Brassicaceae: relationship to reversion of the male sterile phenotype in some cybrids". In: *Molecular and General Genetics* 257.2, pp. 177–185.

Belliard, G., F. Vedel, and G. Pelletier (Oct. 1979). "Mitochondrial recombination in cytoplasmic hybrids of *Nicotiana tabacum* by protoplast fusion". In: *Nature* 281.5730, pp. 401–403.

Bender, A. et al. (Apr. 2006). "High levels of mitochondrial DNA deletions in substantia nigra neurons in aging and Parkinson disease". In: *Nature Genetics* 38.5, pp. 515–517.

Bendich, A. J. and L. P. Gauriloff (Feb. 1984). "Morphometric analysis of cucurbit mitochondria: The relationship between chondriome volume and DNA content". In: *Protoplasma* 119.1, pp. 1–7.

Benson, D. A. et al. (Jan. 2013). "GenBank". In: *Nucleic Acids Research* 41.D1.

Bereiter-Hahn, J. (Jan. 1990). "Behavior of Mitochondria in the Living Cell". In: *International Review of Cytology* 122.C, pp. 1–63.

Bereiter-Hahn, J. and M. Vöth (1994). "Dynamics of mitochondria in living cells: Shape changes, dislocations, fusion, and fission of mitochondria". In: *Microscopy Research and Technique* 27.3, pp. 198–219.

Bidhendi, A. J. et al. (July 2019). "Methods to quantify primary plant cell wall mechanics". In: *Journal of Experimental Botany* 70.14, pp. 3615–3648.

Bilewitch, J. P. and S. M. Degnan (Dec. 2011). "A unique horizontal gene transfer event has provided the octocoral mitochondrial genome with an active mismatch repair gene that has potential for an unusual self-contained function". In: *BMC Evolutionary Biology* 11.1, p. 228.

Boldogh, I. R. and L. A. Pon (May 2006). "Interactions of mitochondria with the actin cytoskeleton". In: *Biochimica et Biophysica Acta (BBA) - Molecular Cell Research* 1763.5-6, pp. 450–462.

Bomba-Warczak, E. et al. (Sept. 2021). "Long-lived mitochondrial cristae proteins in mouse heart and brain". In: *Journal of Cell Biology* 220.9.

Breitling, R. (2010). "What is systems biology?" In: *Frontiers in Physiology* 1, p. 159.

Breuer, D. et al. (July 2017). "System-wide organization of actin cytoskeleton determines organelle transport in hypocotyl plant cells." In: *Proceedings of the National Academy of Sciences of the United States of America* 114.28, E5741–E5749.

Brooks Shera, E. et al. (1990). "Detection of single fluorescent molecules". In: *Chemical Physics Letters* 174.6, pp. 553–557.

Brown, W. M., M. George, and A. C. Wilson (Apr. 1979). "Rapid evolution of animal mitochondrial DNA". In: *Proceedings of the National Academy of Sciences* 76.4, pp. 1967–1971.

Browse, J. et al. (1993). "Mutants of *Arabidopsis* deficient in the synthesis of α-linolenate". In: *Journal of Biological Chemistry* 268.22, pp. 16345–16351.

Bruggeman, F. J., H. V. Westerhoff, and F. C. Boogerd (2002). "BioComplexity: A pluralist research strategy is necessary for a mechanistic explanation of the "live" state". In: *Philosophical Psychology* 15.4, pp. 411–440.

Budar, F. and S. Fujii (Jan. 2012). "Cytonuclear Adaptation in Plants". In: *Advances in Botanical Research*. Vol. 63. Academic Press Inc., pp. 99–126.

Budar, F. and F. Roux (2011). "The role of organelle genomes in plant adaptation: time to get to work!" In: *Plant signaling and behavior* 6.5, pp. 635–639.

Burzyński, A. et al. (Mar. 2003). "Evidence for recombination of mtDNA in the marine mussel *Mytilus trossulus* from the baltic". In: *Molecular Biology and Evolution* 20.3, pp. 388–392.

Busch, K. B., A. Kowald, and J. N. Spelbrink (July 2014). "Quality matters: How does mitochondrial network dynamics and quality control impact on mtDNA integrity?" In: *Philosophical Transactions of the Royal Society B: Biological Sciences* 369.1646.

Butler, P. G. et al. (Mar. 2013). "Variability of marine climate on the North Icelandic Shelf in a 1357-year proxy archive based on growth increments in the bivalve *Arctica islandica*". In: *Palaeogeography, Palaeoclimatology, Palaeoecology* 373, pp. 141–151.

Cao, Z. et al. (June 2018). "Panacea: A low-latency, energy-efficient neighbor discovery protocol for wireless sensor networks". In: *IEEE Wireless Communications and Networking Conference, WCNC* 2018-April, pp. 1–6.

Chen, H. and D. C. Chan (Aug. 2006). "Critical dependence of neurons on mitochondrial dynamics". In: *Current Opinion in Cell Biology* 18.4, pp. 453–459.

Chen, J.-H., C. N. Hales, and S. E. Ozanne (Dec. 2007). "DNA damage, cellular senescence and organismal ageing: causal or correlative?" In: *Nucleic Acids Research* 35.22, pp. 7417–7428.

Chen, X. jie, M. xin Guan, and G. D. Clark-walker (July 1993). "MGM101, a nuclear gene involved in maintenance of the mitochondrial genome in *Saccharomyces cerevisiae*." In: *Nucleic Acids Research* 21.15, p. 3473.

Chen, X. J. (Sept. 2013). "Mechanism of Homologous Recombination and Implications for Aging-Related Deletions in Mitochondrial DNA". In: *Microbiology and Molecular Biology Reviews* 77.3, pp. 476–496.

Chevalier, B. S. and B. L. Stoddard (Sept. 2001). "Homing endonucleases: Structural and functional insight into the catalysts of intron/intein mobility". In: *Nucleic Acids Research* 29.18, pp. 3757–3774.

Chevigny, N. et al. (Jan. 2020). "DNA repair and the stability of the plant mitochondrial genome". In: *International Journal of Molecular Sciences* 21.1.

Christensen, A. C. (June 2014). "Genes and junk in plant mitochondria-repair mechanisms and selection". In: *Genome Biology and Evolution* 6.6, pp. 1448–1453.

Christie, J. M. and M. D. Zurbriggen (2021). "Optogenetics in plants". In: *New Phytologist* 229.6, pp. 3108–3115.

Chudakov, D. M. et al. (July 2010). "Fluorescent proteins and their applications in imaging living cells and tissues". In: *Physiological Reviews* 90.3, pp. 1103–1163.

Chustecki, J. M., R. D. Etherington, et al. (Oct. 2021). "Altered collective mitochondrial dynamics in an *Arabidopsis* msh1 mutant compromising organelle DNA maintenance". In: *bioRxiv*, p. 2021.10.22.465420.

Chustecki, J. M., D. J. Gibbs, et al. (May 2021). "Network analysis of *Arabidopsis* mitochondrial dynamics reveals a resolved tradeoff between physical distribution and social connectivity". In: *Cell Systems* 12.0, pp. 1–13.

Clavel, M. and Y. Dagdas (Oct. 2021). "Proteasome and selective autophagy: Brothers-in-arms for organelle quality control". In: *Current Opinion in Plant Biology* 63, p. 102106.

Cohen, S., A. M. Valm, and J. Lippincott-Schwartz (Aug. 2018). "Interacting organelles". In: *Current Opinion in Cell Biology* 53, pp. 84–91.

Cole, L. W. (Aug. 2016). "The Evolution of per-cell Organelle Number". In: *Frontiers in Cell and Developmental Biology* 4, p. 85.

Collins, T. J. et al. (Apr. 2002). "Mitochondria are morphologically and functionally heterogeneous within cells". In: *The EMBO Journal* 21.7, pp. 1616–1627.

Cordero, O. X. et al. (Sept. 2012). "Ecological populations of bacteria act as socially cohesive units of antibiotic production and resistance". In: *Science* 337.6099, pp. 1228–1231.

Crick, F. (1970). "Central Dogma of Molecular Biology". In: *Nature* 227.5258, pp. 561–563.

Damon, P. E. et al. (Apr. 1974). "Dendrochronologic Calibration of the Radiocarbon Time Scale". In: *American Antiquity* 39.2.1, pp. 350–366.

Daniell, H. et al. (June 2016). "Chloroplast genomes: Diversity, evolution, and applications in genetic engineering". In: *Genome Biology* 17.1, pp. 1–29.

Davila, J. I. et al. (Sept. 2011). "Double-strand break repair processes drive evolution of the mitochondrial genome in *Arabidopsis*". In: *BMC Biology* 9.1, pp. 1–14.

Day, D. A., A. Millar, and J. Whelan (2004). *Plant Mitochondria: From Genome to Function.* Kluwer Academic Publishers, p. 325.

De Col, V. et al. (July 2017). "ATP sensing in living plant cells reveals tissue gradients and stress dynamics of energy physiology". In: *eLife* 6.

De Las Rivas, J., J. J. Lozano, and A. R. Ortiz (Apr. 2002). "Comparative analysis of chloroplast genomes: Functional annotation, genome-based phylogeny, and deduced evolutionary patterns". In: *Genome Research* 12.4, pp. 567–583.

De Vos, K. J., V. J. Allan, et al. (Apr. 2005). "Mitochondrial Function and Actin Regulate Dynamin-Related Protein 1-Dependent Mitochondrial Fission". In: *Current Biology* 15.7, pp. 678–683.

De Vos, K. J. and M. P. Sheetz (Jan. 2007). "Visualization and Quantification of Mitochondrial Dynamics in Living Animal Cells". In: *Methods in Cell Biology* 80, pp. 627–682.

Dieteren, C. E. et al. (May 2011). "Solute diffusion is hindered in the mitochondrial matrix". In: *Proceedings of the National Academy of Sciences of the United States of America* 108.21, pp. 8657–8662.

Dodig, S., I. Čepelak, and I. Pavić (Oct. 2019). "Hallmarks of senescence and aging". In: *Biochemia Medica* 29.3.

Dolgin, E. (Mar. 2019). "How secret conversations inside cells are transforming biology". In: *Nature* 567.7747, pp. 162–164.

Doniwa, Y., S.-i. Arimura, and N. Tsutsumi (Dec. 2007). "Mitochondria use actin filaments as rails for fast translocation in *Arabidopsis* and tobacco cells". In: *Plant Biotechnology* 24.5, pp. 441–447.

Dopp, I. J., X. Yang, and S. A. Mackenzie (Apr. 2021). "A new take on organelle-mediated stress sensing in plants". In: *New Phytologist*, nph.17333.

Durand-Smet, P. et al. (July 2020). "Cytoskeletal organization in isolated plant cells under geometry control". In: *Proceedings of the National Academy of Sciences of the United States of America* 117.29, pp. 17399–17408.

Edwards, D. M. et al. (Apr. 2021). "Avoiding organelle mutational meltdown across eukaryotes with or without a germline bottleneck". In: *PLoS Biology* 19.4, e3001153.

Eisner, V., M. Picard, and G. Hajnóczky (June 2018). "Mitochondrial dynamics in adaptive and maladaptive cellular stress responses". In: *Nature Cell Biology 2018 20:7* 20.7, pp. 755–765.

Ekanayake, S. B. et al. (Apr. 2015). *Imaging and analysis of mitochondrial dynamics in living cells*. Springer New York, pp. 223–240.

El Zawily, A. M. et al. (Oct. 2014). "FRIENDLY Regulates Mitochondrial Distribution, Fusion, and Quality Control in *Arabidopsis*". In: *Plant Physiology* 166.2, pp. 808–828.

Endo, M. et al. (Nov. 2020). "The msh1 gene is responsible for short life span mutant natural death and functions to maintain mitochondrial DNA integrity". In: *Fungal Genetics and Biology* 144.

Erdös, P. and A. Rényi (Oct. 2011). "On the evolution of random graphs". In: *Publ. Math. Inst. Hung. Acad. Sci* 9781400841, pp. 38–82.

Fallon, S. J. et al. (Apr. 2010). "A simple radiocarbon dating method for determining the age and growth rate of deep-sea sponges". In: *Nuclear Instruments and Methods in Physics Research Section B: Beam Interactions with Materials and Atoms* 268.7-8, pp. 1241–1243.

Fan, Y. et al. (Oct. 2021). "The crucial roles of mitochondria in supporting C4 photosynthesis". In: *New Phytologist* 233 (3), pp. 1083–1096.

Federhen, S. (Jan. 2012). "The NCBI Taxonomy database". In: *Nucleic Acids Research* 40.D1, pp. D136–D143.

Fehrenbacher, K. L. et al. (Nov. 2004). "Live Cell Imaging of Mitochondrial Movement along Actin Cables in Budding Yeast". In: *Current Biology* 14.22, pp. 1996–2004.

Feng, X. et al. (Oct. 2004). "Isolation of mutants with aberrant mitochondrial morphology from *Arabidopsis thaliana*". In: *Genes and Genetic Systems* 79.5, pp. 301–305.

Ferrante, M. and M. Saltalamacchia (2014). "The coupon collector's problem". In: *Materials Matemàtics* 35.2, pp. 1–35.

Figge, M. T. et al. (June 2012). "Deceleration of fusion-fission cycles improves mitochondrial quality control during aging". In: *PLoS Computational Biology* 8.6, p. 1002576.

Flajolet, P., D. Gardy, and L. Thimonier (Nov. 1992). "Birthday paradox, coupon collectors, caching algorithms and self-organizing search". In: *Discrete Applied Mathematics* 39.3, pp. 207–229.

Flamholz, A., R. Phillips, and R. Milo (Nov. 2014). "The quantified cell". In: *Molecular Biology of the Cell* 25.22, pp. 3497–3500.

Fonseca, R. R. da et al. (Dec. 2016). "Next-generation biology: Sequencing and data analysis approaches for non-model organisms". In: *Marine Genomics* 30, pp. 3–13.

Franke, W. W. and J. Kartenbeck (1971). "Outer mitochondrial membrane continuous with endoplasmic reticulum". In: *Protoplasma* 73.1, pp. 35–41.

Frederick, R. L. and J. M. Shaw (Dec. 2007). "Moving mitochondria: Establishing distribution of an essential organelle". In: *Traffic* 8.12, pp. 1668–1675.

Fricker, M. D., L. Heaton, N. Jones, B. Obara, et al. (2018). "Quantitation of ER Structure and Function". In: *Methods in Molecular Biology* 1691, pp. 43–66.

Fricker, M. D., L. L. M. Heaton, N. S. Jones, and L. Boddy (May 2017). "The Mycelium as a Network". In: *Microbiology Spectrum* 5.3.

Fricker, M. D., J. A. Lee, et al. (2008). "The Interplay between Structure and Function in Fungal Networks". In: *Topologica* 1.1, p. 004.

Fuchs, P. et al. (Jan. 2020). "Single organelle function and organization as estimated from *Arabidopsis* mitochondrial proteomics". In: *The Plant Journal* 101.2, pp. 420–441.

Fujie, M. et al. (1994). "Behavior of organelles and their nucleoids in the shoot apical meristem during leaf development in *Arabidopsis thaliana*". In: *Source: Planta* 194.3, pp. 395–405.

Fukui, K. et al. (Dec. 2018). "The GIY-YIG endonuclease domain of *Arabidopsis* MutS homolog 1 specifically binds to branched DNA structures". In: *FEBS Letters* 592.24, pp. 4066–4077.

Garcia, L. E. et al. (2019). "Elucidating genomic patterns and recombination events in plant cybrid mitochondria". In: *Plant Molecular Biology* 100, pp. 433–450.

Garone, C. et al. (2018). "The mitochondrial DNA genetic bottleneck: inheritance and beyond". In: *Essays in biochemistry* 62.3, pp. 225–234.

Germond, A. et al. (June 2016). "Design and development of genetically encoded fluorescent sensors to monitor intracellular chemical and physical parameters". In: *Biophysical Reviews* 8.2, pp. 121–138.

Giannakis, K., J. M. Chustecki, and I. G. Johnston (Oct. 2021). "Encounter networks from collective mitochondrial dynamics support the emergence of effective mtDNA genomes in plant cells". In: *bioRxiv*, p. 2021.10.01.462720.

Gilkerson, R. W. et al. (June 2008). "Mitochondrial nucleoids maintain genetic autonomy but allow for functional complementation". In: *Journal of Cell Biology* 181.7, pp. 1117–1128.

Gray, M. W. (Sept. 2012). "Mitochondrial evolution". In: *Cold Spring Harbor Perspectives in Biology* 4.9.

Gray, M. W., G. Burger, and B. F. Lang (Mar. 1999). "Mitochondrial evolution". In: *Science* 283.5407, pp. 1476–1481.

Green, B. R. (Apr. 2011). "Chloroplast genomes of photosynthetic eukaryotes". In: *The Plant Journal* 66.1, pp. 34–44.

Grisi-Filho, J. H. H. et al. (June 2013). "Scale-Free Networks with the Same Degree Distribution: Different Structural Properties". In: *Physics Research International* 2013.

Gualberto, J. M., D. Mileshina, et al. (2014). "The plant mitochondrial genome: Dynamics and maintenance". In: *Biochimie* 100.1, pp. 107–120.

Gualberto, J. M. and K. J. Newton (Apr. 2017). "Plant Mitochondrial Genomes: Dynamics and Mechanisms of Mutation". In: *Annual Review of Plant Biology* 68.1, pp. 225–252.

Guo, C. et al. (July 2013). "Oxidative stress, mitochondrial damage and neurodegenerative diseases". In: *Neural Regeneration Research* 8.21, p. 2003.

Harman, D. (1956). "Aging: a theory based on free radical and radiation chemistry." In: *Journal of Gerontology* 11.3, pp. 298–300.

— (1972). "The Biologic Clock: The Mitochondria?" In: *Journal of the American Geriatrics Society* 20.4, pp. 145–147.

Hildebrandt, T., E. Meyer, and M. Schwarzländer (Nov. 2021). "Die Proteinausstattung eines einzelnen pflanzlichen Mitochondriums". In: *BIOspektrum* 27.7, pp. 715–718.

Hofmann, N. R. (Sept. 2011). "MutS HOMOLOG1 Stabilizes Plastid and Mitochondrial Genomes". In: *The Plant Cell* 23.9, p. 3085.

Hofstatter, P. G. et al. (Oct. 2016). "Evolution of bacterial recombinase A (recA) in eukaryotes explained by addition of genomic data of key microbial lineages". In: *Proceedings of the Royal Society B: Biological Sciences* 283.1840.

Hoitzing, H., I. G. Johnston, and N. S. Jones (June 2015). "What is the function of mitochondrial networks? A theoretical assessment of hypotheses and proposal for future research". In: *BioEssays* 37.6, pp. 687–700.

Hollenbeck, P. J. and W. M. Saxton (Dec. 2005). "The axonal transport of mitochondria". In: *Journal of Cell Science* 118.23, pp. 5411–5419.

Howard, J. (Nov. 2014). "Quantitative cell biology: the essential role of theory". In: *Molecular Biology of the Cell* 25.22, p. 3438.

Howe, C. J., R. E. R. Nisbet, and A. C. Barbrook (Mar. 2008). "The remarkable chloroplast genome of dinoflagellates". In: 59.5, pp. 1035–1045.

Huang, S. et al. (July 2020). "Protein turnover rates in plant mitochondria". In: *Mitochondrion* 53, pp. 57–65.

Huttlin, E. L. et al. (May 2021). "Dual proteome-scale networks reveal cell-specific remodeling of the human interactome". In: *Cell* 184.11, 3022–3040.e28.

Hyde, B. B., G. Twig, and O. S. Shirihai (2010). "Organellar vs cellular control of mitochondrial dynamics". In: *Seminars in Cell and Developmental Biology* 21.6, pp. 575–581.

Ichas, F., L. S. Jouaville, and J.-P. Mazat (June 1997). "Mitochondria Are Excitable Organelles Capable of Generating and Conveying Electrical and Calcium Signals". In: *Cell* 89.7, pp. 1145–1153.

Islam, M. S. and S. Takagi (Feb. 2010). "Co-localization of mitochondria with chloroplasts is a light-dependent reversible response". In: *Plant Signaling and Behavior* 5.2, pp. 146–147.

Islam, M. S., T. Van Nguyen, et al. (Sept. 2020). "Phototropin- and photosynthesis-dependent mitochondrial positioning in *Arabidopsis thaliana* mesophyll cells". In: *Journal of Integrative Plant Biology* 62.9, pp. 1352–1371.

Islam, M. S., Y. Niwa, and S. Takagi (June 2009). "Light-Dependent Intracellular Positioning of Mitochondria in *Arabidopsis thaliana* Mesophyll Cells". In: *Plant and Cell Physiology* 50.6, pp. 1032–1040.

Jackson, M. D. B., S. Duran-Nebreda, and G. W. Bassel (Oct. 2017). "Network-based approaches to quantify multicellular development". In: *Journal of The Royal Society Interface* 14.135, p. 20170484.

Jacoby, R. P. et al. (Oct. 2012). "Mitochondrial Composition, Function and Stress Response in Plants". In: *Journal of Integrative Plant Biology* 54.11, pp. 887–906.

Jaipargas, E.-A., K. A. Barton, et al. (2015). "Mitochondrial pleomorphy in plant cells is driven by contiguous ER dynamics." In: *Frontiers in plant science* 6, p. 783.

Jaipargas, E.-A., N. Mathur, et al. (Feb. 2016). "High Light Intensity Leads to Increased Peroxule-Mitochondria Interactions in Plants". In: *Frontiers in Cell and Developmental Biology* 0.2, p. 6.

Jakubke, C. et al. (Sept. 2021). "Cristae-dependent quality control of the mitochondrial genome". In: *Science Advances* 7.36.

Janicka, S. et al. (Nov. 2012). "A RAD52-like single-stranded DNA binding protein affects mitochondrial DNA repair by recombination". In: *The Plant Journal* 72.3, pp. 423–435.

Javanmardi, Y. et al. (Nov. 2021). "Quantifying cell-generated forces: Poisson's ratio matters". In: *Communications Physics* 4.1, pp. 1–10.

Johnston, I. G. (Nov. 2019a). "Varied mechanisms and models for the varying mitochondrial bottleneck". In: *Frontiers in cell and developmental biology* 7, p. 294.

— (June 2019b). "Tension and Resolution: Dynamic, Evolving Populations of Organelle Genomes within Plant Cells". In: *Molecular Plant* 12.6, pp. 764–783.

Johnston, I. G. and B. P. Williams (Feb. 2016). "Evolutionary inference across eukaryotes identifies specific pressures favoring mitochondrial gene retention". In: *Cell Systems* 2.2, pp. 101–111.

Jones, D. P. (1986). "Intracellular diffusion gradients of O_2 and ATP". In: *American Journal of Physiology - Cell Physiology* 250.5.1, pp. C663–75.

Jones, O. R. et al. (Dec. 2013). "Diversity of ageing across the tree of life". In: *Nature* 505.7482, pp. 169–173.

Jouhet, J. et al. (Dec. 2004). "Phosphate deprivation induces transfer of DGDG galactolipid from chloroplast to mitochondria". In: *The Journal of Cell Biology* 167.5, p. 863.

Kang, J. S. et al. (Jan. 2008). "Docking of Axonal Mitochondria by Syntaphilin Controls Their Mobility and Affects Short-Term Facilitation". In: *Cell* 132.1, pp. 137–148.

Karbowski, M. and R. J. Youle (Aug. 2003). "Dynamics of mitochondrial morphology in healthy cells and during apoptosis". In: *Cell Death and Differentiation* 10.8, pp. 870–880.

Kaya, A. et al. (Nov. 2021). "Evolution of natural lifespan variation and molecular strategies of extended lifespan". In: *eLife* 10.

Kekenes-Huskey, P. M., C. E. Scott, and S. Atalay (Aug. 2016). "Quantifying the Influence of the Crowded Cytoplasm on Small Molecule Diffusion". In: *Journal of Physical Chemistry B* 120.33, pp. 8696–8706.

Kennedy, S. R. et al. (Sept. 2013). "Ultra-sensitive sequencing reveals an age-related increase in somatic mitochondrial mutations that are inconsistent with oxidative damage". In: *PLoS genetics* 9.9.

Khacho, M. et al. (Aug. 2016). "Mitochondrial Dynamics Impacts Stem Cell Identity and Fate Decisions by Regulating a Nuclear Transcriptional Program". In: *Cell Stem Cell* 19.2, pp. 232–247.

Kitano, H. (Nov. 2002). "Computational systems biology". In: *Nature* 420.6912, pp. 206–210.

Kleier, C. and P. W. Rundel (Aug. 2004). "Microsite requirements, population structure and growth of the cushion plant *Azorella compacta* in the tropical Chilean Andes". In: *Austral Ecology* 29.4, pp. 461–470.

Klucnika, A. and H. Ma (2020). "Mapping and editing animal mitochondrial genomes: Can we overcome the challenges?" In: *Philosophical Transactions of the Royal Society B: Biological Sciences* 375.1790.

Kmiec, B., M. Woloszynska, and H. Janska (June 2006). "Heteroplasmy as a common state of mitochondrial genetic information in plants and animals". In: *Current Genetics* 50.3, pp. 149–159.

Kost, B. and N. H. Chua (Jan. 2002). "The Plant Cytoskeleton: Vacuoles and Cell Walls Make the Difference". In: *Cell* 108.1, pp. 9–12.

Kozik, A. et al. (2019). "The alternative reality of plant mitochondrial DNA: One ring does not rule them all". In: *PLoS Genetics* 15.8, e1008373.

Krishnan, K. J. et al. (Feb. 2008). "What causes mitochondrial DNA deletions in human cells?" In: *Nature Genetics* 40.3, pp. 275–279.

Krupinska, K. et al. (June 2020). "Genome communication in plants mediated by organelle–nucleus-located proteins". In: *Philosophical Transactions of the Royal Society B: Biological Sciences* 375.1801.

Kukat, C., K. M. Davies, et al. (Sept. 2015). "Cross-strand binding of TFAM to a single mtDNA molecule forms the mitochondrial nucleoid". In: *Proceedings of the National Academy of Sciences of the United States of America* 112.36, pp. 11288–11293.

Kukat, C., C. A. Wurm, et al. (Aug. 2011). "Super-resolution microscopy reveals that mammalian mitochondrial nucleoids have a uniform size and frequently contain a single copy of mtDNA". In: *Proceedings of the National Academy of Sciences of the United States of America* 108.33, pp. 13534–13539.

Labbé, K., A. Murley, and J. Nunnari (Oct. 2014). "Determinants and functions of mitochondrial behavior". In: *Annual review of cell and developmental biology* 30.1, pp. 357–391.

Ladoukakis, E. D. and E. Zouros (2001). "Direct evidence for homologous recombination in mussel (*Mytilus galloprovincialis*) mitochondrial DNA". In: *Molecular Biology and Evolution* 18.7, pp. 1168–1175.

Ladoukakis, E. D. and E. Zouros (2017). "Evolution and inheritance of animal mitochondrial DNA: Rules and exceptions". In: *Journal of Biological Research (Greece)* 24.1.

Lagouge, M. and N.-G. Larsson (June 2013). "The role of mitochondrial DNA mutations and free radicals in disease and ageing". In: *Journal of Internal Medicine* 273.6, pp. 529–543.

Lakshmanan, L. N. et al. (Oct. 2018). "Clonal expansion of mitochondrial DNA deletions is a private mechanism of aging in long-lived animals". In: *Aging Cell* 17.5, e12814.

Lawless, C. et al. (May 2020). "The rise and rise of mitochondrial DNA mutations". In: *Open Biology* 10.5.

Lee, C. P., H. Eubel, et al. (June 2012). "Mitochondrial proteome heterogeneity between tissues from the vegetative and reproductive stages of *Arabidopsis thaliana* development". In: *Journal of proteome research* 11.6, pp. 3326–3343.

Lee, H. C., P. H. Yin, et al. (2005). "Mitochondrial genome instability and mtDNA depletion in human cancers". In: *Annals of the New York Academy of Sciences* 1042, pp. 109–122.

Lewis, M. R. and W. H. Lewis (1914). "Mitochondria in tissue culture". In: *Science* 39.1000, pp. 330–333.

Lewis, T. L., S.-K. Kwon, et al. (Nov. 2018). "MFF-dependent mitochondrial fission regulates presynaptic release and axon branching by limiting axonal mitochondria size". In: *Nature Communications* 9.1, pp. 1–15.

Li, G. M. (Jan. 2008). "Mechanisms and functions of DNA mismatch repair". In: *Cell Research* 18.1, pp. 85–98.

Li, L., C. J. Nelson, et al. (Mar. 2017). "Protein Degradation Rate in *Arabidopsis thaliana* Leaf Growth and Development". In: *The Plant Cell* 29.2, pp. 207–228.

Li, L., H. Peng, et al. (May 2014). "Chaos–order transition in foraging behavior of ants". In: *Proceedings of the National Academy of Sciences* 111.23, pp. 8392–8397.

Lieber, T. et al. (May 2019). "Mitochondrial fragmentation drives selective removal of deleterious mtDNA in the germline". In: *Nature* 570.7761, pp. 380–384.

Liesa, M. and O. S. Shirihai (Apr. 2013). "Mitochondrial dynamics in the regulation of nutrient utilization and energy expenditure". In: *Cell Metabolism* 17.4, pp. 491–506.

Life, E. of (2021). *Encyclopedia of Life: Global access to knowledge about life on Earth* Date accessed 1 Dec 2020. URL: https://eol.org/.

Lim, S. L. et al. (Dec. 2020). "*In planta* study of photosynthesis and photorespiration using NADPH and NADH/NAD+ fluorescent protein sensors". In: *Nature Communications* 11.1, pp. 1–12.

Lin, Z., M. Nei, and H. Ma (Dec. 2007). "The origins and early evolution of DNA mismatch repair genes - Multiple horizontal gene transfers and co-evolution". In: *Nucleic Acids Research* 35.22, pp. 7591–7603.

Ling, F., F. Makishima, et al. (Aug. 1995). "A nuclear mutation defective in mitochondrial recombination in yeast". In: *EMBO Journal* 14.16, pp. 4090–4101.

Ling, F. and T. Shibata (Sept. 2002). "Recombination-dependent mtDNA partitioning: *in vivo* role of Mhr1p to promote pairing of homologous DNA". In: *The EMBO Journal* 21.17, p. 4730.

Liu, J., M. Zhou, et al. (May 2017). "A comparative study of network robustness measures". In: *Frontiers of Computer Science* 11.4, pp. 568–584.

Liu, X., D. Weaver, et al. (Oct. 2009). "Mitochondrial 'kiss-and-run': Interplay between mitochondrial motility and fusion-fission dynamics". In: *The EMBO Journal* 28.20, pp. 3074–3089.

Logan, D. C., I. Scott, and A. K. Tobin (Nov. 2003). "The genetic control of plant mitochondrial morphology and dynamics". In: *The Plant Journal* 36.4, pp. 500–509.

Logan, D. C. (Mar. 2006a). "The mitochondrial compartment." In: *Journal of Experimental Botany* 57.6, pp. 1225–43.

— (June 2010a). "Mitochondrial fusion, division and positioning in plants". In: *Biochemical Society Transactions* 38.3, pp. 789–795.

— (Jan. 2010b). "The dynamic plant chondriome". In: *Seminars in Cell and Developmental Biology* 21.6, pp. 550–557.

Logan, D. C., I. Scott, and A. K. Tobin (2004). "ADL2a, like ADL2b, is involved in the control of higher plant mitochondrial morphology". In: *Journal of Experimental Botany* 55.397, pp. 783–785.

Logan, D. C. (Nov. 2003). "Mitochondrial dynamics". In: *New Phytologist* 160.3, pp. 463–478.

— (2006b). "Plant mitochondrial dynamics". In: *Biochimica et Biophysica Acta (BBA) - Molecular Cell Research* 1763.5, pp. 430–441.

Logan, D. C. and C. J. Leaver (May 2000). "Mitochondria-targeted GFP highlights the heterogeneity of mitochondrial shape, size and movement within living plant cells". In: *Journal of Experimental Botany* 51.346, pp. 865–871.

Logan, D. C. and G. Paszkiewicz (Apr. 2018). "The Dynamic Chondriome: Control of Number, Shape, Size and Motility of Mitochondria". In: *Annual Plant Reviews online*, pp. 67–110.

Lonsdale, D. M. et al. (May 1988). "The Plant Mitochondrial Genome: Homologous Recombination as a Mechanism for Generating Heterogeneity". In: *Philosophical Transactions of the Royal Society B: Biological Sciences* 319.1193, pp. 149–163.

López-Otín, C. et al. (June 2013). "The Hallmarks of Aging". In: *Cell* 153.6, pp. 1194–1217.

Ma, J. et al. (Mar. 2021). "Friendly mediates membrane depolarization-induced mitophagy in *Arabidopsis*". In: *Current Biology* 31.0, pp. 1–14.

MacAskill, A. F., T. A. Atkin, and J. T. Kittler (July 2010). "Mitochondrial trafficking and the provision of energy and calcium buffering at excitatory synapses". In: *European Journal of Neuroscience* 32.2, pp. 231–240.

Mackenzie, S. A. (Apr. 2018). "The Unique Biology of Mitochondrial Genome Instability in Plants". In: *Annual Plant Reviews online*. John Wiley and Sons, Ltd, pp. 36–49.

Mahapatra, K. et al. (Aug. 2021). "An Insight Into the Mechanism of Plant Organelle Genome Maintenance and Implications of Organelle Genome in Crop Improvement: An Update". In: *Frontiers in Cell and Developmental Biology* 0, p. 2209.

Mano, S., T. Miwa, et al. (Jan. 2008). "The plant organelles database (PODB): A collection of visualized plant organelles and protocols for plant organelle research". In: *Nucleic Acids Research* 36.S.1, p. D929.

Mano, S., T. Miwa, et al. (Dec. 2009). "Seeing is believing: On the use of image databases for visually exploring plant organelle dynamics". In: *Plant and Cell Physiology* 50.12, pp. 2000–2014.

— (Feb. 2011). "The plant organelles database 2 (PODB2): An updated resource containing movie data of plant organelle dynamics". In: *Plant and Cell Physiology* 52.2, pp. 244–253.

Mano, S., T. Nakamura, et al. (Jan. 2014). "The plant organelles database 3 (PODB3) update 2014: Integrating electron micrographs and new options for plant organelle research". In: *Plant and Cell Physiology* 55.1, e1–e1.

Manzoni, C. et al. (Mar. 2018). "Genome, transcriptome and proteome: the rise of omics data and their integration in biomedical sciences". In: *Briefings in Bioinformatics* 19.2, pp. 286–302.

Maréchal, A. and N. Brisson (Apr. 2010). "Recombination and the maintenance of plant organelle genome stability". In: *New Phytologist* 186.2, pp. 299–317.

Martínez, D. E. (May 1998). "Mortality Patterns Suggest Lack of Senescence in *Hydra*". In: *Experimental Gerontology* 33.3, pp. 217–225.

Martínez-Zapater, J. M. et al. (Aug. 1992). "Mutations at the *Arabidopsis* CHM locus promote rearrangements of the mitochondrial genome". In: *Plant Cell* 4.8, pp. 889–899.

Martinière, A. et al. (2013). "Development and properties of genetically encoded pH sensors in plants". In: *Frontiers in Plant Science* 4.12.

Mathur, J. (2021). "Organelle extensions in plant cells". In: *Plant Physiology* 185.3, pp. 593–607.

Mathur, J., A. Mammone, and K. A. Barton (Nov. 2012). "Organelle Extensions in Plant Cells". In: *Journal of Integrative Plant Biology* 54.11, pp. 851–867.

McHugh, D. and J. Gil (Jan. 2018). "Senescence and aging: Causes, consequences, and therapeutic avenues". In: *Journal of Cell Biology* 217.1, pp. 65–77.

Mehrshahi, P. et al. (July 2013). "Transorganellar complementation redefines the biochemical continuity of endoplasmic reticulum and chloroplasts". In: *Proceedings of the National Academy of Sciences of the United States of America* 110.29, pp. 12126–12131.

Mendel, G. (Jan. 1951). "Versuche Über pflanzen-hybriden". In: *Journal of Heredity* 42.1, p. 3.

Menzies, R. A. and P. H. Gold (Apr. 1971). "The Turnover of Mitochondria in a Variety of Tissues of Young Adult and Aged Rats". In: *Journal of Biological Chemistry* 246.8, pp. 2425–2429.

Miller, R. A. et al. (Nov. 2002). "Longer life spans and delayed maturation in wild-derived mice". In: *Experimental Biology and Medicine* 227.7, pp. 500–508.

Milo, R. and R. Phillips (Dec. 2015). *Cell Biology by the Numbers*. Garland Science.

Mironov, S. L. (2007). "ADP regulates movements of mitochondria in neurons". In: *Biophysical journal* 92.8, pp. 2944–2952.

MitoAge (2021). *MitoAge Database* Date accessed 15 Oct 2020. URL: https://www.mitoage.info/.

Møller, I. M. (2001). "Plant mitochondria and oxidative stress: Electron transport, NADPH turnover, and metabolism of reactive oxygen species". In: *Annual Review of Plant Biology* 52, pp. 561–591.

Møller, I. M. (July 2016). "What is hot in plant mitochondria?" In: *Physiologia Plantarum* 157.3, pp. 256–263.

Møller, I. M., A. G. Rasmusson, and O. Van Aken (Oct. 2021). "Plant mitochondria – past, present and future". In: *The Plant Journal* 108.4, pp. 912–959.

Moore, A. S. and E. L. Holzbaur (June 2018). "Mitochondrial-cytoskeletal interactions: dynamic associations that facilitate network function and remodeling". In: *Current Opinion in Physiology* 3, pp. 94–100.

Moore, C. and M. Newman (2000). “Epidemics and percolation in small-world networks”. In: *Physical Review E - Statistical Physics, Plasmas, Fluids, and Related Interdisciplinary Topics* 61.5, pp. 5678–5682.

Morley, S. A. and B. L. Nielsen (Jan. 2017). “Plant mitochondrial DNA”. In: *Frontiers in Bioscience - Landmark* 22.6, pp. 1023–1132.

Morré, D. J., W. D. Merritt, and C. A. Lembi (Mar. 1971). “Connections between mitochondria and endoplasmic reticulum in rat liver and onion stem”. In: *Protoplasma* 73.1, pp. 43–49.

Mouli, P. K., G. Twig, and O. S. Shirihai (May 2009). “Frequency and selectivity of mitochondrial fusion are key to its quality maintenance function”. In: *Biophysical Journal* 96.9, pp. 3509–3518.

Mueller, S. J. and R. Reski (Dec. 2015). “Mitochondrial dynamics and the ER: The plant perspective”. In: *Frontiers in Cell and Developmental Biology* 3.12, p. 78.

Muller, H. J. (May 1964). “The relation of recombination to mutational advance”. In: *Mutation Research - Fundamental and Molecular Mechanisms of Mutagenesis* 1.1, pp. 2–9.

Mullineaux, P. M. et al. (June 2020). “Spatial chloroplast-to-nucleus signalling involving plastid–nuclear complexes and stromules”. In: *Philosophical Transactions of the Royal Society B: Biological Sciences* 375.1801.

Muthye, V. and D. V. Lavrov (Sept. 2021). “Multiple Losses of MSH1, Gain of mtMutS, and Other Changes in the MutS Family of DNA Repair Proteins in Animals”. In: *Genome Biology and Evolution* 13.9.

Nakamura, S. et al. (May 2021). “Autophagy Contributes to the Quality Control of Leaf Mitochondria”. In: *Plant and Cell Physiology* 62.2, pp. 229–247.

Nardozzi, J. D. et al. (Oct. 2012). “A properly configured ring structure is critical for the function of the mitochondrial DNA recombination protein, Mgm101”. In: *The Journal of biological chemistry* 287.44, pp. 37259–37268.

Neff, M. M. et al. (1998). "dCAPS, a simple technique for the genetic analysis of single nucleotide polymorphisms: Experimental applications in *Arabidopsis thaliana* genetics". In: *The Plant Journal* 14.3, pp. 387–392.

Nelson, C. J. et al. (July 2013). "Degradation rate of mitochondrial proteins in *Arabidopsis thaliana* cells". In: *Journal of Proteome Research* 12.7, pp. 3449–3459.

Nicholls, T. J. and C. M. Gustafsson (Nov. 2018). "Separating and Segregating the Human Mitochondrial Genome". In: *Trends in Biochemical Sciences* 43.11, pp. 869–881.

Nielsen, J. et al. (Aug. 2016). "Eye lens radiocarbon reveals centuries of longevity in the Greenland shark (*Somniosus microcephalus*)". In: *Science* 353.6300, pp. 702–704.

Nietzel, T. et al. (2019). "The fluorescent protein sensor roGFP2-Orp1 monitors *in vivo* H_2O_2 and thiol redox integration and elucidates intracellular H_2O_2 dynamics during elicitor-induced oxidative burst in *Arabidopsis*". In: *New Phytologist* 221.3, pp. 1649–1664.

Nunnari, J. et al. (Oct. 1997). "Mitochondrial transmission during mating in *Saccharomyces cerevisiae* is determined by mitochondrial fusion and fission and the intramitochondrial segregation of mitochondrial DNA". In: *Molecular Biology of the Cell* 8.7, pp. 1233–1242.

Nurse, P. (Sept. 2021). "Biology must generate ideas as well as data". In: *Nature* 597.7876, p. 305.

Nystedt, B. et al. (May 2013). "The Norway spruce genome sequence and conifer genome evolution". In: *Nature* 497.7451, pp. 579–584.

O'Leary, N. A. et al. (2016). "Reference sequence (RefSeq) database at NCBI: Current status, taxonomic expansion, and functional annotation". In: *Nucleic Acids Research* 44.D1, pp. D733–D745.

Odahara, M., Y. Kishita, and Y. Sekine (Aug. 2017). "MSH1 maintains organelle genome stability and genetically interacts with RECA and RECG in the moss *Physcomitrella patens*". In: *The Plant Journal* 91.3, pp. 455–465.

Ogata, H. et al. (Jan. 2011). "Two new subfamilies of DNA mismatch repair proteins (MutS) specifically abundant in the marine environment". In: *ISME Journal* 5.7, pp. 1143–1151.

Oikawa, K. et al. (Mar. 2021). "Mitochondrial movement during its association with chloroplasts in *Arabidopsis thaliana*". In: *Communications Biology* 4.1, pp. 1–13.

Okamoto, K. and J. M. Shaw (Dec. 2005). "Mitochondrial Morphology and Dynamics in Yeast and Multicellular Eukaryotes". In: *Annual Review of Genetics* 39.1, pp. 503–536.

Ono, T. et al. (2001). "Human cells are protected from mitochondrial dysfunction by complementation of DNA products in fused mitochondria". In: *Nature Genetics* 28.3, pp. 272–275.

Ottino-Löffler, B., J. G. Scott, and S. H. Strogatz (2017). "Takeover times for a simple model of network infection". In: *Physical Review E* 96.1, p. 12313.

Pain, C. et al. (Feb. 2019). "Quantitative analysis of plant ER architecture and dynamics". In: *Nature Communications* 10.1, pp. 1–15.

Palmer, J. D., J. M. Nugent, and L. A. Herbon (Feb. 1987). "Unusual structure of *Geranium* chloroplast DNA: A triple-sized inverted repeat, extensive gene duplications, multiple inversions, and two repeat families". In: *Proceedings of the National Academy of Sciences* 84.3, pp. 769–773.

Palmer, J. and L. Herbon (Dec. 1988). "Plant mitochondrial DNA evolves rapidly in structure, but slowly in sequence". In: *Journal of molecular evolution* 28.1-2, pp. 87–97.

Pan, R. and J. Hu (2015). "Plant mitochondrial dynamics and the role of membrane lipids". In: *Plant Signaling and Behavior* 10.10.

Paredez, A. R., C. R. Somerville, and D. W. Ehrhardt (June 2006). "Visualization of cellulose synthase demonstrates functional association with microtubules". In: *Science* 312.5779, pp. 1491–1495.

Parr, C. S. et al. (Apr. 2014). "The Encyclopedia of Life v2: Providing Global Access to Knowledge About Life on Earth". In: *Biodiversity Data Journal* 2, e1079.

Paszkiewicz, G. et al. (Feb. 2017). "*Arabidopsis* Seed Mitochondria Are Bioenergetically Active Immediately upon Imbibition and Specialize via Biogenesis in Preparation for Autotrophic Growth". In: *The Plant Cell* 29.1, pp. 109–128.

Patel, P. K., O. Shirihai, and K. C. Huang (July 2013). "Optimal Dynamics for Quality Control in Spatially Distributed Mitochondrial Networks". In: *PLoS Computational Biology* 9.7, e1003108.

Penrose, M. (2003). *Random geometric graphs*. Vol. 5. Oxford University Press.

Peremyslov, V. V. et al. (Oct. 2015). "Myosin-Powered Membrane Compartment Drives Cytoplasmic Streaming, Cell Expansion and Plant Development". In: *PLoS ONE* 10.10, e0139331.

Perico, C. and I. Sparkes (Oct. 2018). "Plant organelle dynamics: cytoskeletal control and membrane contact sites". In: *New Phytologist* 220.2, pp. 381–394.

Pesaresi, P. et al. (Dec. 2007). "Interorganellar communication". In: *Current Opinion in Plant Biology* 10.6, pp. 600–606.

Petersen, G. et al. (May 2017). "Mitochondrial genome evolution in Alismatales: Size reduction and extensive loss of ribosomal protein genes". In: *PLoS ONE* 12.5, e0177606.

Petralia, R. S., M. P. Mattson, and P. J. Yao (2014). "Aging and longevity in the simplest animals and the quest for immortality". In: *Ageing research reviews* 0.1, p. 66.

Picard, M., M. J. McManus, et al. (Feb. 2015). "Trans-mitochondrial coordination of cristae at regulated membrane junctions". In: *Nature Communications* 6.1, pp. 1–8.

Picard, M. and C. Sandi (July 2021). "The social nature of mitochondria: Implications for human health". In: *Neuroscience and Biobehavioral Reviews* 120, pp. 595–610.

Pizzo, P. and T. Pozzan (Oct. 2007). "Mitochondria–endoplasmic reticulum choreography: structure and signaling dynamics". In: *Trends in Cell Biology* 17.10, pp. 511–517.

Pont-Kingdon, G. et al. (1998). "Mitochondrial DNA of the coral *Sarcophyton glaucum* contains a gene for a homologue of bacterial MutS: A possible case of gene transfer from the nucleus to the mitochondrion". In: *Journal of Molecular Evolution* 46.4, pp. 419–431.

Poovathingal, S. K. et al. (Nov. 2009). "Stochastic Drift in Mitochondrial DNA Point Mutations: A Novel Perspective *Ex Silico*". In: *PLoS Computational Biology* 5.11, e1000572.

Porat-Shliom, N., Y. Chen, et al. (Oct. 2014). "*In Vivo* Tissue-wide Synchronization of Mitochondrial Metabolic Oscillations". In: *Cell Reports* 9.2, pp. 514–521.

Porat-Shliom, N., O. J. Harding, et al. (Jan. 2019). "Mitochondrial Populations Exhibit Differential Dynamic Responses to Increased Energy Demand during Exocytosis *In Vivo*". In: *iScience* 11, pp. 440–449.

Preuten, T. et al. (Dec. 2010). "Fewer genes than organelles: extremely low and variable gene copy numbers in mitochondria of somatic plant cells". In: *The Plant Journal* 64.6, pp. 948–959.

Prole, D. L., P. F. Chinnery, and N. S. Jones (Dec. 2020). "Visualizing, quantifying, and manipulating mitochondrial DNA *in vivo*". In: *The Journal of Biological Chemistry* 295.51, p. 17588.

Rafelski, S. M. (Dec. 2013). "Mitochondrial network morphology: building an integrative, geometrical view". In: *BMC Biology* 11.1, p. 71.

Rafelski, S. M. et al. (Nov. 2012). "Mitochondrial network size scaling in budding yeast". In: *Science* 338.6108, pp. 822–824.

Raghavendra, A. S. and K. Padmasree (Nov. 2003). "Beneficial interactions of mitochondrial metabolism with photosynthetic carbon assimilation". In: *Trends in Plant Science* 8.11, pp. 546–553.

Rahbari, R. et al. (Feb. 2016). "Timing, rates and spectra of human germline mutation". In: *Nature genetics* 48.2, pp. 126–133.

Rédei, G. P. (May 1973). "Extra-chromosomal mutability determined by a nuclear gene locus in *Arabidopsis*". In: *Mutation Research - Fundamental and Molecular Mechanisms of Mutagenesis* 18.2, pp. 149–162.

Rédei, G. P. and S. B. Plurad (1973). "Hereditary structural alterations of plastids induced by a nuclear mutator gene in *Arabidopsis*". In: *Protoplasma: An International Journal of Cell Biology* 77.2, pp. 361–380.

Reenan, R. A. and R. D. Kolodner (1992). "Characterization of insertion mutations in the *Saccharomyces cerevisiae* MSH1 and MSH2 genes: Evidence for separate mitochondrial and nuclear functions". In: *Genetics* 132.4, pp. 975–985.

Reitzel, A. M., K. Pang, and M. Q. Martindale (Aug. 2016). "Developmental expression of "germline"- and "sex determination"-related genes in the ctenophore *Mnemiopsis leidyi*". In: *EvoDevo* 7.1, pp. 1–16.

Rendeková, J. et al. (Dec. 2016). "Mgm101: A double-duty Rad52-like protein". In: *Cell cycle* 15.23, pp. 3169–3176.

Revell, L. J. (2012). "phytools: An R package for phylogenetic comparative biology (and other things)." In: *Methods in Ecology and Evolution* 3, pp. 217–223.

Rintoul, G. L. et al. (Aug. 2003). "Glutamate Decreases Mitochondrial Size and Movement in Primary Forebrain Neurons". In: *Journal of Neuroscience* 23.21, pp. 7881–7888.

Robinson, S. and C. Kuhlemeier (June 2018). "Global Compression Reorients Cortical Microtubules in *Arabidopsis* Hypocotyl Epidermis and Promotes Growth". In: *Current Biology* 28.11, 1794–1802.e2.

Romagnoli, S. et al. (Feb. 2007). "Microtubule- and Actin Filament-Dependent Motors are Distributed on Pollen Tube Mitochondria and Contribute Differently to Their Movement". In: *Plant and Cell Physiology* 48.2, pp. 345–361.

Rose, R. J. (June 2021). "Contribution of massive mitochondrial fusion and subsequent fission in the plant life cycle to the integrity of the mitochondrion and its genome". In: *International Journal of Molecular Sciences* 22.11, p. 5429.

Rossignol, R. et al. (2003). "Mitochondrial threshold effects". In: *Biochemical Journal* 370.3, pp. 751–762.

Rowland, A. A. and G. K. Voeltz (Oct. 2012). "Endoplasmic reticulum-mitochondria contacts: Function of the junction". In: *Nature Reviews Molecular Cell Biology* 13.10, pp. 607–615.

Sage, R. F., P. A. Christin, and E. J. Edwards (May 2011). "The C4 plant lineages of planet Earth". In: *Journal of Experimental Botany* 62.9, pp. 3155–3169.

Sage, R. F., T. L. Sage, and F. Kocacinar (June 2012). "Photorespiration and the Evolution of C4 Photosynthesis". In: *Annual Review of Plant Biology* 63.1, pp. 19–47.

Sage, T. L. and R. F. Sage (Apr. 2009). "The Functional Anatomy of Rice Leaves: Implications for Refixation of Photorespiratory CO_2 and Efforts to Engineer C4 Photosynthesis into Rice". In: *Plant and Cell Physiology* 50.4, pp. 756–772.

Sakamoto, W. et al. (Aug. 1996). "Altered Mitochondrial Gene Expression in a Maternal Distorted Leaf Mutant of *Arabidopsis* Induced by chloroplast mutator". In: *The Plant Cell* 8.8, pp. 1377–1390.

Salguero-Gómez, R., R. P. Shefferson, and M. J. Hutchings (May 2013). "Plants do not count... or do they? New perspectives on the universality of senescence". In: *Journal of Ecology* 101.3, pp. 545–554.

Sanchez-Puerta, M. V., M. K. Zubko, and J. D. Palmer (Apr. 2015). "Homologous recombination and retention of a single form of most genes shape the highly chimeric mitochondrial genome of a cybrid plant". In: *New Phytologist* 206.1, pp. 381–396.

Sandhu, A. P. S., R. V. Abdelnoor, and S. A. Mackenzie (Feb. 2007). "Transgenic induction of mitochondrial rearrangements for cytoplasmic male sterility in crop plants". In: *Proceedings of the National Academy of Sciences of the United States of America* 104.6, pp. 1766–1770.

Santo-Domingo, J. et al. (July 2013). "OPA1 promotes pH flashes that spread between contiguous mitochondria without matrix protein exchange". In: *EMBO Journal* 32.13, pp. 1927–1940.

Sato, S. et al. (1999). "Complete structure of the chloroplast genome of *Arabidopsis thaliana*". In: *DNA research* 6.5, pp. 283–290.

Sbalzarini, I. and P. Koumoutsakos (Aug. 2005). "Feature point tracking and trajectory analysis for video imaging in cell biology". In: *Journal of Structural Biology* 151.2, pp. 182–195.

Schaible, R. et al. (Dec. 2015). "Constant mortality and fertility over age in *Hydra*". In: *Proceedings of the National Academy of Sciences of the United States of America* 112.51, pp. 15701–15706.

Schattat, M. et al. (Apr. 2011). "Plastid stromule branching coincides with contiguous endoplasmic reticulum dynamics". In: *Plant Physiology* 155.4, pp. 1667–1677.

Schmid, M. et al. (May 2005). "A gene expression map of *Arabidopsis thaliana* development". In: *Nature genetics* 37.5, pp. 501–506.

Schofield, M. J. and P. Hsieh (2003). "Dna Mismatch Repair: Molecular Mechanisms and Biological Function". In: *Annual Review of Microbiology* 57, pp. 579–608.

Schrader, M. et al. (Sept. 2015). "The different facets of organelle interplay– An overview of organelle interactions". In: *Frontiers in Cell and Developmental Biology* 3.9, p. 56.

Schuler, M. H. et al. (Aug. 2017). "Miro1-mediated mitochondrial positioning shapes intracellular energy gradients required for cell migration". In: *Molecular Biology of the Cell* 28.16, pp. 2159–2169.

Schwarzländer, M., M. D. Fricker, et al. (Aug. 2008). "Confocal imaging of glutathione redox potential in living plant cells". In: *Journal of microscopy* 231.2, pp. 299–316.

Schwarzländer, M., D. C. Logan, et al. (Mar. 2012). "Pulsing of membrane potential in individual mitochondria: A stress-induced mechanism to regulate respiratory bioenergetics in *Arabidopsis*". In: *Plant Cell* 24.3, pp. 1188–1201.

Scott, I. and D. C. Logan (Nov. 2007). "Mitochondrial morphology transition is an early indicator of subsequent cell death in *Arabidopsis*". In: *New Phytologist* 177.0, pp. 90–101.

— (Jan. 2008). "Mitochondrial morphology transition is an early indicator of subsequent cell death in *Arabidopsis*". In: *New Phytologist* 177.1, pp. 90–101.

Scott, I., I. A. Sparkes, and D. C. Logan (Sept. 2007). "The missing link: inter-organellar connections in mitochondria and peroxisomes?" In: *Trends in Plant Science* 12.9, pp. 380–381.

Scott, I., A. K. Tobin, and D. C. Logan (Mar. 2006). "BIGYIN, an orthologue of human and yeast FIS1 genes functions in the control of mitochondrial size and number in *Arabidopsis thaliana*". In: *Journal of Experimental Botany* 57.6, pp. 1275–1280.

Seguí-Simarro, J. M., M. J. Coronado, and L. A. Staehelin (Nov. 2008). "The mitochondrial cycle of *Arabidopsis* shoot apical meristem and leaf primordium meristematic cells is defined by a perinuclear tentaculate/cage-like mitochondrion." In: *Plant physiology* 148.3, pp. 1380–93.

Seguí-Simarro, J. M. and L. A. Staehelin (Mar. 2009). "Mitochondrial reticulation in shoot apical meristem cells of *Arabidopsis* provides a mechanism for homogenization of mtDNA prior to gamete formation." In: *Plant signaling and behavior* 4.3, pp. 168–71.

Shai, N., M. Schuldiner, and E. Zalckvar (May 2016). "No peroxisome is an island - Peroxisome contact sites". In: *Biochimica et Biophysica Acta - Molecular Cell Research* 1863.5, pp. 1061–1069.

Shai, N., E. Yifrach, et al. (May 2018). "Systematic mapping of contact sites reveals tethers and a function for the peroxisome-mitochondria contact". In: *Nature Communications* 9.1, pp. 1–13.

Shao, M. R. et al. (Feb. 2017). "Stress-responsive pathways and small RNA changes distinguish variable developmental phenotypes caused by MSH1 loss". In: *BMC Plant Biology* 17.1, pp. 1–14.

Shaw, J. M. and J. Nunnari (Apr. 2002). "Mitochondrial dynamics and division in budding yeast". In: *Trends in Cell Biology* 12.4, pp. 178–184.

Shcherbo, D. et al. (2007). "Bright far-red fluorescent protein for whole-body imaging". In: *Nature Methods* 4.9, pp. 741–746.

Sheahan, M. B., D. W. McCurdy, and R. J. Rose (Dec. 2005). "Mitochondria as a connected population: Ensuring continuity of the mitochondrial genome during plant cell dedifferentiation through massive mitochondrial fusion". In: *The Plant Journal* 44.5, pp. 744–755.

Shearer, T. L. et al. (Dec. 2002). "Slow mitochondrial DNA sequence evolution in the Anthozoa (Cnidaria)". In: *Molecular Ecology* 11.12, pp. 2475–2487.

Shedge, V. et al. (Apr. 2007). "Plant Mitochondrial Recombination Surveillance Requires Unusual RecA and MutS Homologs". In: *The Plant Cell* 19.4, pp. 1251–1264.

Shimmen, T. and E. Yokota (Feb. 2004). "Cytoplasmic streaming in plants". In: *Current Opinion in Cell Biology* 16.1, pp. 68–72.

Shimomura, O., F. H. Johnson, and Y. Saiga (1962). "Extraction, purification and properties of aequorin, a bioluminescent". In: *Journal of Cellular and Comparative Physiology* 59.3, pp. 223–239.

Shu, Y. and J. McCauley (Mar. 2017). "GISAID: Global initiative on sharing all influenza data – from vision to reality". In: *Eurosurveillance* 22.13.

Shutt, T. E. and H. M. McBride (Feb. 2013). "Staying cool in difficult times: Mitochondrial dynamics, quality control and the stress response". In: *Biochimica et Biophysica Acta - Molecular Cell Research* 1833.2, pp. 417–424.

Sia, E. A. and D. T. Kirkpatrick (Feb. 2005). "The yeast MSH1 gene is not involved in DNA repair or recombination during meiosis". In: *DNA Repair* 4.2, pp. 253–261.

Silva, B. S. et al. (Nov. 2020). "Maintaining social contacts: The physiological relevance of organelle interactions". In: *Biochimica et Biophysica Acta (BBA) - Molecular Cell Research* 1867.11, p. 118800.

Simmen, T. and M. Tagaya (2017). "Organelle Communication at Membrane Contact Sites (MCS): From Curiosity to Center Stage in Cell Biology and Biomedical Research". In: *Advances in Experimental Medicine and Biology* 997, pp. 1–12.

Simula, L. and S. Campello (2018). "Monitoring the Mitochondrial Dynamics in Mammalian Cells". In: *Mitochondrial Bioenergetics: Methods and Protocols*. New York, NY: Springer New York, pp. 267–285.

Skippingtona, E. et al. (July 2015). "Miniaturized mitogenome of the parasitic plant *Viscum scurruloideum* is extremely divergent and dynamic and has lost all NAD genes". In: *Proceedings of the National Academy of Sciences of the United States of America* 112.27, E3515–E3524.

Sloan, D. B., Z. Wu, and J. Sharbrough (Mar. 2018). "Correction of Persistent Errors in *Arabidopsis* Reference Mitochondrial Genomes." In: *The Plant cell* 30.3, pp. 525–527.

Sloan, D. B., A. J. Alverson, et al. (Jan. 2012). "Rapid evolution of enormous, multichromosomal genomes in flowering plant mitochondria with exceptionally high mutation rates". In: *PLoS Biology* 10.1.

Spillane, M. et al. (Dec. 2013). "Mitochondria Coordinate Sites of Axon Branching through Localized Intra-axonal Protein Synthesis". In: *Cell Reports* 5.6, pp. 1564–1575.

Stenton, S. L. and H. Prokisch (June 2020). "Genetics of mitochondrial diseases: Identifying mutations to help diagnosis". In: *EBioMedicine* 56.

Sukhorukov, V. M., D. Dikov, et al. (Oct. 2012). "Emergence of the Mitochondrial Reticulum from Fission and Fusion Dynamics". In: *PLoS Computational Biology* 8.10, e1002745.

Sukhorukov, V. M. and M. Meyer-Hermann (Sept. 2015). "Structural Heterogeneity of Mitochondria Induced by the Microtubule Cytoskeleton". In: *Scientific Reports* 5.

Tacutu, R. et al. (Jan. 2018). "Human Ageing Genomic Resources: New and updated databases". In: *Nucleic Acids Research* 46.D1, pp. D1083–D1090.

Tagu, D., J. K. Colbourne, and N. Nègre (July 2014). "Genomic data integration for ecological and evolutionary traits in non-model organisms". In: *BMC Genomics* 15.1.

Takagi, S., M. S. Islam, and K. Iwabuchi (2011). "Dynamic behavior of double-membrane-bounded organelles in plant cells". In: *International Review of Cell and Molecular Biology* 286.C, pp. 181–222.

Takanashi, H. et al. (2006). "Different amounts of DNA in each mitochondrion in rice root". In: *Genes and Genetic Systems* 81.3, pp. 215–218.

Tam, Z. Y. et al. (Oct. 2013). "Mathematical Modeling of the Role of Mitochondrial Fusion and Fission in Mitochondrial DNA Maintenance". In: *PLoS ONE* 8.10, e76230.

Tinevez, J. Y. et al. (Feb. 2017). "TrackMate: An open and extensible platform for single-particle tracking". In: *Methods* 115, pp. 80–90.

Tominaga, M. and K. Ito (2015). "The molecular mechanism and physiological role of cytoplasmic streaming". In: *Current Opinion in Plant Biology* 27.

Toren, D. et al. (2016). "MitoAge: a database for comparative analysis of mitochondrial DNA, with a special focus on animal longevity". In: *Nucleic Acids Research* 44.D1, p. D1262.

Twig, G., A. Elorza, et al. (Jan. 2008). "Fission and selective fusion govern mitochondrial segregation and elimination by autophagy". In: *The EMBO Journal* 27.2, pp. 433–446.

Twig, G., X. Liu, et al. (Aug. 2010). "Biophysical properties of mitochondrial fusion events in pancreatic beta-cells and cardiac cells unravel potential control mechanisms of its selectivity." In: *American journal of physiology– Cell physiology* 299.2, pp. C477–87.

Unseld, M. et al. (Jan. 1997). "The mitochondrial genome of *Arabidopsis thaliana* contains 57 genes in 366,924 nucleotides". In: *Nature Genetics 1997 15:1* 15.1, pp. 57–61.

Valm, A. M. et al. (June 2017). "Applying systems-level spectral imaging and analysis to reveal the organelle interactome". In: *Nature* 546.7656, pp. 162–167.

Van Dingenen, J. et al. (Dec. 2016). "Plants grow with a little help from their organelle friends". In: *Journal of Experimental Botany* 67.22, pp. 6267–6281.

Van Gestel, K., R. H. Köhler, and J. P. Verbelen (2002). "Plant mitochondria move on F-actin, but their positioning in the cortical cytoplasm depends on both F-actin and microtubules". In: *Journal of Experimental Botany* 53.369, pp. 659–667.

Van Oppen, M. J. H. et al. (1999). "Gene Content and Organization in a Segment of the Mitochondrial Genome of the Scleractinian Coral *Acropora tenuis*: Major Differences in Gene Order Within the Anthozoan Subclass Zoantharia". In: *Mol. Biol. Evol* 16.12, pp. 1812–1815.

Van Regenmortel, M. H. (Nov. 2004). "Reductionism and complexity in molecular biology". In: *EMBO Reports* 5.11, p. 1016.

Vance, J. E. (Apr. 2014). "MAM (mitochondria-associated membranes) in mammalian cells: Lipids and beyond". In: *Biochimica et Biophysica Acta (BBA) - Molecular and Cell Biology of Lipids* 1841.4, pp. 595–609.

Vasudevan, S. et al. (2009). "Neighbor Discovery in Wireless Networks and the Coupon Collector's Problem". In: *Proceedings of the 15th annual international conference on Mobile computing and networking*.

Viana, M. P. et al. (Mar. 2020). "Mitochondrial Fission and Fusion Dynamics Generate Efficient, Robust, and Evenly Distributed Network Topologies in Budding Yeast Cells". In: *Cell Systems* 10.3, 287–297.e5.

Virdi, K. S. et al. (2016). "MSH1 Is a Plant Organellar DNA Binding and Thylakoid Protein under Precise Spatial Regulation to Alter Development". In: *Molecular Plant* 1.9(2), pp. 245–260.

Voon, C. P. et al. (Nov. 2018). "ATP compartmentation in plastids and cytosol of *Arabidopsis thaliana* revealed by fluorescent protein sensing". In: *Proceedings of the National Academy of Sciences of the United States of America* 115.45, E10778–E10787.

Wada, M. and N. Suetsugu (Dec. 2004). "Plant organelle positioning". In: *Current Opinion in Plant Biology* 7.6, pp. 626–631.

Wagner, S. et al. (Apr. 2015). *Analysis of plant mitochondrial function using fluorescent protein sensors*. Vol. 1305. Methods Mol Biol, pp. 241–252.

Wallace, D. C. and D. Chalkia (2013). "Mitochondrial DNA genetics and the heteroplasmy conundrum in evolution and disease". In: *Cold Spring Harbor perspectives in biology* 5.11, a021220.

Wang, C., M. Taki, et al. (Aug. 2019). "A photostable fluorescent marker for the super-resolution live imaging of the dynamic structure of the mitochondrial cristae". In: *Proceedings of the National Academy of Sciences of the United States of America* 116.32, pp. 15817–15822.

Wang, P. and P. J. Hussey (June 2015). "Interactions between plant endomembrane systems and the actin cytoskeleton". In: *Frontiers in Plant Science* 6, p. 422.

Wang, Y., O. Berkowitz, et al. (July 2018). "Stress responsive mitochondrial proteins in *Arabidopsis thaliana*". In: *Free Radical Biology and Medicine* 122, pp. 28–39.

Watanabe, W. et al. (Mar. 2007). "Single-organelle tracking by two-photon conversion". In: *Optics Express* 15.5, pp. 2490–2498.

Watson, J. D. and F. H. Crick (Apr. 1953). "Molecular Structure of Nucleic Acids: A Structure for Deoxyribose Nucleic Acid". In: *Nature* 171.4356, pp. 737–738.

Watts, D. and H. Strogatz (June 1998). "Collective dynamics of 'small-world' networks". In: *Nature* 393.6684, pp. 440–442.

Welchen, E. et al. (Jan. 2014). "Coordination of plant mitochondrial biogenesis: Keeping pace with cellular requirements". In: *Frontiers in Plant Science* 4.1, p. 551.

West, S. A. et al. (Dec. 2007). "The Social Lives of Microbes". In: *Annual Review of Ecology, Evolution, and Systematics* 38, pp. 53–77.

Westerhoff, H. V. and B. O. Palsson (Oct. 2004). "The evolution of molecular biology into systems biology". In: *Nature Biotechnology* 22.10, pp. 1249–1252.

Whelan, J. and M. W. Murcha (Apr. 2015). *Plant mitochondria: Methods and protocols*. Springer New York, pp. 1–303.

White, R. R. et al. (Dec. 2020). "Miro2 tethers the ER to mitochondria to promote mitochondrial fusion in tobacco leaf epidermal cells". In: *Communications Biology* 3.1, pp. 1–8.

Wikipedia (2021). *Wikipedia: List of longest-living organisms*. Date accessed 5 Dec 2020. URL: https://en.wikipedia.org/wiki/List_of_longest-living_organisms.

Williams, B. P., I. G. Johnston, et al. (Sept. 2013). "Phenotypic landscape inference reveals multiple evolutionary paths to C4 photosynthesis". In: *eLife* 2.

Williams, C. F. and C. H. George (Mar. 2019). "Connect and Conquer: Collectivized Behavior of Mitochondria and Bacteria". In: *Frontiers in Physiology* 10, p. 340.

Willingham, T. B., P. T. Ajayi, and B. Glancy (Oct. 2021). "Subcellular Specialization of Mitochondrial Form and Function in Skeletal Muscle Cells". In: *Frontiers in Cell and Developmental Biology* 9, p. 2907.

Witte, L. C. de and J. Stöcklin (Dec. 2010). "Longevity of clonal plants: why it matters and how to measure it". In: *Annals of Botany* 106.6, pp. 859–870.

Wolfram, R. (2018). *Mathematica, Version 11.3.0.0*. Champaign, IL, 2018.

Woloszynska, M. (2010). "Heteroplasmy and stoichiometric complexity of plant mitochondrial genomes-though this be madness, yet there's method in't". In: *Journal of Experimental Botany* 61.3, pp. 657–671.

Woodson, J. D. and J. Chory (May 2008). "Coordination of gene expression between organellar and nuclear genomes". In: *Nature Reviews Genetics* 9.5, pp. 383–395.

Wu, Z. et al. (July 2020). "MSH1 is required for maintenance of the low mutation rates in plant mitochondrial and plastid genomes". In: *Proceedings of the National Academy of Sciences of the United States of America* 117.28, pp. 16448–16455.

Wynn, E., E. Purfeerst, and A. Christensen (Feb. 2020). "Mitochondrial DNA repair in an *Arabidopsis thaliana* uracil N-glycosylase mutant". In: *Plants* 9.2.

Xin, J. C. and R. A. Butow (Sept. 2005). "The organization and inheritance of the mitochondrial genome". In: *Nature Reviews Genetics* 6.11, pp. 815–825.

Xu, X. and D. Wang (Jan. 2021). "Comparative Chloroplast Genomics of *Corydalis* Species (Papaveraceae): Evolutionary Perspectives on Their Unusual Large Scale Rearrangements". In: *Frontiers in Plant Science* 11, p. 2243.

Xu, Y. Z., M. P. Arrieta-Montiel, et al. (Sept. 2011). "Muts homolog1 is a nucleoid protein that alters mitochondrial and plastid properties and plant response to high light". In: *Plant Cell* 23.9, pp. 3428–3441.

Xu, Z., R. Zhang, et al. (June 2021). "A Balance between the Activities of Chloroplasts and Mitochondria Is Crucial for Optimal Plant Growth". In: *Antioxidants* 10.6, p. 935.

Yaffe, M. P. (1999). "Dynamic mitochondria". In: *Nature Cell Biology* 1.6, E149–E150.

Yi, M., D. Weaver, and G. Hajnóczky (Nov. 2004). "Control of mitochondrial motility and distribution by the calcium signal a homeostatic circuit". In: *Journal of Cell Biology* 167.4, pp. 661–672.

Yoshida, K. et al. (Dec. 2006). "Degeneration after sexual differentiation in *Hydra* and its relevance to the evolution of aging". In: *Gene* 385, pp. 64–70.

Yoshinaga, K. et al. (Aug. 2005). "Mitochondrial behaviour in the early stages of ROS stress leading to cell death in *Arabidopsis thaliana*". In: *Annals of Botany* 96.2, pp. 337–342.

Yu, F., A. Fu, et al. (Mar. 2007). "Variegation mutants and mechanisms of chloroplast biogenesis". In: *Plant, Cell and Environment* 30.3, pp. 350–365.

Yu, S. B. and G. Pekkurnaz (Oct. 2018). "Mechanisms Orchestrating Mitochondrial Dynamics for Energy Homeostasis". In: *Journal of Molecular Biology* 430.21, pp. 3922–3941.

Yu, Y., H. C. Lee, et al. (2016). "Inner membrane fusion mediates spatial distribution of axonal mitochondria". In: *Scientific Reports* 6.

Yui, R., Y. Ohno, and E. T. Matsuura (June 2003). "Accumulation of deleted mitochondrial DNA in aging *Drosophila melanogaster*". In: *Genes and Genetic Systems* 78.3, pp. 245–251.

Zainabadi, K. (Apr. 2018). "A brief history of modern aging research". In: *Experimental Gerontology* 104, pp. 35–42.

Zamponi, N. et al. (Dec. 2018). "Mitochondrial network complexity emerges from fission/fusion dynamics". In: *Scientific Reports* 8.1, pp. 1–10.

Zhao, J., U. Lendahl, and M. Nistér (2013). "Regulation of mitochondrial dynamics: Convergences and divergences between yeast and vertebrates". In: *Cellular and Molecular Life Sciences* 70.6, pp. 951–976.

Zheng, M., M. Beck, et al. (June 2009). "Actin Turnover Is Required for Myosin-Dependent Mitochondrial Movements in *Arabidopsis* Root Hairs". In: *PLoS ONE* 4.6, e5961.

Zheng, M., Q. Wang, et al. (Mar. 2010). "The speed of mitochondrial movement is regulated by the cytoskeleton and myosin in *Picea wilsonii* pollen tubes". In: *Planta* 231.4, pp. 779–791.

Zorov, D. B., M. Juhaszova, and S. J. Sollott (July 2014). "Mitochondrial reactive oxygen species (ROS) and ROS-induced ROS release". In: *Physiological Reviews* 94.3, pp. 909–950.